STATUS OF THESIS

Title of thesis	Polyetherimide-Montmorillonite Hollow Fibre Mixed Matrix Membranes for CO_2/CH_4 Separation

I MUHAMMAD ASIF JAMIL

hereby allow my thesis to be placed at the Information Resource Center (IRC) of Universiti Teknologi PETRONAS (UTP) with the following conditions:

1. The thesis becomes the property of UTP
2. The IRC of UTP may make copies of the thesis for academic purposes only.
3. This thesis is classified as

   ☐ Confidential

   ☑ Non-confidential

If this thesis is confidential, please state the reason:

____

____

The contents of the thesis will remain confidential for ___________ years.

Remarks on disclosure:

____

____

	Endorsed by
____________________	____________________
Signature of Author	Signature of Supervisor
Permanent address:	Name of Supervisor
55 B- Agrics Town, Raiwind Road	Dr. Oh Pei Ching
Lahore - Pakistan	
Date : ____________________	Date : ____________________

UNIVERSITI TEKNOLOGI PETRONAS

POLYETHERIMIDE-MONTMORILLONITE HOLLOW FIBRE MIXED MATRIX MEMBRANES FOR CO_2/CH_4 SEPARATION

By

MUHAMMAD ASIF JAMIL

The undersigned certify that they have read, and recommend to the Postgraduate Studies Programme for acceptance of this thesis for the fulfillment of the requirements for the degree stated.

Signature: ______________________________

Main Supervisor: Dr. Oh Pei Ching

Signature: ______________________________

Co-Supervisor: Prof. Azmi B M Shariff

Signature: ______________________________

Head of Department: Assoc. Prof. Dr. Suriati Sufian

Date: ______________________________

POLYETHERIMIDE-MONTMORILLONITE HOLLOW FIBRE MIXED MATRIX MEMBRANES FOR CO_2/CH_4 SEPARATION

by

MUHAMMAD ASIF JAMIL

A Thesis

Submitted to the Postgraduate Studies Programme

as a Requirement for the Degree of

DOCTOR OF PHILOSOPHY

CHEMICAL ENGINEERING DEPARTMENT

UNIVERSITI TEKNOLOGI PETRONAS

BANDAR SERI ISKANDAR,

PERAK

AUGUST 2018

DECLARATION OF THESIS

Title of thesis	Polyetherimide-Montmorillonite Hollow Fibre Mixed Matrix Membranes for CO_2/CH_4 Separation

I MUHAMMAD ASIF JAMIL

hereby declare that the thesis is based on my original work except for quotations and citations which have been duly acknowledged. I also declare that it has not been previously or concurrently submitted for any other degree at UTP or other institutions.

Witnessed by

Signature of Author

Signature of Supervisor

Permanent address:
55 B, Agrics Town, Raiwind Road
Lahore - Pakistan

Name of Supervisor
Dr. Oh Pei Ching

Date : ____________________

Date : ____________________

DEDICATION

This dissertation is dedicated to my father Muhammad Jamil, mother Shamim Akhtar, and other members of my family for their unconditional love, support, motivation and encouragement during my PhD studies.

ACKNOWLEDGEMENTS

First of all, I am grateful to Universiti Teknologi PETRONAS (UTP) Malaysia for providing me the opportunity to achieve my academic pursuits.

I am deeply gratified to my supervisor, Dr. Oh Pei Ching for her guidance and support throughout the course of my PhD degree. Her profound knowledge, commitment for work and dedication to research have been a great source of inspiration and stimulation in my professional life. I am highly thankful to my co-supervisor Prof. Azmi M Shariff for his guidance and facilitation throughout my research span.

I would like to express my appreciation to other members of my research group for their help and assistance in my studies. My sincere appreciation to all the lab technologists from Chemical Engineering Department and Centralized Analytical Laboratory (CAL), UTP for their assistance in carrying out my research activities.

I am grateful to my wife, Uzma, for her unswerving, unfaltering and unmitigated love and support. My son, Waleed, deserves the special recognition, as he remained a continuous source of exuberance to me.

Last but not least, I am thankful to all my friends and acquaintances, Salman Naqvi, Umair Sikandar, Babar Azeem, Zia Mustafa, Zubair Shahid, Sahil Garg, M. Shahbaz, Farukh Iqbal, Umair Shahid, Hafiz Ab. Manan and Waqas Yaqub for making this time unforgettable and memorable.

ABSTRACT

Hollow fibre mixed matrix (HFMM) membranes with nano-filler embedded in polymer matrix offer an attractive route for the fabrication of high performance gas separation membranes. However, the major concern is the incompatibility of nano-filler like clay with the organic phase due to its inherent hydrophilic properties. In this work, montmorillonite (MMT) clay was modified with long chain aminolauric acid to impart organophilicity thereby enhance its compatibility towards organic polymer matrix. Furthermore, HFMM membranes comprising polyetherimide (PEI) with various unmodified and modified montmorillonite (MMT and *f*-MMT) ranging from 1 to 4 wt. %, were developed via phase inversion method. Morphological, filler distribution, dispersion, surface topology, thermal, and wettability analyses were carried out for developed hollow fibre (HF) membranes. Pure gas permeation tests using CO_2 and CH_4 were conducted at varying pressure of 2 to 10 bars at ambient conditions. In addition, mixed gas test at CO_2/CH_4 composition of 50/50 v/v % was conducted for selected membranes. Upon modification of MMT, the basal spacing increased from 12.38 to 17.22 Å. The developed mixed matrix membranes (MMMs) incorporating MMT showed decrease in CO_2/CH_4 gas separation performance compared to neat PEI membrane. In contrast, the performance of asymmetric membrane was enhanced by incorporating *f*-MMT in PEI matrix to form MMMs. Uniform dispersion, void-free morphology and hydrophobic properties were observed for the aforementioned membranes. Furthermore, an increasing trend in ideal selectivity was observed up to 2 wt. % *f*-MMT loading against all feed pressures. Thereafter, opposite trend was observed with increasing filler loading due to filler agglomeration. The maximum ideal selectivity achieved was 18.35 with 2 wt. % loading at 4 bar pressure, which is 52.2 % higher than neat PEI hollow fibre membrane. Moreover, for the aforementioned membrane, the mixed gas selectivity of 10.66 was achieved. This implies that polyetherimide-clay HFMM membranes have the potential to be considered for CO_2/CH_4 separation at commercial scale after further improvement.

Finally, various theoretical gas permeation models were adopted for predicting CO_2 permeance in MMMs. The average aspect ratio of the *f*-MMT was found to be 53, with 3 number of stacks per tactoid. Moreover, it was observed that Bhardwaj model showed the least average absolute relative error (%AARE) values up to 3 wt. % *f*-MMT loading in the range of –10.11 to 8.55 for 2 to 10 bar pressure. Hence, Bharadwaj was the best fit model for the experimental data compared to other models.

ABSTRAK

Membran matriks campuran dalam konfigurasi serat berongga dengan pengisi-nano yang tersirat dalam matriks polimer menawarkan kaedah yang memberangsangkan untuk fabrikasi membran berprestasi tinggi bagi tujuan pemisahan gas. Walaubagaimanapun, mencapai penyerakan seragam pengisi-nano dalam polimer perumah menjadi cabaran utama dalam membangunkan membran. Dalam kajian ini, tanah liat MMT diubahsuai dengan asid aminolaurik yang berangkaian panjang untuk memberikan ciri organofilisiti untuk meningkatkan keserasian terhadap matriks polimer organik. Selanjutnya, membran serat campuran matriks yang terdiri daripada polyetherimide (PEI) dengan pelbagai montmorillonite yang tidak diubahsuai (MMT) dan montmorillonite yang diubahsuai (*f*-MMT) dari 1 hingga 4 wt. %, telah disintesis melalui kaedah penyongsangan fasa untuk pemisahan CO_2/CH_4. Serat berongga yang telah di sintesis dicirikan dengan menggunakan mikroskop elektron pengimbasan emisi (FESEM), spektroskopi sinar-X dispersif tenaga (EDX), mikroskopi electron transmisi (TEM), mikroskopi daya atom (AFM), analisis gravimetri termal (TGA), kalorimetri pengimbasan berbeza (DSC), sudut pertemuan dan ujian permeasi gas. Ujian permeasi dijalankan dengan menggunakan gas tulen pada suhu sekeliling (atmosfera) antara 2 hingga 10 bar. Ujian gas bercampur pada komposisi CO_2/CH_4 pada 50/50 v/v % telah dijalankan bagi membran yang optimum.

MMT telah berjaya diubahsuai dan jarak basal meningkat dari 12.38 ke 17.22 Å. Tambahan lagi, MMM yang menggabungkan MMT menunjukkan penurunan dalam prestasi berbanding membran PEI yang tulen. Sebaliknya, prestasi membran tidak simetri dipertingkatkan dengan memasukkan *f*-MMT dalam matrik PEI untuk membentuk MMM. Penyebaran seragam, morfologi bebas dan sifat hidrofobik diperhatikan untuk membran yang disebutkan di atas. Tambahan lagi, arah aliran yang meningkat dalam kepemilihan yang unggul telah diperhatikan sehingga 2 wt. % pemuatan *f*-MMT terhadap semua tekanan suapan. Selepas itu, arah aliran yang bertentangan telah diperhatikan dengan peningkatan penambahan pengisi disebabkan

oleh penggumpalan pengisi. Kepemilihan maksimum unggul yang dicapai ialah 18.35 dengan 2 wt. % pemuatan pada tekanan 4 bar iaitu 52.2% lebih tinggi daripada membran PEI HF yang tulen.

Akhirnya, pelbagai model teori permeasi gas telah digunakan untuk meramalkan tahap perlepasan CO_2 dalam MMM. Nisbah aspek purata *f*-MMT didapati 53, dengan 3 bilangan susunan setiap taktoid. Selain itu, dapat diperhatikan bahawa model Bhardwaj menunjukkan relatif kesilapan purata (% AARE) yang paling rendah mencecah 3 wt. % pemuatan *f*-MMT dalam julat -10.11 hingga 8.55 untuk tekanan 2 hingga 10 bar. Oleh itu, Bharadwaj adalah model terbaik untuk data eksperimen berbanding model yang lain.

TABLE OF CONTENT

LIST OF FIGURES

LIST OF PLATES

LIST OF TABLES

LIST OF ABBREVIATIONS

AARE	Average absolute relative error
AEAPTMS	N-β-(aminoethyl)-γ-aminopropyltrimethoxysilane
AFM	Atomic force microscopy
CA	Cellulose acetate
CEC	Cation-exchange capacity
CMS	Carbon molecular sieve
CNT	Carbon nanotube
DDR	Deca-dodecasil rhombohedral
DSC	Differential scanning calorimetry
DTG	Derivative thermogravimetric
EDX	Energy dispersive X-Ray spectroscopy
EPDM	Ethylene-propylene-diene rubber
EVA	Ethyl vinyl acetate
f-MMT	Functionalized montmorillonite
FESEM	Field emission scanning electron microscopy
FTIR	Fourier transform infrared spectroscopy
GPU	Gas permeation unit
HNT	Halloysite nanotubes
HDPE	High-density polyethylene
HF	Hollow fibre
HFMM	Hollow fibre mixed matrix
MMT	Montmorillonite
MMM	Mixed matrix membrane
Mof	Metal-organic framework
NDP	Number of data points
NMP	*N*-Methyl-2-pyrrolidone
OMMT	Organically modified montmorillonite
PAEK	Poly(aryletherketone)

PBI	Polybenzimidazole
PC	Polycarbonate
PDMS	Polydimethylsiloxane
PEI	Polyetherimide
PES	Polyethersulfone
PI	Polyimide
PP	Polypropylene
PP-g-MA	Polypropylene grafted maleic anhydride
PSf	Polysulfone
PVA	Polyvinyl alcohol
PVDF	Polyvinylidene fluoride
SAPO	Silicoaluminophosphate
SEM	Scanning electron microscopy
TEM	Transmission electron microscopy
TGA	Thermogravimetric analysis
TMA-MMT	Tetramethylammonium intercalated montmorillonite
US	United States of America
XRD	X-ray diffractometry
3D	Three Dimensional
6FDA	2-2’-Bis (3,4 Dicarboxyphenyl) hexafluoropropane dianhydride

LIST OF SYMBOLS

A	Area	cm^2
a	Aspect ratio	-
D	Diffusion coefficient	cm^2/s
I.D	Inner diameter	cm
O.D	Outer diameter	cm
P	Permeability	barrer
P/l	Permeance	GPU
P_c	Permeability of composite membrane	barrer
P_o	Permeability of pure membrane	barrer
Q	Volumetric flow rate	cm^3/s
Ra	Roughness parameter	nm
S	Solubility coefficient	$cm^3(STP)/cm^3.atm$
T	Absolute temperature	˚C
T_g	Glass transition temperature	˚C
Wt.	Weight	g
l	Membrane thickness	cm
Φ	Filler volume fraction	-
α	Ideal selectivity	-
ΔP	Pressure difference	bar

CHAPTER 1

INTRODUCTION

Membrane acts as a semi permeable barrier which permits the transportation of one or more molecules in a selective manner from a multicomponent mixture. Micro molecular selective transport membranes have been around for more than a century; however, membranes have only been used for gas separation application in the recent fifty years [1]. Membrane based separation processes are energy efficient, cost effective and environmental friendly. Therefore, they are more attractive as compared to traditional separation technologies such as absorption, adsorption and distillation. Moreover, membrane based set ups are easy to install and scale up [2, 3].

Nowadays, membrane technology finds application in many aspect of separation engineering, ranging from solid-liquid (microfiltration, ultrafiltration), ion-liquid (nanofiltration), reverse osmosis, forward osmosis, liquid-liquid (pervaporation) and liquid-gas (gas contactor) to gas-gas (gas separation) [2, 4-8]. Membrane technology for liquid-liquid separation has been used for various industrial processes due to its reliability and efficiency. However, membrane technology for gas-gas separation are relatively immature and has not find much applications for industrial processes despite its tremendous industrial potential. In membrane based separation technology, gas-gas separations are rapidly growing industrial processes, and increasingly used for nitrogen separation from air, hydrogen recovery in ammonia synthesis and petroleum cracking plants and for natural gas purification.

1.1 Natural Gas

Nowadays, world’s focus starts changing from fossil fuel to cleaner fuel source for electricity generation, industry and transportation. In this scenario, natural gas has emerged as an important energy resource of the future [9]. Natural gas is considered as a clean fuel in comparison to fossil fuels in terms of their combustion byproducts; however, natural gas found in reservoirs contains impurities such as water, hydrogen sulfide and carbon dioxide. Table 1-1 shows the typical composition of natural gas in pre-refined state.

Table 1-1: Natural gas composition, Terengganu, Malaysia [10].

Components	Feed Content
CH_4	40 - 50 %
C_2H_6	5 - 10 %
C_3H_8	1 – 5 %
CO_2	20 - 30 %
N_2, H_2S	0 - 1 %

These impurities must be removed to very low concentrations before transport through pipeline. Carbon dioxide is one of the most undesired impurity which must be separated from natural gas. Some natural gas reservoirs contain CO_2 composition as high as 70% in Natuna located in Indonesia [10]. In the presence of water, CO_2 is highly corrosive which can corrode gas pipeline and equipment. In addition, it also reduces the calorific value of natural gas stream and increases the cost of production [11]. Moreover, CO_2 also freezes at lower temperature, therefore, its removal from natural gas stream is inevitable to increase its sales value.

1.2 Natural Gas Sweetening Techniques

Natural gas sweetening refers to carbon dioxide removal from natural gas. Various techniques are available for CO_2 removal such as absorption, adsorption, cryogenic distillation and membrane technology [12]. Membrane based separation processes have gained overwhelming attention over conventional separation technologies owing to its small environmental footprint, cleaner production, economic feasibility and energy efficiency [3, 13]. Membrane technology, particularly for CO_2/CH_4 separation, has gained much interests for industrial applications such as water treatment, biogas purification and natural gas sweetening [14]. However, the development of efficient gas separation membranes remains a challenge for researchers.

1.3 Performance enhancement strategies for gas separation membranes

Presently, it is a challenge for gas separation membranes to maintain their favorable economy viability while improving their gas selectivity and durability. These improved membranes would be attractive in potential markets such as CO_2/CH_4, hydrocarbon/H_2 and olefin/paraffin separations. Various aspects are considered to be more favorable in comparison to traditional membrane formation methods. One of the conventional route is to synthesize inorganic membranes over organic membranes as they demonstrate high permeability and durability, but at 1-3 folds higher cost. In contrast, polymer based mixed matrix membranes are next-generation separation membranes that address the need for improved selectivity and durability at lower cost. Similarly, although many published literatures focused on flat sheet membranes, 70 % of industrial membranes are formed in hollow fibre geometry due to higher surface area per unit volume, whereas fewer than 20 % are formed in spiral wound modules [15]. Moreover, asymmetric membranes are more favorable in comparison to dense membranes due to higher permeation and selectivity. These membrane formation aspects could improve the gas separation performance and are considered in this research work.

1.3.1 Geometrical Aspect

Flat sheets are generally provided in plate and frame or spiral wound modules. However, plate and frame is one of the earliest module and has been largely replaced by spiral wound module due to high cost involved. For industrial gas separation applications, hollow fibre technology is the optimized geometry in comparison to flat sheet and spiral wound geometries as it promised compact module design, lower cost, and higher surface to volume ratio. The surface area of hollow fibre membranes available for separation process is much higher as compared to its counterparts [16]. In order to obtain the same separation surface area through flat sheet and spiral wound,

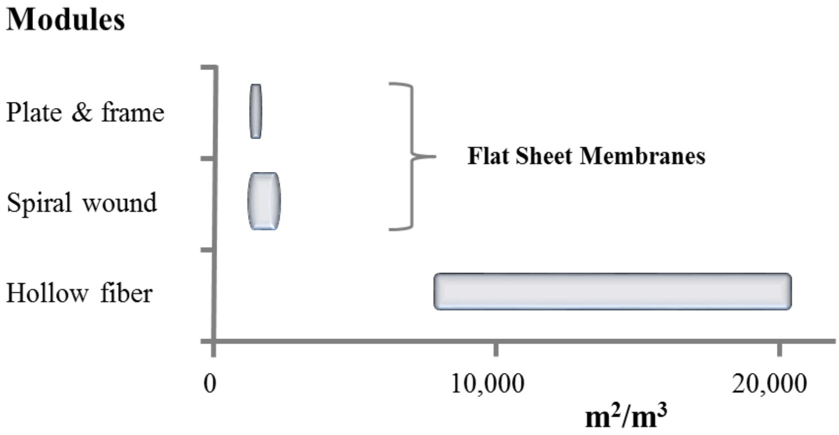

Figure 1-1: Comparison of surface area per unit volume between different membrane modules [16].

much higher investment is required [1]. Figure 1-1 depicts the comparison of surface to volume ratio of flat sheet, spiral wound and hollow fiber membrane. Generally, the outer diameter of hollow fibre membranes are 100-500 µm with surface to volume ratios of 20,000 to 40,000 m^2/m^3. Flat sheet membranes offered surface to volume ratio of 1,000 m^2/m^3, despite being effective in liquid separation or vacuum application [17]. The advantages of using hollow fibre membrane over other geometries are provided in Table 1-2.

Table 1-2: Comparison of different membrane geometries [15, 17].

Property	Membrane geometry		
	Plate and Frame	Spiral wound	Hollow fiber
Manufacturing cost, USD/m^2	50 to 200	10 to 100	2 to 5
Packing density	Low	Low	High
Pressure drop	Low	Low	Low
Suitability for high pressure	Moderate	Yes	Yes
Surface area (per unit volume)	Low	Low	High
Space required	Large	Large	Low

Nowadays, most of the gas separation membranes are developed in hollow fibre modules, with fewer than 20% formed in spiral wound modules. Despite the various benefits associated with hollow fibre geometry, cost effectiveness is one of the major constraints for product commercialization. Hollow fibre module offers a production cost between $ 2 to 5 per unit area, whereas spiral wound costs between $ 10 to 100.

Furthermore, the cylindrical shape of the hollow fibres can withstand high transmembrane pressure difference up to 1000 psi. Another advantage associated with hollow fibre module is the compactness, which results in lower space required for membrane module set up and scale up [15].

The development of membrane from a particular polymer in hollow fibre module further enhance its performance boundaries. The development of hollow fibres is more of an art than a science, as large number of spinning parameters are associated with the spinning process. The morphologies of hollow fibres can be varied by changing the spinning conditions and dope compositions or combination of both. Various morphological structures of a specific polymer hollow fibre membrane showed different separation performance even for the same gas.

1.3.2 Morphological aspect

The morphology of a particular membrane module plays the most important role in determining the separation performance. Hollow fibre membranes are commonly prepared using phase separation mechanism as introduced by Loeb and Surirajan in the 1960s [18]. Due to phase separation, asymmetric morphology is obtained which consists of thin top layer and porous sub-layer beneath it. The top layer comprises thin, dense, non-porous skin layer which performs the gas permeation, supported by the micro porous sub-layer from the same material which induces mechanical strength to the membrane.

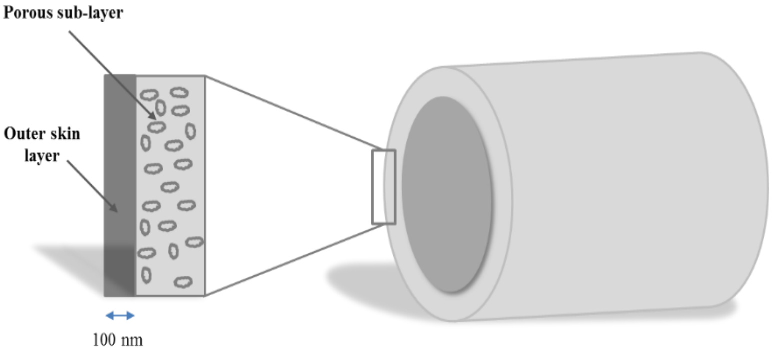

Figure 1-2: Schematic of asymmetric hollow fibre membrane [16].

The asymmetric morphology allows large surface area, maximum driving force and minimum resistance for gas permeation while possibly maintaining the material's intrinsic selectivity [19]. The asymmetric morphology of membranes is formed due to non-solvent induced phase separation. The exchange of solvent and non-solvent takes place at the interface of solvent and coagulation bath, in which the removal of solvent from the membrane results in a porous structure. For membrane development through phase separation mechanism, three methods are frequently used namely dry phase, wet phase and dry-wet phase. Dry phase preparation, also called as air casting, is induced by placing the dope solution under ambient conditions, in which the evaporation of volatile solvent takes place which cause phase separation. In wet phase preparation, which is also termed as immersion casting, solvent exchange takes place between coagulant and solvent, whereas, non-solvent interacts and separates the phases from dope solution. On the other hand, dry-wet phase separation is a combination of air and immersion casting. Phase separation which occurs via dry-wet phase inversion produces a thin outer layer and thick sub-layer as shown in Figure 1-2 [20].

On a commercial scale, asymmetric hollow fibre membranes are preferred, as they enhance separation performance at reduced cost. Moreover, the presence of porous structure in the sub-layer offers ideally negligible permeation resistance and improves the mechanical stability of membrane against high pressure gas feed streams. Subsequently, the thin dense outer layer has a thickness as low as 100 nm and performs gas separation with high productivity. However, due to complication in the spinning process, development of defect-free thin layer remains a challenge.

1.3.2.1 Macrovoids development

In membrane forming processes via phase inversion, macrovoids appear as large elongated pores that can grow across the membrane thickness [21]. Generally, the size of macrovoids reported ranged from a few micrometers to tens of micrometers or even appeared parallel to the membrane phase separation front [22]. Using phase inversion technique, polymer-rich and polymer-lean phases have been produced during solvent exchange process, which is responsible for creating voids on the membrane surface.

The shape and size of macrovoids depend on the rate of solvent exchange; finger-like pores are generated due to instantaneous phase exchange whereas slow exchange produced sponge-like structure [23]. Finger-like pores favor gas permeance whereas sponge-like pores result in selectivity enhancement as the latter are produced due to greater molecular orientation and closely packed molecular chains [24].

A number of theories exist to explain the creation of macrovoids in membrane forming processes. In essence, various parameters which dictate membrane morphology have been studied in literature to suppress the formation of macrovoids such as air gap, polymer concentration, dope viscosity, delayed demixing, surfactant addition and elongation draw [25]. The common feature in these approaches to suppress macrovoids is to increase the dope viscosity either by increasing polymer concentration or by adding additives. The viscosity of dope solution plays a very important role in formation of macrovoids-free hollow fibre membrane morphology. With the increase in dope viscosity, macrovoids formation increases, decreases and increases again. This trend provides the evidence of optimum viscosity for a certain dope solution. The polymer concentration in a dope solution has a significant impact on mean pore size, porosity and permeance of hollow fibre membranes. With the increase in polymer concentration, the solution viscosity and density increased, resulting in depression of void formation in the membrane microstructure. At longer air gaps, macrovoids formation increased to a great extent, similarly, a highly distorted structure was observed when air gap was greatly reduced. Dry processes are the only phenomena that took place in the aforementioned condition whereas wet processes dominate in the latter case. In order to obtain macrovoids-free membrane surface, the processing parameters like dope solution viscosity and air gap distance need to be optimized [21, 26]. The addition of surfactant in the dope solution influences the formation of macrovoids. The addition of hydrophobic surfactant which possesses low affinity towards coagulant is helpful in the suppression of macrovoids due to delayed liquid-liquid demixing process [27]. Macrovoids can be completely eliminated by spinning at higher elongation draw. This causes polymer chain alignment along with inducement of radial outflow of solvents within nascent fibre both to the inner or outer coagulant sides. It also retards the penetration of external coagulant which removes the driving force for macrovoids creation [21].

1.3.3 Mixed matrix membrane

Mixed matrix is another important approach to fabricate high performance membranes. MMM comprises of a polymer phase dispersed with inorganic filler as depicted in Figure 1-3. Although tremendous improvement has been shown by polymeric membranes over the past decade in terms of gas permeance, a balance between permeance and selectivity is yet to be achieved; whereas inorganic membranes are superior in terms of selectivity but their low processing ability, fragile, brittleness and higher capital cost limit their commercial application [28]. The notion behind development of mixed matrix membrane (MMM) was to combine the permeance of polymeric material and selectivity of inorganic material to create a state-of-the-art hybrid membrane.

For gas permeation, numerous polymers have been utilized to fabricate separation membranes. Rigid polymers with high T_g seems appropriate in achieving upper bound performance in comparison to rubbery polymers. Several high-performance polymers containing aromatic rings such as polyimide (PI), polycarbonate (PC), polysulfone (PSf), and poly(aryletherketone) (PAEK) have been widely used. The presence of covalent bonding, phenyl groups, high inter/intra molecular interactions between the bulky polymer chains offer high chemical and mechanical resistance at high temperatures. Nevertheless, the molding of the aforementioned polymers into desired morphologies is a difficult task due to rigidity and poor mobility of the polymer chains. However, the presence of flexible ether group within the bulky and rigid chain of

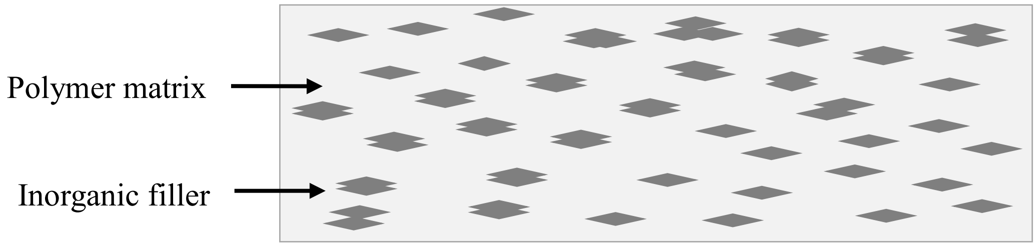

Figure 1-3: Schematic of mixed matrix membrane.

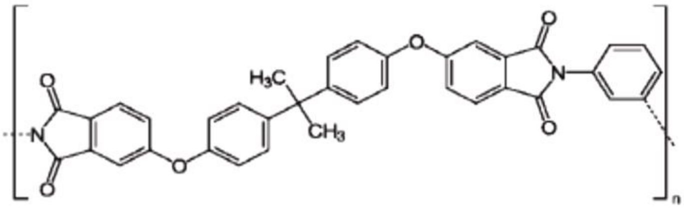

Figure 1-4: Chemical structure of polyetherimide [29].

polyimide makes polyetherimide (PEI) an attractive candidate to improve polymer processability while maintaining high mechanical and chemical resistance as compared to other high-performance polymers [29]. The chemical structure of polyetherimide is provided in Figure 1-4.

In essence, the performance of MMM does not simply depend on the cumulative addition of the individual phase’s intrinsic properties. Many parameters may seriously affect the separation performance of MMM, making it difficult to be understood. Consistent reproduction of successful MMM is often difficult, severely hindering its potential commercialization. In the past, during dense membrane formation, the major challenge was to understand the nature of poor interfacial interactions between polymer and inorganic filler. Much work need to be done to understand the interaction of both phases in dense membranes. However, the organic inorganic phase interactions in asymmetric hollow fibre mixed matrix membrane developed via phase inversion method has yet to be understood due to complexity involved in spinning process [30]. Nowadays, the major concern in MMM research is suitable combination of polymers and inorganic phase in addition to its physical properties like filler dispersion and agglomeration together with organic/inorganic interfacial morphologies [31]. The selection criteria of appropriate inorganic filler are often complicated, in which several parameters like compatibility, durability, productivity and mechanical properties should be considered. Various inorganic fillers have been studied in literature for separation membrane, however, the potential of nano-clay has yet to be considered despite their abundant usage in the composite industry. Good dispersion of nano-clay will enhance the mechanical, chemical and thermal properties at low loading [32].

1.3.3.1 Clay minerals

A common characteristic of clay minerals is their fine grained natural structure with sheet-like geometry. The sheet-structured hydrous silicates are generally referred to as phyllosilicates. Individual natural clay particles are smaller than 0.004 mm in diameter; these can range from 0.002 to 0.001 mm in diameter [33].

The elementary structural units are silica tetrahedron and aluminum octahedral. The cation Si^{+4} is four-fold and possesses tetrahedral coordination with oxygen, while the cation Al^{+3} occurs in six-fold or octahedral coordination. The variety of clay minerals can be described by the arrangement of tetrahedral and octahedral sheets, i.e. 1:1 clay mineral contains one tetrahedral and one octahedral sheet per clay layer; 2:1 clay mineral possesses two tetrahedral sheets and one octahedral sheet sandwiched between the two tetrahedral sheets (montmorillonite is an example of a clay mineral having 2:1 sheet-structure); and 2:1:1 clay minerals are composed of an octahedral sheet adjacent to a 2:1 layer. Therefore, the structure of clay minerals can be described in terms of arrangement of tetrahedral and octahedral sheets [33, 34]. Clay minerals are extensively used in polymer composite industry due to better mechanical, thermal and flame retardant properties.

1.3.4 Membrane surface coating

During membrane development processes, surface defects like microscopic pin holes may appear that often hamper gas separation performance, thereby allowing higher non-selective flux rate [35]. The aforementioned defects can be eliminated by coating the surface which facilitates the permeability and selectivity in gas separation membranes. The general criteria for coating polymer is similar with separating layer; which includes high permeability to avoid transport resistance against the permeating gas molecules. The coated membranes are dependent on certain factors like outer layer morphology, coating methods and convection conditions. It has been reported that a layer of rubbery coating material on the membrane surface is able to suppress the surface defects [36].

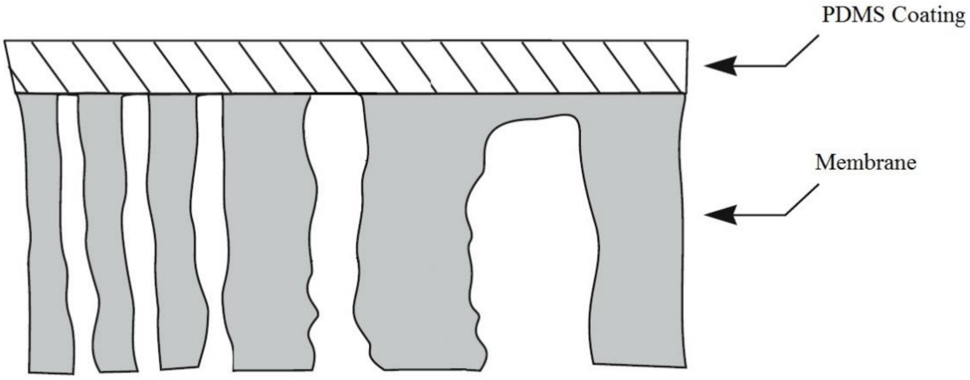

Figure 1-5: Schematic of PDMS coating layer at the membrane’s surface [36].

Polydimethylsiloxane (PDMS) is the most common rubbery material used for membrane coating. PDMS contains favorable structural properties such as unique flexibility of the siloxane backbone, low intermolecular forces between the methyl groups and high bonding energy of the siloxane bond. These properties result in a low glass transition temperature (T_g = -123 ˚C) as well as good thermal, chemical and oxidative stability [37]. Moreover, PDMS provides suitable adhesive properties to the membrane, which is another important characteristic for coating material [38]. Thus, the PDMS coated layer provides the desired permeability and selectivity for gases due to its intrinsic properties as well as sealing the pinholes as shown in Figure 1-5.

The membrane surface can be coated by two methods. In film-casting method, top layer materials are coated on the surface of substrate by film applicators or blades. In dip-coating, the top layer is formed by immersing substrate in an appropriate polymer solution. Film-casting method plugged the surface defects at the outer surface; whereas dip coating technique blocked the pores from both the top and bottom side of membrane [37]. The PDMS layer at the top of membrane surface does not affect the membrane properties, as it does not undergo physical aging and appears to have little or no influence on the underlying glassy layers [2]. In short, the effect of the PDMS layer on CO_2 plasticization behavior of the underlying membrane can be neglected.

1.4 Problem statement

The enrichment of methane gas from CO_2/CH_4 gas mixture is one of the important processes in gas separations. For CO_2 separation, numerous polymers including Matrimid, Udel, cellulose acetate, polyimide, Ultem, and polysulfone have been studied. Despite their good membrane performance, a fine balance between permeability and selectivity has yet to be achieved. The performance of polymers containing aromatic ring is remarkable, however, due to the stiffness of the polymers' main chain, they are often difficult to be processed. Polyetherimide contains both aromatic ring and ether linkage in the main chain. Consequently, the former induced chemical and mechanical strength, whilst the latter results in ease of processing. Mixed matrix membranes have the potential to increase the separation performance of membrane. Studies on MMM showed that the performance does not merely depend on the cumulative intrinsic properties of two phases, but the suitable combination of organic/inorganic phase plays a vital role in determining the separation performance. Nowadays, one of the major challenges in MMM research is the selection of suitable combination of polymers and inorganic phase in addition to its physical properties like filler dispersion and agglomeration together with organic/inorganic interfacial morphologies. Various inorganic fillers have been incorporated for MMM fabrication but non-porous inorganic filler, namely montmorillonite, has yet to receive much attention in MMM development for gas separation applications although it is prominently used in polymer composite industry due to associated advantages like thermal, mechanical, optical, electrical, flammability and economic viability. The major concern pertaining to MMT is negatively charged layers which attracts water and become incompatible to most host polymers due to hydrophilic characteristics. To overcome this issue, MMT is functionalized via cation exchange method to impart hydrophobicity and improve compatibility towards organic polymer.

Mostly, industrial scale membranes are developed in hollow fibre module via phase inversion technique. In the past, during dense membrane formation, the major challenge was to understand the nature of interfacial interactions of polymer and inorganic filler. Numerous work has been done to understand the interaction of both phases in dense membranes. However, the organic inorganic phase interactions in asymmetric hollow fibre MMM developed via phase inversion method has yet to be understood due to complexity in spinning process. Due to complications in phase inversion method, morphological defects such as macrovoids creation are common, causing deterioration in membrane's gas separation performance. Hence, process parameters such as air gap distance and dope viscosity need to be optimized to obtain defect-free morphology. For MMMs incorporating impermeable filler phase, various permeation models are available for validating the experimental performance; however, these models do not consider the effect of filler agglomeration at higher loading.

1.5 Research objectives

- To synthesize modified montmorillonite organoclay nanoparticles with reduced hydrophilicity and enhanced compatibility towards polymer matrix.
- To optimize spinning parameters for fabrication of asymmetric polyetherimide-montmorillonite (unmodified/modified) hollow fibre membrane at various inorganic, polymeric and solvent compositions.
- To investigate the performance of the resultant mixed matrix membranes for CO_2/CH_4 gas separation at varying feed pressures.
- To validate hollow fibre mixed matrix membrane CO_2/CH_4 performance via existing permeation models.

1.6 Scope of study

This research mainly focuses on the development of polyetherimde-montmorillonite mixed matrix hollow fibre membrane for CO2 separation. The uniform dispersion of inorganic phase in polymer matrix is a major issue which needs to be addressed in current MMM development. In this study, montmorillonite was functionalized to ensure compatibility with the polyetherimide matrix. The modified MMT was characterized to confirm the functionalization and interlayer spacing distance. The hollow fibre membranes formation via phase inversion is complicated and might create macrovoids at the membrane surface. In order to suppress macrovoids formation, polyetherimide hollow fibre membranes were spun by varying polymer concentration and air gap distance in order to optimize the spinning parameters. Other methods for macrovoid suppression like delayed demixing, surfactant addition and elongation draw are not considered in this study.

After optimizing spinning parameters, polyetherimide montmorillonite (unmodified/modified) mixed matrix hollow fibre membranes were developed up to 4 wt. % filler loading. The inorganic nanofillers' distribution and spatial dispersion analyses were carried out to ensure homogeneity. Developed hollow fiber membranes were characterized by kinetic study on thermal degradation at multiple heating rates and their performance were also investigated for CO_2/CH_4 gas separation for pressure range of 2 to 10 bar. All relevant parameters were optimized for successful formation of MMMs. Various phenomenological models like Nielsen, Cussler, Yang-Cussler, Lape-Cussler and Bharadwaj were applied for theoretical estimation of MMMs' CO_2/CH_4 separation performance.

1.7 Thesis Organization

The research work presented in this thesis consists of five chapters. The coverage of each chapter is presented as follows:

- Chapter 1 presents the insight of the subject, background and current issues pertaining to the work. Performance enhancement strategies like membrane geometry, material and morphological aspects were discussed. It further elaborates on the problem statement, research objectives and scope of the proposed study.

- Chapter 2 provides the background knowledge of structure and properties of clay fillers. From past literature, MMM containing clay as fillers, their performance for CO_2/CH_4 separation together with the morphological problems associated with the aforementioned membranes are discussed in detail.

Furthermore, various existing permeation models are presented to validate the results.

- Chapter 3 summarizes the methodology for montmorillonite modification and characterization. Moreover, the methods to develop HFMMM, characterization techniques and performance for CO_2/CH_4 gas are also discussed. The equations and formulae used to determine the performance of the HFMMM are also described.

- Chapter 4 provides the result and discussion of the experimental work performed in this study. The characterizations of modified montmorillonite and morphology of the developed neat PEI and mixed matrix membranes are discussed. Furthermore, the CO_2 and CH_4 gas performance testing are presented and explained based on different theories and arguments established in previous literature. The results are further compared with the theoretical results generated via existing permeation models.

- Chapter 5 comprises of all the findings and conclusions generated through the present research work and provides future recommendation for the related work.

CHAPTER 2

LITERATURE REVIEW

The present chapter reviews the working principle, historic background of gas separation membrane and commercialization of CO_2/CH_4 separation membrane. Membrane classification based on geometry, morphology, materials and transport mechanism is discussed, along with performance analysis of polymeric, inorganic, and mixed matrix membrane for CO_2/CH_4 separation. Moreover, the potential of nano-clay as inorganic filler is also analyzed along with challenges and issues pertaining to successful formation of mixed matrix membrane. Furthermore, Section 2.10 highlights the existing gas permeation models which are used in this study.

2.1 Membrane technology

The word membrane originates from a Latin word "Membrana" which means skin of the body [39]. By definition, membrane is a thin layer which separates two phases and allows the selective transport of one or more constituents of a mixture more readily than others [40].

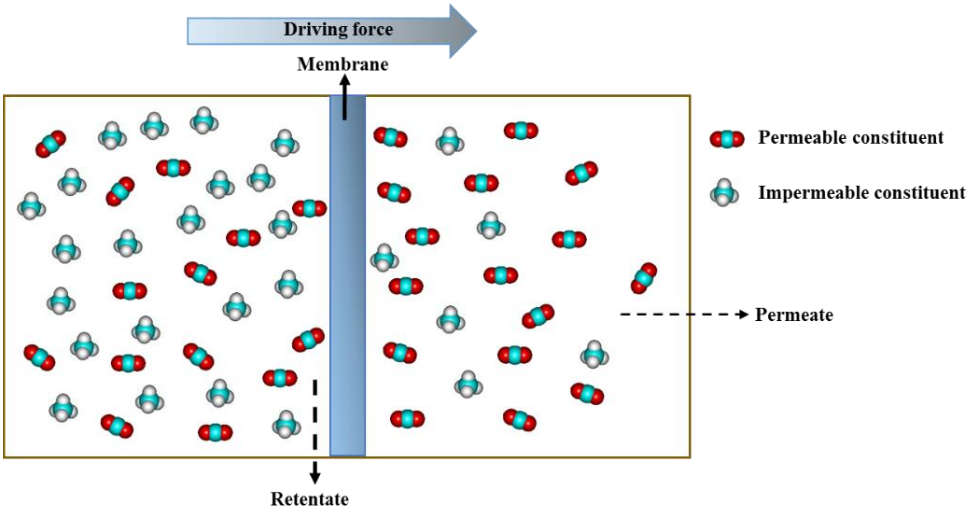

Figure 2-1: Membrane based separation mechanism [40].

Membrane technology is an emerging area which uses semipermeable membranes to differentiate one or more constituents from a mixture based on the applied driving force. The differentiated streams are classified as permeate (stream that passed through membrane) or retentate (stream retained by membrane), as depicted in Figure 2-1. The applied driving force could be temperature, pressure, concentration, or potential gradient. The performance of the membrane processes can be described by permeability coefficient, permeation rate and separation factor. Permeability and separation factor are the intrinsic properties of the membrane material whereas permeance is an extrinsic property that depends on membrane thickness, often given in barrer and GPU. The extent of membrane separation per force is reported as selectivity or enrichment factor. For good performance, membranes should have lower manufacturing cost, resistant against aggressive feed conditions and exhibit higher permeance and selectivity. Due to their versatility and economic feasibility, membrane technology has been applied in various industries like water treatment, textile, food, petrochemical, chemical, metal plating, electronic, pulp and paper, as well as natural gas treatment [41].

2.2 Gas transport mechanism in permeation membranes

The transport of gas molecules through permeation membranes are governed either by viscous flow, Knudsen diffusion, surface diffusion, molecular sieving or solution diffusion mechanism. The permeation of gas molecules across membranes is highly dependent on the membrane morphology, which is either porous or non-porous in nature. The permeance in porous membranes is governed by Knudsen diffusion, molecular sieving and surface diffusion based on the membrane pore size [19, 42, 43].

Solution-diffusion is the common permeation mechanism for non-porous gas separation membranes. In solution-diffusion mechanism, gas molecules sorb (dissolve) at the feed side of the membrane, followed by diffusion through the bulk of membrane and desorb at the permeate side [44]. The gas molecules' kinetic diffusion and thermodynamic sorption result in permeation rate being a function of molecular size and solubility within the membrane. However, the partial pressure difference is regarded as the general driving force for permeation membranes. The major resistance to permeation is the thickness of dense selective layer.

The permeation (P_i) of gas through membrane is described as the product of gas' diffusion (D_i) and sorption (S_i) coefficients. Gas permeability can also be calculated from the pressure and thickness normalized flux through the membrane and usually reported in Barrers as given in equation 2-1 and 2-2. On the other hand, the ratio of the respective gas permeation is known as ideal gas selectivity, as given in equation 2-3.

$$\left(P_i / l \right) = \frac{(Flux_i)}{(\Delta p_i)} \tag{2-1}$$

$$\left(P_i / l \right) = GPU = 10^{-6} \frac{cm^3_{STP}}{cm^2 . \sec . cmHg} \tag{2-2}$$

$$\alpha_{i/j} = \frac{\left(P_i / l \right)}{\left(P_j / l \right)} = \frac{(Flux_i)(\Delta p_i)}{(Flux_j(\Delta p_j)} \tag{2-3}$$

2.3 Membrane classification

Separation membranes are classified based on differences in the transport mechanism, geometry, structural morphology or manufacturing materials as described in Figure 2-2. Based on separation mechanism, membranes are either porous or non-porous. Solution-diffusion or sorption diffusion are the governing mechanisms in gas transport through non-porous membranes. On the other hand, porous membranes discriminate based on size of gas molecules [45]. Moreover, structural geometry plays a vital role in terms of gas molecule segregation through membranes. Hollow fibre membranes provide higher surface to volume ratio for gas molecules, which result in higher separation ability as compared to flat sheet and tubular membranes [46].

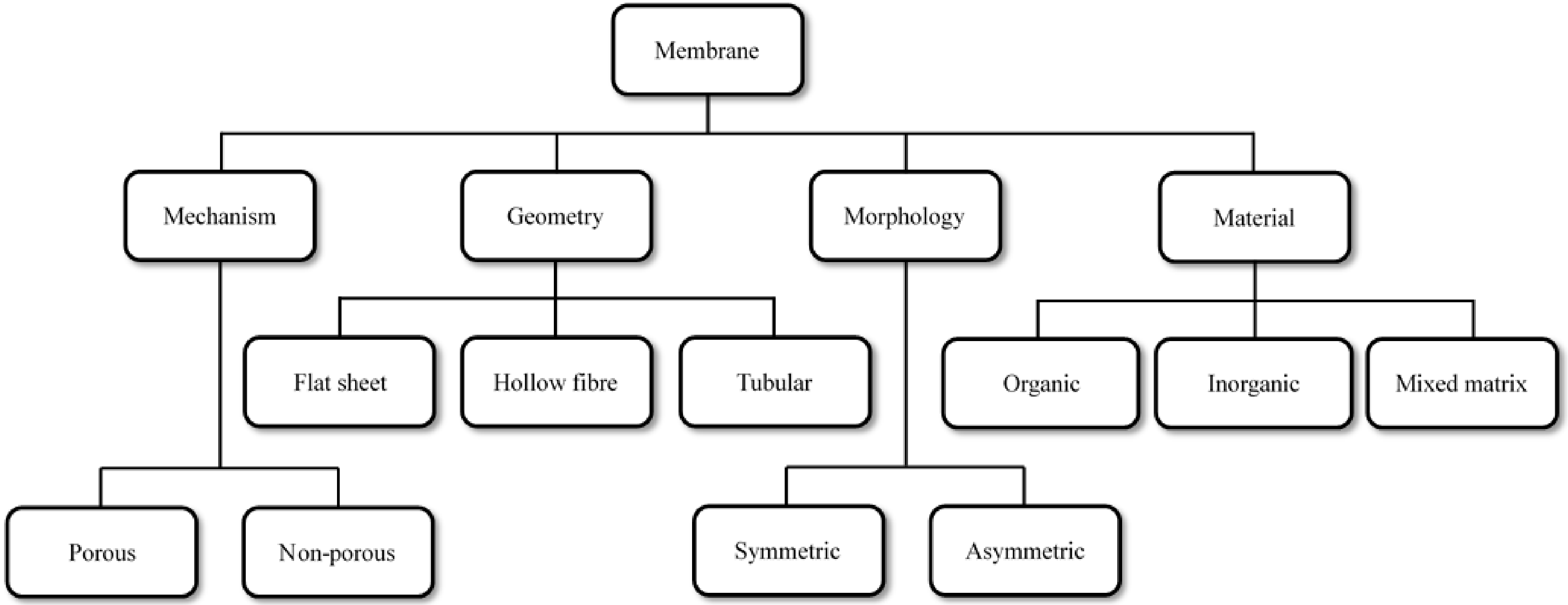

Figure 2-2: General classification of membranes [45].

Additionally, membranes are classified as symmetric or asymmetric based on structural morphology. For symmetric membrane, the pore structure remains the same throughout the membrane, whereas asymmetric membrane does not have the same structure. For the latter, the outer layer consists of a thin skin which contains smaller pore size and plays a major role in selective transport of gas molecules. However, the pore size increases in the sub-layer which acts as supporting layer for outer thin skin layer and improves the mechanical properties of the membrane [47]. In terms of manufacturing materials, organic (polymer), inorganic or organic-inorganic hybrid materials are generally used for membrane fabrication [45].

Membrane technology, due to versatility and economic feasibility, found applications in various industries like water treatment, textile, food, petrochemical, chemical, metal plating, electronic, pulp and paper. However, for gas separation processes, it is relatively new and much work need to be done in order to improve the membranes' separation performance.

2.4 Membrane Technology for Gas separation

The potential of membrane technology was well-known long before the first commercial-scale gas separation membrane was introduced. Thomas Graham was the first to report the use of polymeric membrane for gas separation. Later, he developed Graham's law by his experiment of gas diffusion through a tube with a sealed end [48]. Subsequently, Mitchell reported that gas molecules have different tendencies to pass through rubber membrane [2]. R.M. Barrers and D.A Dynes introduced the method to quantify the diffusion rate through separation membranes [49]. Since then, various polymeric membranes were studied as potential candidates for gas separation membrane. The commercialization of membrane technology for separation purposes were delayed due to lack of facility to develop high performance and economically feasible membrane modules. Loeb and Sourirajan reported a novel phase inversion method to produce cellulose acetate membrane with selective thin layer to sub micrometer level [18]. The phase inversion method laid the foundation stone for commercial application of gas separation membranes. In 1980, Permea PRISM was the first commercial scale polysulfone hollow fibre membrane for hydrogen recovery from purge streams of ammonia plants [40]. The timeline of membrane development is shown in Figure 2-3.

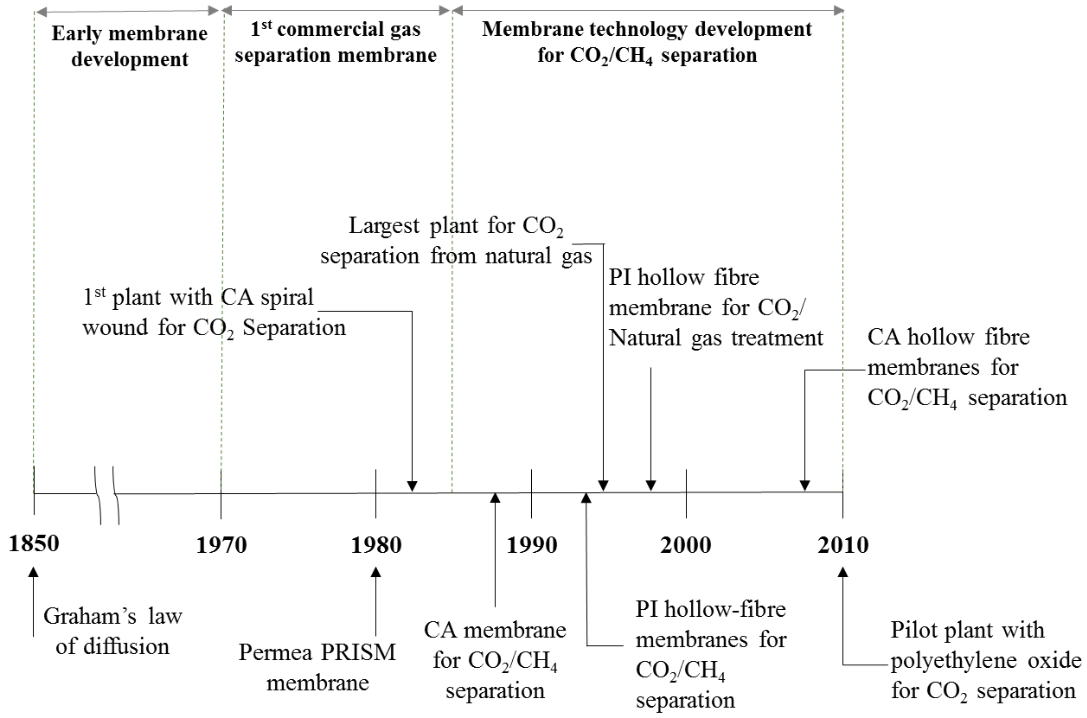

Figure 2-3: Timeline of gas separation membrane development on industrial scale [40, 45].

In recent years, gas separation via membrane technology has gained significant interest due to its versatility in processing, energy efficiency, low capital and operational cost, and small footprint [31, 50]. Many common polymers like polydimethylsiloxane (PDMS), cellulose acetate (CA), polysulfone (PSf), polyethersulfone (PES) and polyimide (PI) were developed as membrane module and applied for various gas separation applications such as hydrogen recovery, nitrogen enrichment, volatile organic recovery and separation of acid gases from natural gas streams and steel industry [2, 43].

2.5 Membrane separation performance for CO_2 from CH_4

Development of membrane for CO_2/CH_4 separation has been started since early 1990's and now there are more than 200 plants operating worldwide. Cellulose acetate and polyimides are the dominating membrane materials at commercial scale. The former is generally used in spiral wound configuration and the latter is used in hollow fibre modules [51-53]. However, the concentration of CO_2 after membrane separation process is still far behind the US pipeline specifications (<2%) [11]. Hence, the development of robust advanced materials with improved CO_2 permeation and selectivity for membrane technology is needed. The heart of membrane based separation process is the membrane itself. Various types of membranes for CO_2 separation from CH_4 gas including inorganic, polymeric and mixed matrix membrane have been reported in literature.

2.5.1 Inorganic membranes

Inorganic membranes with molecular sieves-like properties show significantly higher diffusivity selectivity than polymeric membranes, as shown in Figure 2-4 due to their discriminating ability based on pore sizes and shape. These membranes are also superior in terms of thermal and chemical stability, mechanical strength and have a longer lifespan [54]. Among the inorganic membranes, zeolite and carbon molecular sieve membranes favor CO_2/CH_4 separation due to narrow pore distribution (2 to 20 nm). These membranes are able to withstand swelling induced by CO_2 gas at higher pressure and are stable at higher temperature. In spite of that, their commercial

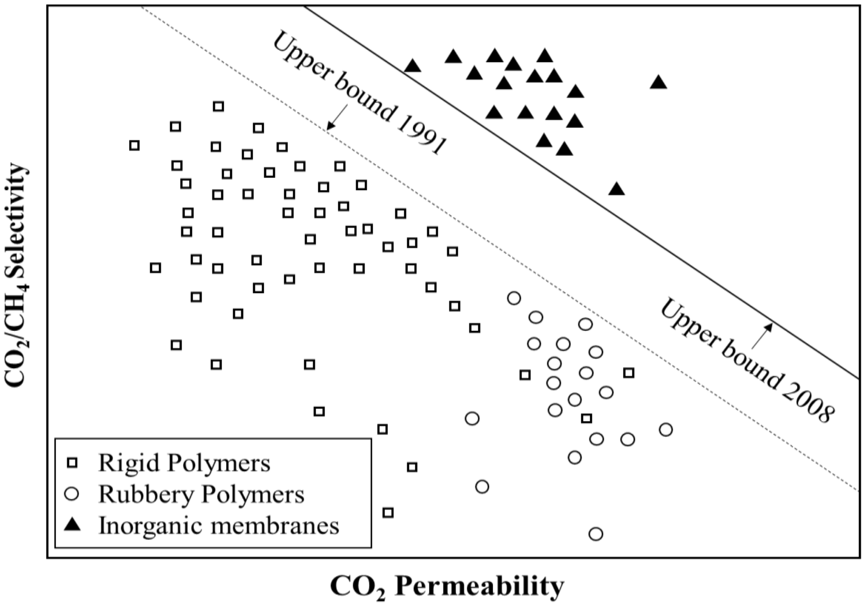

Figure 2-4: Robeson curve for CO_2/CH_4 gas permeability and selectivity.

applications are hindered by the lack of technology to produce defect-free membrane with improved reproducibility and at lower cost [55-57].

The performance of inorganic membranes for CO_2/CH_4 separation is presented in Table 2-1. Zeolites membranes, SAPO-34, MFI, DDR have narrow pore size distribution of 0.40, 0.50 and 0.36 nm, respectively approaching kinetic diameter of CO_2 (0.33 nm) and show better separation selectivity in comparison to silica and carbon membranes. Along with molecular sieving, the adsorption of CO_2 over CH_4 also governed the separation mechanism in zeolite membranes. However, the adsorption decreases with increasing temperature in zeolite membranes like MFI, which results in decrement in CO_2/CH_4 separation performance.

Table 2-1: Inorganic membranes for CO_2/CH_4 separation in literature.

Membrane	**Pressure (bar)**	**Temp. (˚C)**	**Permeance CO_2 (GPU)**	**Selectivity CO_2/CH_4**	**Ref**
SAPO-34 zeolite (on porous stainless steel tube)	2.2	22	1045.9	120	[58]
MFI (on porous alumina disk)	-	170	26.89	8	[59]
DDR zeolite (on porous alumina tube)	5	24	199.22	220	[60]
Carbonized (Polyamic acid)	1.6	100	5.71	70	[61]
Silica (on alumina disk)	1.5-4	25	750.06	326	[62]
DDR zeolite (on porous alumina disk)	5	27	239.06	500	[63]
Silicalite^{-1}	1	30	5755.2	2.4	[64]

2.5.2 Polymeric membrane

Polymeric membranes are typically formed from either glassy or rubbery polymers. The performance of polymer membranes displays trade-off between permeability and selectivity as described by Robeson performance curve, as shown in Figure 2-4. Rigid glassy polymers with small intersegment gaps, crystalline structures, and better chain interaction exhibit high intrinsic selectivity and low permeability. These glassy polymers generally have high chain entanglement and transport gas molecules on the basis of size and shape. In contrast, rubbery polymers show the opposite behavior; they exhibit poor selectivity but relatively high permeability due to the lack of crystallinity, paucity of polar groups and low degree of crosslinking. These rubbery polymers which consist of extremely flexible chains permit gas molecules to pass through without obstruction, resulting in the high permeability but low selectivity.

For gas permeation, numerous polymers have been utilized to fabricate separation membranes. Despite their promising separation performance, polymeric membranes are limited by Robeson upper bound performance curve. The performance of polymeric membranes for CO_2/CH_4 separation are summarized in Table 2-2. It is depicted that polyimides are most widely used and show better CO_2/CH_4 separation performance as compared to other glassy polymers because of their good chemical, thermal, mechanical and high selectivity. 6FDA, a type of aromatic polyimide, has been identified as a promising membrane material as it exhibits higher gas permeability and selectivity as compared to non-fluorinated polyimides. This is attributed to the presence of bulky –$C(CF_3)_2$- group which hinders intra segmental mobility and disrupts inter chain packing and stiffens backbone [65, 66]. The stiff back bone polymer chain made it difficult to process and spin.

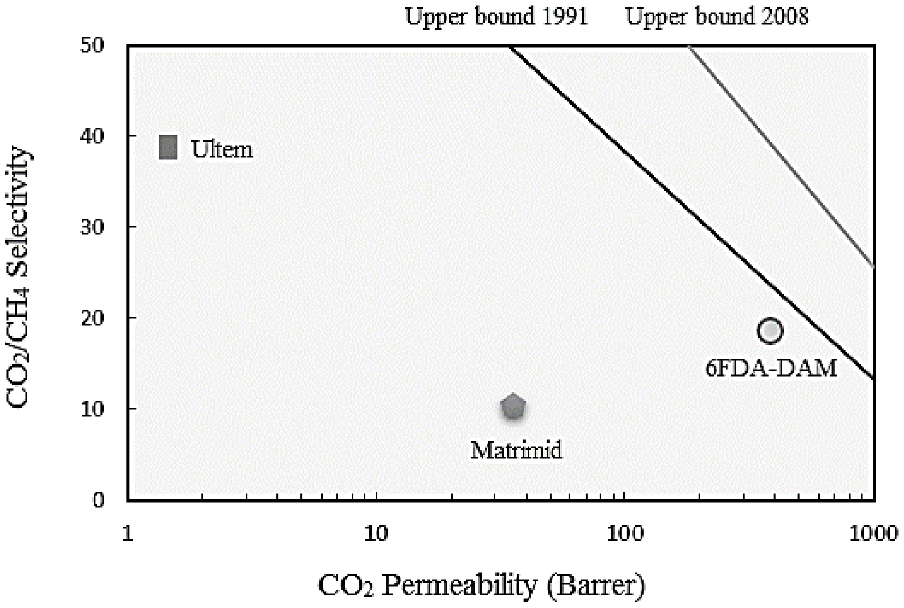

Figure 2-5: The CO_2/CH_4 separation performance of various polyimide membranes [66].

Table 2-2: CO_2/CH_4 separation performance of polymeric membranes.

Year	**Material**	**Config.**	**Pressure**	**Temp.**	**CO_2 permeance/permeability**	**Selectivity (CO_2/CH_4)**	**Test type (CO_2 Vol.%)**	**Ref.**
2003	6FDA-BAPAF	FS	30	21	24.6 GPU	22.78	S	[67]
2003	6FDA-DAP	FS	30	21	38.57 GPU	77.82	S	[67]
2003	6FDA-DABA	FS	30	21	26.3 GPU	46.96	S	[67]
2002	6FDA-1,5-NDA	FS	10	35	22.6 Barrer	49.00	S	[68]
2003	6FDA-durene	FS	10	35	458 Barrer	16.1	S	[69]
2003	Matrimid® 5218	HF	34.5	35	10 Barrer	35.71	S	[70]
2004	Matrimid® 5218	FS	1.1	25	28.5 GPU	50	M	[71]
2004	Matrimid® 5218 (fluorintaed)	FS	1.1	25	18.7 GPU	93.5	M	[71]
2004	PDMS	FS	2-4	23	3800 Barrer	3.17	S	[38]
2007	Polycarbonate	FS	20	30	2 Barrer	27.2	M (40%)	[72]
1995	Polyamide	FS	2	35	11 Barrer	36.3	S	[73]
2002	6FDA-DAT	HF	7	20	59 GPU	40	M (40%)	[74]
2003	6FDA-DAT	HF	2	35	55 GPU	60	M (40%)	[75]

Table 2-2 (Contd.): CO_2/CH_4 separation performance of polymeric membranes

Year	**Material**	**Config.**	**Pressure**	**Temp.**	**CO_2 permeance/permeability**	**Selectivity (CO_2/CH_4)**	**Test type (CO_2 Vol.%)**	**Ref.**
1997	PSf	HF	5	25	80.7 GPU	40.2	S	[76]
2010	Matrimid	HF	15	20	11 GPU	67	M	[77]
2007	Cellulose Accetate	FS	8	35	2.5 GPU	20	M (50%)	[78]
2004	Matrimid/PES	FS	10	22	9.5 GPU	40	M (40%)	[79]
2016	Matrimid 5218	FS	8	25	6.46 Barrer	26.58	S	[80]
2016	Matrimid 5218 (Brominated)	FS	12	25	13.89 GPU	23.38	S	[80]
2014	PSf	FS	2	–	33.4 GPU	9.54	S	[81]
2014	PSf/PDMS	FS	2	–	12.5 GPU	4.46	S	[81]
2010	ODPA-TAPOB	FS	1	35	0.63 Barrer	98	S	[82]
2010	6FDA-TAPOB	FS	1	35	7.4 Barrer	75	S	[82]
2001	6FDA-6FmDA	FS	10	35	5.1 Barrer	63.8	S	[82]
2007	Ultem 1000	HF	7.8	35	13.8 GPU	39.6	S	[1]

Polyetherimide is another derivative of polyimide (PI) with flexible ether group introduced onto rigid and highly polar imide chain structure, in order to improve the processing and spinning ability while maintaining all other outstanding PI properties. The processing of PEI is much easier due to lower softening temperature (218˚C) relative to PI (260˚C) [29]. Moreover, due to flexible chains as compared to Matrimid and 6FDA, the chain packing is high with lower free volume available for gas molecules to pass through, the permeability of penetrating gas molecules is very low as shown in Figure 2-5. The lower free volume available discriminates gas molecules based on molecular size. As a result, despite its lower gas transport rate, the high selectivity makes PEI suitable for gas separation applications.

2.5.3 Mixed Matrix Membrane

To overcome the limitations of polymeric and inorganic membranes, mixed matrix membranes (MMMs) have emerged as one of the alternative approaches which afford enhanced gas separation performance. In this approach, the superior gas separation properties (i.e. selectivity) of inorganic molecular sieve materials are combined with the desirable permeability, mechanical properties and economical processability of polymers, to fabricate a state-of-the-art hybrid membrane [54]. In the early 1970s, Paul and Kemp started to embark on MMM research by incorporating 5A zeolite in polydimethyl siloxane (PDMS) to study the delayed diffusion time lag effect for CO_2 and CH_4 gas [83]. To date, Matrimid, Udel and Ultem are commercially available as viable polymers for incorporation of inorganic fillers in order to ameliorate gas separation properties [84-86].

Nonetheless, even though usage of polymers with high glass transition temperature coupled with inorganic fillers is expected to produce MMMs which surpass the upper bound performance, poor combination of polymer/inorganic filler as well as poor adhesion at the polymer/inorganic filler interface, among others, caused deteriorated gas separation performance [87-89]. Hence, during selection of the appropriate inorganic filler to be incorporated into the organic phase, its shape, size and interaction towards the penetrating molecules should also be considered for better membrane performance. In this regard, it is found that inorganic particles with spherical shape minimize agglomeration whereas layered structures maximize polymer-filler contact. Micro-sized fillers often required large amount of filler in the polymer matrix and result in composite bulkiness and loss of transparency; whereas desired properties are achieved at low volume fraction with nano-sized fillers [90]. Since the selection of appropriate polymer/inorganic filler combination is important in determining MMM performance, the next section reviews the feasibility of using different inorganic source.

2.6 MMM penetrated with inorganic fillers

In essence, inorganic fillers are classified as porous or non-porous in nature as depicted in Figure 2-6. The mode of gas molecules transportation through porous structure is diffusion mechanism whereas solubility selectivity is the transportation phenomenon for non-porous fillers. Inorganic fillers containing porous structure include zeolite, carbon molecular sieve (CMS) and carbon nanotube (CNT) whereas nanoclay, silica and metal-organic framework (MOF) represent non-porous structure [31, 91-94]. In past literature, MMMs containing porous fillers, which are governed by diffusion as the dominating transport mechanism, have been extensively analysed for CO_2/CH_4 application; however, less attention is paid for sorption selective systems. Non-porous fillers improve the gas separation performance of MMM by creating tortuous surfaces and decreasing diffusion of large gas molecules. Moreover, non-porous fillers disrupt polymer chain packing and increase free volume which ultimately enhance gas diffusion.

In polymer-layered silicate MMM, the mechanism for gas absorption and transportation is based on solubility. For CO_2/CH_4 gas pair, due to lower critical temperature, CO_2 is more soluble compared to CH_4. Besides that, the kinematic diameter for CO_2 (0.33 nm) is low compared to CH_4 (0.40 nm) which promotes faster diffusion. Solubility is a thermodynamic property and depends on the polarity of incident gas and polymer matrix. It is also interesting to note that polymers which contain polar groups such as ether oxygen, nitrile and acetate exhibit the highest CO_2

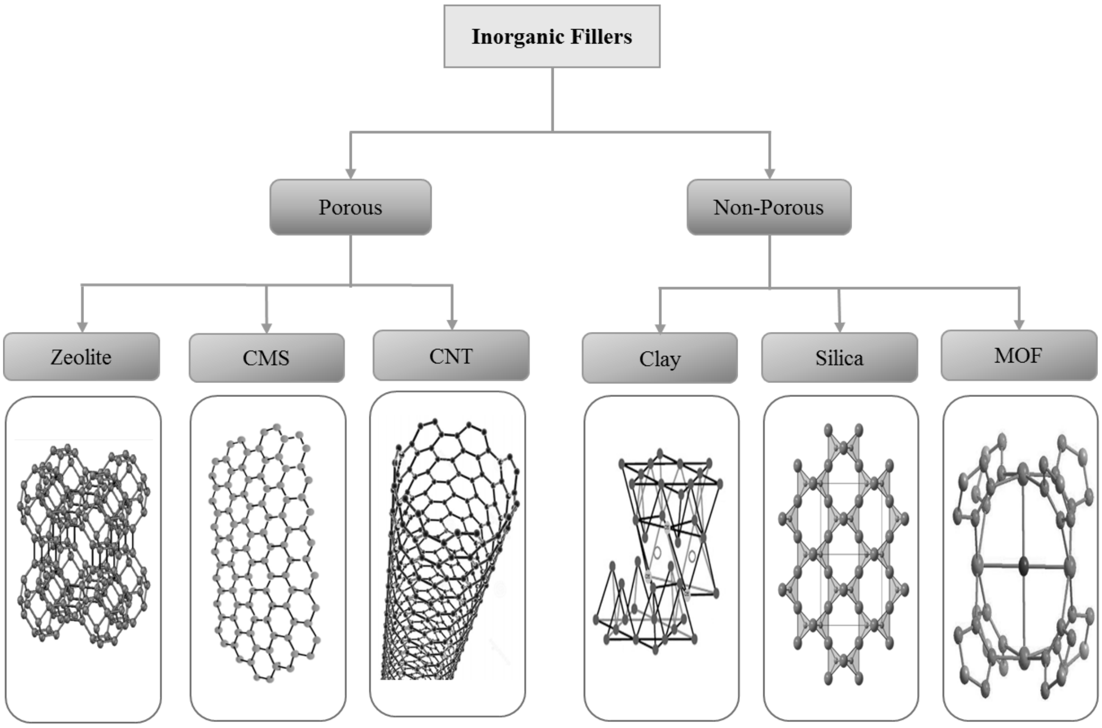

Figure 2-6: Classification of inorganic fillers [31, 91-94].

solubility selectivity. For example, when the ether oxygen concentration (polar in nature) increases from polybutadiene to poly(tetramethylene) to poly(ethylene oxide), the CO_2 solubility also increases in the same order. Apart from this, the CO_2/CH_4 solubility selectivity of polymers also improves as the concentration of carbonyl and sulfone group increases [85, 95, 96].

Table 2-3 analysed the performance of MMM incorporating filler in CO_2/CH_4 separation from the literature. Non-porous fillers Cloisite 15 A incorporated in PEI matrix showed excellent selectivity of 50 even at high pressure of 15 bar. Zeolite is one of the most widely used porous inorganic fillers incorporated in MMMs for CO_2/CH_4 separation. PSf/Matrimid hollow fibre membranes showed 50% increase in selectivity by adding zeolite to their selective skin layers [57, 70]. In comparison to neat polymers, addition of CMS to Matrimid and Ultem increases the membrane selectivity by 45% and 40% respectively for CO_2/CH_4 systems [90]. Much of this is due to the pore structure of porous fillers which provides discrimination of gas penetrants, thus improves selectivity. Non-porous fillers, however, increase the free volume, dislocate chain packing, and result in higher permeability. Poor adhesion with polymer matrix at nanofiller surface might cause void formation that could result in permeability rise.

Table 2-3: Mixed matrix membrane for CO_2/CH_4 separation.

Polymer matrix	**Inorganic filler**		**Config.**	**Pressure (bar)**	**Temp. (°C)**	**CO_2 Permeance**	**Selectivity**	**Ref.**
PSf	MCM-41 silica (0%)	Non-Porous Fillers	FS	4	35	4.5 Barrer	23	[97]
PSf	MCM-41 silica (10%)		FS	4	35	6.6 Barrer	23	[97]
PSf	MCM-41 silica (20%)		FS	4	35	7.8 Barrer	23	[97]
PSf	MCM-41 silica (40%)		FS	4	35	14.8 Barrer	15	[97]
Matrimid 9725	MOFs (0%)		FS	4	35	10 GPU	18	[98]
Matrimid 9725	$[Cu_3(BTC)_2]$ (30%)		FS	10	35	17 GPU	23	[98]
Polyurethane	Alumina (10%)		FS	10	-	88.35 Barrer	15.61	[99]
Polyurethane	Alumina (30%)		FS	10	-	74.67 Barrer	23.48	[99]
Polyetherimide	Cloisite 15 A		FS	15	25	0.93 GPU	50.00	[100]

Table 2-3 (Contd.): Mixed matrix membrane for CO_2/CH_4 separation.

Polymer matrix	**Inorganic filler**		**Config.**	**Pressure (bar)**	**Temp. (˚C)**	**CO_2 Permeance**	**Selectivity**	**Ref.**
Matrimid 9725	ZIF-8 (30%)	Porous Fillers	FS	10	35	22 GPU	20	[98]
6FDA-DAM	ZIF-90 (15%)		FS	2	25	720 Barrer	37	[66]
Matrimid 9725	MIL-53(Al) (30%)		FS	10	35	19 GPU	22	[98]
Matrimid 5218	CMS (17%)		HF	3.4	35	10.3 Barrer	44.78	[101]
Matrimid 5218	CMS (33%)		HF	3.4	35	11.5 Barrer	47.92	[101]
Ultem 1000	Grignard treated zeolites (13.5%)		HF	7.8	35	6.8 GPU	46.9	[1]
PEI	SAPO-34 (5%)		FS	2	30	1.3 Barrer	60	[102]
Matrimid	ZIF-8 (30%)		FS	4	22	21.35 Barrer	29.3	[103]

By the addition of hydrated silica (non-porous inorganic filler) to poly-benzimidazole (PBI), a solubility rise of condensable gases is reported in literature. The presence of polar hydroxyl groups (-OH) in polymer matrix plays a vital role towards solubility increase.

Unlike solution diffusion mechanism for gas transportation of hybrid membranes, in neat PBI membranes, diffusion permeation mechanism is responsible for gas transportation; thus decreased permeation of non-condensable gases is observed leading to gas separation in the presence of silica particles [38]. Nanoclay is another type of non-porous inorganic filler used extensively in the polymer composite industry, which exhibits good potential to be incorporated in MMM for gas separation systems. According to literature, very low clay loadings (i.e. ≤10 mass% clay) have resulted in enhanced thermal, mechanical, optical, electrical, and barrier properties specifically for large kinematic diameter gas molecules [104, 105].

2.7 Layered silicate

Layered silicates are naturally occurring or synthetically made minerals, and consist of very thin layers which are bonded to each other by counterions. The basic building block of layered silicates consists of two core individual sheets; tetrahedral sheet in which silicon is surrounded by four oxygen atoms, and octahedral sheet composed of aluminium surrounded by eight oxygen atoms [106]. Different combinations and arrangements of these tetrahedral and octahedral sheets form different kinds of molecular structure. For instance, in 1:1 layered structure, a tetrahedral sheet is fused with an octahedral sheet and oxygen atoms are shared. In 2:1 layered structure, an octahedral sheet is sandwiched between two tetrahedral sheets [33]. Figure 2-7 shows the crystal lattice of 2:1 phyllosilicates. It consists of two dimensional layers where a central octahedral sheet of alumina is fused to two external silica tetrahedral sheets with shared apical oxygen atoms. Each layer is approximately 1 nm thick and lateral dimensions vary from 300 Å to several microns. The aspect ratio is usually greater than 1000 [34, 107]. Although layered silicates have achieved considerable commercial success as nanocomposites, their application in mixed matrix membranes are still in infancy stage and several fundamental issues (i.e. polymer-filler compatibility,

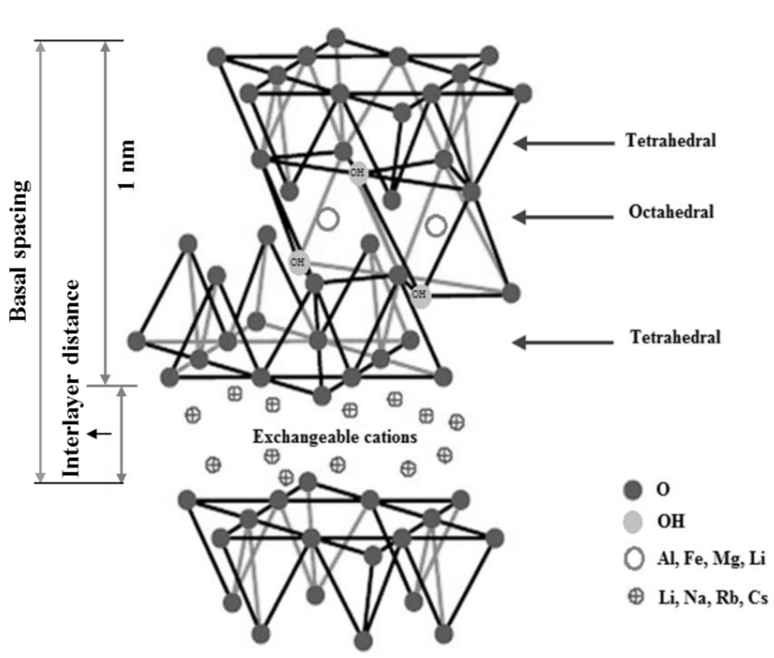

Figure 2-7: Structure of 2:1 phyllosilicate [106].

dispersion etc.) need to be addressed. Often, surface modification is performed to improve compatibility between layered silicates and the polymer matrix when synthesizing mixed matrix membranes. Various clay minerals are naturally occurring such as clay minerals, AMH-3 and MCM-22. Several other synthetically modified layered silicates have been used, such as Laponite, UZAR-S1, NU-6 and ITQ-2 [108-110].

2.7.1 Amherst-3

Amherst-3 (AMH-3) comprises layered silicate structure with strontium cations, sodium cations and water molecules between the layers. It has pores in 3-D planes with 8-membered rings (8MRs) and pore size of 3.4 Å [111]. Figure 2-8 depicts the AMH-3 structure, in which each layer is formed by bonding two silicate sheets containing 4MRs and 8MRs. AMH-3 possesses micropores in both parallel and perpendicular direction, promising state-of-the-art properties. In a recent study, AMH-3 is used for fabrication of MMMs for gas separation applications to enhance permselectivity due to its unique 3-D microstructure [112]. In polymer matrix, the microporosity of AMH-3

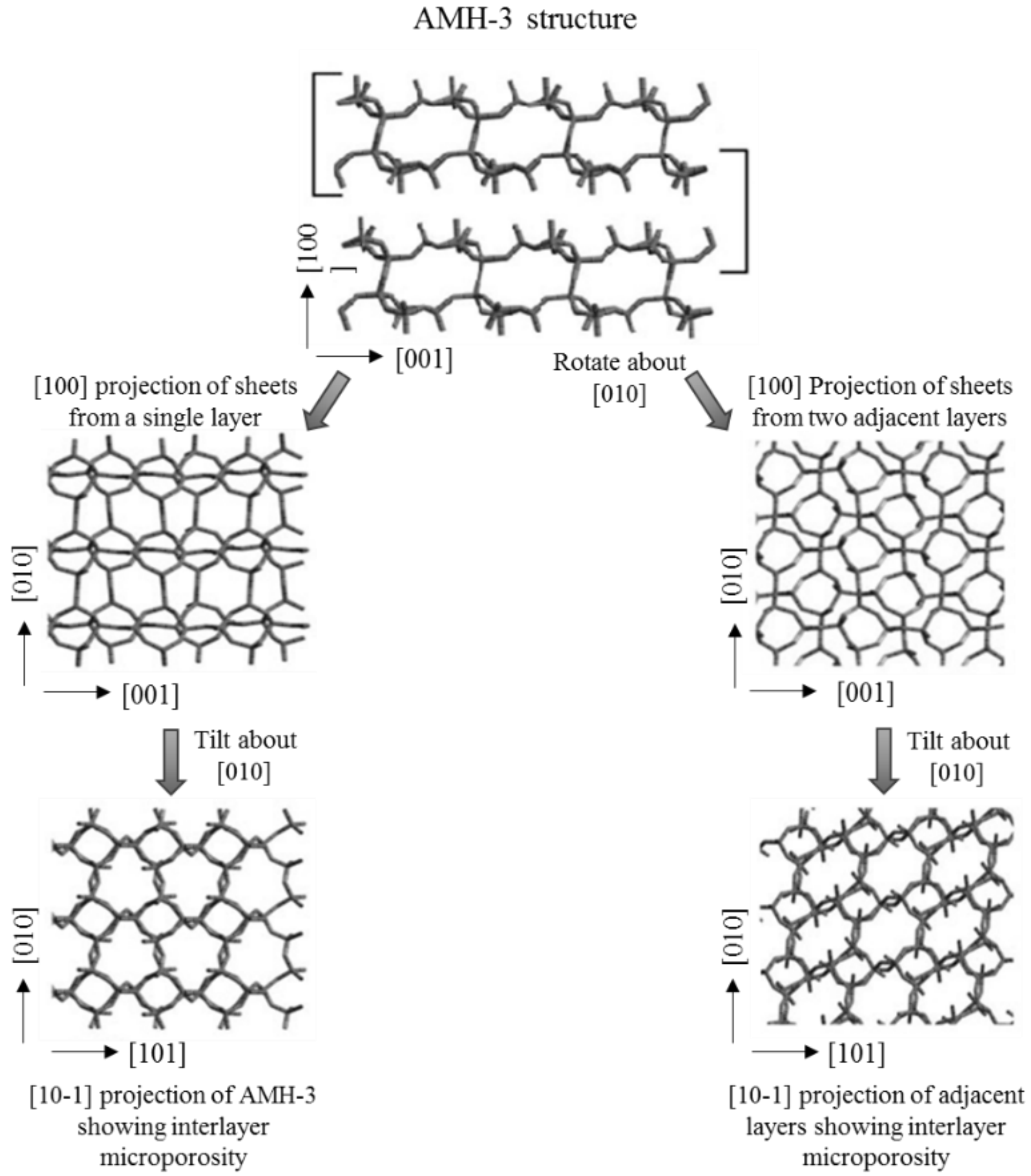

Figure 2-8: Projections of the AMH-3 structure. Top left: Projection of a single AMH-3 layer down [100]. Bottom left: Projection of the same layer along [101] showing 8MRs in the layer. Top right: Projection down [100] of two sheets from adjacent layers. Bottom right: Projection of the same down [10-1] showing an interlayer transport path through 8MRs. Red = Si, Blue = O [111].

enhanced exfoliation in polymer matrix, reduced permeation of larger gas molecules by creating tortuous path and as a result, high selectivity is achieved. Recently, it has been found that swelled AMH-3 with larger interlayer distance shows better gas separation properties than intercalated phase. Nevertheless, the presence of silanol groups on AMH-3 surface and the existence of charge balancing cations between the inter gallery spaces hinder AMH-3 swelling. In a study, Choi introduced an innovative method, i.e. by sequential intercalation of dodecyl amine after proton exchange in the presence of amino acid, for the swelling of AMH-3 because the routine methods used for swelling of clays are not applicable for AMH-3 due to its strong interlayer bonding [113]. Also, conventional methods of dispersion and sonication do not guarantee exfoliation of AMH-3 in polymer matrix. Hence, shear stress and viscosity of polymer should be sufficiently high in order to achieve high degree of exfoliation [114].

2.7.2 MCM-22

MCM-22 which consists of 2-D aluminosilicate layered structure has found a variety of applications due to its versatile framework [115]. MCM-22 contains two independent porous systems; a sinusoidal and bidirectional channel with internal diameter of 0.52 nm and other supercavities with 0.71 nm internal diameter. Both porous systems are accessible through 10MR windows [116]. Figure 2-9 represents the schematic structure of MCM-22, highlighting the two independent porous systems. Kim et al. reported on functionalization of the layer surfaces of MCM-22 with hydrocarbon chain to increase hydrophobicity, as well as perform interlayer swelling [117]. It is also found that amine functionalised MCM-22 has promising features in CO_2 adsorption [118]. Thus, these

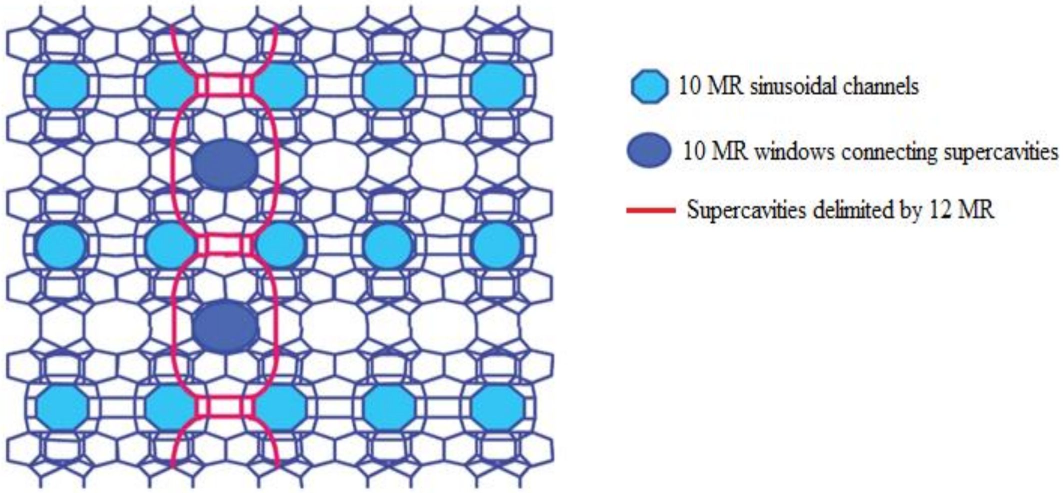

Figure 2-9: Graphical representation of MCM-22 [116].

characteristics made evident the potential of using MCM-22 as fillers in CO_2/CH_4 gas separation membranes [119].

2.7.3 Clay Minerals

Clay minerals are layered silicates which belong to the phyllosilicate subclass and can be characterized based on their fine grained natural structure with sheet-like geometry. They exist in nature as tactoids with hundreds to thousands of silicate layers. Individual natural clay particles are generally smaller than 0.004 mm in diameter [120]. Clay minerals are further classified into subgroups such as smectite, illite, kaolinite, chlorite or sepiolite. Montmorillonite (MMT), a member of the smectite family, has been extensively used as reinforcing filler in the automotive industry since the 1990s. Toyota Research group emerged as the pioneer in this regard, successfully commercializing nylon-6-MMT nanocomposite [121]. According to their findings, with a small addition of MMT (4.2 wt.%), the modulus and tensile strength increased by 50%. Since then, researchers have thoroughly investigated MMT application in thermoplastic nanocomposites due to their superior mechanical, barrier, thermal, flame retardant and abrasive properties [122-124].

The presence of charge in the tetrahedral and octahedral sheets influences the layered structure of clay minerals. The electronegative nature of the silicate layers attracts the exchangeable cations (like Li^+, Na^+, Rb^+, and Cs^+) in interlayer gallery spacing [125, 126]. The replacement of an element with another element in mineral crystal without modifying its chemical structure is called isomorphous substitution and mainly results in charge development. For example, Al^{+3} can replace Si^{+4} in tetrahedral coordination, and replacement of Al^{+3} is possible by Mg^{+2}, Fe^{+2}, and Fe^{+3} in octahedral coordination [33]. In MMT, divalent Mg^{+2} replaces Al^{+3} and this creates surface charge disturbance which is balanced by Na^{+1}or Ca^{+2} ions. The interlayer spacing varies according to the size of the ions. Since these ions have affinity for polar groups, water and other polar solvents can easily migrate inside the layer and cause it to expand [127]. This causes MMT to possess high cationic exchange capacity, thus is a promising inorganic filler for MMM development [128].

Table 2-4: Transport properties of various layered silicates in polymer matrix for CO_2/CH_4 separation.

Polymer	**Nanofiller**	**Pressure (bar)**	**Temp. (˚C)**	**Polymer Permeability**	**MMM Permeability**	**Selectivity of Polymer**	**Selectivity of MMM**	**Ref.**
PEI	Cloisite15A (0.5%)	15	25	0.63 barrer	0.78 barrer	79.6	101.89	[100]
PSf	Cloisite15A (1%)	5	25	4.97 barrer	18.72 barrer	23.12	20.98	[106]
PEI	HNT (0.5%)	15	25	0.63 barrer	0.80 barrer	79.6	85.97	[129]
PDMS	Sepiolite (20%)	13.8	-	-	-	5.75	14.03	[130]
PDMS	TMA-MMT (15%)	13.8	-	-	-	5.75	10.98	[130]
PBMA	Modified cloisite 15A (5%)	4	25	56.3 barrer	24.6 barrer	9.4	10.25	[131]
PES	MMT-Na (2%)	2	25	1.97 barrer	7.15 barrer	24.5	9.8	[132]
CA	AMH-3 (6%)			7.55 barrer	11.59 barrer	29.61	29.71	[133]
PES	Cloisite 15A (0.25 %) Coated with PDMS	3	25	2.70 barrer	9.77 barrer	28.38	33.49	[134]
PSF	C 5A (0.05%)	5	25	19.88 GPU	5.48 GPU	23.12	14.81	[135]
PSF	C 15A (0.05 %)	5	25	19.88 GPU	4.53 GPU	23.12	52.67	[135]
PSF	C 30B (0.05 %)	5	25	19.88 GPU	4.02 GPU	23.12	36.55	[135]

Table 2-4 summarizes the performance of clay as inorganic filler in MMM for CO_2/CH_4 separation. It is evident that the selectivity of MMM increases in comparison to nascent polymer membranes except for PES-MMT-Na (2 wt. %) and PSF/C 5A (0.05 wt. %) MMM which is due to interfacial defects and are discussed in section 2.9.

Along with MMT, bentonite, hectorite, saponite and laponite are clays that are used as reinforcing fillers in polymer composite industry [136]. These clay fillers play an important role in the polymer nanocomposite industry due to their economic viability, availability, flame retardancy and reinforcement characteristics. The interlayer space or "gallery", intercalation ability and exfoliation of these layered clays enhanced their attractiveness as a component in polymer nanocomposites [122, 137].

2.7.4 Surface modification of clay platelets

The hydrophilic nature of layered silicate makes it poorly suited to mixing and interacting with most polymer matrices. Moreover, the stacks of clay platelets are held together by electrostatic forces, whereby the counterions can be shared by two neighbouring platelets, resulting in stacks of platelets that are held tightly together. Nanocomposites employing untreated clay would not demonstrate much effectiveness, because most of the clay would form aggregates, involving very limited interaction between the matrix and the individual platelets. A popular and relatively easy method of modifying the clay surface, to render it more compatible with an organic matrix, involves exchange of inorganic cations (Na^+ or Ca^{+2}). As can be seen in Figure 2-10, the inorganic cations are not strongly bound to the clay surface; thus organic cations can replace them in the clay. For example, if sodium ions are replaced by quaternary ammonium ions (R_4N^+) with long alkyl chains, the clay would be more compatible with an organic matrix. This is due to the fact that the length of the alkyl chain imparts hydrophobicity in MMT. Therefore, by treating it with various organic cations, MMT clay can be compatibilized with a wide variety of matrix polymers [138].

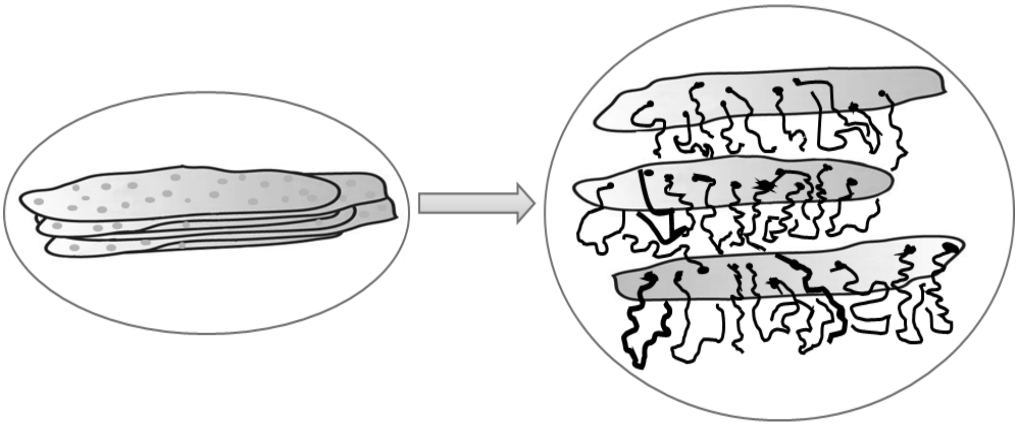

Figure 2-10: Schematic picture of ion exchange reaction. The relatively small inorganic ions (i.e. Na^{+1}) are exchanged by more voluminous organic onium cations [127].

Generally, two types of chemical modification (non-covalent or covalent) can be performed on layered silicates. Non-covalent modification involves intercalation modification without covalent bonding through hydrogen bonding, Van der Waals interaction, dipole-dipole interactions and acid base reactions. On the other hand, covalent bonding occurs through silylation, condensation and esterification of $SiOH/SiO_2$ groups. The bonding forces involved in non-covalent modifications provide weaker interactions than covalent modifications. Besides that, organic cations provide functional groups that can interact or initiate polymerization of monomers to improve the strength of interface adhesion between the inorganic component and polymer phase. Thus, covalent modification not only increases the filler distribution but improves the MMM performance as well. Figure 2-11 summarizes the covalent and non-covalent modification of layered silicates with their possible applications [120, 139]. Defontaine et al has reported a considerable increase in membrane selectivity for CO_2/CH_4, by incorporating sepiolite and tetramethylammonium intercalated montmorillonite (TMA-MMT) nanoclays in polydimethylsiloxane (PDMS) matrix [140]. A covalent bond was formed between the nanoclay surface and polymer chains by the silanol group. Addition of sepiolite nanofiller in PDMS matrix resulted in an increase of 144% in CO_2/CH_4 selectivity, due to the Si-O-Si bonding which occurred between the polymer chain and silicate layers due to the abundance of silanol groups present at the external surfaces. Whereas for TMA-MMT/PDMS MMMs, a 91% increase in CO_2/CH_4 selectivity was achieved because of the lower density of edged silanol groups in MMT.

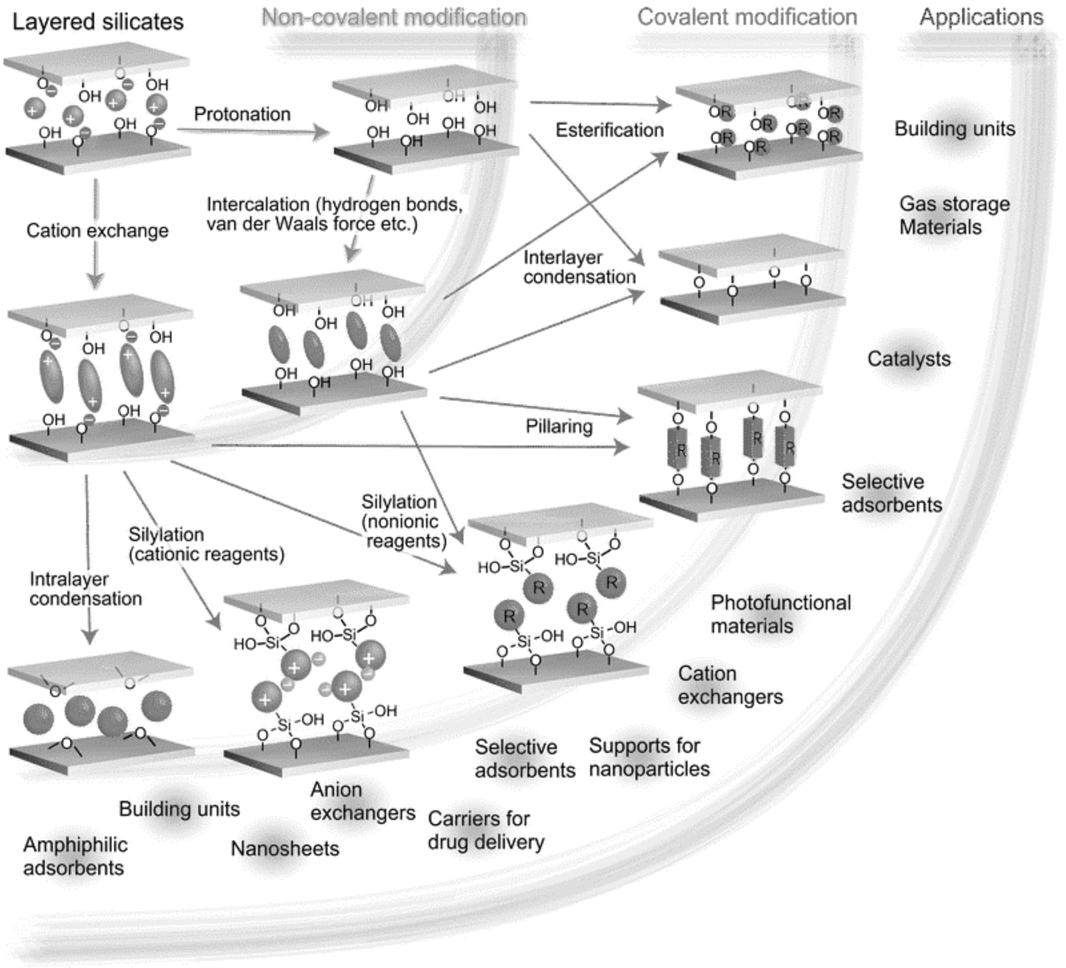

Figure 2-11: Types of modifications for layered silicates and their potential applications area [139].

Along with covalent and non-covalent approach, ion exchange is a relatively rapid method to achieve organophilicity of clay. For ion exchange method, the interlayer ability to swell plays an important role. If alkali is present between the layers of clay, swelling is possible because divalent or trivalent atoms hinder the water molecules from penetrating the layers and inhibit the swelling process. The swelling flakes increase the selectivity for small molecules by creating higher tortuous path for larger molecules. The common types of alkali cations used are sodium based alkali cations such as octosilicate ($Na_8[Si_{32}O_{64}(OH)_8].32H_2O$ also known as ilerite or RUB-18, α-Na_2 Si_2O_5, and β-$Na_2Si_2O_5$, as well as non-sodium based alkali cations such as $KHSi_2O_5$, $LiNaSi_2O_5.2H_2O$ (silinaite). The alkali cations present between the clay layers provide the opportunity for organic cations and surfactants to replace them. Furthermore, the presence of interlayer organic cations decreases the surface energy, thus, interaction between polymer and modified clay improved significantly. The long chained surfactants tethered at the surface of clay resulted in increased gallery space. This will attract polymer chains to diffuse into the gallery space and improve interaction towards polymer matrix. Ultimately, the compatibility of filler towards polymer is also tremendously improved [117]. Figure 2-10 shows the ion exchange reaction of layered silicate, in which Na^+ ion is replaced by voluminous onium ion. After surface modification of layered silicate with surfactant molecules, the interlayer distance increased.

Alonso and co-workers modified naturally occurring MMT through ion exchange method with [2-(acryloyloxy)ethyl]-trimethylammonium which creates tethered reactive groups on the surface of the silicate layer [141]. The modified MMT and poly(*n*-butylmethacrylate) are subsequently emulsion-polymerised to form nanocomposite membrane. The tethered groups on the MMT surface were found to react with the acrylate monomers and exfoliate the silicate layers. Due to exfoliation, tortuous path increases for the permeating gas, and as a result, reduction in permeance is observed, in spite of the increase in selectivity. This trend holds true for increasing filler loading. With 1 to 5wt.% filler loading, the selectivity increased by approximately 37% whereas CO_2 permeability decreased by 31% [142]. In another study, Alonso used similar modified MMT in poly(*n*-butylacrylate) to produce nanocompsite membrane through *in situ* polymerization, which leads to exfoliated clay morphology within the polymer matrix. It was also found that with increasing modified MMT loading, the permeance reduction of CO_2 was approximately 56% whereas 9.3% enhancement in selectivity was achieved.

Cation-exchange capacity (CEC) represents the extent of negative charge on the surface of MMT and its ability to exchange ions. CEC is dependent on the isomorphous substitution in tetrahedral or octahedral layers of MMT. The CEC for MMT varies from 0.9–1.2mequiv./g depending on the mineral origin. For non-polar polymers, quaternary alkyl having long alkyl chains is preferentially used; whereas quaternary ammonium containing hydroxyl groups are considered to be suitable for polar polymer matrices [143]. Various types of MMT clay have been produced by changing the intercalated cations, each with its unique characteristic based on the interlayer distance. Table 2-5 summarizes some industrially available modified MMT and their interlayer distances.

Table 2-5: Types of commercially available montmorillonite and their properties.

Filler	**Interlayer cations**	**Interlayer distance (Å)**
Cloisite Na	Na^+	12.1
Cloisite 10A	$(CH_3)_2N^+CH_2(C_6H_6)$(Hydrogenated Tallow)	19.2
Cloisite 20A	$(CH_3)_2N^+$(Hydrogenated Tallow)$_2$	22.1
Cloisite 25A	$(CH_3)_2N^+$(Hydrogenated Tallow)(2-ethylhexyl)	20.7
Cloisite 30B	$(CH_3)_2N^+$(Tallow)$(CH_2CH_2OH)_2$	18.5
Nanomer 1.28E	$CH_3N^+(CH_2)_{17}CH_3$	24.0-26.0
Nanomer 1.30E	$H_3N^+(CH_2)_{17}CH_3$	18.0-22.0
Nanomer 1.31PS	$H_3N^+(CH_2)_{17}CH_3,H_3N^+(CH_2)_3Si(OC_2H_5)_3$	18.0-22.0
Nanomer 1.34TCN	$CH_3N^+(C_2H_4OH)_2$(Hydrogenated Tallow)	18.0-22.0
Nanomer 1.44P	$CH_3(CH_2)_{17}N^+(CH_3)2(CH_2)_{17}CH_3$	24.0-26.0
Nanofil 757	Na^+	12.2
Nanofil 15	$(CH_3)_2N^+$(Hydrogenated Tallow)$_2$	29.0
Nanofil 919	$(CH_3)_2N^+$(Tallow)$(CH_2C_6H_5)$	18.8
Nanofil 804	CH_3N^+(Tallow)$(OH)_2$	18.0

2.8 Morphology of polymer-clay MMM

In fabricating enhanced performance MMMs for gas separation, material selection remains the most crucial factor. In MMMs, polymer phase enhances permeation whereas dispersed fillers assist in improving selectivity. When layered silicates are incorporated, three different types of morphological changes may take place; dispersion, phase separated and intercalated or exfoliated, as shown in Figure 2-12 [94]. These morphologies offer significant improvement in terms of mechanical, thermal and barrier properties of polymer-nanoclay hybrid materials [34, 126].

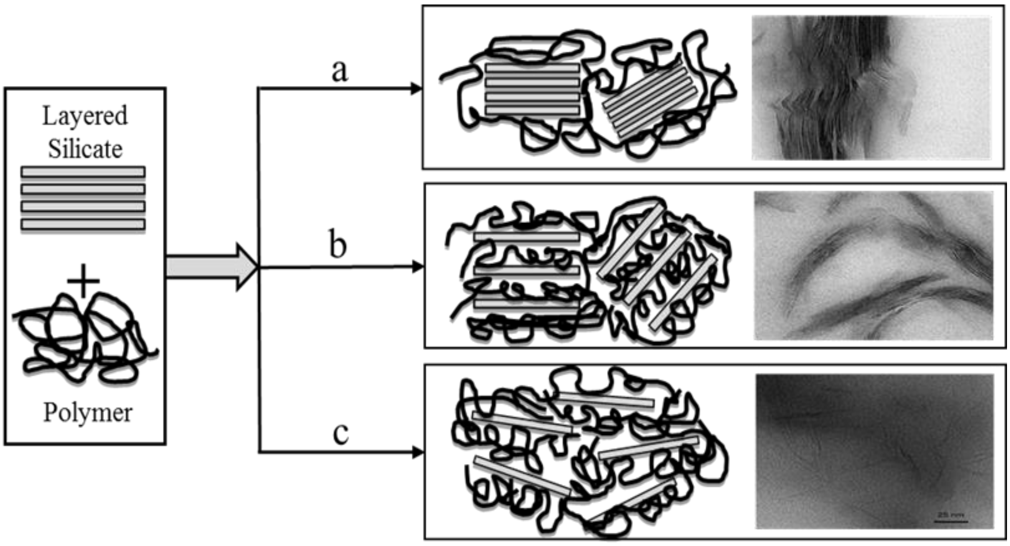

Figure 2-12: Schematic diagrams and TEM micrographs of layered silicates and polymer interfacial morphology showing a) Phase separated, b) Intercalated, and c) Exfoliated morphology [134].

Principally, layered silicate affects the sorption of condensable gas by diffusion pathways obstruction and reduction of free volume in polymer systems [94, 144-146]. The exfoliated morphology creates a tortuous path for penetrating gas molecules, as a result, permeance decreases at the expense of improved selectivity. Intercalation gives enhanced permeation but the risk of surface defects and void formation remains high due to lower filler distribution. Figure 2-13 shows the scheme of tortuous path induced by exfoliated clay layers in polymer matrix.

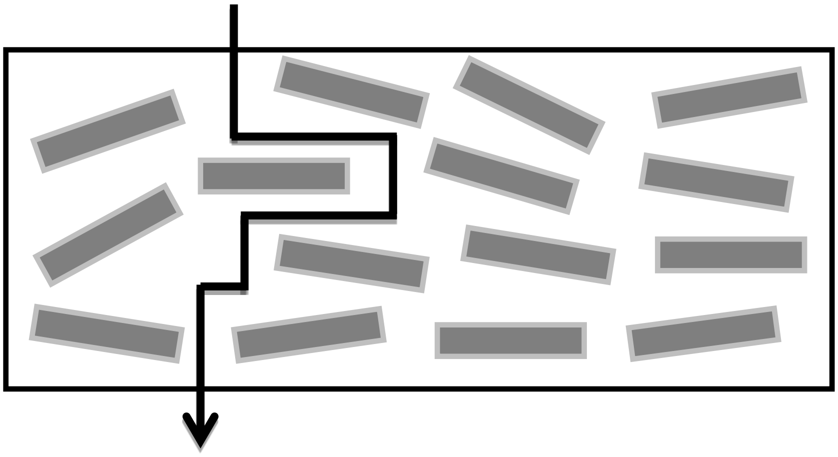

Figure 2-13: Schematic diagram of tortuous path induced by exfoliated structure in polymer matrix.

The interface morphology between polymer and filler is also crucial in defect-free membrane development. The interface interaction actually decides the selective passage of one gas over the other, thus affecting the permeability and selectivity of gas molecules. Poor interaction leads to non-ideal morphologies as shown in Figure 2-14. These include (a) sieve-in-a-cage, (b) chain rigidification, (c) leaky interface, and (d) plugged interface. If polymer-filler adhesions are weak, interfacial voids will be formed at the polymer-filler interface, also known as "sieve-in-a-cage" morphology. These voids caused non-selective passage of the gas molecules, resulting in much higher permeability than the neat polymer, whereas selectivity may vary depending on the void size. When these interfacial voids become large enough that gas molecules pass through without any resistance, the structure is known as "leaky interface", which results in increased permeability but decreased selectivity. In "chain rigidification", polymer chains are rigidified at the polymer-filler interface. This inhibits polymer chain mobilization at the interface, which lowers permeability as well as selectivity. Chain rigidification also causes pore blockage. Immobilized polymer chains may block the pores of the filler, resulting in "plugged fillers". All these defects in interface morphology seriously affect membrane performance. For this reason, various techniques are developed to reduce non-idealities in morphology such as priming

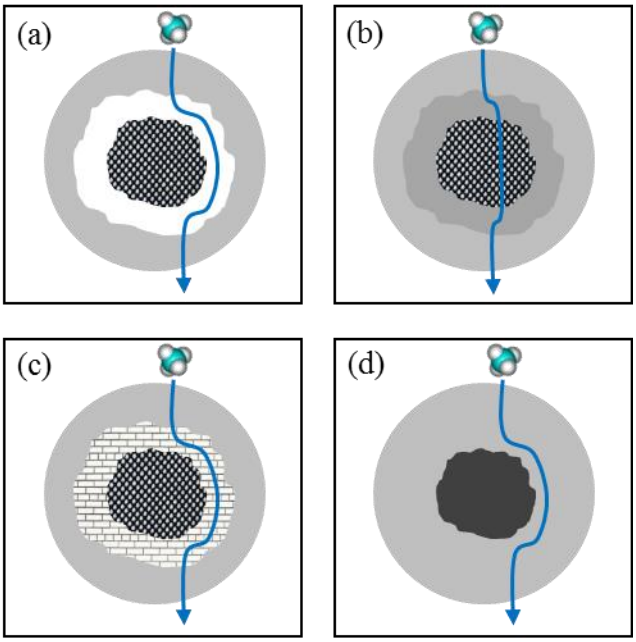

Figure 2-14: Non ideal polymer-filler morphology and transportation of gas [114].

protocol, selection of glassy polymers above T_g, grafting, use of silane coupling agents and cross-linking techniques [94, 95, 114].

During membrane formation, the selection of solvent plays a vital role on membrane morphology. Whilst selecting the appropriate solvent, the interaction of solvent towards polymer and filler should be carefully considered. There should be strong polymer-filler interaction, fair polymer-solvent interaction and weak filler-solvent interaction. If polymer-solvent interaction is too strong, the polymer chains do not approach close to the filler surface. Conversely, if filler-solvent interaction is too strong, it will be difficult for the solvent to desorb from the filler surface when the polymer chains approach the filler. Consequently, the order of interaction should be polymer/filler followed by polymer/solvent and filler/solvent [114].

2.9 Challenges and issues in successful MMM formation

Various challenges are faced by researchers in successful membrane formation. This section presents the problems and proposed solutions associated with successful membrane development.

2.9.1 Clay dispersion in organic phase

Dispersion of nano-sized inorganic particles in polymer matrix is the foremost challenge in MMM development. Generally, nanofillers disperse poorly in the polymer matrix, thus are likely to agglomerate in the MMM [147]. This tends to lead to the formation of numerous stress concentrated points which can deteriorate the mechanical stability of MMM, especially at high inorganic filler concentrations. In order to promote dispersion, surface priming protocol can be employed. In priming, a small amount of polymer is added to the nanofiller solution in order to decrease the interfacial stress between the polymer and nanofiller. This protocol is usually performed before the addition of bulk polymers to the nanofiller suspension. Hashemifard demonstrated an interesting technique of modifying halloysite nanotubes (HNT), a type of clay family to improve the dispersion properties in polymer matrix. In his work, the modification of HNT was performed with N-β-(aminoethyl)-γ-aminopropyltrimethoxysilane (AEAPTMS) and incorporated in PEI matrix to analyse the adhesion and distribution [75]. Initially, the selectivity for HNT/PEI MMM decreased but the optimization of priming protocol and sonication extended the selectivity and dispersion of HNT platelets. His work also demonstrated that increased concentration of silane molecules leads to higher degree of tortuosity and ultimately higher selectivity. Moreover, the presence of amine group in AEAPTMS/HNT/PEI MMM is also effectual in terms of CO_2 adsorption and improving CO_2 permeability and selectivity through membrane. The optimum results achieved with 0.5 wt.% of silylated HNT showed an increase of 28 % and 7% in permeance and selectivity, respectively as compared to pristine PEI membrane.

2.9.2 Void formation at the filler surface

Poor interaction of polymer chains and filler surface causes the formation of interfacial voids and results in poor membrane performance in terms of gas separation. To eliminate defects at the bulk polymer and dispersed filler interface, priming protocol and silane coupling treatment have been proposed and reported in literature [57]. Silane coupling agents are effective in eliminating the interfacial voids by creating chemical linkages between the filler phase and organic matrix. They can react with hydroxyl groups, amino groups and other functional groups from layered silicates and/or the polymer matrix to enhance the compatibility between the phase boundaries [57].

Hashemifard et al has reported a considerable increase in membrane selectivity for CO_2/CH_4, by incorporating raw and commercially modified MMT such as Cloisite 15A, in polyetherimide (PEI) matrix [67]. According to the study, Cloisite 15A provides better adhesion towards PEI matrix due to the presence of dimethyl dehydrogenated tallow quaternary ammonium in the layered structure, which enhances MMM separation properties by minimizing void formation. Cloisite 15A not only improved adhesion due to the presence of tallow interlayer gallery, its higher aspect ratio also favored the degree of tortousity in the dense skin layer of MMM. As a result, a selectivity increase of 28% is observed as compared to pristine polymer as shown in Figure 2-15. However, increasing the Cloisite 15A loading beyond the critical value

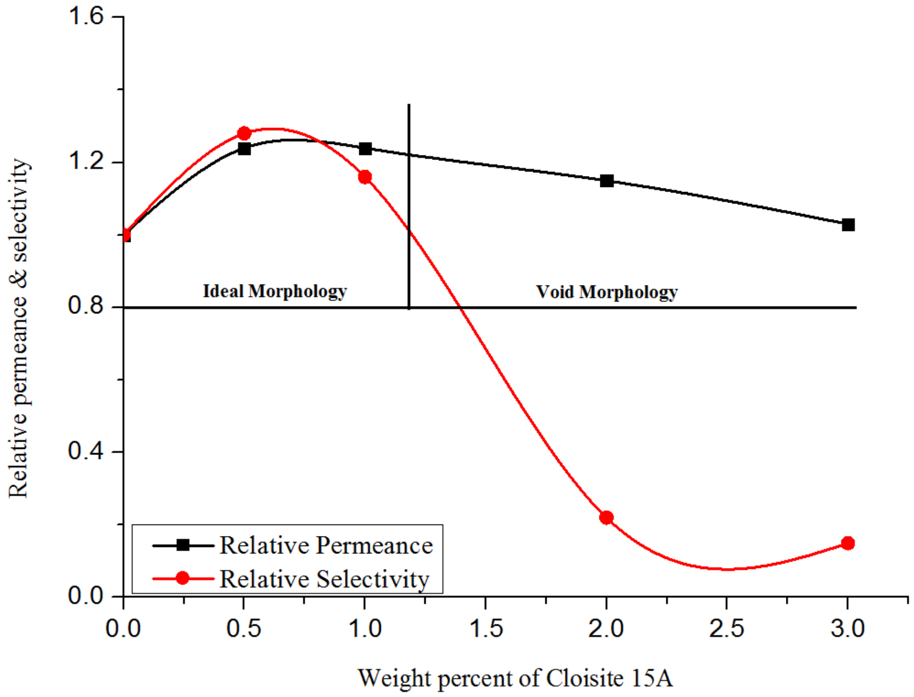

Figure 2-15: Effect of Cloisite 15A loading on PEI/Cloisite 15A MMM CO_2 permeance and CO_2/CH_4 selectivity [67].

resulted in agglomeration and void formation. The optimum membrane selectivity performance is observed at 0.5% Cloisite 15A loading in PEI matrix.

Liang and co-workers also conducted a study on polyethersulfone (PES)-based MMM with incorporation of Na-MMT as the inorganic filler [148]. The interlayer distance of MMT was found to increase with increasing filler loading, which suggested that polymer chains are intercalated in the gallery space. Nevertheless, at high filler loading, Na-MMT was found to agglomerate. This phenomenon is evident as the permeability for CO_2 increased with Na-MMT loading but beyond 10 wt. %, CO_2/CH_4 selectivity was greatly reduced. The authors speculate that the presence of interfacial voids leads to the decrease in membrane selectivity since gas transport occurs via Knudsen diffusion.

2.9.3 Distribution morphology of clay platelets

Distribution of layered silicates in polymer matrix is the most important parameter in order to control membrane performance. Intercalated morphology leads to better permeation whereas exfoliated morphology favours selectivity by controlling the permeation of large sized molecules. By using polysulfone (PSf) as polymer matrix and Cloisite 15A as filler, an asymmetric MMM was synthesized by Zulhairun which showed that at low Cloisite 15A loadings, there was a 270% enhancement in CO_2 permeability compared to neat PSf; without affecting CO_2/CH_4 selectivity [126]. The results were contrary to the concept that incorporation of clay filler caused permeability decrease. This may be largely dependent on how the clay minerals were dispersed in polymer matrix; whether they were non-intercalated or phase-separated clay tactoids which might increase permeance. The authors have further speculated that unexfoliated clay layers may generate high degree of perturbation in polymer chains packing, causing an increased permeance. Figure 2-16 showed the distribution morphology of Cloisite 15A in PSf matrix, in which void morphology can be observed around filler particle at 2 wt.% loading. Thus, nanometer gaps around inorganic phase causing possible Knudsen diffusion through clay galleries and polymer-clay interface might also affect permeability. By increasing path length across MMM for large diffusion gases by capitalizing on the barrier properties of inorganic filler, the selectivity of small condensable gas could be increased among the gas mixture.

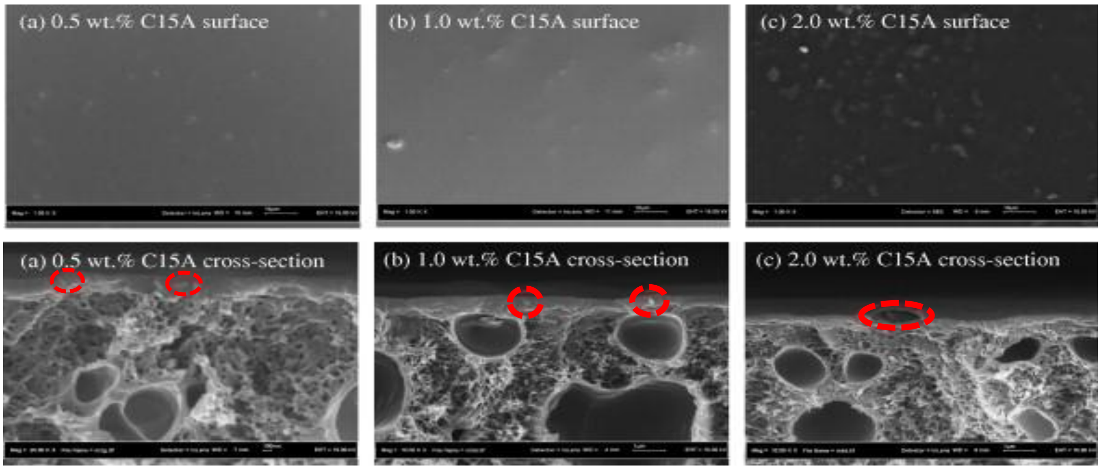

Figure 2-16: FESEM images of the surface and cross-section morphology of PSf MMMs containing (a) 0.5 wt.% C15A, (b) 1.0 wt.% C15A, and (c) 2.0 wt.% C15A [126].

Nanocomposites of poly(ε-caprolactone) containing Na-MMT and Cloisite 30B were prepared by melt blending and *in situ* polymerization, and their gas barrier properties were analysed by Gain and co-workers [149]. According to their study, along with clay platelets distribution in polymer matrix, the processing technique and the interaction of polymer chains towards clay surface are factors that affect the nanocomposite morphology. The intercalated spacing of Na-MMT and Cloisite 30B were 13.1Å and 18.5Å, respectively in the polymer matrix. Among others, melt processing and *in situ* polymerization are the most studied techniques to prepare polymer clay nanocomposite. Melt processing is an environmental friendly technique without usage of solvent whereas *in situ* intercalative polymerization involves the intercalation of monomer in gallery space of clay followed by polymerization. *In situ* polymerization leads towards intercalated or exfoliated morphology which increases the platelet dispersion and delamination. The permeability of CO_2 decreases and it is found that crystallinity of polymer remains unchanged by the presence of nanoclay. The permeability decrease is higher for composites containing Cloisite 30B prepared through *in situ* polymerization despite their higher inter gallery spacing. With the presence of hydroxyl functional groups, the grafting density increases, thus, less specific sites are available in the clay for gas sorption.

2.9.4 Polymer clay compatibility

The compatibility of layered silicate towards polymer matrix is another important aspect to be considered in mixed matrix membrane development. In order to increase polymer-filler compatibility, chemicals such as compatibilizers can be added to enhance the interaction of the polymer matrix and layered silicates. Crystalline state is impermeable in nature; thus, decreasing crystallinity of polymer phase leads to increasing permeability of penetrating gases. In previous research, highly crystalline high-density polyethylene (HDPE) and nanoclay (pristine and modified) nanocomposite films have been developed. It is observed that the crystallinity of HDPE is not affected by the addition of clay despite the permeability increase. This rise in permeability of HDPE/MMT-based nanocomposite membrane is due to the weak interaction between the polymer and filler interface. Therefore, addition of more polar maleic anhydride as compatibilizer increases intercalation, dispersion, exfoliation and tortuous path, hence decreases permeability [143].

In recent literature, copolymer-layered silicate composite membranes are reported to be used for gas separation. Goodarzi prepared polypropylene (PP)/ethyl vinyl acetate (EVA)/clay nanocomposite membrane to analyse the effect of morphology on gas permselectivity [150]. According to his research, EVA imparts better permeability properties in the polymer blend as compared to crystalline PP. The morphology and gas separation properties of nanocomposite membrane have been investigated in the presence of organically modified montmorillonite (OMMT) and compatibilizer such as polypropylene grafted maleic anhydride (PP-*g*-MA). With the addition of OMMT, the carbonyl groups of EVA and hydroxyl group of OMMT results in intercalation. On the other hand, the presence of compatibilizer helps increase the gallery space of OMMT and leads to exfoliated morphology as shown in Figure 2-17. The addition of compatibilizer changed the OMMT morphology from intercalated to exfoliated. The higher the compatibilizer (PP-*g*-MA) content in the blend, the higher the distribution of OMMT in the composite. Addition of OMMT and compatibilizer to the PP/EVA blend causes reduction in gas permeability and increase in selectivity due to the reduction in free volume fraction and increase in tortuous path. The CO_2 permeability in PP/EVA 75/25 blend decreases to 21.5 barrer when 5 wt.% OMMT is added as compared to

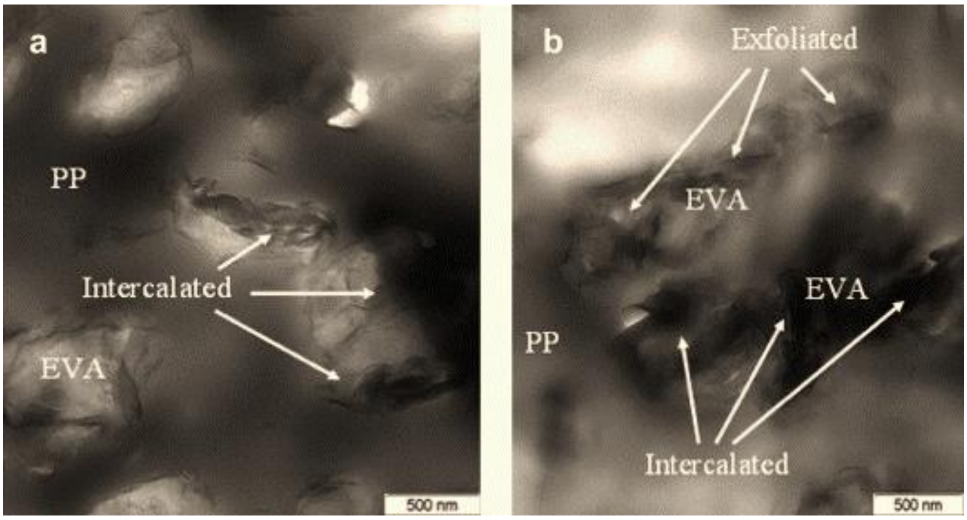

Figure 2-17: PP/EVA/OMMT composite membrane; a) without compatibilizer and b) with compatibilizer [150].

blend without OMMT (25.6 barrer). Also, a further addition of 5 wt. % compatibilizer reduced the permeability to 18.6 barrer.

Similar results were reported when organo (alkyl ammonium modified) clay was added in PP/ethylene-propylene-diene rubber (EPDM) blend by solvent blending technique. The irregular shaped EPDM exists in dispersed phase in PP matrix with 50/50 composition blend. By the addition of organo clay, the dispersed phase transformed to almost spherical shape. An antioxidant generally known as Irgan is used as compatibilizer for better dispersion of nanoclay in PP/EPDM blend. The presence of compatibilizer increases the gallery space of nanoclay, as a result, exfoliation morphology is obtained thus tortuous path increases for diffusing molecules. Despite the decrease in crystallinity of PP, the permeability of CO_2 decreases with increase in organo clay content [151]. Whilst the compatibilizer increases the compatibility of polymer and nanoclay, it also changes the morphology of polymer blend which results in higher flake aspect ratio and exfoliated geometry that help in decreasing the permeation of CO_2 gas. On top of this, by increasing the tortuous path, selectivity increases as well.

2.9.5 Polymer clay MMM surface defects

Since the surface structure of membrane is crucial in enhancing membrane performance, extensive research has been carried out with regards to this aspect. Loeb and Sourirajan are the pioneer in developing integrally-skinned asymmetric membrane dated back to the 1960s [152]. An integrally-skinned asymmetric membrane consists of two layers of the same material; a very thin and dense skin layer (0.1 to 1µm) is overlaid above a thick and highly porous sublayer (100-200 µm, void size 0.1 to 1 µm). It is the skin layer that controls the diffusion and permeation of penetrating gases whereas the sublayer only provides mechanical support. High permeability can be achieved via the active thin skin layer, thus, any defect will lead towards poor gas separation performance [153].

PVDF-hydrophilic MMT hollow fibre MMMs are commonly used in gas separation applications. PVDF is hydrophobic in nature, thus, its concentration decreases during wet phase inversion near the outer surface resulting in a very thin skin layer. This is due to the fact that during membrane casting, tap water is used as external coagulant, nevertheless, the solvent and non-solvent do not diffuse out of the PVDF solution during phase inversion due to high hydrophobicity of PVDF. A decrease in dope viscosity with increment in solvent/coagulant exchange capacity is observed in the presence of MMT, due to the weaker polymer-clay interaction which reduces the thermodynamic stability of polymer solution. Similar phenomenon is observed with the addition of sepiolite clay in chitosan and polyvinyl alcohol (PVA) by Huang et al [154]. This decrease in polymer viscosity causes morphological change and formation of finger-like pores beneath the outer surface of the membrane. As a result, pores are generated in the thin skin layers, followed by finger-like structure in the substrate which meets sponge-like structure in the middle of the membrane. With increasing MMT loading, surface porosity and finger-like structure increases whereas sponge-like zone gradually reduces which leads to permeation enhancement. The maximum increment is observed at 5wt.% MMT loading where 21% greater permeance is obtained compared to neat PVDF [155].

Another new approach which involves the incorporation of “selective flake” that possesses lower thickness and higher aspect ratio leads to improved permeability without compromising the selectivity. Kim investigated the intercalation of primary amines in porous AMH-3 with cellulose acetate (CA) by using high shear rate in order to obtain better exfoliation and higher aspect ratio [112]. The AMH-3 is also reacted with dodecylamine to induce swelling. The dodecylamine interlayer spacing is 30Å whereas in AMH-3, the interlayer spacing decreased to 20Å due to high normal forces induced by a high shear driving force mixer. Also, some of the dodecylamine molecules are extracted due to the shear force from the layers of AMH-3, leaving behind layers in close contact. The number of stacks of layer per tactoid is 3-8 for 2-6 % AMH-3. The CO_2/CH_4 gas separation performance of the AMH-3/cellulose acetate composite membrane is found to increase substantially with increasing flakes loading. The CO_2 permeability is increased by 54 % whereas selectivity remained very close to that of pure CA matrix (i.e. 29.61). Thus, one envisages the future prospect of developing nano-flakes hybrid membranes which combines the advantages of high permeability while retaining the selectivity of the matrix.

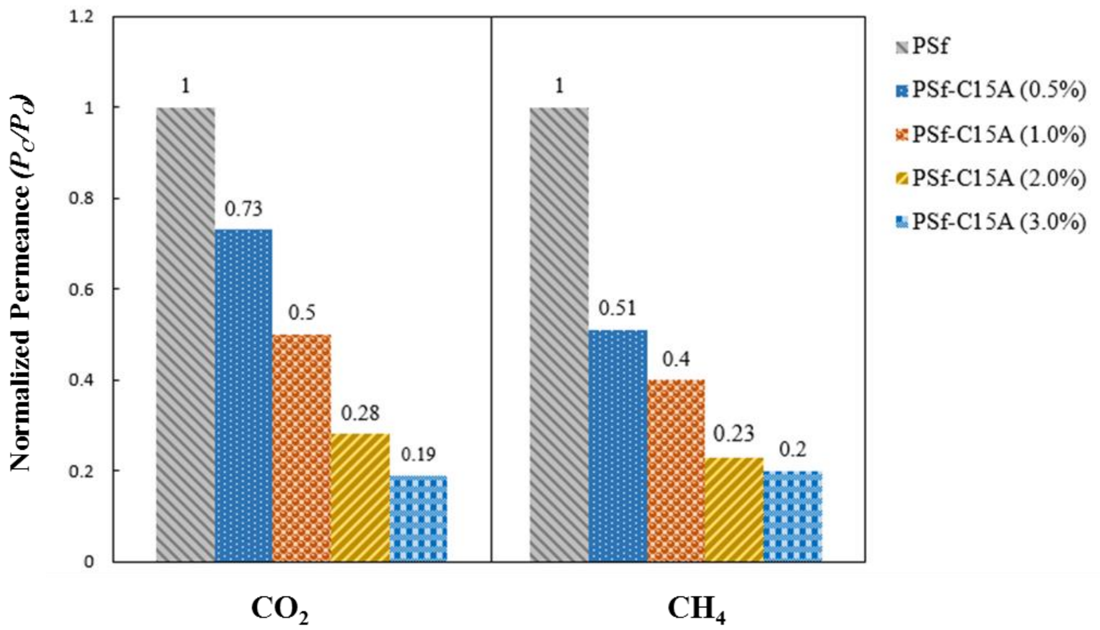

Figure 2-18: Gas permeation behavior of PSF-C15A MMM as a function of clay loading. Normalized permeance represent the MMM over pure PSF membrane [156].

Zulhairun also prepared MMMs by using high aspect ratio of filler in order to avoid high filler loading that lead towards agglomeration, membrane surface defects, non-uniform morphology and poor gas separation performance [156]. Closite 15A which is embedded in PSf is chemically modified with quaternary ammonium to render the hydrophilic surface hydrophobic along with basal space increase to 3.46Å. The initial dope solution is sonicated to disperse clay uniformly and flat sheet PSf-Closite 15A is fabricated. According to his findings, higher filler loading leads to diffusion path blockage and permeability decrease for gas molecules. By merely increasing 3 wt.% of clay loading, the permeability of PSf-clay membrane goes down by 80%, and the optimum performance is observed at 0.5 wt% filler loading as shown in Figure 2-18. The increase in clay loading leads to lower delamination or exfoliation of layers. As a result, lower inter gallery space is available for polymer molecules to intercalate, which contributes to lower distribution of clay within the polymer matrix. The number of stakes per tactoid reported to show optimal dispersion is 2 to 4. Excellent particle dispersion and interlayer void-free morphology is obtained, resulting in higher selectivity (by 144%) for CO_2/CH_4 gases.

2.9.5.1 PDMS coating of membrane surface

Generally, surface defects in the thin skin layer can be minimised by controlling the casting shear rate, evaporation time, and by coating the membrane surface with a rubbery polymer. In a study, Ismail and co-workers prepared flat sheet MMMs using PES and Cloisite 15A [157]. According to their findings, layered silicates bring about morphological changes in the polymer matrix and converted finger-like microvoids to sponge-like microvoids. At higher evaporation time, the skin layer obtained is thicker with aligned nanoparticles, as a result, the selectivity increase is significant as compared to lower evaporation time, due to tortuous path near the surface. At 0.25 wt.% Closite 15A loading, the permeability and selectivity decrease due to the development of thin skin layer with nanoparticles coagulated near the surface. However, by increasing the evaporation time, the membrane performance improved due to circulation and distribution in the skin layer. Besides that, coating the membrane surface with polydimethylsiloxane (PDMS) showed improvement in selectivity at the expense of permeability. The selectivity rise for coated membrane is approximately 227 % as compared to uncoated membrane at the same evaporation time.

On top of that, PES is extensively used for gas separation applications. Madaeni et al. prepares asymmetric PES membrane and later applied PDMS coating on membrane surface via dip coating and film casting methods [37]. The membrane coated with film casting method exhibits higher (CO_2, CH_4) ideal selectivity compared to dip coating procedure for similar PDMS concentration via single coating technique. The ideal selectivity for 5 wt. % PDMS solution coating increased to 58.3 % in film casting method, whereas only 33.3 % increment was observed for dip-coated membrane. This is due to the thicker coating layer formed in film casting procedure which results in permeance reduction. In contrast, for sequential coating procedure, dip coating showed promising selectivity compared to film casting procedure. This is due to when dip coating was applied, pores from both top and bottom of membranes are plugged and PDMS penetrate inside pores. Film-casting was applied only on the top surface of developed asymmetric membrane. After 5 sequential coating, the CO_2/CH_4 ideal selectivity increased to 9.3 and 5.0 for dip-coating and film-casting procedures, respectively.

In another study, PSF asymmetric membrane was developed and coated with PDMS and applied for CO_2/CH_4 separation. The permeance of both gases for PDMS coated membrane was compared to uncoated membrane. The PDMS coated membrane showed increased ideal selectivity to 4.7 from 3.65 for pure PSF membrane. The PDMS coating plugged the surface defects and increased the separation performance of developed gas separating membranes [81].

2.9.6 Macrovoids creation

Generally, surface defects or voids have been created during phase separation process using conventional membrane forming techniques. These voids ranged from a few to tens of micrometers in length and in several cases, it moves parallel to the membrane phase separation front [22, 158]. The solvent coagulant exchange in phase inversion process produced polymer rich and polymer lean phases, which generated unstable membrane structure. The subsequent solidification process provide stability. The exchange process between solvent and coagulant trigger the macrovoids formation which are mostly shaped as finger-like or sponge-like structure. The formation of finger-like and sponge-like structure depends on the rate of phase separations. Finger-like structure formed because of instantaneous demixing whereas delay in demixing produced sponge-like macrovoids [23]. Finger-like pores favour gas permeance whereas sponge-like pores result in selectivity enhancement as the latter are produced due to greater molecular orientation and closely packed molecular chains [24]. Along with aforementioned pores, there are other undesired macrovoids which exist in membrane morphology that influence membrane performance, as shown in Figure 2-19. These macrovoids appear in various shapes like tear drop, micelle-like and elliptical. Different theories have been presented to explain the formation and suppression of macrovoids. According to Frommer, osmotic pressure between solvent and coagulation is the driving force in phase inversion technique. The membrane surface porosity or voids creation can be controlled by reducing this osmotic pressure [159]. This can be achieved by the addition of salt in coagulation bath in order to limit water activity. Also, the addition of solvent in coagulation bath could reduce the concentration gradient for phase separation and porosity is controlled [160].

Along with these techniques, macrovoids formation can be minimized by controlling spinning parameters like dope viscosity, air gap, polymer concentration, delayed demixing, addition of high viscous component, surfactant addition, high shear rate spinning, increasing coagulation bath temperature, or high elongational draw [25]. In all the aforementioned approaches, the easiest choice is to increase dope solution viscosity either by introducing highly viscous additive or by increasing polymer concentration. The polymer concentration in a dope solution has a significant impact on mean pore size, porosity and permeance of hollow fibre membranes. With the increase in polymer concentration, solution viscosity and density increased, resulting in depression of void formation in the membrane microstructure [161]. Kesting et al. claimed in his patent that a membrane with critical polymer concentration of 30 wt.% and viscosity around 5×10^4 cp would produce macrovoid-free membrane. This was the initial attempt to quantitatively correlate dope viscosity and macrovoid-free structures [162]. Peng et al. studies the effect of dope viscosity, air gap and take up speed on the morphological structure of polysulfone, p84 and cellulose acetate. According to his findings, optimum morphological structure for improved separation performance can be obtained by optimizing all the aforementioned parameters [21]. Wang et al. prepared PEI asymmetric hollow fibre membrane using a dope containing NMP as solvent and ethanol as non-solvent additive. According to findings, at longer air gaps, macrovoids formation increased to a great extent, similarly a highly distorted structure was observed when air gap was greatly reduced. Dry processes are the only phenomenon that took

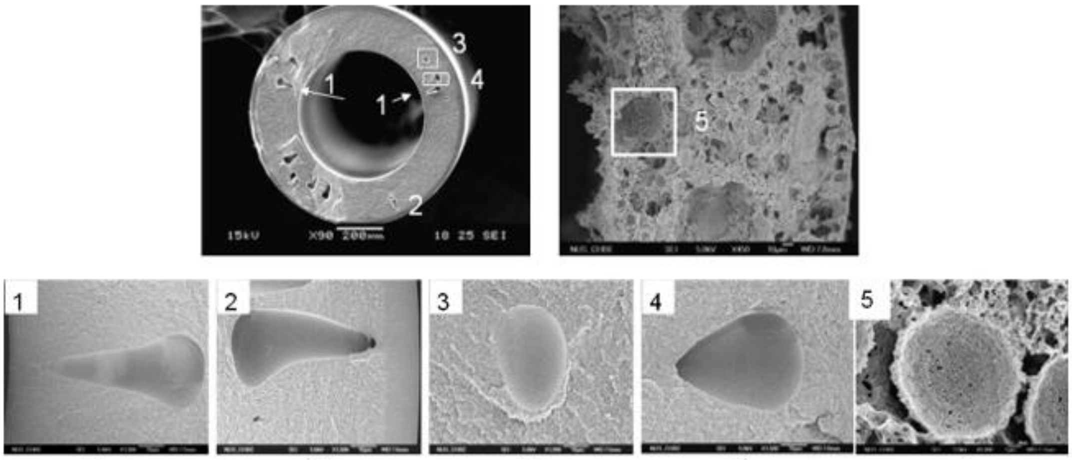

Figure 2-19: Five types of macrovoids and trace of intrusion. 1: Inward-pointed, 2: outward-pointed, 3: elliptical, 4: tear drop, and 5: micelle-like macrovoid [162].

place in the aforementioned condition whereas wet processes dominate in the latter case. It was proven that the gas separation performance can be enhanced by optimizing the air gap distance [163]. Similar results were obtained by Tsai et al for polysulfone hollow fibre membrane with variation in air gap distance [164].

2.9.7 Plasticization

Plasticization is a phenomenon that takes place when the concentration of sorbing molecules increases to an extent that it swells the polymer matrix. Swelling typically occurs as a result of disturbance in chain mobility which ultimately reduces the separation ability of membrane against the penetrating molecules. Generally, polymers having polar groups are more prone to plasticize because of the polarising nature of CO_2 molecule. For instance, $–OCOCH_3$ and $–COOCH_3$ are polar and flexible pendent groups in polymethyl methacrylate and polyethylmethacrylate (PEMA). These polymers are more likely to plasticise at higher CO_2 concentration [165]. In literature, several techniques have been proposed to address this issue, such as thermal treatment, polymer blending and usage of crosslinking agents [166-170]. Thermal treatment suppresses membrane plasticization by densification of the polymer matrix and restricting chain mobility. On the other hand, heat treatment decreases the free volume by improving the polymer chain packing [165]. In polymer blending, a polymer with high plasticization tendency is blended with another polymer which is stable against CO_2-induced plasticization. It has been reported that Matrimid blended with PSf showed better plasticisation resistance in mixed gas environment [171].

2.10 Gas permeation modelling

The transportation of gas molecules through layered silicates is a complex phenomenon governed by diffusion/solubility mechanism. Generally, the transportation of gas molecules through polymer phase consists of four processes, the sorption of penetrant gas molecules at the membrane surface; gas dissolution inside membrane; diffusion through membrane; followed by desorption from the other surface [172]. The permeation of penetrant molecules led to solution-diffusion mechanism and can be explained via Fickian diffusion which states that the permeation coefficient depends on both diffusion coefficient and solubility coefficient as given in Eq. 2-4.

$$P = D \cdot S \qquad (2\text{-}4)$$

Diffusion coefficient, *D*, describes the kinetic properties of penetrant molecules which depends on its mobility in polymer phase whereas solubility coefficient, *S*, is the thermodynamic factor which reflects the interactions between organic and inorganic phase [173].

The penetrant molecules have faced increased diffusion path due to the presence of impermeable inorganic filler particles. The tortuosity of the layered silicates plays a major role in permeation reduction and is dependent on three factors; volume fraction, orientation of platelets and aspect ratio. As the volume fraction of impermeable inorganic phase increased, the available volume of organic permeable phase decreased, subsequently the permeability and solubility factor of MMM also decreased.

The orientation of MMT in PEI matrix plays a key role in determining the permeability of gas molecules through the membrane. The perpendicular orientation of layered silicate to the diffusion path results in decrement of diffusion coefficient of penetrant molecules, whereas, the opposite behavior is observed with parallel orientation. The aspect ratio defined the state of delamination and exfoliation of layered silicate in polymer matrix; higher aspect ratio favors exfoliation and dispersion of individual layer in the polymer matrix which increase the tortuous path for penetrant gas molecules and reduce the permeation. Delamination of layered silicate represents the intercalation of polymer chain in the intergallery space whereas exfoliation represents the complete separation of platelets which is required to enhance the membrane properties even at lower loading. However, in most cases, delaminated morphology or mixed morphology of the clay platelets are observed rather than complete exfoliation [174].

Table 2-6: Phenomenal models used to calculate gas permeance through MMM using layered silicates as fillers.

Models	**Equation**	**Ref.**	**Description**
Nielsen	$\frac{P_C}{P_O} = \frac{1-\varphi}{1+\frac{\alpha.\varphi}{2}}$	[175]	Where P_c, Permeability of composite, P_0, Neat polymer membrane permeability φ, Filler volume fraction α, Aspect ratio S, Order factor S = 0 for Random orientation S = -1/2 for parallel orientation to the direction of flow S = 1 for Horizontal orientation to the flow direction
Cussler	$\frac{P_C}{P_O} = \left(1+\frac{\alpha^2\varphi^2}{1-\varphi}\right)$	[176]	
Yang-Cussler	$\frac{P_C}{P_O} = \frac{1-\varphi}{\left[1+\frac{1}{2}(\alpha^2\varphi^2)\right]}$	[177]	
Lape-Cussler	$\frac{P_C}{P_O} = \frac{1-\varphi}{[1+(2/3)\alpha\varphi]^2}$	[178]	
Bharadwaj	$\frac{P_C}{P_O} = \frac{1-\varphi}{[1+(1/3)\alpha\varphi(S+1/2)]}$	[179]	

Several theoretical models are available in literature to predict gas permeation through polymer layered silicates membrane as given in Table 2-6. Nielsen proposed a simple permeation model by considering the regular and horizontal arrangement of platelets to the diffusion path, therefore this model is often referred as "tortuous path" model [175]. The nanoparticles with rectangular shape are evenly distributed with finite width, *L*, and thickness, *D*, in the polymer matrix. Cussler improved the model by considering the nanoparticles arranged in layered form with each layer separated by narrow slits [176]. This model is more sensitive with regards to aspect ratio and volume fraction for permeability prediction as compared to Nielsen Model. Yang-Cussler further improved the model by considering the monodispersed nanoparticles with parallel alignment and varied aspect ratio [177]. Whereas Lape-Cussler considered the rectangular platelets with similar aspect ratio are dispersed randomly in polymer matrix and aligned parallel to each other along the diffusion path [178]. All the above stated models are based on the consideration that nanoparticles are aligned horizontally to the penetrant diffusion path. In later years, Bharadwaj developed a model which takes into account the platelet orientation factor [179]. This factor includes various dimensions whether horizontal, parallel or random distribution in the direction of the diffusion path. Most models assumed complete exfoliation of nanoparticles, nevertheless, this model describes the state of delamination and complete exfoliation.

2.11 Summary

In summary, scientists are searching for robust new membrane materials to provide enhanced gas separation properties. Much work has been performed on polymeric membranes, nevertheless, their performance is not competitive at the industrial level. Inorganic membranes are too delicate to process and handle, however, they are capable of withstanding higher pressure and temperature without reduction in separation ability. To date, polymeric membranes are still dominating the membrane gas separation market due to their ease of processing, despite their 5 to 10 times lower selectivity. To address this issue, mixed matrix membranes (MMMs) are developed to fill the gap due to the inefficiency of polymeric and inorganic membranes. In the past, various types of nanofillers, both porous and non-porous have been studied for gas separation applications. Based on size and shape, porous fillers allow gas molecules to pass through whereas non-porous fillers are acknowledged to alter the chain orientation of polymers and improve the separation ability of polymer matrix. Among the non-porous fillers, layered silicate exhibits promising ability to alter polymer chain orientation. The selection of suitable polymeric material as matrix for layered silicate is essential for successful formation of membrane. Typically, the phase boundary defects between nano-clay and polymer phase results in poor membrane performance, nevertheless, these can be solved via crosslinking, thermal treatment and priming protocol. The orientation of clay platelets is also a critical factor in defining the gas separation performance of MMM, thus it should be carefully controlled during membrane casting. The development of high aspect ratio and nanosized fillers open an interesting pathway to the fabrication of asymmetric mixed matrix hollow fibre membrane with ultra-thin selective layers. The development of state-of-the-art ultra-thin skinned layered MMM could boost the performance of MMMs. For further advancement in this area, high aspect ratio of layered silicates, and low number of stakes per tactoids should be ensured for low filler loading and enhanced dispersion. The polymer-layered silicate interface void formation and distribution morphology are immediate challenges that need to be addressed. Along with improvement in existing materials, membrane researchers need to discover new materials to functionalize the nano-clay surfaces which may pave the way towards better dispersion and adhesion. In addition, various theoretical permeation models have been discussed for polymer-layered silicate mixed matrix membranes.

CHAPTER 3

METHODOLOGY

This chapter provides the information about the materials, methodology and equipment used to synthesize and characterize PEI-clay hollow membranes. Section 3.1 narrates the details of the materials that are used to in the development of asymmetric hollow fibre membranes. Moreover, the experimental procedure for montmorillonite modification is described in Section 3.2. Subsequently, Section 3.3 and 3.4 present the optimization of spinning parameters, characterization of neat PEI membrane and synthesis of mixed matrix membrane. Furthermore, the membrane coating method is discussed in Section 3.5. Section 3.6 highlights the details of the existing gas permeation models which are used in this study.

3.1 Materials and methods

In this research, various chemicals and materials were used to synthesize the modified MMT and to develop the neat PEI, PEI-MMT and PEI-*f*-MMT membranes at various loadings to study the carbon dioxide/methane separation. Table 3-1 presents the details of all the materials used to carry out this research. All chemicals used in this study are of analytical grades.

Table 3-1: Chemicals used in this study.

Chemicals	Mol. Formula	Assay (%)	Density (g/cm^3)	Brand	CAS No.
Montmorillonite	$Si_8(Al_{3.34}Mg_{0.66})Na_{0.66}O_{20}(OH)_4$	98.5	0.3-0.4	Kunimine Ind. Co. Japan	-
Polyetherimide	$(C_{39}H_{30}N_2O_6)_n$	-	1.27	Sigma Aldrich	61128-46-9
N-methyl-*2*-pyrrolidone	C_5H_9NO	99.5	1.03	Sigma Aldrich	872-50-4
Hydrochloric acid	HCl	37	1.19	Merck	7647-01-0
ω-aminolauric acid	$NH_2(CH_2)_{11}COOH$	95	-	Sigma Aldrich	693-57-2
Loctite Hysol EA 0151 TM Epoxy	-	-	-	Ellsworth Adhesives	-
PDMS	$[Si(CH_3)_2O-]_x$	96	5	Fisher Scientific	9016-00-6

3.1.1 Equipment

The details of all the equipment used for clay modification, MMM development and gas permeation performance are provided in Table 3-2. The properties of spun HF membranes were characterized using analytical techniques as provided in Table 3-3.

Table 3-2: List of equipment used in this research.

Equipment	Brand
Weighing balance	METTLER TOLEDO, MS303S
Magnetic stirrer	DAIHAN, Wisd Multi Hot Plates
Sonicator	Fisherbrand, FB15061
Viscometer	Fungilab Rotational viscometer
HF spinning machine	AMTEC, Malaysia
Permeation rig	DIXSON FA, Malaysia
Digital dubble flow meter	SUPELCO, Optiflow 520
Vacuum oven	Memmert, Germany
Platinum coater	Qorum Q150RS

Table 3-3: List of analytical equipment used for characterization.

Analytical Equipment	Brand
Fourier Transform Infrared (FT-IR)	Perkin Elmer 1650
Thermo gravimetric Analyzer (TGA)	Perkin Elmer, STA 6000
Differential scanning calorimetry (DSC)	TA Instruments, Q2000
Small angle X-ray diffraction (SAX)	BRUKER, XRD/D8
Scanning electron microscopy (SEM)	HITACHI TM3030
Field Emission Scanning Electron Microscope (FESEM)	Zeiss Supra55 VP
Energy dispersive x-ray (EDX)	Oxford Instruments, INCAx-act
Contact angle measuring system	OCA 20, DataPhysics

3.1.2 Research Layout

Research layout of polyetherimide-montmorillonite hollow fibre membranes is given in Figure 3-1.

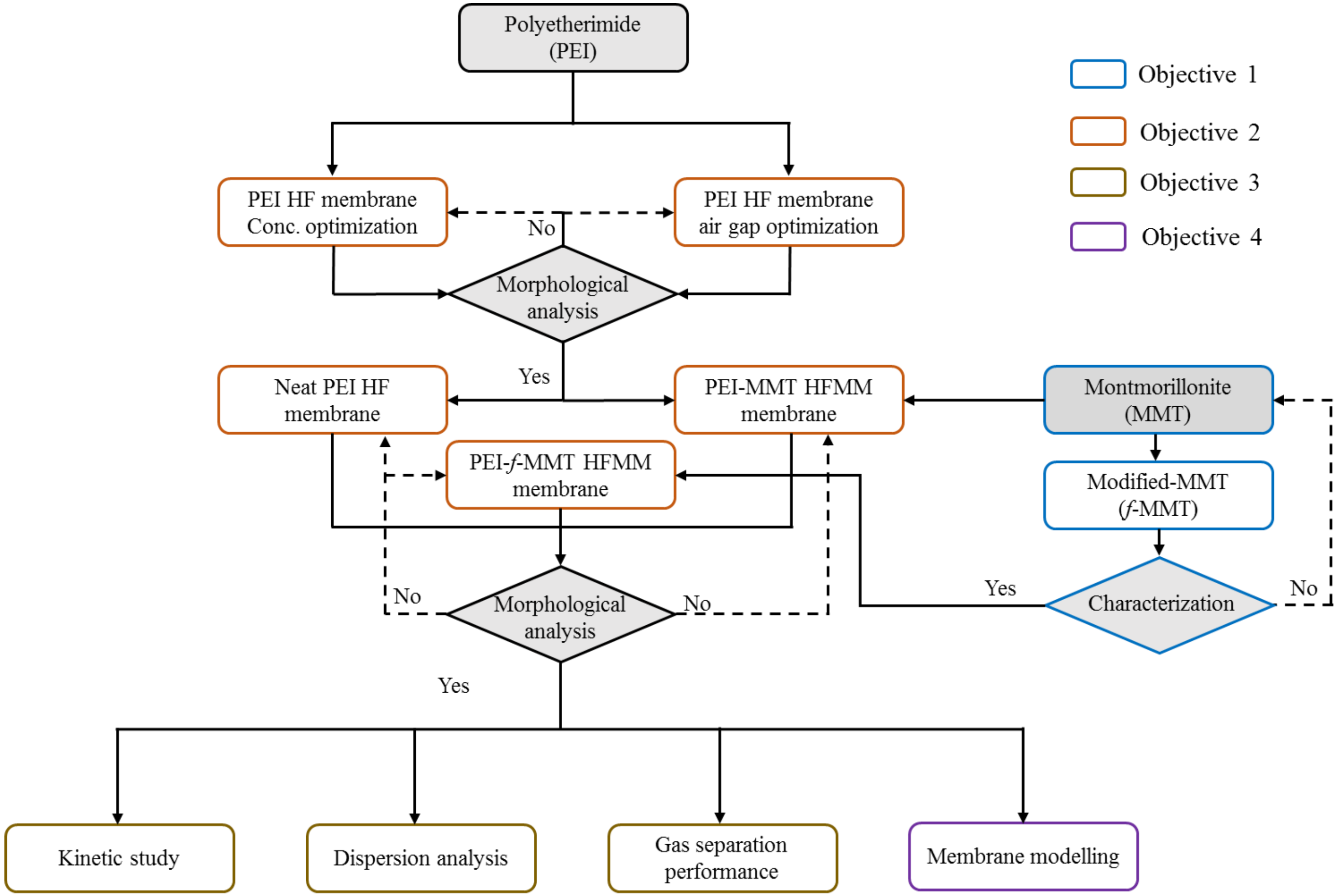

Figure 3-1: Research work layout for PEI/MMT HFMM membranes

3.1.3 Research phases

This research work was conducted in five different phases which are elaborated in the Table 3-4.

Table 3-4: Research phases involved in this study.

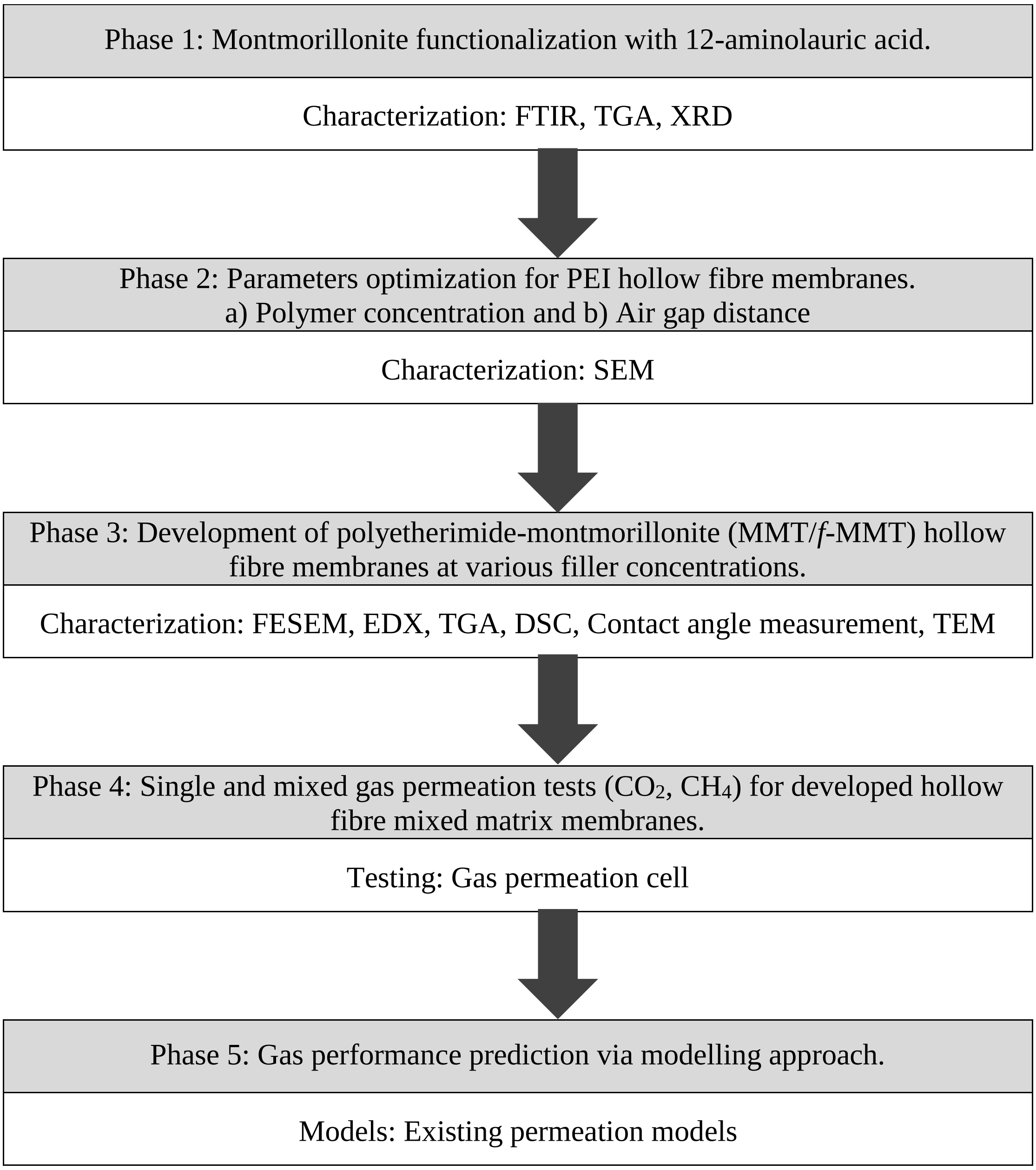

Phase 1: Montmorillonite functionalization with 12-aminolauric acid.

Characterization: FTIR, TGA, XRD

Phase 2: Parameters optimization for PEI hollow fibre membranes.
a) Polymer concentration and b) Air gap distance

Characterization: SEM

Phase 3: Development of polyetherimide-montmorillonite (MMT/*f*-MMT) hollow fibre membranes at various filler concentrations.

Characterization: FESEM, EDX, TGA, DSC, Contact angle measurement, TEM

Phase 4: Single and mixed gas permeation tests (CO_2, CH_4) for developed hollow fibre mixed matrix membranes.

Testing: Gas permeation cell

Phase 5: Gas performance prediction via modelling approach.

Models: Existing permeation models

3.2 Modification of Na-MMT

The modification of inorganic MMT to organic MMT is depicted in Figure 3-2. 100 ml of water was heated up to 80˚C in a 500 ml beaker. 1.2 ml of concentrated hydrochloric acid and 12 mmol of ω-aminolauric acid were added with continuous stirring. ω-aminolauric acid solution was poured in another solution which contained 5 g of Na-MMT in 500 ml hot water. The mixture was heated and stirred vigorously. When white precipitates appeared, the product was filtered and washed with hot water and dried in vacuum oven at 90˚C for 24 hours. The solid product was crushed in mortar and grinded to powder form [122].

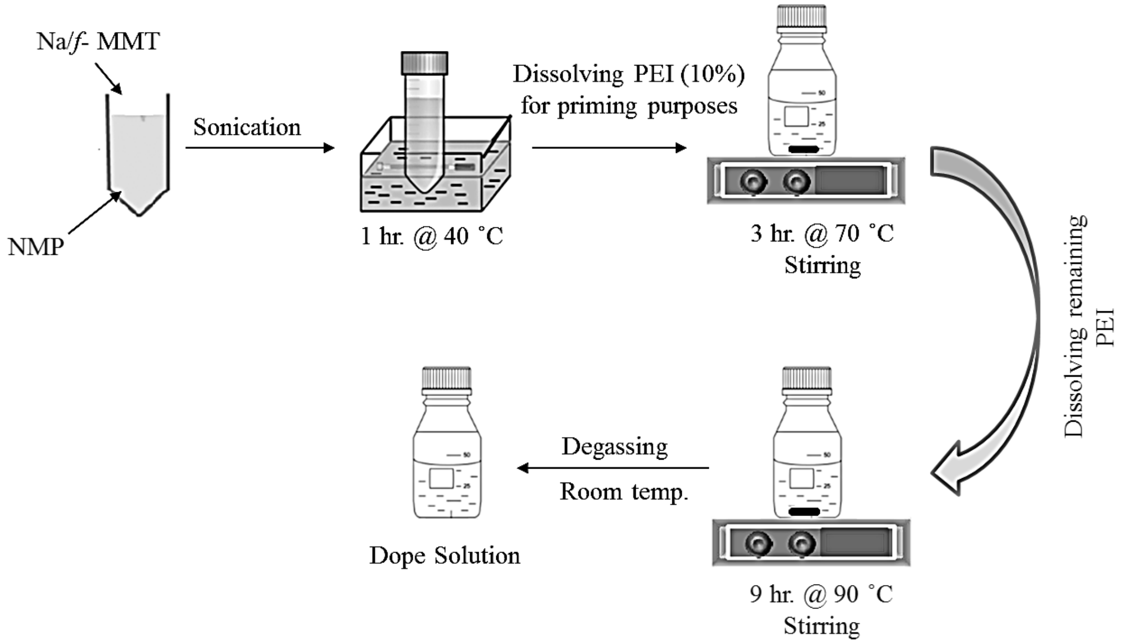

Figure 3-2: Schematic diagram of organic modification of inorganic MMT.

3.2.1 Functional group identification

The possible functional groups attached to *f*-MMT were identified by Fourier transform Infrared (FT-IR) Perkin Elmer 1650. The spectra of both MMT and *f*-MMT samples were obtained in the range of 400 to 3900 cm^{-1}.

3.2.2 Content of amino functionalization

The content of ω-aminolauric acid moiety in MMT was determined by using thermogravimetric analyzer (Perkin Elmer, STA6000). The MMT and *f*-MMT were heated from room temperature to 800˚C at the heating rate of 10˚C/min under nitrogen atmosphere [123].

3.2.3 Interlayer spacing of *f*-MMT

SAX (BRUKER, XRD/D8) was used with CoKα radiation (0.15414 nm) to measure the interlayer distance of both MMT and *f*-MMT.

3.3 Optimizing parameters to minimizing morphological defects

In order to prepare defect-free PEI hollow fibre membrane morphology, parameters like dope viscosity and air gap distance were varied while keeping all other parameters constant. The effect of air gap and dope viscosity on fibres' morphology were studied by adopting the following methodology.

3.3.1 Optimizing dope viscosity

The dope solution viscosity is controlled by PEI concentration in the solution. In this study, all other parameters are kept constant except PEI concentration.

3.3.1.1 Dope Preparation

PEI was dried in vacuum prior to use in order to remove moisture. Five different dope solutions with varied PEI concentrations of 10, 15, 20, 25, 28 wt. % were prepared. Dried PEI was added in NMP solvent and heated while stirring at 70˚C for 3 hours followed by 9 hours heating at 90˚C. After 12 hours of heating and stirring, the prepared solution was placed at ambient conditions for 24 hours in order to remove the trapped gas [163].

3.3.1.2 PEI HF membrane spinning

Lab scale hollow fibre membrane set up was used to spun PEI HF membranes by phase inversion method as shown in Figure 3-3. For dope extrusion, tube in orifice spinneret was used with 0.8 mm outer and 0.4 mm inner diameter. The spinneret assembly is shown in Plate 3-1. The dope solution was pumped to spinneret at constant flow rate and under the nitrogen pressure of 1 bar. Water was used as bore fluid and pumped to spinneret through syringe pump. The nascent spun HF membranes passed through coagulation bath containing water as external coagulant for solvent exchange and collected by take up drum [1]. All the membranes were spun at ambient condition and at constant humidity. Afterwards, the spun membranes were immersed in tap water for complete removal of residual solvent for three days at room temperature followed by fibre drying at room temperature. The spinning conditions for PEI HF membranes are described in Table 3-5.

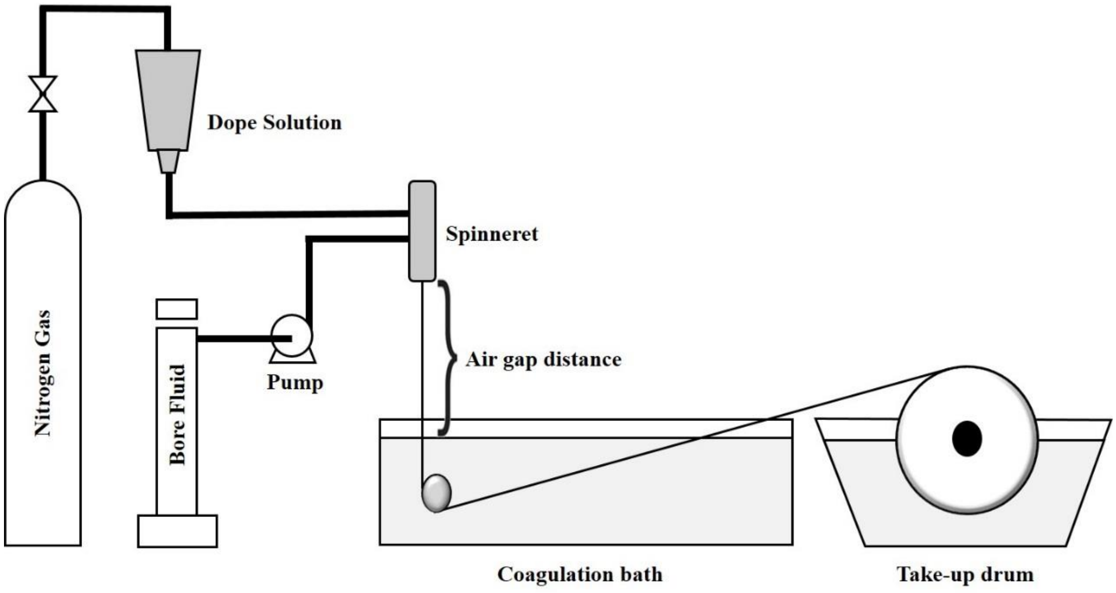

Figure 3-3: Schematic of dry jet, wet quench spinning apparatus.

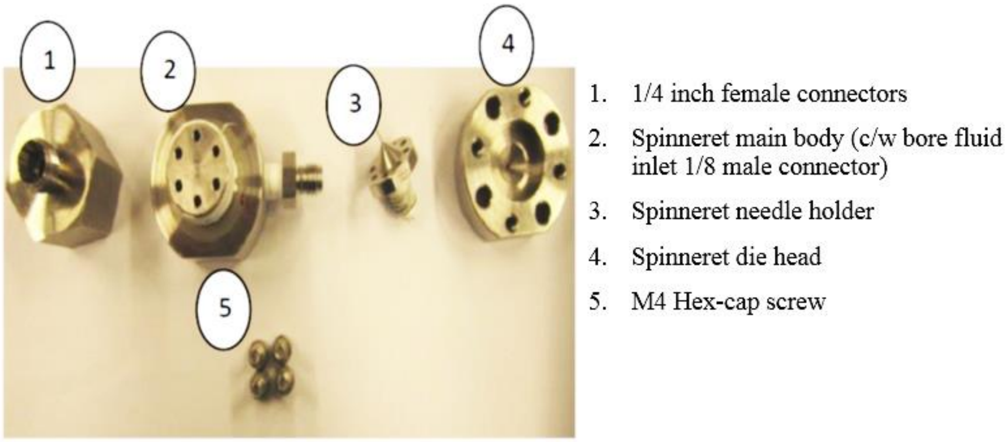

1. 1/4 inch female connectors
2. Spinneret main body (c/w bore fluid inlet 1/8 male connector)
3. Spinneret needle holder
4. Spinneret die head
5. M4 Hex-cap screw

Plate 3-1: Spinneret assembly used in this study.

Table 3-5: PEI NMP HF membrane spinning condition.

Spinning Conditions	Parameters
Temperature	25˚C
O.D/I.D (mm)	0.8/0.4
Relative humidity	Constant
Coagulant	Water
PEI concentration	10, 15, 20, 25, 28 wt. %
Air gap	10 cm
Dope solution flow rate	0.8 ml/min
Bore water flow rate	1 ml/min
Take up velocity	Free fall

3.3.2 Optimization of air gap for PEI/NMP HF membrane

The effect of air gap on PEI/NMP HF membrane morphology is studied in order to develop defect-free membranes. In this formulation, every other parameter remained constant except for air gap distance, which represents the distance from spinneret to the coagulant solvent surface in coagulant bath as shown in Figure 3-4.

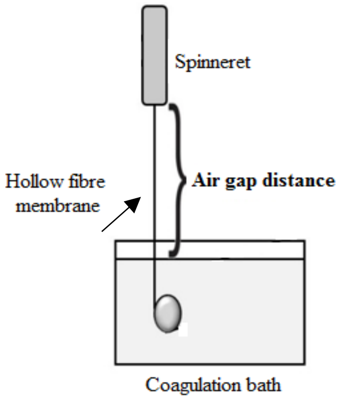

Figure 3-4: Schematic diagram showing air gap distance.

3.3.2.1 Dope solution preparation

Prior to dope preparation, 23 g of PEI was dried in vacuum oven in order to remove moisture. Dried PEI was immersed in NMP solvent. Initially, the solution was stirred at 70˚C for 3 hours, afterwards temperature was increased to 90˚C for 9 hours. The solution was stirred thoroughly for uniform mixing and degassed.

3.3.2.2 Fabrication of hollow fibre membranes

PEI HF membranes were produced at ambient conditions by phase inversion method using lab scale experimental set up. All other parameters were kept constant except air gap distance as described in Table 3-6.

Table 3-6: PEI/NMP hollow fibre membrane spinning parameters.

Spinning conditions	**Parameters**
Temperature (˚C)	25
O.D/I.D (mm)	0.8/0.4
Coagulant	Water at room temp.
Air gap (cm)	0, 5, 10, 15, 20, 25, 30, 35
Dope solution flow rate (ml/min)	0.8
Bore water flow rate (ml/min)	1
Take up velocity	Free fall

3.4 Synthesizing hollow fibre mixed matrix membranes

This section elaborates the steps to develop hollow fibre mixed matrix membrane containing PEI host polymer with MMT and *f*-MMT as filler phase.

3.4.1 PEI-MMT HF membrane

After optimizing the parameters for PEI HF membranes, mixed matrix membranes (MMM) were produced containing MMT as inorganic filler and PEI as host polymer.

3.4.1.1 Dope solution preparation

The dope solution of PEI/MMT HF membrane consists of 23 wt. % of PEI in 75 ml of NMP with varied amount of MMT (0, 1, 2 ,3, 4 wt.% of solid PEI). The desired amount of MMT was dispersed in NMP solvent and sonicated at 40˚C for 60 min in order to disperse uniformly. After dispersion, 10% of PEI was added in the sonicated mixture for priming purpose with stirring at 70˚C for 3 hours. Later, the remaining PEI was gradually added for complete dissolution followed by increase in temperature to 90˚C for 9 hours. The prepared dope solution was degassed for 12 hours at room temperature to remove air bubbles. Viscosity measurements were taken 3 hours prior to membrane spinning.

3.4.1.2 PEI-MMT HF membrane spinning

HF asymmetric membrane was produced at ambient conditions by phase inversion method using lab-scale HF spinning experimental set up as shown in Figure 3-2. Tube in orifice type of spinneret was used for extrusion with 0.8 mm and 0.4-mm inner diameter. The dope solution was pumped to spinneret at constant flow rate of 0.8 ml/min and constant N_2 pressure was applied at 1 bar. Water was used as bore fluid at ambient condition and delivered through syringe pump at the constant flow rate of 1 ml/min. Water was also used as external coagulant at room temperature and air gap was fixed at 15 cm. The nascent spun fibre were free falling and passed through coagulation bath for solvent exchange. Subsequently, the spun hollow fibers were immersed in distilled water for solvent exchange for 3 days with daily water change to remove solvent residues, followed by fibre drying at ambient conditions.

3.4.2 PEI-*f*-MMT HF membrane

After incorporating MMT in PEI, mixed matrix membranes containing *f*-MMT were developed by adopting the following methods.

3.4.2.1 Dope solution preparations

The dope preparation method was based on similar procedures as described for PEI-MMT HF membranes. The concentrations of PEI and NMP were fixed at 23 wt. % and 77 wt. %, respectively; whereas air gap distance was held constant at 15 cm. Four different concentrations of *f*-MMT (1 to 4 wt. % of total solid PEI) were added into the dope solution with stirring. Initially, *f*-MMT was added in the NMP solvent and sonicated for 60 minutes at 40˚C to disintegrate the clay layers for uniform mixing in the solvent. After sonication, 10 wt. % of PEI was added in the solution for priming purpose and stirred at 70˚C for 3 hours. Subsequently, the temperature was raised to 90˚C for 9 hours and the remaining PEI was added gradually for complete dissolution in the solvent. After preparation, the dope solution was kept at room temperature for 12 hours in order to evacuate the trapped air as well as for polymer chain relaxation.

3.4.2.2 Development of PEI-f-MMT HF membrane

The PEI-*f*-MMT hollow fibres were developed by using lab scale experimental set up by dry-wet phase inversion method. The spinneret used to spin HF membrane consists of 0.8 mm outer diameter and 0.4 mm inner diameter. The dope solution was pumped through the spinneret under 1 bar of nitrogen pressure, whereas tap water was used as internal coagulant and pumped through syringe pump to spinneret. The air gap distance was maintained at 15 cm for all dope solutions prepared. After extrusion through spinneret, hollow fibre membrane passed through coagulation bath at ambient conditions. The nascent fibres were collected under free fall. The spinning conditions for PEI-*f*-MMT HF membranes are described in Table 3-7. The spun HF membranes were immersed in tap water for 72 hours for complete removal of residual NMP from the fibres. The water was replaced with fresh water after every 24 hours. The spun PEI-*f*-MMT HF membranes were dried at room temperature.

Table 3-7: PEI/NMP hollow fibre membrane spinning parameters.

Spinning conditions	**Dope solution**
Temperature (˚C)	25
O.D/I.D (mm)	0.8/0.4
Relative humidity	Constant
Coagulant	Water
Coagulant temperature (˚C)	25
Air gap (cm)	15
Dope solution flow rate (ml/min)	0.8
Bore water flow rate (ml/min)	1
Take up velocity	Free fall

3.5 Characterization of developed membranes

Various characterization methods were used to analyze the developed polymeric and mixed matrix hollow fibre membranes. These are categorized as morphological, filler distribution, spatial dispersion, and thermal characterizations.

3.5.1 Viscosity measurement

In order to determine the critical dope viscosity to prepare PEI hollow fibre membrane with minimum morphological defects, the viscosity of the prepared dope solutions was measured by using Fungilab rotational viscometer at 12 rpm and at ambient conditions. All viscosity measurements were made 3 hours prior to membrane spinning.

3.5.2 Morphological characterization

In order to study the surface and cross-section morphology of the membranes, the fibres were fractured in liquid nitrogen and coated with platinum using Qorum Q150RS platinum coater. HITACHI TM3030 scanning electron microscopy (SEM) was used to observe the morphological structure of the fibres.

The developed PEI-*f*-MMT HF membranes were spun through dry wet phase inversion method. The morphology of spun membranes was studied through Zeiss Supra55 VP field emission scanning electron microscopy (FESEM) analyses.

Furthermore, surface topology of the developed membranes was analyzed via Nano Navi E-sweep atomic force microscopy (AFM). AFM provides the 3D images of membrane surface.

3.5.3 Filler distribution study in PEI matrix

The modified MMT possessed organophilic attributes which enhanced its dispersion in organic polymer phase. The distribution of *f*-MMT in PEI matrix was studied by EDX analysis.

RMC Boekeler ultramicrotome (PT-PC PowerTome) was used to slice the membrane samples in trapezoidal shape. The sliced samples were transferred onto a copper grid for transmission electron microscopy (TEM) analysis. Subsequently, the spatial dispersion of MMT or *f*-MMT in polymer matrix was analyzed via FEI Tecnai F20S TEM.

3.5.4 Thermal characteristics of PEI-*f*-MMT HF membranes

Perkin Elmer STA6000 thermogravimetric analyzer (TGA) was used to study the thermal behavior of PEI-*f*-MMT HF membranes. The thermal profile was analyzed using a heating rate of 10˚C/min under nitrogen environment.

The amorphous behavior of spun HF membranes was analyzed using TA Instruments Q2000 differential scanning calorimetry (DSC) to determine the glass transition temperature (T_g) of the developed membranes. Filler loadings affect the glassy nature of the polymer and influence the thermal properties of the developed membranes.

3.5.5 Hydrophobicity of PEI-*f*-MMT HF membranes

The hydrophobic behavior of developed membranes through dry-wet phase inversion method was analyzed by using OCA20 DataPhysics contact angle measuring system. The water droplet contact angle on membrane surface was captured and analyzed for hydrophobic/philic behavior of membranes.

3.5.6 Pure gas permeation test

Gas permeation tests for spun HF membranes were carried out by using lab scale permeation cell as shown in Appendix A-1. Figure 3-5 demonstrates the schematic diagram of the permeation rig. For gas transport through membranes, 99.99 % pure CO_2 and CH_4 gases were used at room temperature and at pressure of 2 to 10 bars. A pile containing 3 fibres was fixed in the module with one end glued with epoxy resin to avoid gas passage, whereas the other end of the pile was accessible to the inlet gases [36]. Permeation was carried out by passing the desired gas through the lumen side of the hollow fibres as depicted in Figure 3-6.

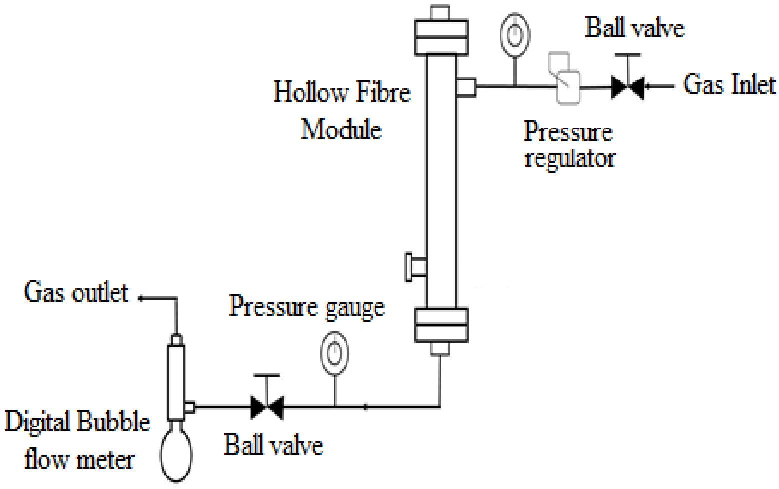

Figure 3-5: Schematic of hollow fibre permeation cell used in this work.

The total length of the HF pile was 15 cm with an effective area of approximately 11.31 cm^2. A digital bubble flow meter was attached to the gas permeate side in order to measure the flow rate of gas through the membrane. The permeance was calculated by using Eq. (3-1).

$$\frac{P_i}{l} = \frac{Q}{A\Delta P}\frac{273.15}{T} \tag{3-1}$$

Pi/l is the gas permeance in GPU [1GPU=1*10^{-6} cm^3(STP)/cm^2.s.cm.Hg]. Subscript *i* represents the penetrating gas, i.e. CO_2 or CH_4, *A* is the effective surface area of the membrane, *ΔP* is the pressure difference across membrane in cmHg and

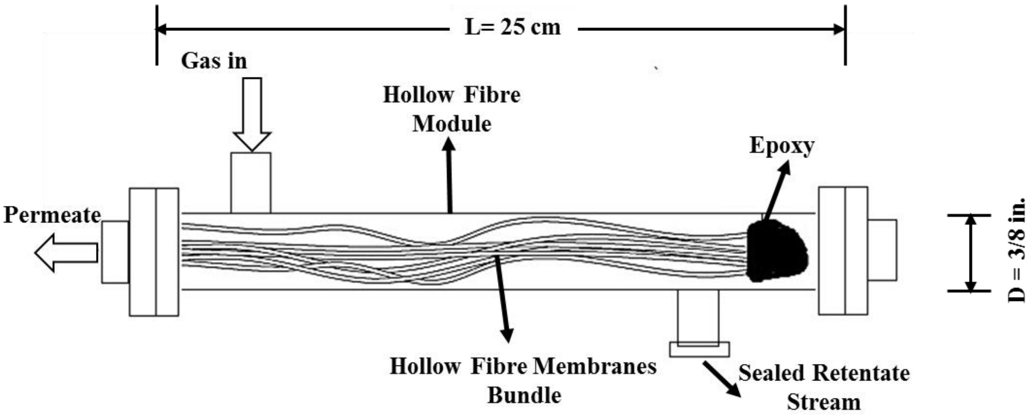

Figure 3-6: Schematics of hollow fibre bundle preparation.

T (K) is the temperature at which permeation was carried out. The ideal selectivity is the ratio of permeance of fast gas to slow gas and was calculated by using Eq. (3-2).

$$\alpha_{ij} = \frac{P_i/l}{P_j/l} \tag{3-2}$$

αij represents ideal selectivity of gas i to j. Whereas Pi/l and Pj/l represents permeation of gas i and j, respectively.

3.5.6.1 Gas permeation performance

The gas permeation performance of PEI-*f*-MMT HF membranes was carried out by using 99.999 % pure CO_2 and CH_4 gases at room temperature at a pressure of 2 to 10 bars. The desired gas was supplied through the lumen side of the membrane bundle. For permeation tests, 3 fibres were taken as a pile and one end of the pile was sealed using epoxy glue. After 3 hours, another coat of epoxy was applied, followed by 24 hours of drying. After 24 hours, the pile of fibres were fixed inside the module and glued so that no gas can pass through except through the fibres' lumen side. Before gas permeation, the entire permeation cell was vacuumed. The specifications of the module are given in Table 3-8. Membrane permeance and selectivity for CO_2 and CH_4 were calculated by using equation (3-1) and (3-2), respectively [106].

Table 3-8: Module specifications.

Specifications	**Values**
Module I.D (mm)	12.7
Fibre effective length (mm)	151
Number of fibres	3
Effective membrane area (cm^2)	11.39
Hollow fibre O.D/I.D (mm)	0.8/0.4

3.6 PDMS coating of developed hollow fibre membranes

Poly(dimethylsiloxane) (PDMS) coating protocols were used in order to remove the surface defects on the outer layer of developed membranes. Dried hollow fibres were immersed in a coating solution which consists of 5 wt. % of PDMS in *n*-hexane for 60 minutes. Afterwards, membranes were cured in oven at 80˚C for 3 days. After the curing process, the coated membranes were stored for gas permeation testing.

3.7 Mixed gas (CO_2/CH_4, 50/50 v/v %) permeation test

The mixed gas performance for coated neat PEI and PEI-*f*-MMT (2) samples was carried out at 4 bar feed pressure with 50/50 v/v % composition of CO_2 and CH_4 gas, respectively. Moreover, the module contained 10 hollow fibres and cross flow arrangement was used for mixed gas test. The permeate gas mixture was then analyzed under gas chromatography (GC) to evaluate the gas composition of the mixture that permeate through the aforementioned membranes.

3.8 Chapter summary

This chapter provides the detailed methods and procedures from material preparation to design of experiments. Montmorillonite clay was functionalized with organic cation to improve its compatibility towards polymer matrix. The functionalized clay was characterized in order to determine the extent of functionalization. PEI hollow fibre membrane was spun to investigate the optimum parameters required to fabricate defect-free membrane morphology. Furthermore, MMT and functionalized MMT were incorporated in PEI matrix to develop hollow fibre membranes. The morphology, thermal behavior and gas separation characteristics of aforementioned membranes were analyzed. Subsequently, mixed gas test at CO_2/CH_4 composition of 50/50 v/v % was carried out for selected membranes.

CHAPTER 4

RESULTS AND DISCUSSION

This chapter presents the experimental results of montmorillonite (MMT) modification as well as synthesis of neat polyetherimide (PEI), PEI-MMT and PEI-*f*-MMT hollow fibre mixed matrix membrane. The chapter is divided into four sections; characterization of modified MMT is discussed in section 4.1. Section 4.2 narrated the optimization of spinning parameters for development of neat PEI membrane in hollow fibre geometry. Section 4.3 provided the results from characterization through analytical methods for PEI-MMT HFMM membrane, whereas, PEI-*f*-MMT HFMM membrane characterization is discussed in section 4.4. Section 4.5 discussed on the CO_2 and CH_4 permeance and selectivity for pure gases through spun hollow fibre membranes. Moreover, the last section deals with the various phenomenological models for evaluation of various experimental results obtained via gas permeation test.

4.1 Characterization of modified-MMT

The characterization of *f*-MMT was conducted in order to confirm the successful modification and basal spacing of *f*-MMT.

4.1.1 Functional group identification

Figure 4-1 shows the FTIR spectra of native montmorillonite (MMT) and amino functionalized MMT. Native MMT displays characteristics peaks at wavenumber 521, 1041, 1637, and 3467 cm^{-1}, which represent Al-O-Si deformation, Si-O stretching, H-O-H bending and Al-O stretching, respectively.

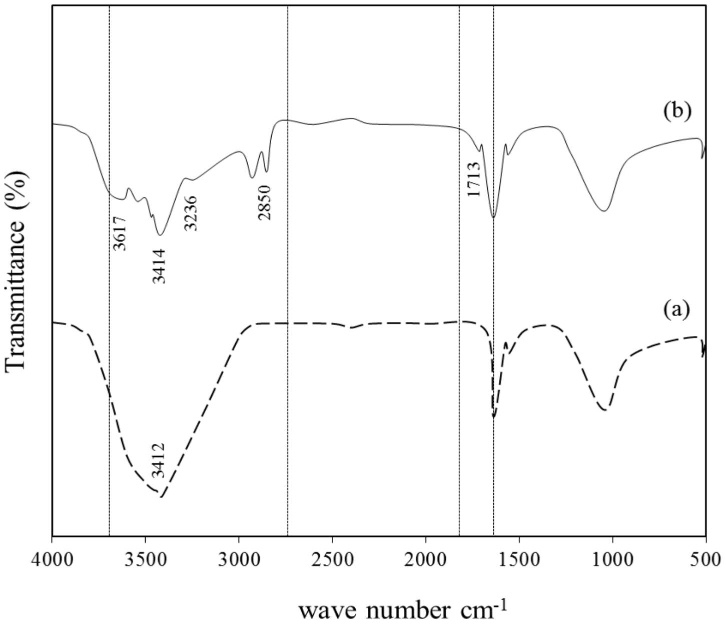

Figure 4-1: FTIR spectrum of a) MMT and b) *f*-MMT.

In amino-functionalized MMT (*f*-MMT), several new peaks appeared at approximately 1713, 2850, 3236 and 3617 cm^{-1}. These peaks are associated with the stretching vibration of carbonyl group, C-H bond stretching, N-H stretching and structural stretching of hydroxyl (OH) group [180, 181]. All the important bands and assignments of functional groups are tabulated in Table 4-1. Therefore, the FTIR spectra suggested the attachment of ω-aminolauric acid to the MMT surface.

Table 4-1: FTIR peaks and bonds assigned.

SN	Wave Number (cm^{-1})		Bonds Assigned	Theoretical Range (cm^{-1})
	MMT	*f*-MMT		
1	521	521	Al-O-Si deformation	-
2	1041	1048	Si-O stretch	1030-1045
3	1637	1638	H-O-H bending	1610-1650
4		1713	Carbonyl group	1690-1760
5		2850	C-H stretching	2850-2960
6		3236	N-H stretch	-
7	3412	3414	H-O-H stretch	3410-3445
8		3617	Structural OH stretch	3597-3645

4.1.2 Thermal analyses

Figure 4-2 presents the thermal analysis performed by TGA whereas DTG (derivative thermo-gravimetric) curve is depicted in Figure 4-3. Only a single mass loss stage appeared for Na-MMT, which happened at approximately 250˚C. Subsequently, mass loss took place gradually but no sharp peak was observed. This mass loss stage was related to the decomposition of functional groups (Na^{+1}) present in the MMT. Generally, the presence of functional groups in clay minerals are possible at three locations; a) interlayer space, b) external surface and c) edges of the clay layer [182]. For MMT, the mass loss was due to the presence of inorganic cations in interlayer gallery as only a single mass loss stage appeared.

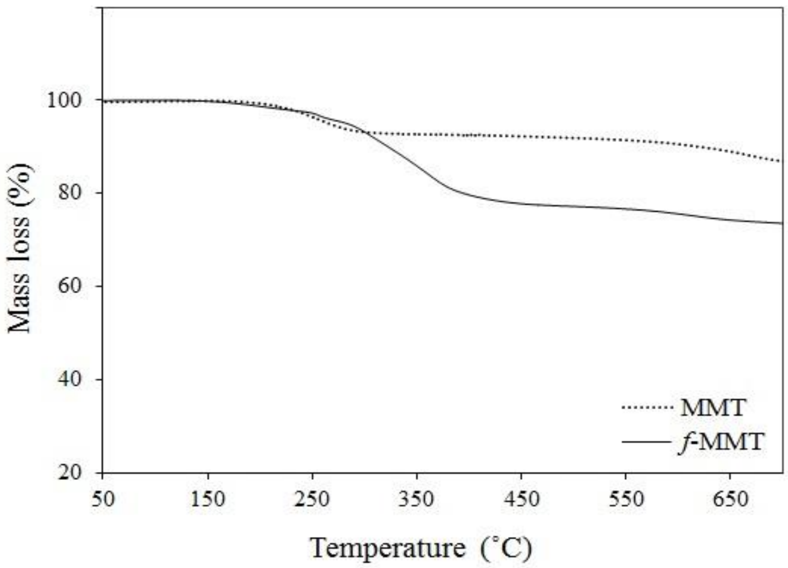

Figure 4-2: TGA analysis of MMT and *f*-MMT.

However, for *f*-MMT, the mass loss occurred in two stages at 260 and 358˚C as depicted by Figure 4-3. The first mass loss implied the presence of organic cation in the intercalated space which decomposed at 260˚C. The decomposition at the second stage implied the loss of organic groups at the external surface which were grafted onto Si-OH and Al-OH groups. Due to covalent bonding, these groups are stable compared to intercalated functional groups.

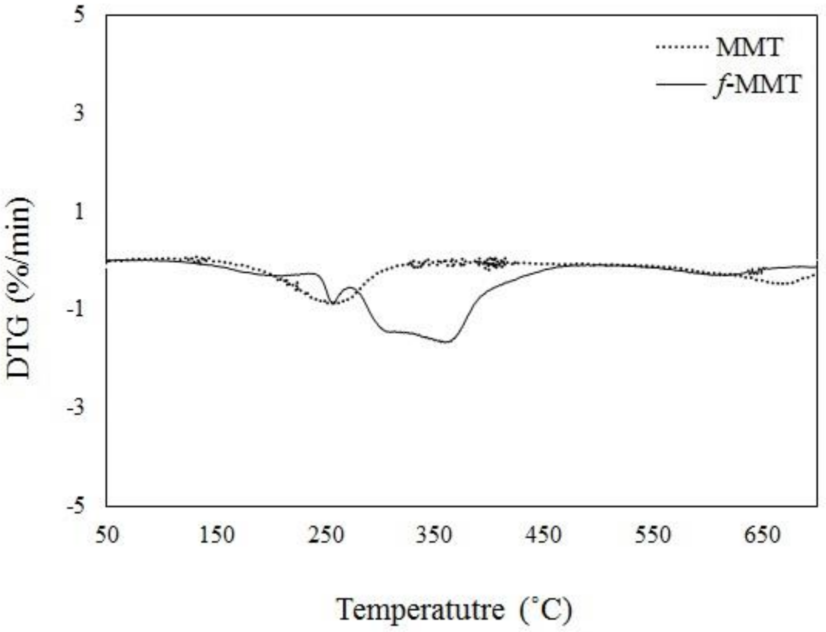

Figure 4-3: DTG curve for MMT and *f*-MMT.

From TGA and DTG analyses, it was observed that the decomposition temperature for *f*-MMT is well above the operating temperature for most processes. Moreover, the extent of attachment can be estimated from the difference between mass loss (%) in MMT and *f*-MMT, which is approximately 21 %. For *f*-MMT, mass loss from 120 to 800˚C was due to organic contents and structurally absorbed water. The mass loss for MMT was 7 % from 210 to 300˚C whereas a significant mass loss of 21 % was observed for *f*-MMT from 240 to 460˚C. The absorbed water content was believed to be 7 % and organic content was significant at approximately 21 %. The weight percent for structural water observed is similar to past literature, where 6.86 % of the structural water content was reported for MMT by TGA analysis [183].

4.1.3 Interlayer spacing evaluation

The interlayer distance of MMT which promotes dispersion in PEI matrix was measured by using X-Ray diffraction as shown in Figure 4-4. The basal spacing of Na-MMT calculated by Bragg's equation was 12.38 Å, which is consistent with the reported value of 12.397 Å [184].

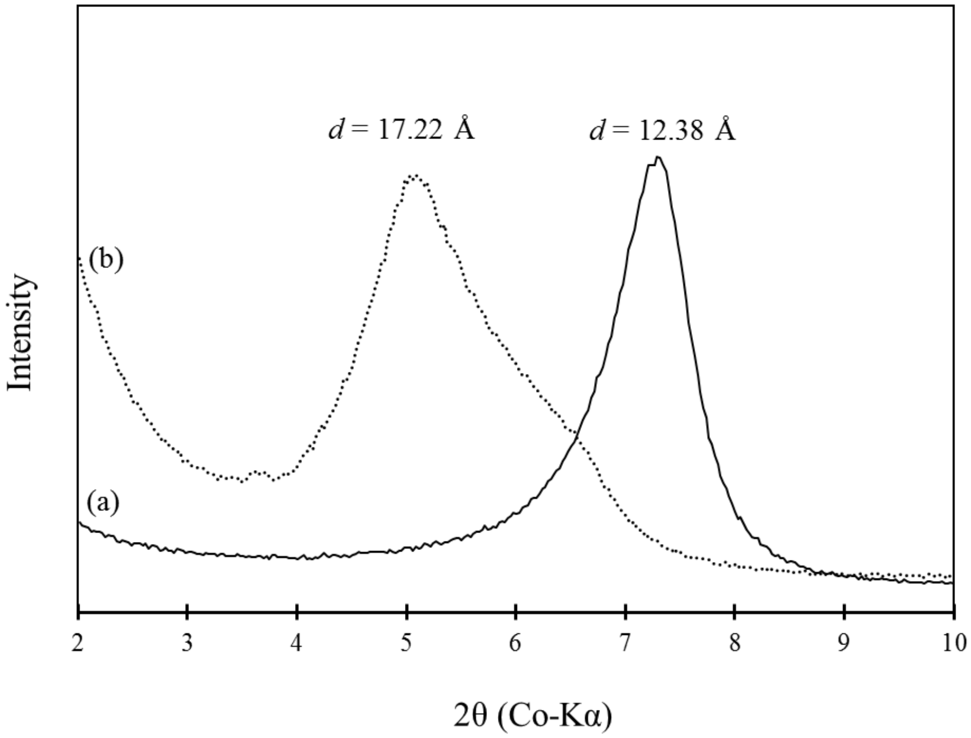

Figure 4-4: X-ray diffractogram of a) MMT and b) *f*-MMT.

The interaction between 12-aminolauric acid and Na-MMT gave lower 2θ value for *f*-MMT (17.22 Å), implying that the interlayer distance of *f*-MMT has expanded. Okada and Usuki who modified Na-MMT with the same organic cation also reported basal spacing as 17.2 Å, which further emphasized on the effectiveness of ω-aminolauric acid in increasing the interlayer distance of MMT [122]. The enhanced interlayer distance further weakened the interlayer van der Waals forces, which helped in MMT exfoliation in polymer matrix. The exfoliated form of MMT increased the dispersion within host polymer.

4.1.4 Dispersibility test

Table 4-2 presents the observations made by dispersing MMT and *f*-MMT in various solvents. MMT showed very good dispersibility in water due to its hydrophilic nature; however, it showed demixing when dispersed in ethanol. Zhou et al. reported similar observation when dispersing MMT in water and ethanol [184].

Table 4-2: Dispersibility[a] test of MMT and *f*-MMT in water and ethanol.

Samples	Water	Ethanol
MMT	++	+-
f-MMT	-	++

[a], ++: better dispersibility, uniform supernatant, lower sample is swelling.

+: good dispersibility, non-uniform supernatant, lower sample is swelling.

+-: bad dispersibility, clear supernatant, lower sample is swelling.

-: worse dispersibility, clear supernatant, lower sample is not swelling.

In contrast, *f*-MMT exhibited an opposite behavior in both water and ethanol. It showed worse dispersibility in water, but very good dispersion in ethanol. This is mainly due to the presence of long alkyl chains associated with the alkylammonium cations in *f*-MMT which increased its affinity towards organic solvent. Therefore, this dispersibility analysis depicts the hydrophobic nature of *f*-MMT, which made it suitable for uniform dispersion in hydrophobic PEI matrix.

4.2 Spinning parameters optimization for neat PEI hollow fibre membrane

In conventional membrane forming techniques, surface defects or voids are often created during phase separation process. These voids ranged from a few to tens of micrometers in length. In some cases, they move parallel to the phase separation front [22]. During phase inversion process, solvent and coagulant exchange produced polymer-rich and polymer-lean phases, which generate an unstable membrane structure. This exchange process may trigger void formation, which are mostly shaped as finger-like or sponge-like structure. Finger-like structure is generally formed due to instantaneous demixing whereas delayed demixing produced sponge-like macrovoids [23]. Different theories have been presented to explain the formation and suppression of macrovoids. According to Frommer, osmotic pressure between solvent and coagulant is the driving force in phase inversion technique. Therefore, the membrane surface porosity or voids creation can be controlled by reducing the osmotic pressure [159]. This can be achieved by the addition of salt in coagulation bath in order to limit water activity. Also, the addition of solvent in coagulation bath could reduce the concentration gradient for phase separation thus control macrovoids [160].

Along with these techniques, macrovoid formation can be minimized by controlling spinning parameters like dope viscosity, air gap, polymer concentration, delayed demixing, addition of highly viscous component, surfactant addition, high shear rate spinning, increasing coagulation bath temperature, or high elongational draw [23, 25, 26]. Between the aforementioned approaches, the easiest choice is to increase dope solution viscosity either by introducing highly viscous additive or by increasing polymer concentration. Kesting et al. claimed that a membrane with critical polymer concentration of 30 wt. % and viscosity of 5×10^4 cP would produce macrovoid-free membrane. This was the initial attempt to quantitatively correlate dope viscosity and macrovoid-free structures [162]. Peng et al. analyzed the effect of dope viscosity, air gap and take-up speed on the morphological structure of polysulfone, P84 and cellulose acetate. According to his findings, these parameters are closely associated to each other. The critical value of aforementioned parameters was studied and it was concluded that spinning of hollow fibres at critical parameters helped to eliminate macrovoids from polymer spun hollow fibre membranes [21].

4.2.1 Dope viscosity optimization

The polymer concentration in a dope solution has a significant impact on mean pore size, porosity and permeance of hollow fibre membranes. With the increase in polymer concentration, the solution viscosity and density increased, resulting in depression of void formation in the membrane microstructure [185]. For an asymmetric membrane consisting of porous sublayer and thin-skinned layer, only the upper thin-skinned layer is crucial in determining the separation properties of membranes. Thus, it is essential to fabricate membranes with a defect-free thin upper layer as it would lead to enhanced membrane performance. The spinning of hollow fibre membrane from a dilute polymer solution often leads to porous membrane with improved permeability but lower selectivity. On the other hand, higher concentration of polymer in the dope solution complicates the spinning procedure and often form upper skin layer with increased thickness, resulting in low permeance but high selectivity. In order to produce hollow fibre membranes with optimum performance and defect-free structural morphology, it is important to obtain the critical polymer concentration and dope viscosity [186]. The effect of polyetherimide (PEI) concentration on the structure of PEI hollow fibre membrane was studied while keeping all other parameters constant such as air gap, coagulant and coagulation bath temperature, take up velocity, and bore fluid flow rate.

Figure 4-5 represents the viscosity curve for PEI/NMP binary dope solution. The viscosity increased steadily with increasing polymer concentration. Nevertheless, above a specific limit, the slope suddenly becomes steeper. The extrapolation of the relatively linear sections of the viscosity curve generated an interception point which represents the critical polymer concentration. This extrapolated critical viscosity curve has been used extensively and proved to be valid for synthesis of asymmetric membranes. For PEI in NMP solvent, the critical dope viscosity was found at approximately 25 wt. % PEI concentration. This critical dope viscosity corresponds to the degree of chain entanglement for the particular polymer concentration. Above this critical point, the polymer chains exhibited significant entanglement which hinders the intrusion of non-solvent through the surface, resulting in reduced formation of

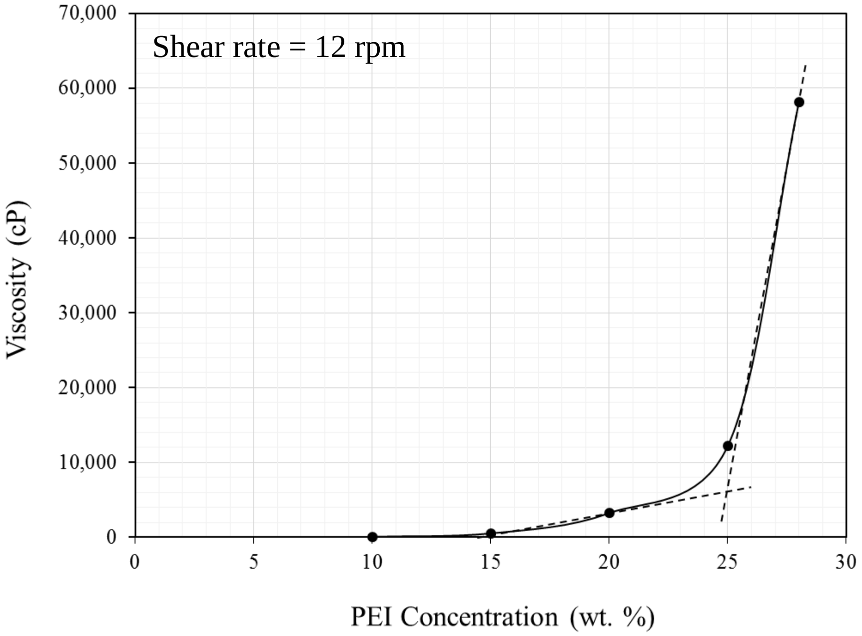

Figure 4-5: Dope (PEI/NMP) viscosity at room temperature vs PEI concentration.

macrovoids. For polymer concentration below the critical point, the chains are loosely packed; thus are able to move freely, which allows the non-solvent to penetrate through diffusion mechanism to form macrovoids on the membrane surface. In other words, the critical viscosity is the point at which a balance is observed between the highly dense structure and porous structure of membranes to achieve optimum separation performance [186].

Figure 4-6 displays the SEM images of PEI hollow fibre membranes spun at various polymer concentration. Figure 4-6 (a) shows the morphological structure of 10 wt. % PEI in NMP. A very thin top skin followed by narrow finger-like pores were observed. The low concentration of PEI in dope solution led to loosely packed structure, therefore, the non-solvent penetrated the inner surface of the hollow fibre membrane and created pores on the membrane surface. During membrane formation, the phase separation process was so instantaneous that finger-like pores that extended all the way to the outer surface were created. Similar morphology was found for 15 wt. % PEI/NMP dope solution as shown in Figure 4-6 (b). This indicated that 10 and 15 wt. % PEI concentration in NMP solvent was too low to form outer skin layer. Benjamin prepared PES/NMP/AL_2O_3 hollow fibre membrane and reported that extended finger-like morphology lead to poor separation performance and low mechanical strength [187].

At 20 wt. % PEI concentration, finger-like pores existed but the length and width of the pores have been greatly enhanced forming macrovoids. Also, thin-skinned layer was observed and finger-like pore structure dominated the outer skin layer. The presence of outer skinned layer may improve gas separation performance but the presence of macrovoids in the surface morphology suggested a membrane with higher permeance but lower selectivity. As shown in Figure 4-6 (d), at 25 wt. % PEI composition, finger-like structure was initiated from the inner skin layer which extended to the outer skin layer. For this polymer concentration, void formation was greatly reduced as compared with Figure 4-6 (e). The size and shape of finger-like structure was also uniform throughout the membrane surface. Membrane spun at this critical PEI composition will exhibit improved mechanical strength and separation performance.

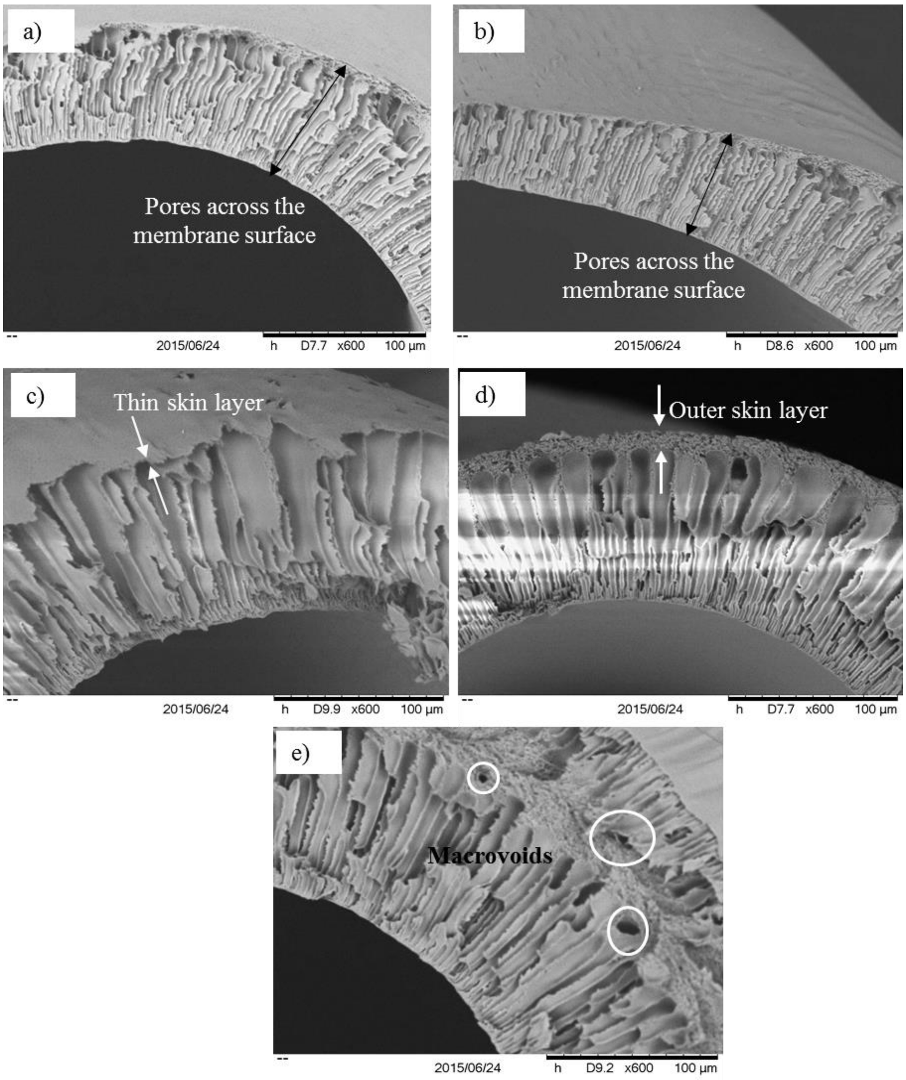

Figure 4-6: SEM cross sectional micrographs (magnification: 600) of PEI/NMP HF membranes with a) 10 wt.%, b) 15 wt.%, c) 20 wt.%, d) 25 wt.%, and e) 28 wt. % PEI concentration.

Hollow fibre membrane could not be spun at 30 wt. % PEI concentration due to exceedingly high viscosity value. Hence, 28 wt. % PEI concentration was considered as the upper limit. Figure 4-6 (e) revealed that at this polymer concentration, the pore structure was extremely distorted and non-uniform. Due to the dense and highly entangled polymer chains, the diffusion of internal solvent through the inner membrane surface was limited. Besides that, large spherical pores were also observed. The mechanical strength of this membrane was expected to increase. Nevertheless, its gas separation performance might be reduced due to the presence of macrovoids.

The optimum PEI concentration for PEI-/NMP hollow fibre membrane development was obtained at 25 wt. % concentration wherein a uniform, defect-free outer skin layer was observed and possessed uniform finger-like pores underneath the outer skin layer.

4.2.2 Air gap optimization

Air gap distance is another important parameter that influenced the membrane morphology and gas separation performance. Figure 4-7 (a, b, c) shows the hollow fibre membranes spun at small air gaps (0, 5, 10 cm). It was found that solidification process took place along with water penetration from the outer layer. This created highly non-uniform and larger voids which will ultimately affect membrane separation properties. For shorter air gaps, coagulation front will not have enough time to move to the outer skin layer before the nascent outer skin layer solidifies in the coagulation bath. Thus, the resulting membranes exhibit the desired defect-free structure. The membranes with air gap of 15 to 20 cm exhibit the same uniform structure around the periphery of the membranes as shown Figure 4-7 (d, e). This uniformity of microstructure brings mechanical strength and improved separation performance in hollow fibre membrane.

The presence of water as internal coagulant increased the polymer-coagulant interaction in solvent exchange process [188]. As a result, for longer air gaps, the dry process dominates due to longer time in air which ultimately provides opportunity for the internal coagulant to diffuse in the outer skin layer. During dry phase inversion, the occurrence of liquid-liquid phase separation forms a distorted nascent dense skin due to coalescence and deformation of polymer aggregates. The finger-like pores produced as a result of longer air gaps are larger in size as shown in Figure 4-7 (f, g, h) for air gaps 25, 30 and 35 cm. Occasionally, for very long air gaps, the coagulation front reached the outer skin layer before it touches the external coagulant in coagulation bath. As a result, porous or thin skin layer was obtained. Similar findings were reported by Wang et al., when PEI asymmetric hollow fibre membrane was developed using a dope containing NMP as solvent and ethanol as non-solvent additive. Pre- and post-treated PEI membranes were analysed to optimise the gas separation performance. At longer

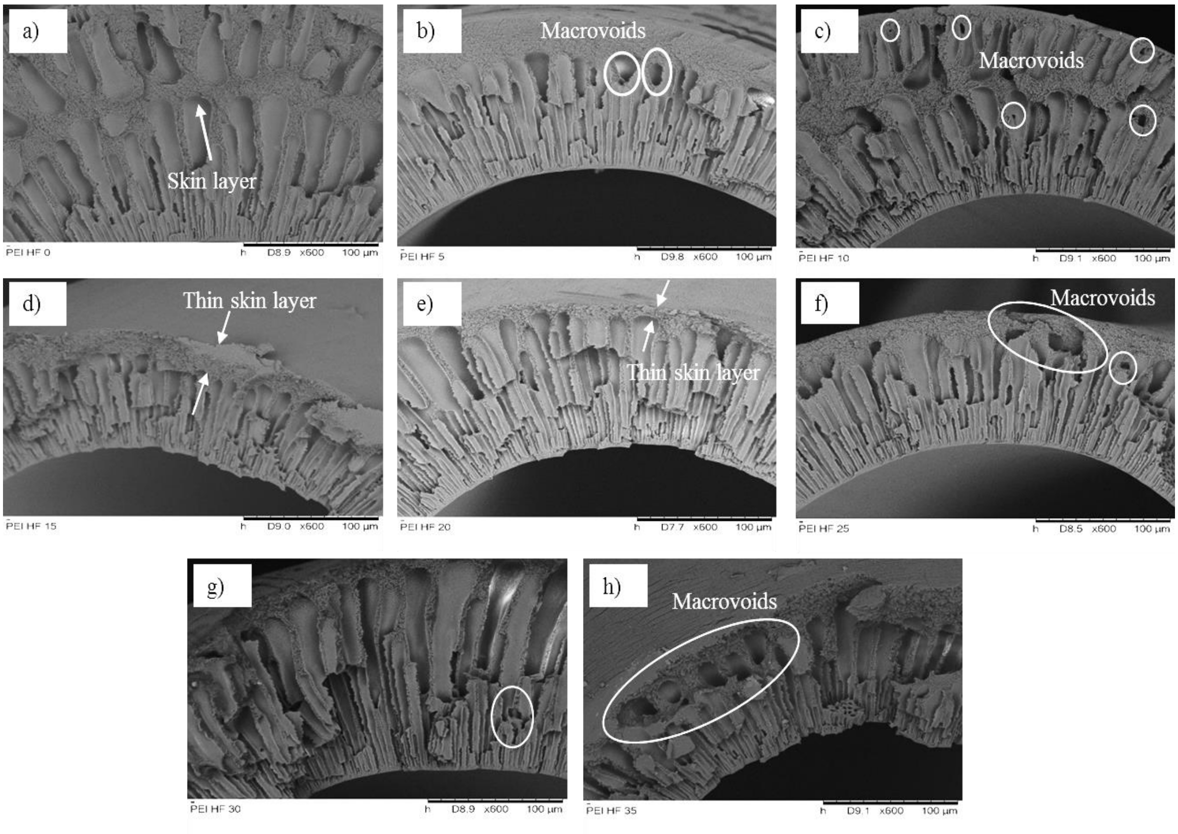

Figure 4-7: SEM cross sectional micrographs (magnification: 600) of 25 wt. % PEI/NMP hollow fibre membranes at (a) 0 cm, (b) 5 cm, (C) 10 cm, (d) 15 cm, (e) 20 cm, (f) 25 cm, (g) 30 cm, and (h) 35 cm air gap distance.

air gaps, macrovoids formation increased to a great extent; similarly, a highly distorted structure was observed when air gap was greatly reduced [189]. Dry processes were the only phenomenon that took place in the aforementioned condition whereas wet processes dominated in the latter case. It was proven that the gas separation performance can be enhanced by optimizing the air gap distance [163]. Similar results were obtained by Tsai et al for polysulfone hollow fibre membrane with variation in air gap distance [164].

In short, asymmetric membranes consist of porous sub-layer and thin skinned outer layer, in which the latter is the active participant in separation process whereas the former acts as support only [190]. Thus, the fabrication of defect-free outer thin-skinned layer is essential to produce high performance membranes. This is not only dependent on evaporation and coalescence in dry process but also highly dependent on the subsequent wet process and internal coagulation rate. The optimum air gap distance for PEI/NMP hollow fibre membrane was 15 or 20 cm where a very thin, defect-free outer skin was observed with uniform finger-like pores under the outer thin skin. This pore structure favors gas permeation through the membrane.

4.2.3 PEI-MMT HF membrane

After optimizing the spinning parameters for PEI polymer, MMT clay was incorporated in PEI matrix to develop PEI-MMT hollow fibre mixed matrix membranes. This section covers the morphological and thermal decomposition behavior of developed HFMM membranes. Moreover, the dispersion state of MMT within PEI matrix is also presented.

4.2.4 Morphological analysis

The morphology of developed PEI-MMT hollow fibre mixed matrix membranes was studied by using FESEM. Figure 4-8 shows the cross sectional morphology of PEI-MMT HFMM membranes at various MMT loading. The PEI-MMT hollow fibre membrane contains long finger-like pores and thin outer skin layer. The membranes with different MMT loadings show uniform pore size. However, the pores were larger

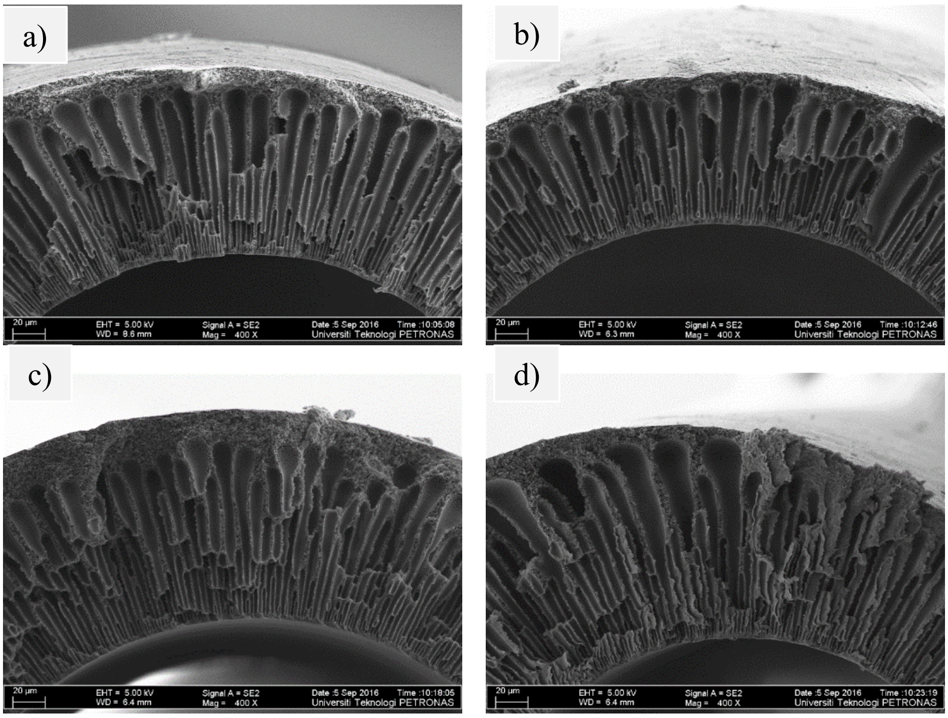

Figure 4-8: FESEM cross sectional images (Mag: 400) of PEI-MMT HFMM membrane containing a) 1 wt.%, b) 2 wt.%, c) 3 wt.% and d) 4 wt.% of MMT.

for 4 wt. % MMT loading, as observed in Figure 4-9 (d). This is due to the presence of higher concentration of hydrophilic MMT, hence PEI-MMT (4) attracts water at a faster rate compared to other membranes with low MMT loadings.

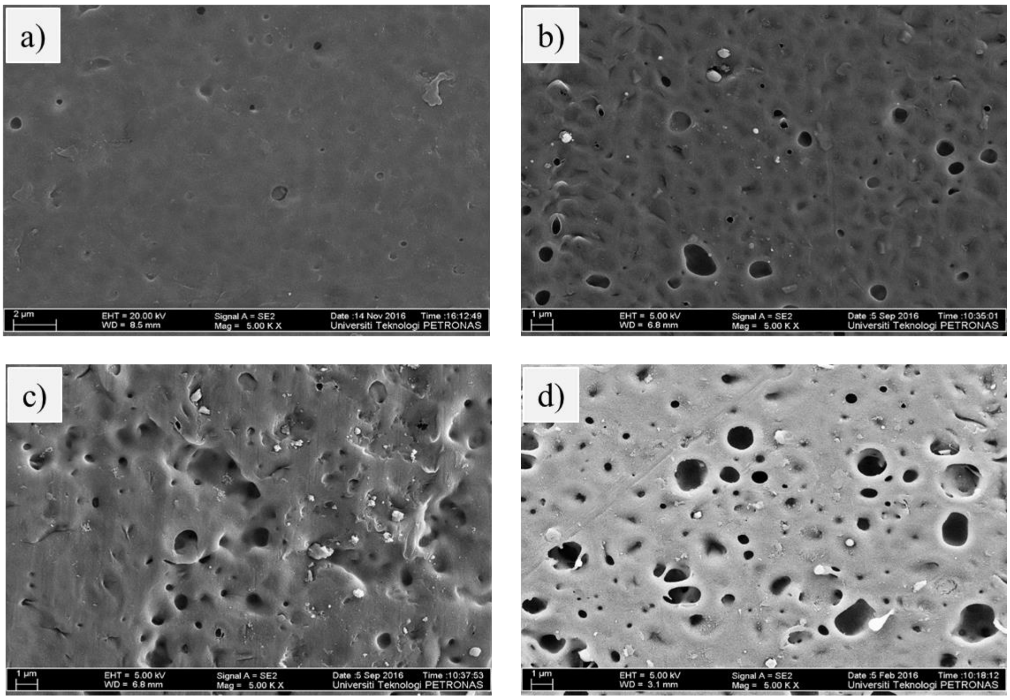

Figure 4-9: PEI-MMT hollow fibre membrane with a) 1 wt.%, b) 2 wt.%, c) 3 wt.% and d) 4 wt. % of MMT (Mag: 5K).

Moreover, since instant dissolution took place between solvent and coagulant during phase inversion process, finger-like pores with almost no macrovoids were formed due to the optimized synthesis parameters. All the developed PEI-MMT HFMM membranes have different surface morphology, as the membranes possess different affinity for water depending on their respective MMT loading. Also, the coagulant water during phase inversion brought the MMT to the surface which is evident from Figure 4-9. In addition, the size of voids at the surface of the membrane increased with increasing MMT loading in polymer matrix. These large-sized voids at the membrane surface have contrary effect on the membrane’s separation characteristics [191].

4.2.5 MMT distribution in PEI matrix

EDX analysis was carried out to study the distribution of MMT in PEI matrix. Uniform MMT dispersion provides similar hindrance for incident gas molecules to pass through the MMM. Agglomeration of MMT leads to weak MMT and PEI interfacial interactions which deteriorate gas separation performance of developed membrane.

Figure 4-10 presents the EDX micrographs of developed PEI-MMT membranes at various MMT loadings. Si or Al elements represent the presence of MMT in the polymer matrix. Moreover, it is evident that the presence Si increased from PEI-MMT (1) to PEI-MMT (4). The micrographs show uniform dispersion of MMT in host PEI matrix; however, the concentration of Si or Al appeared to be low.

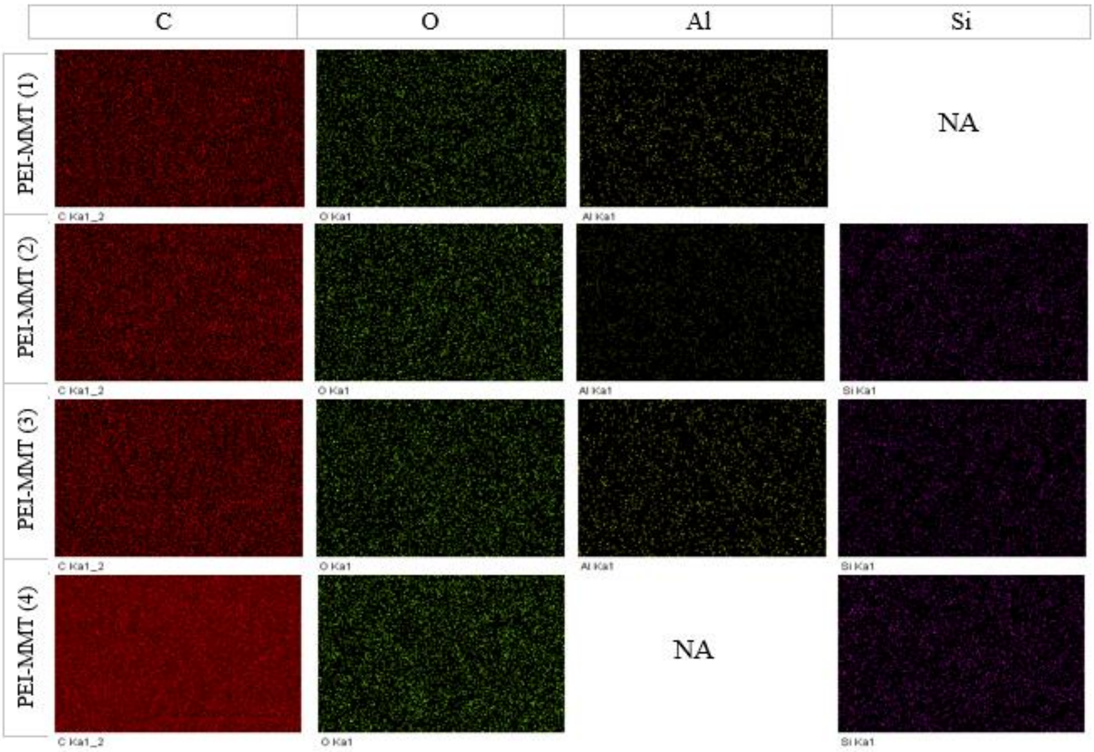

Figure 4-10: EDX micrograph of developed PEI-MMT HFMM membrane.

Table 4-3 presents the elemental analysis of developed membrane at the outer surface. It is noticed that Si or Al concentration increases with MMT loading, however, the concentration of Si at the surface is very low. This was most probably due to the presence of agglomerated MMT in the polymer matrix as evident in the cross-sectional micrographs.

Table 4-3: Elemental analysis of PEI-MMT HFMM membranes.

Elements	PEI-MMT (1) wt. (%)	PEI-MMT (2) wt. (%)	PEI-MMT (3) wt. (%)	PEI-MMT (4) wt. (%)
C	77.87	76.89	77.25	77.34
O	22.03	23.03	22.56	22.44
Si	-	0.06	0.08	0.21
Al	0.09	0.02	0.12	-
Totals	100.00	100.00	100.00	100.00

Figure 4-11 shows the cross-sectional images of MMMs with 3 and 4 wt. % MMT loadings. It is noticed that MMT agglomeration started at 3 wt. % loading and worsen at 4 wt. %. This agglomeration forming tendency of MMT limits its loading in polymer matrix as it showed adverse properties in terms of separation applications.

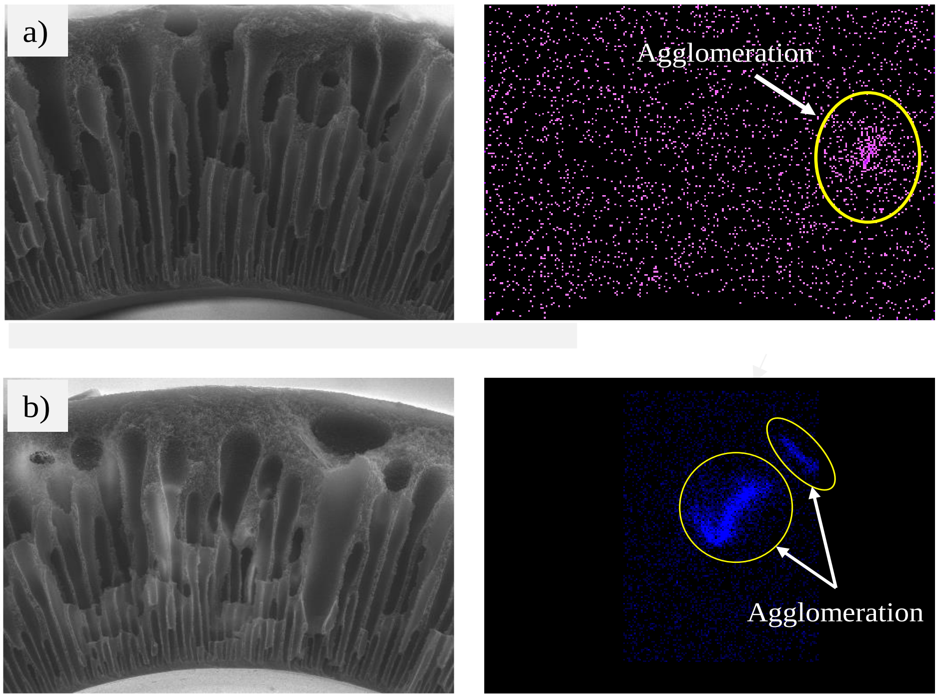

Figure 4-11: EDX mapping for cross sectional surface of (a) PEI-MMT (3) and (b) PEI-MMT (4)

4.2.6 MMT dispersion in PEI

TEM provides the visualization for distinctive dispersion of MMT in PEI matrix and comprehensive internal morphological characteristics of the investigated material. The dispersion of nano-clay in polymer matrix is classified as intercalated, exfoliated or tactoid/agglomerated.

Figure 4-12 (a, b) shows the TEM micrographs of PEI-MMT (2) and PEI-MMT (4) hollow fibre membranes. It is observed that MMT is present in tactoid form in PEI matrix, which is in agreement with FESEM micrographs. The dark lines indicate MMT tactoids or non-exfoliated layers; whereas the distant, displaced layers in lighter-grey indicate the intercalated form of MMT. Exfoliated forms exist in the absence of interactions between MMT layers and are marked with arrows. It can be observed that for PEI-MMT (2) membranes, MMT exists largely in tactoid form with low number of silicate layers. Several exfoliated layers are also available in the membrane matrix.

For PEI-MMT (4) membrane, the width of tactoid and number of layered silicate present in the tactoid also increased. This is due to the fact that MMT at higher concentration formed agglomeration and phase separated from the polymer matrix. Moreover, this particular trend of MMT in PEI matrix indicated weak MMT and PEI interfacial interactions which is mainly due to the organophobic nature of MMT. These observations are consistent with dispersibility analysis and EDX micrographs in Figure 4-10.

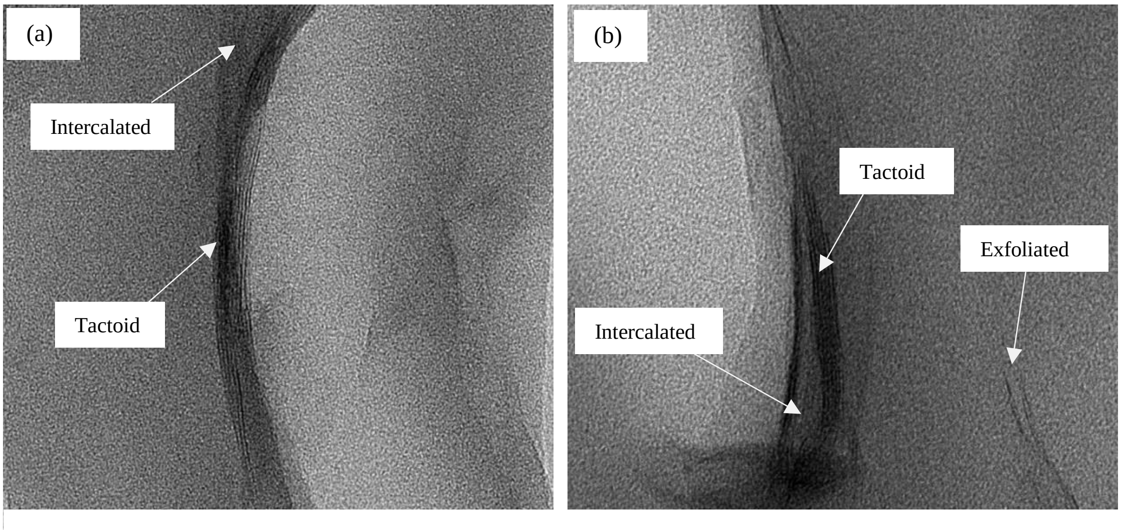

Figure 4-12: TEM micrograph of (a) PEI-MMT (2) and (b) PEI-MMT (4).

4.2.7 Surface roughness of PEI-MMT HFMM membranes

The surface topology of developed PEI-MMT HF membranes were studied via atomic force microscopy (AFM) in order to analyze the effect of MMT contents on the surface structure. Figure 4-13 presents the surface roughness of PEI-MMT MMMs containing 2 and 4 wt. % of MMT. The mean surface roughness parameter (Ra) that was dependent on the concentration of MMT increased with loading. For 2 wt. % MMT loading, the surface roughness was 22.38 nm which increased to 41.79 with 4 wt. % loading. This increase in surface roughness was due to high filler accumulation and less dispersion [192]. Similarly, increasing surface roughness by addition of MMT filler in poly(vinyl alcohol) was reported by Yeh et al. [193]. Moreover, Rezaei et al. prepared PVDF-MMT hollow fibre membranes and observed that surface roughness of developed membranes increased with increasing MMT loading [194]. In addition, the surface roughness affects the hydrophobic/philic properties and gas separation characteristics of developed membranes. Moreover, EDX analysis revealed that beyond 2 wt. % of MMT, agglomeration occurred which increased the concentration of voids at the membrane surface, as displayed in Figure 4-10.

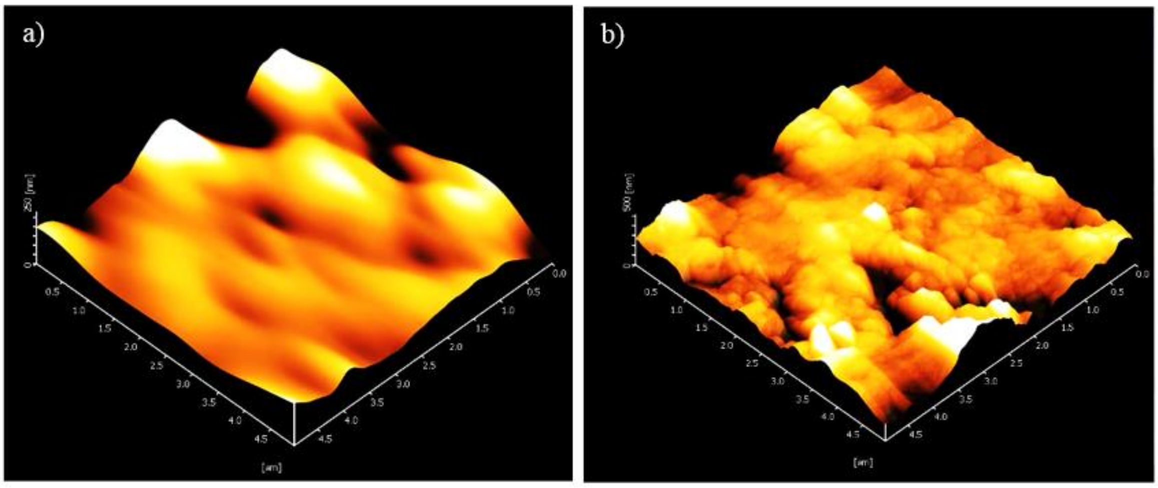

Ra = 22.38   Ra = 41.79

Figure 4-13: AFM 3D topography image of a) PEI-MMT (2) and b) PEI-MMT (4) HFMM membranes.

4.2.8 Thermal properties of PEI-MMT HF membrane

The thermal characteristics of PEI-MMT were analyzed through TGA and DSC analytical methods. TGA was used to determine the weight loss of spun PEI-MMT hollow fibre membranes with thermal treatment in the presence of nitrogen gas.

4.2.8.1 Thermal analysis

The thermal decomposition profile for PEI hollow fibre membranes at various MMT loading is shown in Figure 4-14. For simplicity, decomposition temperature was considered at 5 % weight loss. The thermograms showed that no weight loss occurred below 400˚C, which is due to complete solvent removal from the spun membranes.

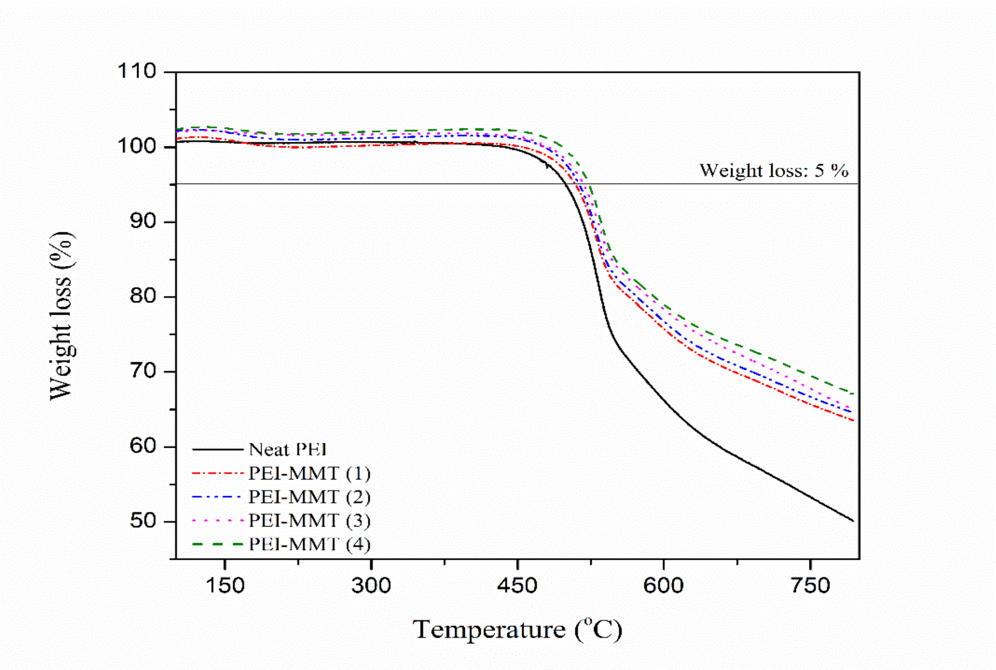

Figure 4-14: TGA analysis of PEI-MMT HFMM membranes.

The decomposition temperature for neat PEI membrane is 500.23˚C. However, the addition of 1 wt. % MMT enhanced the thermal stability to 523.27 ˚C. This improvement is attributed to the inherent thermal characteristics of MMT, as it absorbed a great amount of heat [132]. In addition, nano-fillers which settled between the polymer chains hindered the inter-chain segmental motion, which enhanced the energy

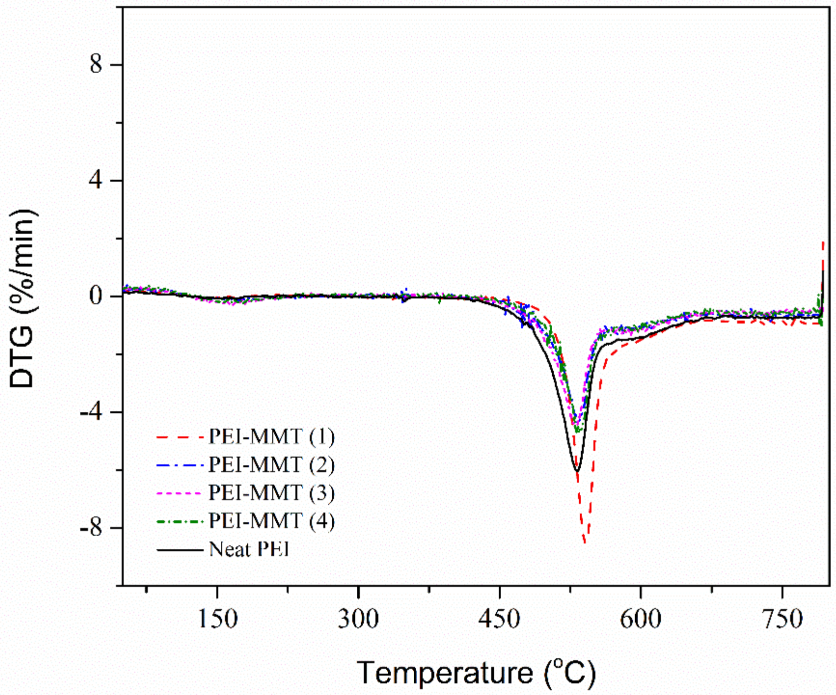

Figure 4-15: DTG curve of PEI-MMT HFMM membranes.

needed for polymer chain movement [195]. Moreover, the addition of 2, 3, and 4 wt. % MMT increased the decomposition temperature to 508.74, 514.09, and 517.27˚C, respectively.

Similar trend was observed by C-Y Liang when incorporating MMT filler in PES membrane [132]. The addition of MMT (2 to 20 wt. %) consistently improved the thermal stability of the MMM. J. M Herrra-Alonso also observed similar findings when mixing Cloisite Na^+ in PBMA [196]. The onset degradation temperature increased from 222 to 260˚C with the addition of clay from 0 to 5 wt. %. PMMA clay nanocomposite also showed similar trend, in which thermal stability improved due to higher amount of alumino silicate in MMT. Moreover, the addition of MMT in PSf matrix increased the decomposition temperature of the membrane. This improvement in decomposition temperature is due to the layered morphology of clay which restricted the diffusion of oxygen into the polymer matrix. The heat provided is absorbed by the clay platelets and delayed the decomposition process [20].

4.2.8.2 Glass transition analyses

DSC analysis was carried out in order to determine the effect of MMT loading on PEI-MMT mixed matrix hollow fibre membrane. It should be noted that the glass transition provides a qualitative evaluation of polymer chain flexibility in MMM [197]. Figure 4-16 presents the effect of MMT loadings on the glass transition temperature of PEI hollow fibre membrane.

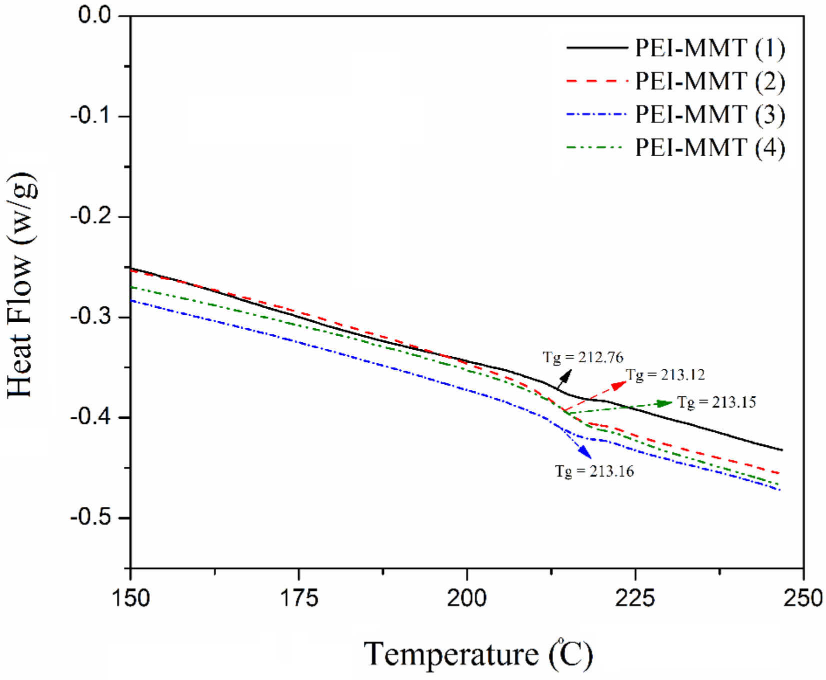

Figure 4-16: DSC curve for PEI-MMT HF membranes.

The addition of MMT resulted in a slight increase in T_g, which resulted in decreased amorphous phase of PEI-MMT MMM. The increase in T_g attributed to higher restricted segmental chain motion of polymer chains due to interfacial interactions with clay layers. C.Y Liang found similar observation when MMT clay was incorporated in PES polymer matrix [132]. The increase in T_g represents the chain rigidification when MMT was added in PES matrix. This might be due to the poor interaction between polymer and filler [198]. An increment of 1.03˚C is observed with 1 wt. % MMT loadings which increased up to 1.43˚C for 4 wt. % MMT loading. This increase in T_g with filler loading showed poor interfacial interaction between two phases with increased MMT loading.

Oh P. C and Mansur prepared PSf-MMT asymmetric MMM with 1, 3 and 5 wt. % loading of MMT and reported the increasing trend of T_g with filler loading [20]. It was speculated that the stiff clay platelets act as reinforcement to polymer chains at molecular level; which consequently obstruct the localized motion of polymer chains. As a result, membrane structure became more crystalline with MMT addition.

4.3 PEI-*f*-MMT HF membrane

The morphological and thermal characteristics of PEI-*f*-MMT HFMM membranes are discussed in this section. Subsequently, the dispersion of *f*-MMT in PEI matrix is studied via EDX analysis.

4.3.1 Morphological analysis

The cross-sectional morphology of spun PEI-*f*-MMT hollow fibre membranes is shown in Figure 4-17. The lower dope solution viscosity along with hydrophobicity resulted in instant solvent exchange during spinning. As a result, finger-like pores dominated in PEI-*f*-MMT HF membranes. All membranes consisted of thin outer skin layer and porous sub-layer. The thin outer skin layer is crucial in determining gas separation performance, whereas the inner layer only acts as the substrate. For all *f*-MMT concentrations, the outer skin layer obtained was uniform, whereas the inner sub-layers consisted of longer finger-like pores throughout the periphery of the membrane. These long finger-like pores were formed due to instant demixing of PEI and NMP. Water molecules diffused from the inner wall of spun HF, whilst NMP solvent migrated to the coagulant liquid. In addition, MMT particles were not observed from the micrographs. This suggests that *f*-MMT particles were dispersed uniformly throughout the matrix due to vigorous sonication of dope solution and organic modification of MMT particles [199]. The presence of long alkyl group in between the layers weaken the van der Waals interaction, thus, layered exfoliation took place during sonication.

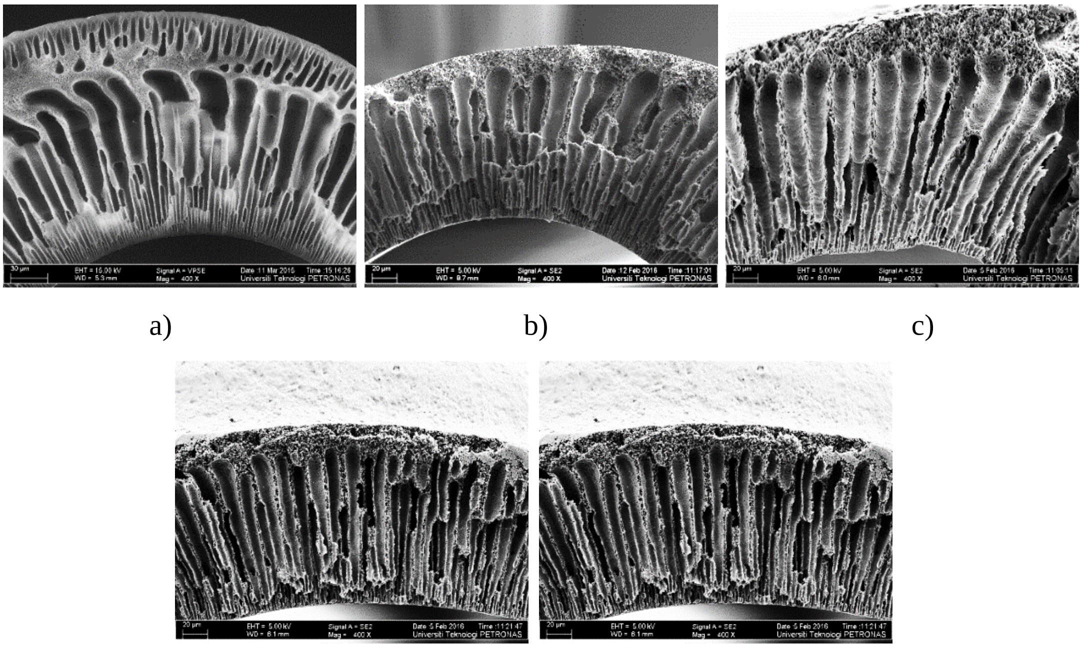

a) b) c)

d) e)

Figure 4-17: FESEM images of a) Neat PEI, b) PEI-*f*-MMT(1), c) PEI-*f*-MMT(2), d) PEI-*f*-MMT(3), and e) PEI-*f*-MMT(4) hollow fibre membranes.

The membrane morphology and mechanical properties are governed by phase inversion method. In particular, the thermodynamic and kinetic principles involved in phase inversion technique such as polymer-solvent interactions, solvent-coagulant interactions and dope viscosity affected membrane morphology [200]. With the increase in dope solution viscosity, non-solvent diffusion rate in polymer matrix reduced, therefore, the overall membrane forming process is slowed which resulted in irregular pores structure and thick outer skin formation [192]. Depending on the solvent/non-solvent interactions, various types of pores are created i.e. finger-like or sponge-like. The former is created as a result of instant solvent exchange with low molecular orientations whereas the latter is produced with slow exchange of solvent at higher chain orientations [201]. The length of these pores varies from several nanometers to tens of micrometers [202]. Finger-like pores promote gas permeance; however, if the pore size is too large, it will result in weak mechanical strength of HF membrane. Sponge-like fibers are helpful in producing highly selective membrane with good mechanical properties [22]. The pore formation continues until membrane surface touches the external coagulant which solidifies the structure and form dense outer skin layer.

4.3.2 Distribution analysis of *f*-MMT

Generally, the degree of filler dispersion in any polymer phase is a major concern which affects membrane separation performance. The energy dispersive X-ray spectroscopy (EDX) mapping in Figure 4-18 shows that distribution of Si elements on the membrane outer surface was uniform.

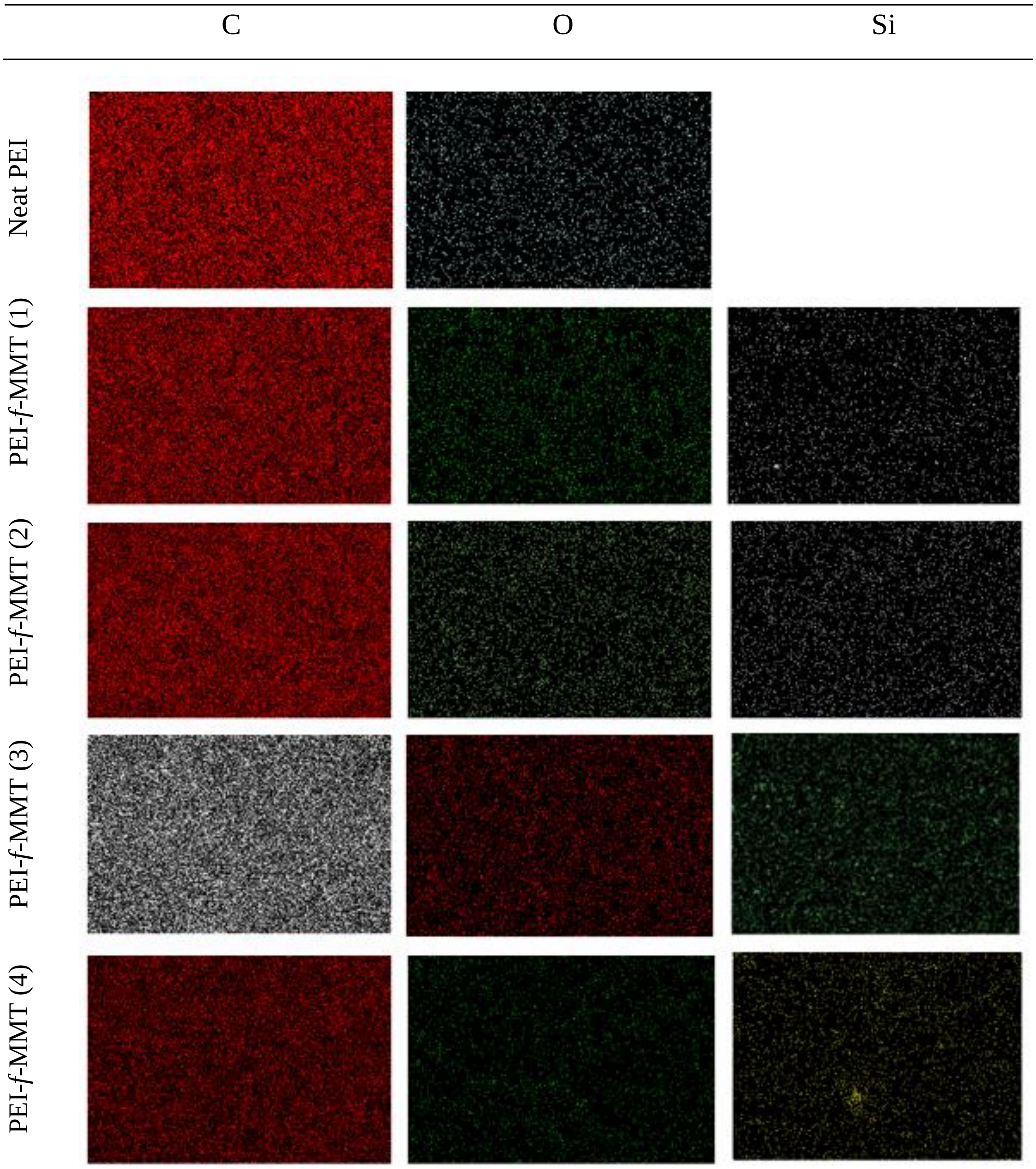

Figure 4-18: EDX mapping of C, O, Si elements in a) Neat PEI, b) PEI-*f*-MMT (1), c) PEI-*f*-MMT (2), d) PEI-*f*-MMT (3), and e) PEI-*f*-MMT (4) hollow fibre membranes.

The weight percentage of Si increased gradually from neat PEI HF membrane to 4 wt. % *f*-MMT due to the increased *f*-MMT loading. The concentration of *f*-MMT increased from inner to outer surface because elongation of fibre took place during dry wet phase inversion method. The fibre front moved inward and may facilitate the incompressible dope solvent to move outward which resulted in *f*-MMT migration to the outer layer [106].

Table 4-4: EDX elemental analysis of C, O, Si atoms at the outer surface of PEI-*f*-MMT hollow fibre membranes.

Elements	Neat PEI wt. (%)	PEI-*f*-MMT (1) wt. (%)	PEI-*f*-MMT (2) wt. (%)	PEI-*f*-MMT (3) wt. (%)	PEI-*f*-MMT (4) wt. (%)
C	78.63	78.93	78.15	76.74	77.40
O	21.37	20.65	21.11	22.18	20.70
Si		0.43	0.74	1.07	1.90
Total	100.00	100.00	100.00	100.00	100.00

The presence of *f*-MMT at the outer thin skin layer increases the gas selectivity due to the selective properties of clay towards the desired gas. Table 4-4 provides the atomic and weight percentage of atoms present at the HF membrane outer surface. The atomic and weight percent of Si increased gradually at the outer skin layer of spun HF membrane at increasing *f*-MMT concentration. At 4 wt. % *f*-MMT, small agglomeration was observed, but the overall distribution was uniform across the rest of the surface.

4.3.3 Dispersion study of *f*-MMT in PEI

Figure 4-19 (a, b) shows the TEM micrographs of PEI-*f*-MMT (2) and PEI-*f*-MMT (4) hollow fibre mixed matrix membranes, respectively. It is noticed that *f*-MMT showed better dispersibility in PEI matrix, compared to MMT as observed in Figure 4-12. This is due to the fact that *f*-MMT has higher basal spacing compared to MMT as depicted by XRD analysis (Figure 4-4). In addition, *f*-MMT is present in exfoliated and intercalated morphology as depicted by Figure 4-17 (a). Furthermore, dark grey lines showed tactoid morphology; however, the width of the tactoid is very low, signifying that only several layers of *f*-MMT combined to form tactoids.

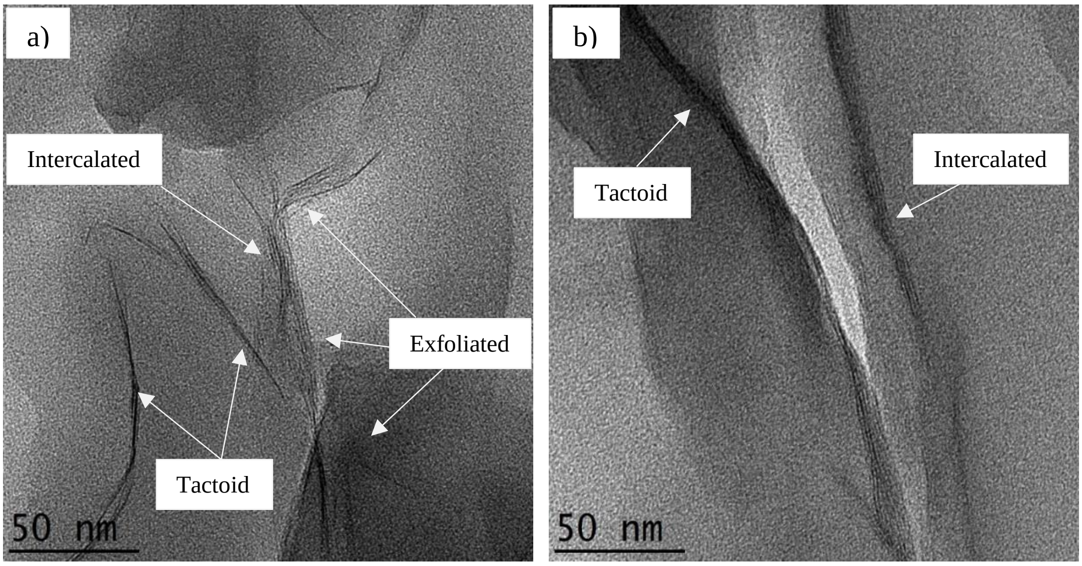

Figure 4-19: TEM micrographs of a) PEI-*f*-MMT (2) and b) PEI-*f*-MMT (4).

In contrast, when the concentration was increased to 4 wt. %, *f*-MMT formed agglomerates which exist largely in tactoid and intercalated morphology as depicted by Figure 4-19 (b). These observations are supported by EDX micrographs in Figure 4-18. Ismail incorporated Cloisite 15A, a type of clay, in PES matrix and observed that at 1 wt. % of filler, both intercalated and exfoliated morphology existed [134]. Furthermore, when cloisite15A concentration increased to 5 wt. %, layered silicates showed only intercalated morphology. Hence, it is noticed that lower clay concentration allows better dispersion of silicate layers in PEI matrix as depicted by the combination of exfoliated and intercalated morphology for 2 wt. % *f*-MMT loading.

4.3.4 Surface topography of PEI-*f*-MMT HFMM membranes

Figure 4-20 presents the 3D topographic images of PEI-*f*-MMT HFMM membranes. It is noticed that for 2 wt. % *f*-MMT loading, the developed membrane showed uniform surface topology with the mean roughness parameter (Ra) value of 12.57 nm. This is due to uniform *f*-MMT dispersion in PEI matrix as supported by Figure 4-17. The low surface roughness parameter indicates uniform dispersion and exfoliation of MMT filler [194]. Moreover, with increase in *f*-MMT loading from 2 to 4 wt. %, Ra increased from 12.57 to 16.75 nm. This increase in surface roughness was due to the fact that at

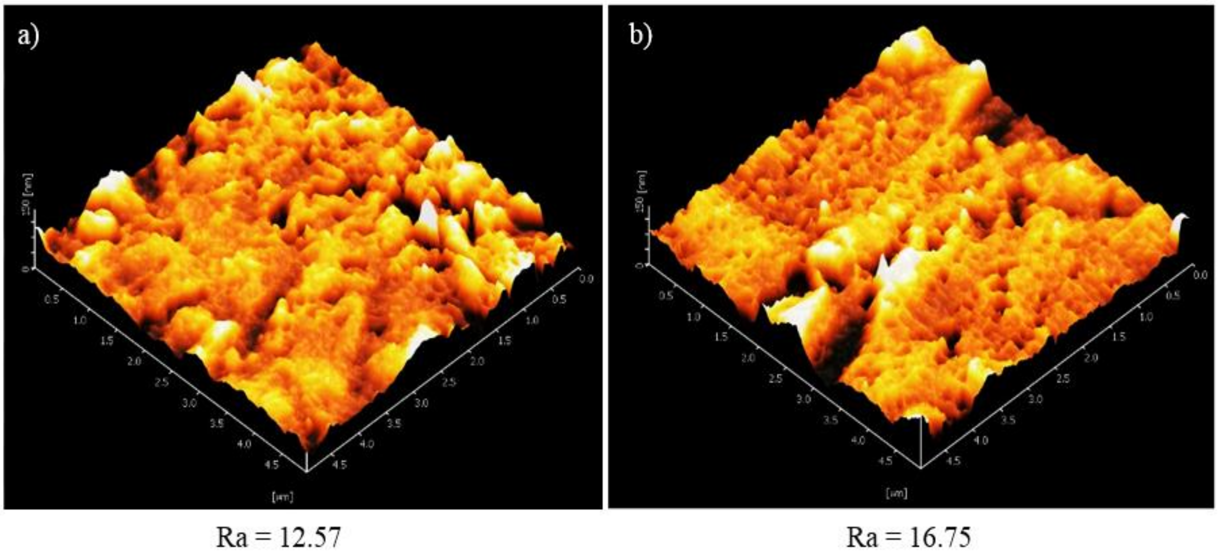

Figure 4-20: AFM 3D topography of PEI-*f*-MMT with a) 2 wt. % and b) 4 wt. % *f*-MMT loading.

4 wt. % loading, agglomeration occurred, which affects the surface structure and surface properties of PEI-*f*-MMT HF membranes [192], such as hydrophobicity and gas permeation behavior.

4.3.5 Thermal properties of PEI-*f*-MMT HF membrane

The thermal properties of spun HF membranes were studied using TGA and DSC. TGA measured the weight loss, whereas glass transition behavior was observed via DSC for the developed PEI-*f*-MMT hollow fibre membranes.

4.3.5.1 Thermal analysis

All fibers exhibited single major weight loss in the decomposition curve as shown in Figure 4-21. The onset degradation temperature for neat PEI HF membrane was approximately 438.16°C, whereas for other compositions of *f*-MMT, the weight loss was approximately 483.26°C. The +45 °C shift in degradation temperature implies that the thermal properties of hybrid membranes were enhanced. This increase in thermal stability resulted from the inherently good thermal properties of MMT [203].

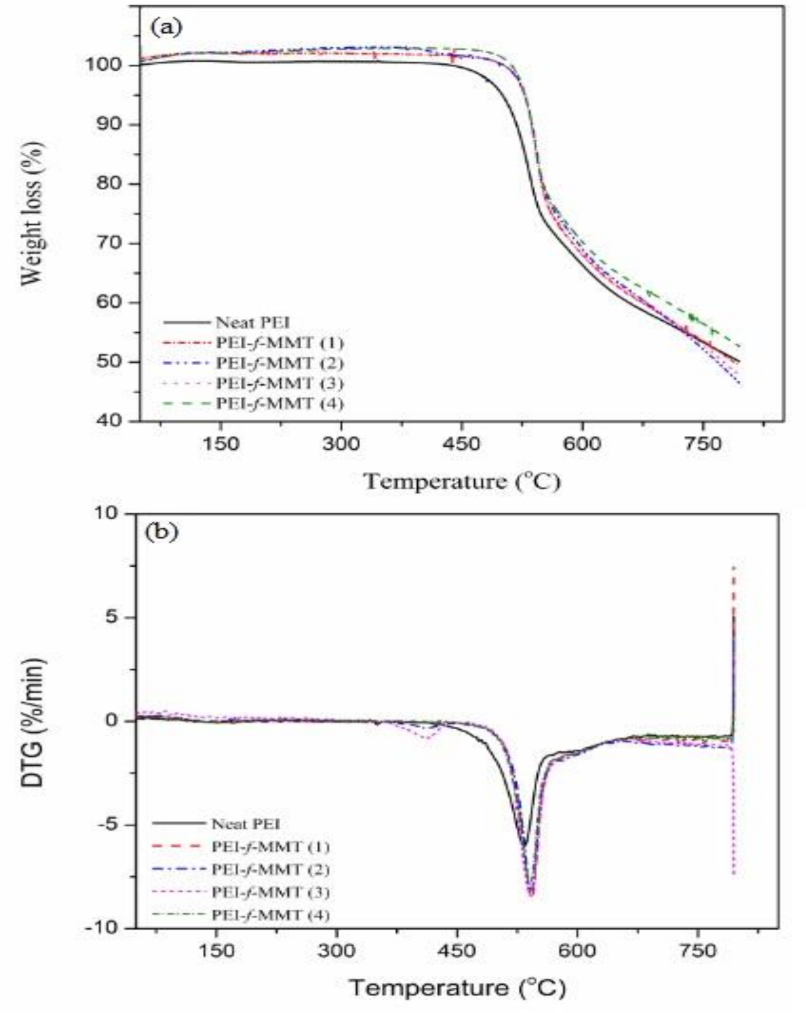

Figure 4-21: Thermal decomposition curves showing a) TGA and b) DTG profile for PEI-*f*-MMT HF membranes

Moreover, the enhancement in thermal stability is closely related to the interaction between clay particles and the polymer matrices [204]. The MMT generated an insulating layer at the polymer surface which hindered the decomposition of more volatile compounds at polymer decomposition stage. The shift of degradation temperature showed good interaction between *f*-MMT and PEI matrix. However, with increasing *f*-MMT loading, no significant improvement in decomposition temperature was observed. It is possible that at high loading, clay formed agglomerates, which weaken the interactions of two phases, hence formed active sites for degradation of polymer [131]. At low loading, the insulating properties were prominent which decreased at higher loading.

4.3.5.2 Glass transition analyses

Table 4-5 tabulates the glass transition temperatures of the spun fibers. With the addition of *f*-MMT, the T_g reduced gradually, signifying an increment in the amorphous phase of PEI-*f*-MMT MMM. Hsiao found similar decreasing trend in polyimide-clay hybrid film and speculated that the dodecyl groups in organophilic clays provided significant plasticization effect, resulting in reduction of glass transition temperature. This reduction in T_g is significant in MMT hybrid film due to its better dispersion [205]. The dispersed MMT particles hindered the polymer chain orientation, as a result, crystalline phase decreased.

Table 4-5: Glass transition temperature of spun membranes.

Sample	T_g (°C)
Neat PEI	211.73 ± 0.01
PEI-*f*-MMT (1)	209.81 ± 0.01
PEI-*f*-MMT (2)	209.09 ± 0.01
PEI-*f*-MMT (3)	209.08 ± 0.01
PEI-*f*-MMT (4)	208.74 ± 0.01

4.3.6 Hydrophobic/philic characteristics of developed HF membranes

Contact angle analysis of PEI-*f*-MMT is performed to determine the hydrophobic/philic attributes of spun hollow fibres. Measuring the contact angle is the simplest method to quantify the hydrophobicicity/philicity of the membranes. Water droplet is used as the contacting liquid. Figure 4-22 presents the PEI HF membrane contact angle measurement for PEI-MMT (1) membrane. Table 4-6 shows the contact angle for developed PEI, PEI-MMT and PEI-*f*-MMT HFMM membranes.

Neat PEI HF membrane has an average contact angle of 61.75˚. With the addition of hydrophilic MMT in PEI matrix, the contact angle reduced, which showed the increase in hydrophilic attributes of PEI-MMT HF membranes. In addition, with increasing MMT loadings in PEI matrix, the contact angle values decreased.

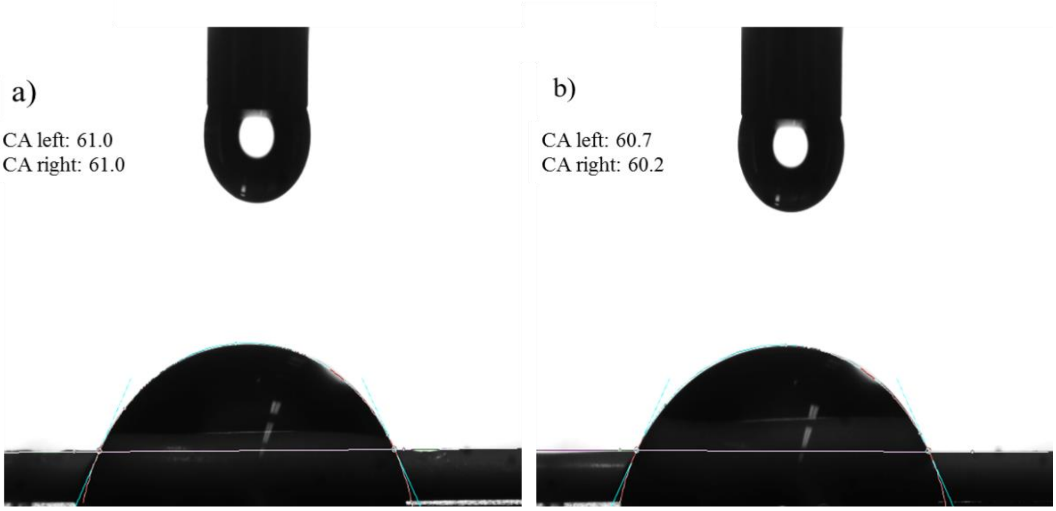

Figure 4-22: Contact angle measurement for PEI-MMT (1) HF membrane of a) Sample 1 and b) Sample 2.

Table 4-6: Contact angle measurements of spun HF membranes.

Membrane	Sample 1	Sample 2	Average Value
Neat PEI	61.6°	61.9°	61.75° ± 0.15
PEI-MMT (1)	61.0°	60.7°	60.85° ± 0.15
PEI-MMT (2)	60.0°	59.4°	59.70° ± 0.30
PEI-MMT (3)	59.5°	58.5°	59.00° ± 0.50
PEI-MMT (4)	59.4°	52.5°	55.95° ± 3.45
PEI-*f*-MMT (1)	63.1°	63.0°	63.05° ± 0.05
PEI-*f*-MMT (2)	74.9°	72.7°	73.80° ± 1.10
PEI-*f*-MMT (3)	71.0°	69.7°	70.35° ± 0.65
PEI-*f*-MMT (4)	63.2°	61.9°	62.55° ± 0.65

In contrast to MMT, modified MMT contains hydrophobic attributes which improve the filler dispersion and surface morphology of PEI-*f*-MMT HF membranes. The improved surface morphology leads to increased hydrophilic characteristics. There is a trend of increasing contact angle with increased *f*-MMT loading in hydrophobic PEI matrix. Since the contact angle values depend on material characteristics and surface topology, the sudden decrease for 4 wt. % *f*-MMT is due to increased surface roughness as a result of *f*-MMT agglomeration. DashtArzhandi reported similar observations when hydrophobic MMT was incorporated in PEI matrix [199]. The contact angle increased to 86˚ with 1 wt. % addition compared to neat PEI membrane's value of 77˚. However, further addition of hydrophobic MMT (3 wt. % and 5 wt. %) decreased the hydrophilic characteristics due to filler agglomeration.

4.4 Gas permeation performance

The developed asymmetric hollow fibre membranes at various filler loading and pressure variations were evaluated on the basis of gas separation characteristics. The separation characteristics are determined by the permeance of CO_2 and CH_4 gases at room temperature and 2 to 10 bar feed pressures. The permeance and selectivity were calculated by using equation (3-2) and (3-3), respectively. Since the membrane thickness varies in asymmetric membranes, the gas transport is calculated in pressure normalized flux or permeance in GPU units.

The following section covers the effect of MMT, *f*-MMT and PDMS coated membranes at various pressure.

4.4.1 Single gas performance of PEI HF membrane

This section elaborates on the performance of PEI-MMT HFMM membrane for CO_2 and CH_4 gases at various feed pressure and MMT loadings.

4.4.1.1 Effect of pressure on neat PEI HF membrane

Figure 4-23 presents the CO_2 and CH_4 permeance at 2 to 10 bar feed pressure. CO_2 permeance increased from 323.98 GPU at 2 bar to 344.23 at 4 bar. Above 4 bar pressure, a decline in CO_2 permeance was observed until 8 bar. Since PEI is glassy in nature, there are available free volume between the stiff polymer chains. However, when

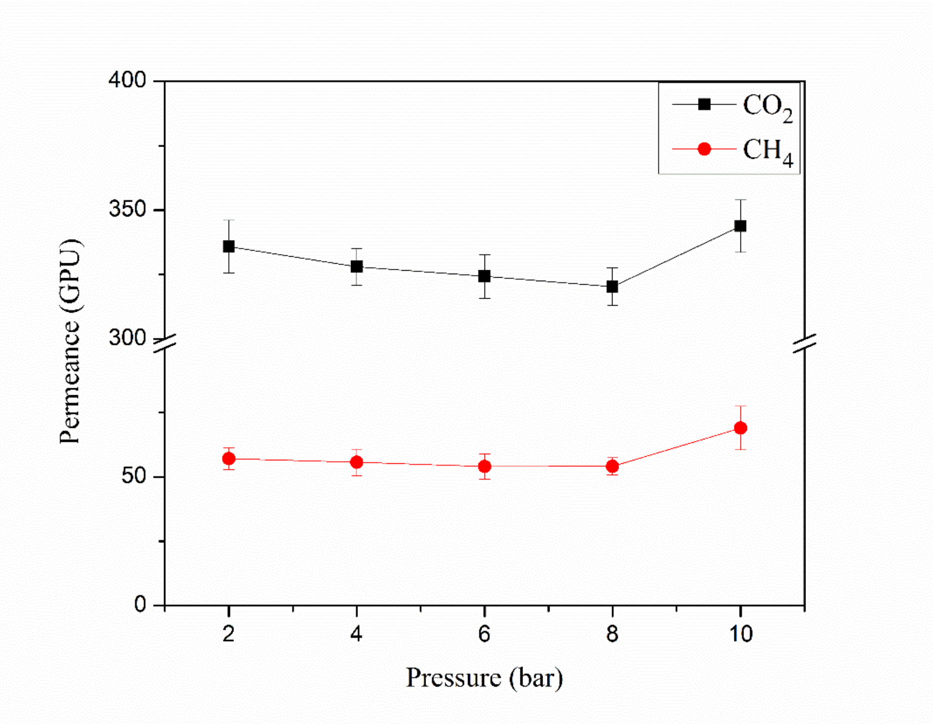

Figure 4-23: Permeance of pure CO_2 and CH_4 gases for neat PEI HF membrane.

pressure increased, the polymer chains are packed more closely. This ultimately reduced the available free volume and gas transport mobility through the matrix [206]. Moreover, the sorption of gases in glassy polymers is complicated. This may be explained by dual-sorption model, which consists of Henry's law of dissolution for rubbery phases, whereas Langmuir behavior is associated with micro voids available which are present in glassy polymers [207]. With increasing pressure, the micro voids start diminishing. As a result, Henry's law of dissolution applied, in which with increasing pressure, the solubility of CO_2 increases initially but reaches a constant value [208, 209]. Similar observation is observed from 2 to 8 bar; however, increasing trend after 8 bar is due to CO_2 induced plasticization effect. The reason for such low plasticization pressure is the asymmetric morphology of the membrane. Generally, for asymmetric membranes, the plasticization behavior of polymer does not only depend on the pressure alone. It is also affected by the thickness of the membrane. J. Xia prepared thin skinned layered membrane with Extem, a type of PEI [210]. According to his findings, plasticization was observed beyond 8 bar pressure. The chain packing in integrally skinned asymmetric membrane is more compact compared to dense membrane and is responsible for the plasticization behavior [211].

Unlike CO_2 permeance which has high affinity towards PEI matrix, the transportation of CH_4 gas through the membrane is governed by solution-diffusion mechanism which depends on the relative size of gas molecules. Due to smaller in size and linear structure of CO_2 compared to CH_4 gas, CO_2 mobility is higher than CH_4 gas in polymer matrix. However, a slight decrease of CH_4 permeance is observed up to 8 bar. At lower pressure, the CH_4 gas molecules diffused in inter-segmental packing defects. Nevertheless, with further pressure increase, the diffusivity in aforementioned defects reached its maximum limit and gas transportation rate decreases [212]. Similar decreasing trend for CH_4 gas is observed by various researchers with increasing feed pressure [213, 214].

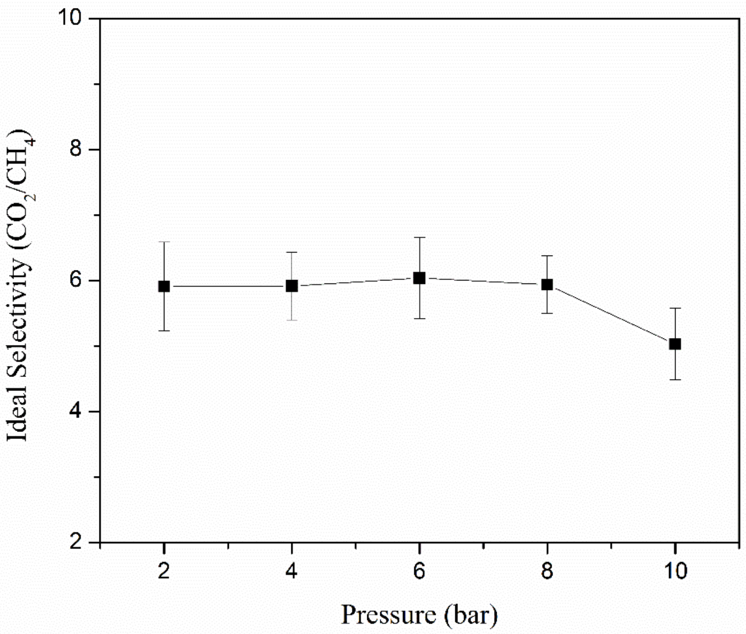

Figure 4-24: Ideal selectivity of neat PEI membrane at various pressure.

Figure 4-24 shows the ideal selectivity (CO_2/CH_4) curve for PEI HF membrane at feed pressure of 2 to 10 bar for CO_2 and CH_4 gases. The ideal selectivity displays an increasing trend until 8 bar. This is due to the decrease in CH_4 diffusivity with increasing feed pressure, since CH_4 possesses larger kinematic diameter compared to CO_2. An opposite selectivity behavior is observed beyond 8 bar pressure due to CO_2

induced plasticization. This reversed-selective performance beyond plasticization pressure was reported by many researchers [2, 210].

4.4.2 Single gas permeation of PEI-MMT HFMM membranes

The performance of PEI-MMT HFMM membranes in terms of permeance and ideal selectivity at various gas feed pressure and filler loadings are evaluated and compared with neat PEI HF membrane.

4.4.2.1 Effect of pressure on PEI-MMT HFMM membrane

Figures 4-25 and 4-26 show the permeance of CO_2 and CH_4 gases at various feed pressure and at room temperature across PEI-MMT HFMM membranes. The permeance of both CO_2 and CH_4 gases increased with pressure from 2 to 10 bar. This upward trend is due to the weak interfacial interaction between hydrophobic polymer and hydrophilic MMT, which ultimately results in MMT agglomeration and microvoids generation at the surface layer as described in Figure 4-9. When the transmembrane

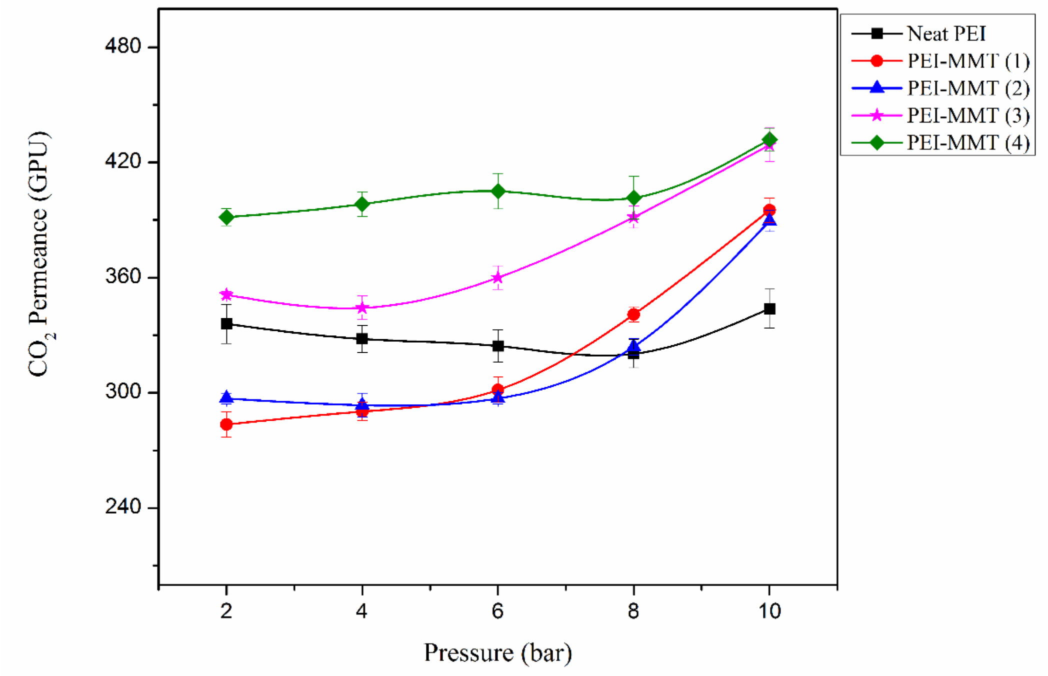

Figure 4-25: CO_2 permeance of PEI-MMT HFMM membranes at various feed pressure.

pressure increased, the micro voids widened. As a result, the permeance of both CO_2 and CH_4 gases increased contrary to neat PEI HF membrane. The permeance increase for 1, 2, 3 and 4 wt. % MMT loading is 39.4, 31.1, 22.3, and 10.3 % higher for 10 bar pressure than at 2 bar pressure. Since PEI-MMT with 4 wt. % loading contains more surface defects as depicted in Figure 4-9, the CO_2 permeance is 20.8 % higher than neat PEI membrane at 2 bar.

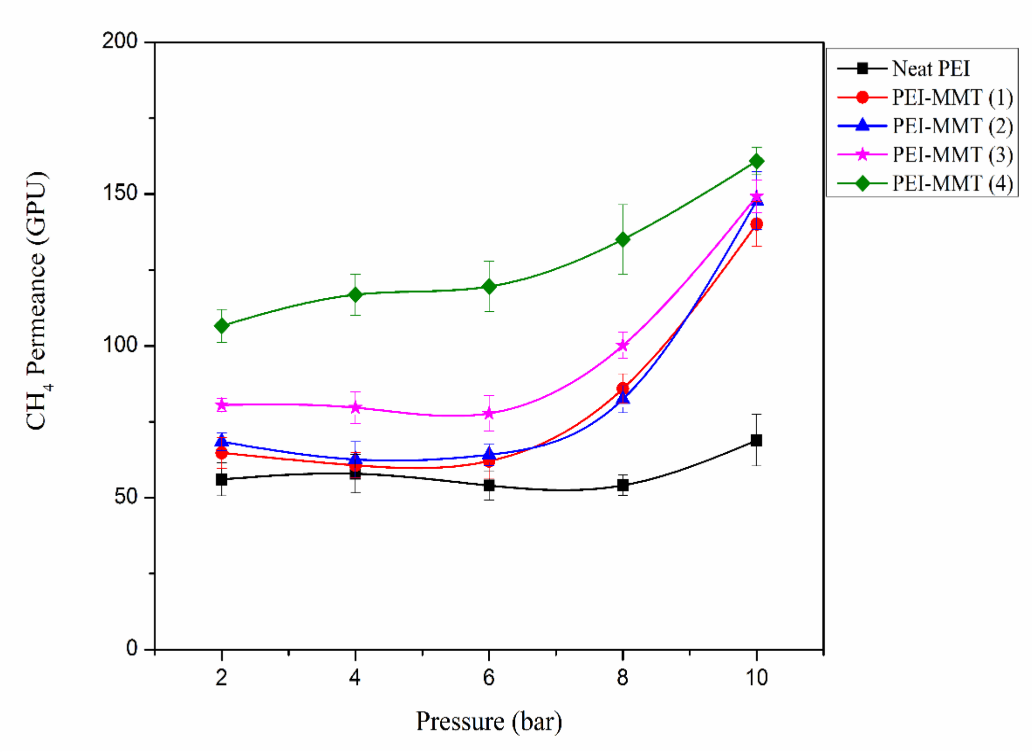

Figure 4-26: CH_4 permeance of PEI-MMT HFMM membranes at various feed pressure.

Figure 4-26 shows the permeance of CH_4 through PEI-MMT HFMM membranes at various feed pressure. The CH_4 permeance showed similar upward trend as observed for CO_2 gas. Although, CH_4 gas molecules are larger than CO_2 molecules, the permeance values are lower compared to CO_2. However, with increasing feed pressure, the permeance showed an increasing trend, which is opposite to neat PEI HF membrane. The CO_2 permeance increase for PEI-MMT (1), PEI-MMT (2), PEI-MMT (3), and PEI-MMT (4) is 12.8, 20.5, 44.6, 92.8 % higher than PEI membrane at 2 bar.

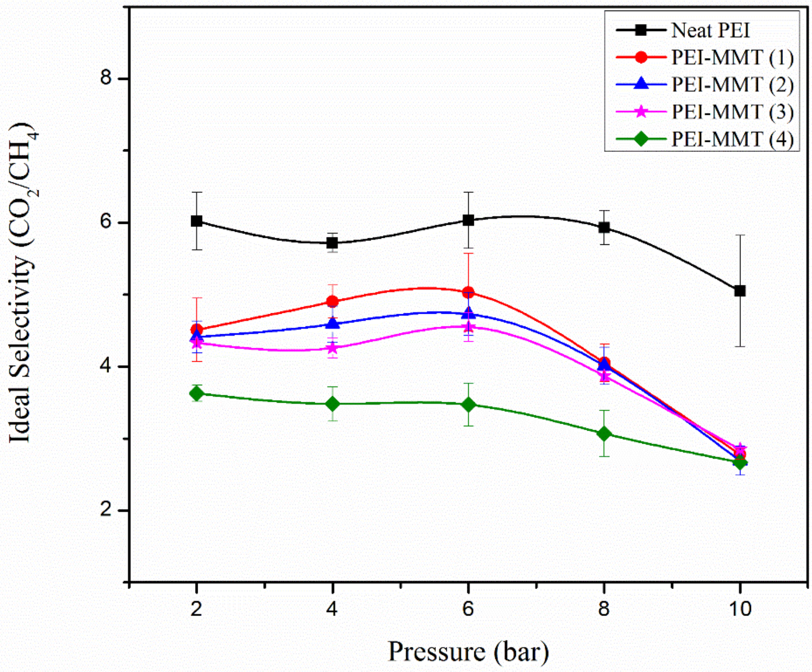

Figure 4-27: Ideal selectivity of PEI-MMT HFMM membranes at various feed pressure.

Figure 4-27 shows the ideal CO_2/CH_4 selectivities for neat PEI and PEI-MMT HFMM membranes at various feed pressure. Due to the existence of MMT agglomeration and microvoids, the selectivity of MMMs are found to be lower than neat PEI membranes. PEI-MMT (1) shows better CO_2/CH_4 separation performance compared to other MMMs, however, there was 22.4 % decrement compared to neat PEI membrane at 2 bar. These findings are consistent with literature, where Hashemifard developed MMM with hydrophilic MMT incorporated in PEI matrix, and reported that ideal CO_2/CH_4 selectivity reduced to 11.06 from 43.10 for neat PEI membrane [100].

4.4.2.2 Effect of filler loading on PEI-MMT HFMM membranes

Filler concentration may affect the gas separation performance of MMMs, therefore, MMT loading is one of the parameters considered for this study. Figure 4-25 shows the CO_2 permeance of PEI-MMT HFMM membrane with increasing filler concentration. At 1 wt. % addition of MMT, the CO_2 permeance decreased compared to neat PEI membrane at 2, 4, and 6 bar pressure, however, an opposite trend is observed at 8 and10 bar pressure. Moreover, 2 wt. % MMT loading also shows similar trend. For 1 and 2 wt. % MMT, the filler dispersed uniformly through the PEI matrix and created tortuous path in the gas pathways as observed in Figure 4-12. This ultimately restricted the mobility of incident gas molecules and decreased the gas permeance through the membrane. However, at 3 wt. % loading, MMTs tend to form agglomerates within the host polymer which created weak interfacial interactions, as observed in Figure 4-11. Generally, the MMMs showed an increase in CO_2 permeation for all MMT loading and feed pressure. Greater chain perturbed orientations, Knudsen diffusion or absence of polymer chain intercalation at interlayer space of clay are the common issues that resulted in lowering the polymer clay interfacial interactions and enhanced the CO_2 permeance through the membrane [100]. In addition, the aforementioned issues become more adverse at higher feed pressures.

A similar trend is observed for CH_4 gas permeance across PEI-MMT HFMM membrane as shown in Figure 4-26. Since diffusion is the prominent gas transport mechanism for CH_4 molecules through PEI matrix, the permeance is low compared to CO_2 gas due to molecular size variation. Moreover, the dispersion of clay platelets creates tortuous path which also forms obstacles especially for larger molecules of CH_4 gas. CH_4 permeance increased consistently with MMT loading and showed higher values for 4 wt. % loading. This increase in CH_4 permeance for PEI-MMT (4) was due to the presence of surface defects as observed in Figure 4-9. Liang et al. found that the use of higher loadings of MMT can lead to severe agglomeration, causing pinholes or other defects to the membrane [132].

Moreover, PEI-MMT HFMM membrane showed higher mobility for CH_4 gas molecules compared to neat PEI HF membrane due to weak interfacial interactions, particularly at 10 bar pressure. In addition, the surface defects or chain rigidification takes place around MMT platelets. Hence, higher CH_4 permeance is observed at 8 and 10 bar pressure compared to neat PEI membrane. At 10 bar pressure for 3 and 4 wt. % loading, the increase in CH_4 permeance is 118.4 and 135.0 % higher compared to neat PEI.

Figure 4-27 presents the ideal selectivity of PEI-MMT HFMM membrane. As can be seen, the membrane selectivity decreases compared to neat membrane. Subsequently, the PEI-MMT MMM CO_2/CH_4 separation performance decreases consistently with increasing pressure. This is true for all MMT loading at all pressure. Similar observations with hydrophilic MMT incorporated in PEI matrix was reported by Hashemifard [100]. At 1 wt. % MMT loading, the relative selectivity for MMM reduced by 74 %. This phenomenon was governed by the void morphology that was developed due to local agglomeration of MMT that exceeded the selective skin layer of asymmetric PEI-MMT MMM.

4.4.3 Single gas permeation of PEI-*f*-MMT HFMM membrane

This section elaborates on the performance of PEI-*f*-MMT HFMM membrane for CO_2 and CH_4 gases at various feed pressure and *f*-MMT loadings.

4.4.3.1 Effect of pressure on PEI-f-MMT HFMM membrane

Modified MMT (*f*-MMT) was incorporated at various loading in PEI matrix and spun in hollow fibre geometry. Figure 4-28 displays the CO_2 permeance of PEI-*f*-MMT HFMM membranes.

With increasing pressure, CO_2 permeance showed downward trend. These variations with pressure is consistent with dual-sorption model for glassy polymers. The perturbed chains in glassy polymers increased the free volume for incident gas molecules. With increasing pressure, the free volume decreased the sorption capacity of PEI matrix. As a result, the sorption behavior depends on Henry’s diffusion law and increasing pressure caused decrement in CO_2 diffusion through the PEI membrane. Similar decreasing trend is observed for all PEI-*f*-MMT HFMM membranes until 8 bar pressure. As mentioned earlier, the plasticization pressure for PEI thin layer membrane reduced with decrease in membrane top layer thickness. Beyond the plasticization pressure, the permeance of CO_2 gas through the membrane increases to a great extent.

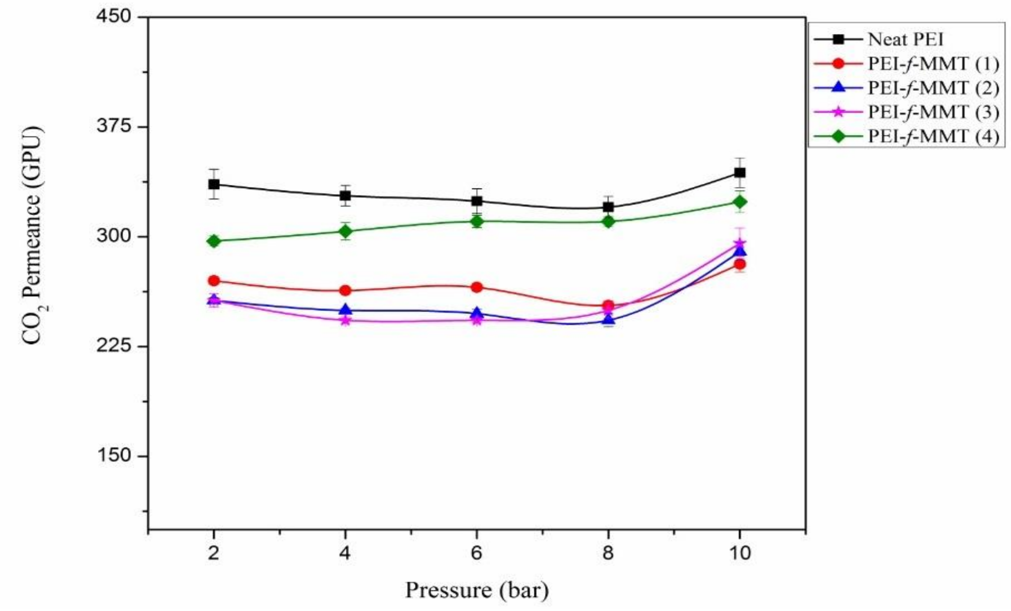

Figure 4-28: CO_2 permeance for PEI-*f*-MMT HFMM membranes against various feed pressure.

Similar with CO_2 permeance behavior for PEI-*f*-MMT MMM, CH_4 gas showed similar decreasing trend with pressure, as shown in Figure 4-29. CH_4 gas transports via diffusion mechanism through PEI membrane. Since CH_4 has higher kinematic diameter

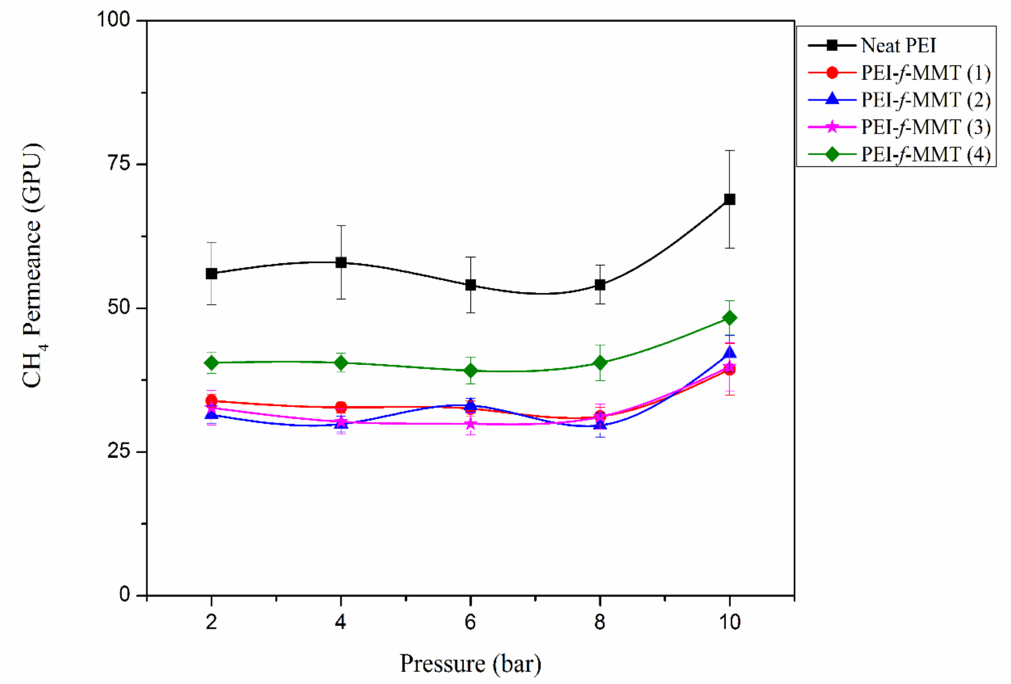

Figure 4-29: CH_4 permeance for PEI-*f*-MMT HFMM membranes against various feed pressure.

compared to CO_2 molecules, CH_4 molecules face more resistance in order to pass through the thin layer of PEI-*f*-MMT HFMM membranes. This trend is similar to previous studies [209, 215].

The permeance of both CO_2 and CH_4 gases for PEI-*f*-MMT MMMs are lower than PEI-MMT MMMs. It is due to the larger interlayer distance of *f*-MMT compared to MMT. According to XRD analysis (Figure 4-4), the degree of exfoliation of *f*-MMT is higher compared to MMT, therefore gas transport is affected by the tortuous gas diffusion pathways [191]. Moreover, the interfacial defects would be reduced due to the compatibility of organic modification. For 1 wt. % *f*-MMT loading, the CO_2 permeance of MMM at 2 bar decreased by 4.8% compared to MMT at similar loading. Subsequently, other filler loadings showed similar trend.

Figure 4-30 shows the ideal selectivity of PEI-*f*-MMT HFMM membranes at various feed pressure. Contrary to PEI-MMT MMMs, the PEI-*f*-MMT HFMM membranes showed improved ideal selectivity compared to neat PEI HF membrane. The ideal selectivity for all developed MMMs for all *f*-MMT loadings showed an

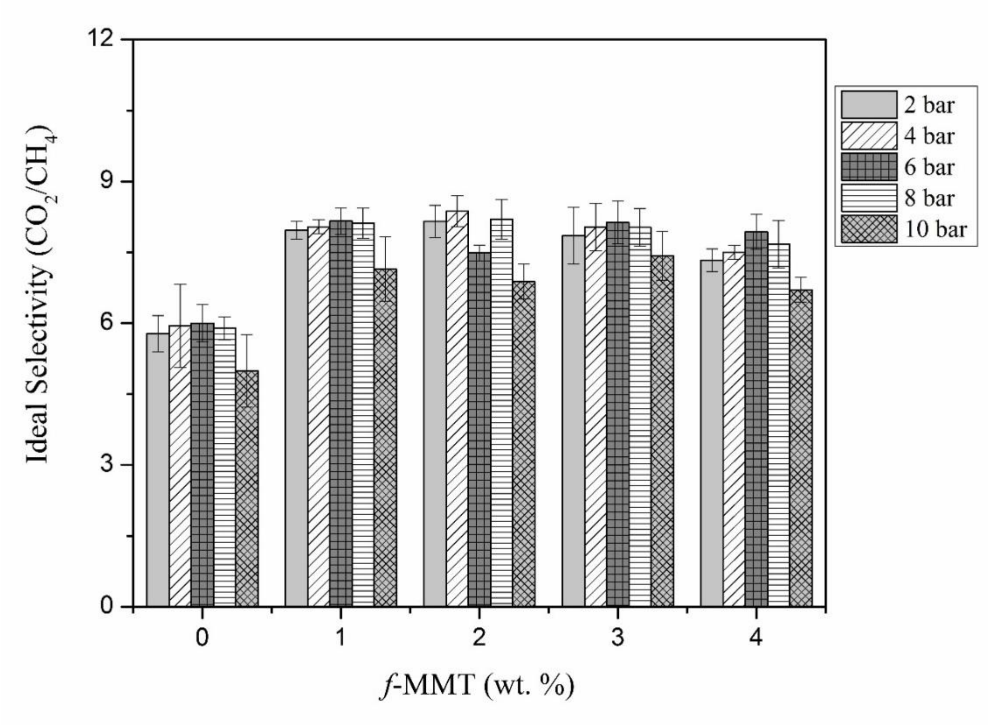

Figure 4-30: Ideal selectivities for PEI-*f*-MMT HFMM membranes at various feed pressure.

upward trend until 6 bar pressure. This trend is similar to other reported literature [210]. Above 6 bar, plasticization pressure of PEI is reached, causing a decrease in membrane separation performance. Moreover, compared to other membranes, PEI-*f*-MMT (2) showed the highest ideal selectivity before plasticization. Beyond this *f*-MMT loading, agglomerates are formed which resulted in void morphology, as verified by EDX analysis in Figure 4-17. Hashemifard incorporated Cloisite 15 in PEI matrix and observed similar results [100]. Ideal morphology existed below 2 wt. % of filler loading, upon which increment caused void morphology and deteriorated the MMMs separation performance.

4.4.3.2 Effect of filler loading on PEI-f-MMT HFMM membranes

CO_2 permeance of hollow fibre membranes was performed from 2 to 10 bar at various *f*-MMT loadings as described in Figure 4-28. With increasing *f*-MMT loading up to 3 wt.%, the CO_2 permeance decreases for 2 to 6 bar feed pressure. The CO_2 permeance shows 29.4% decrease compared to neat PEI membrane at 4 bar pressure for PEI-*f*-MMT (3). This phenomenon is governed by the tactoid structure of clays; fully exfoliated form provides interfacial interactions towards host polymer matrix and tortuous path for the gas to pass through. The tortuous path increases diffusion path length which leads to reduction in gas permeance [135, 216].

Compared to neat PEI membranes, CO_2 permeance decreases continuously up to 3 wt.% *f*-MMT loading. This phenomenon is attributed to the intercalated phase's interlayer space which was packed with PEI chains and distributed throughout the host polymer, ultimately increases tortuous path for both gases. This could also be due to *f*-MMT was well distributed in the polymer phase. However, with further increase in filler loading (i.e. 4 wt. %), the *f*-MMT particles tend to form agglomerates which lead to phase separated distribution, which is confirmed by EDX analysis (Figure 4-18). Similar trend was observed for CH_4 gas transportation through polymer matrix as depicted in Figure 4-29. Since the diffusion of large sized gas molecules through the tortuous path is more restricted, the CH_4 molecule's mobility is adversely affected compared to CO_2 molecules.

Figure 4-30 presents the ideal selectivity of CO_2/CH_4 gases at various filler loadings. The maximum ideal selectivity is observed for 2 wt. % *f*-MMT loading at 2, 4 and 8 bar pressures. This rise in selectivity is 41.0, 40.8, and 39.1 % higher compared to neat PEI HFMM membrane. At this loading, gas molecules encountered more obstacles induced by extended tortuous path as compared to other loadings. At 1 and 2 wt. % *f*-MMT loadings, the exfoliated platelets are higher in concentration compared to 3 and 4 wt. % loadings. Moreover, the long alkyl chains at the clay surface suppressed the void morphology. As a result, the selectivity is higher; however, intercalated morphology exists beyond these loadings, particularly at 4 wt. %, agglomeration of clay is evident in Figure 4-17. Therefore, PEI-*f*-MMT (2) HFMM membrane has the highest ideal selectivity values at 2, 4 and 8 bar pressure whereas PEI-*f*-MMT (4) has the lowest value except at 6 bar pressure.

4.4.4 Gas separation performance of PDMS coated hollow fibre membranes

4.4.4.1 Effect of coating on neat PEI HF membrane

Due to complications involved in phase inversion method, the spun PEI HF membranes may contain surface defects which inversely affect gas transport behavior. In order to minimize the effect of surface defects of spun HF membrane, the surface is coated with highly permeable PDMS polymer. Figure 4-31 shows the permeance of PDMS coated PEI membrane at various feed pressure. With increase in CO_2 feed pressure, a decrease in CO_2 permeance is observed until 8 bar pressure. However, CH_4 showed nearly constant permeance at all feed pressure. Compared to uncoated membranes, coated membrane shows reduction in CO_2 permeance by 54.75 % at 2 bar pressure. As described in previous section, methane gas follows the sorption diffusion model, as a result, the transportation of CH_4 gas remained almost constant for the entire pressure range. Similar trend is also observed by various researchers [209, 213].

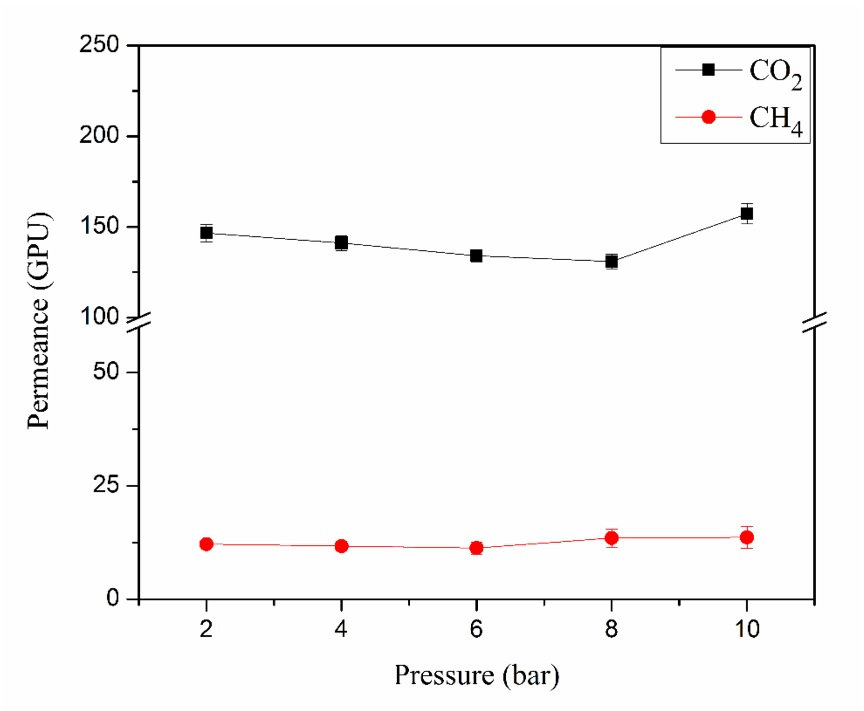

Figure 4-31: Pure CO_2 and CH_4 permeance for coated neat PEI HF membrane.

Figure 4-32 shows the ideal selectivity of coated PEI membrane. It is observed that the selectivity of the coated membrane has increased by 52.1 % compared to uncoated membrane at 2 bar pressure. This increase in selectivity is governed by the elimination

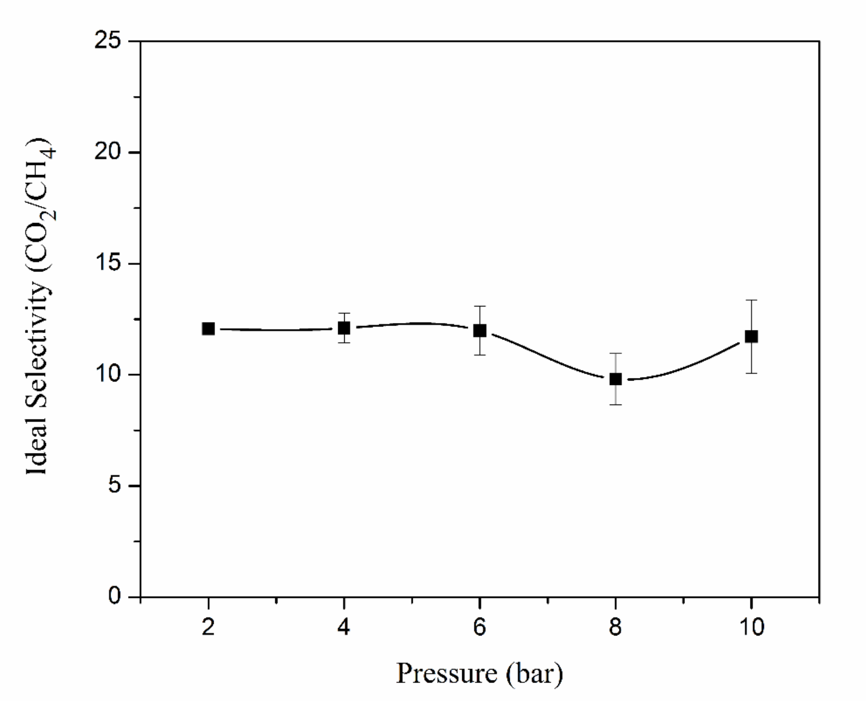

Figure 4-32: Ideal selectivity behavior of coated PEI HF membrane.

of micro voids at the membrane surface. The coated PDMS polymer created a layer on the surface of the membrane which is highly permeable in nature; however, it covered the macrovoids produced at the surface during the membrane formation process. Similar results have been found by other researchers when membranes were coated with PDMS [37, 81]. Ismail coated PES asymmetric membrane with PDMS and reported selectivity improvement from 7.89 to 28.38 [134].

4.4.4.2 PEI-MMT HFMM membrane performance enhancement via PDMS coating

The developed uncoated PEI-MMT HFMM membranes show reduced gas separation performance due to surface and morphological defects present at the outer surface, as confirmed by Figure 4-9. These morphological defects affect the membrane pore size and surface porosity which in turn affect the selectivity [217]. Therefore, a standard PDMS coating procedure was applied to overcome the surface defects. Generally, for coated membranes, the ideal selectivity increased while normalized pressure permeance

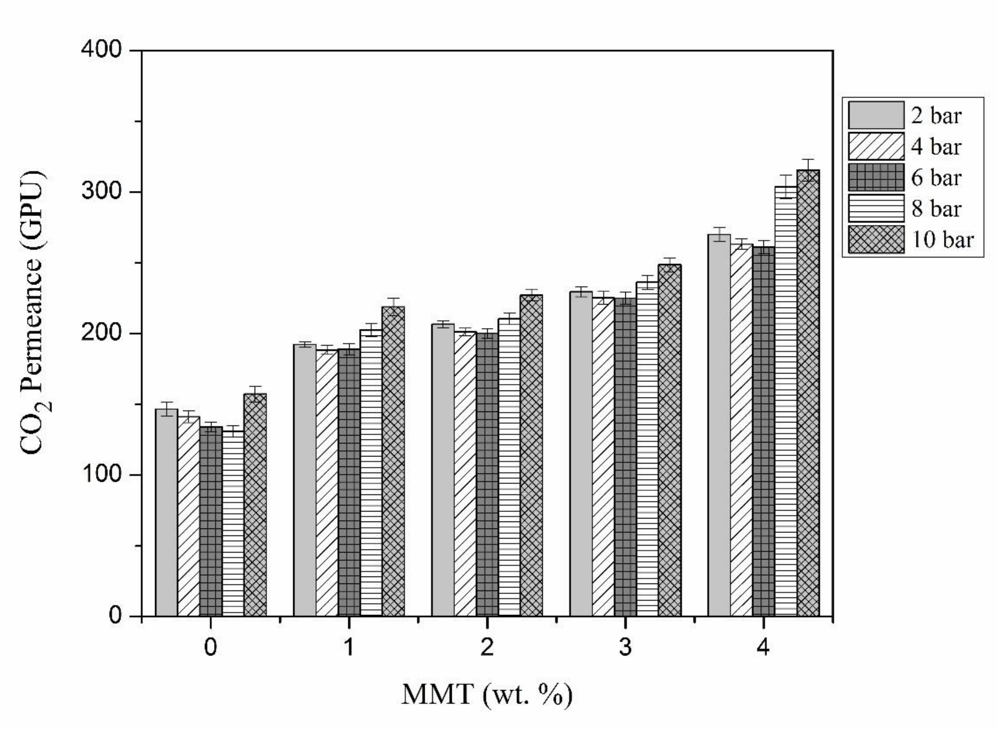

Figure 4-33: CO_2 permeance of coated PEI-MMT HFMM membrane at various MMT loadings.

for both CO_2 and CH_4 reduced. The permeance of coated PEI-MMT HFMM membranes are provided in Figure 4-33 and 4-34 for CO_2 and CH_4 gas, respectively.

Compared to neat PEI, for coated PEI-MMT MMM, the CO_2 permeance increased at all feed pressure and MMT loading. At 2 bar pressure, the permeance (GPU) of CO_2 has increased to 31.1, 40.9, 56.5, and 84.1 % for 1, 2, 3, and 4 wt. % MMT, respectively. Furthermore, in comparison to uncoated PEI-MMT MMMs, coated membranes show lower CO_2 permeance for all MMT loading and feed pressure. For coated PEI-MMT MMMs, the CO_2 permeance compared to its uncoated counterparts displays 47.5, 43.8, 53.0 and 45.0 % decrement for 1, 2, 3, and 4 wt. % MMT loading at 2 bar pressure.

Subsequently, methane gas finds more restricted mobility in coated membranes due to blockage of surface defects. Like CO_2 permeance, CH_4 permeance for coated PEI-MMT MMMs has decreased compared to their uncoated counterparts. A decrement of 63.9, 65.8, 65.0 and 64.4 % for 1, 2, 3, and 4 wt. % MMT loading was observed at 2 bar pressure.

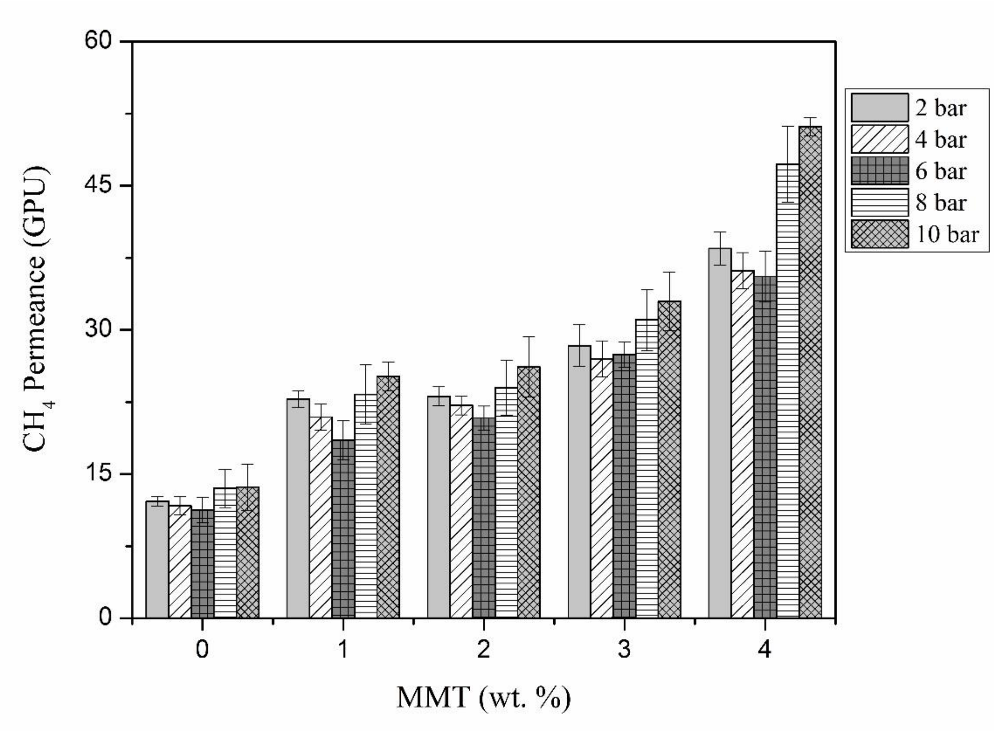

Figure 4-34: CH_4 permeance of coated PEI-MMT HFMM membranes at various MMT loadings.

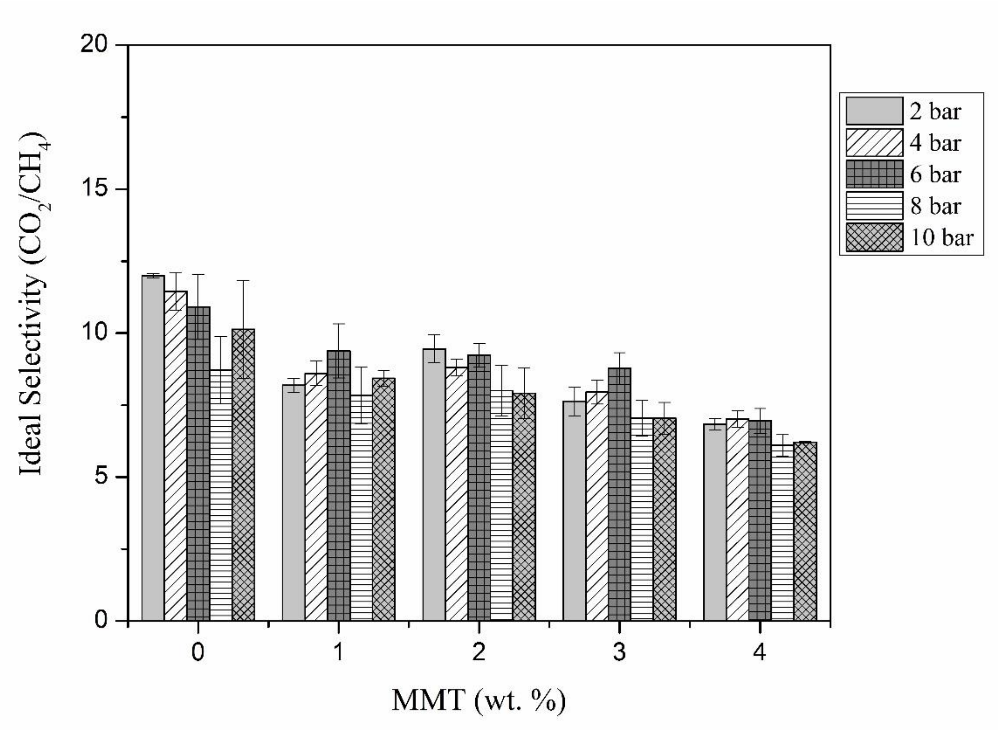

Figure 4-35: Ideal selectivity of coated PEI-MMT HFMM membranes at various MMT loadings.

The PDMS coating protocols for membranes affect the CO_2 and CH_4 permeance as well as selectivity. The ideal selectivity trend remains the same for all feed pressure as shown in Figure 4-35. However, the values of ideal selectivity have improved by almost 100 % compared to uncoated MMMs. For PEI-MMT (1), the coating protocols improved the ideal selectivity from 5.0 to 10.21 at 6 bar pressure. N. M Ismail reported that the CO_2/CH_4 ideal selectivity for PES-C15A1 MMM has improved from 2.29 to 18.72, since the PDMS coating reduced the effects of void morphology for MMM [134].

4.4.4.3 Effect of PDMS coating on PEI-f-MMT HFMM membranes

The presence of long alkyl chains at the surface of *f*-MMT enhanced the interfacial contact with PEI matrix. As a result, void morphology is suppressed in PEI-*f*-MMT HFMM membranes. However, since phase inversion method was used to develop the membranes, the presence of voids at the surface cannot be neglected. The surface morphology defects can be further suppressed by PDMS coating on the membrane surface.

Figure 4-36 and 4-37 present the CO_2 and CH_4 permeance at various filler loadings. The CO_2 permeance decreased gradually with increasing *f*-MMT loading, which is similar to uncoated PEI-*f*-MMT HFMM membranes as described in the previous section. However, decrement in CO_2 permeance for coated PEI-*f*-MMT membranes is noticed compared to uncoated MMMs. For instance, at 2 bar feed pressure, the permeance decrease for 1, 2, 3 and 4 wt. % membranes are 47.7, 48.6, 50.2, and 49.1% respectively. This downward trend in CO_2 permeance indicates the suppression of voids at the membrane outer surface when PDMS coating was applied.

Moreover, similar observations were found for CH_4 gas diffusion through the membranes as depicted in Figure 4-37. Due to larger kinematic diameter, CH_4 molecules face more hindrance. Subsequently, the decreasing trend in CH_4 permeance through developed PEI-*f*-MMT MMMs is noticeable. At 2 bar feed pressure, the permeance decrease for 1, 2, 3 and 4 wt. % PEI-*f*-MMT HFMM membranes are 72.1,

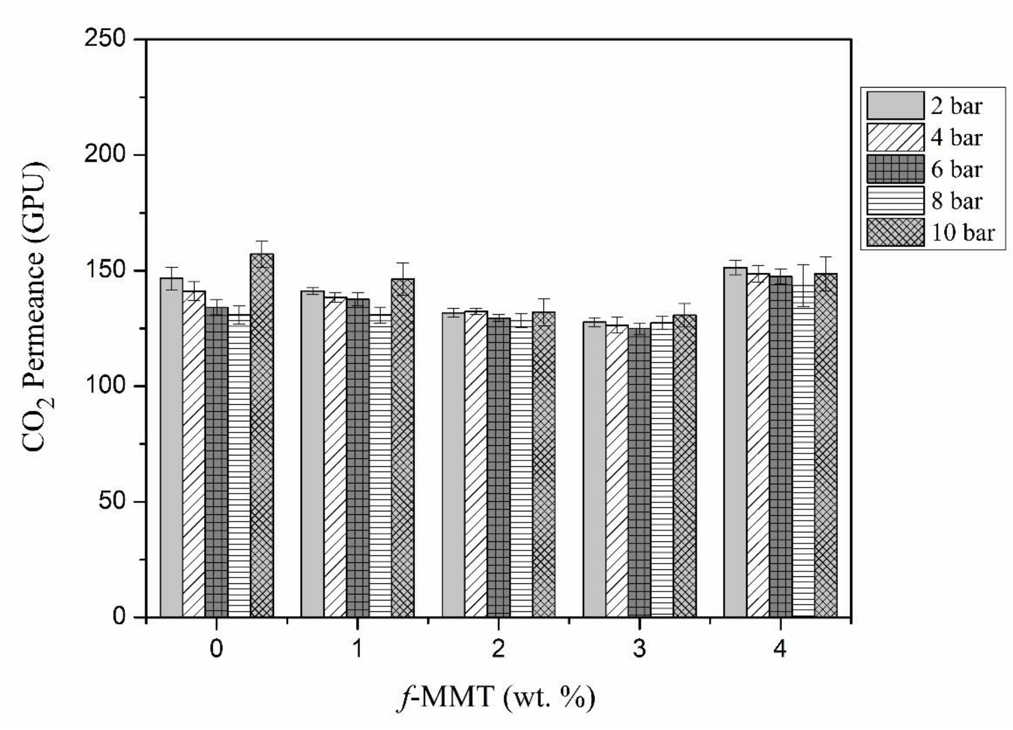

Figure 4-36: CO_2 permeance of coated PEI-*f*-MMT HFMM membranes at various *f*-MMT loadings.

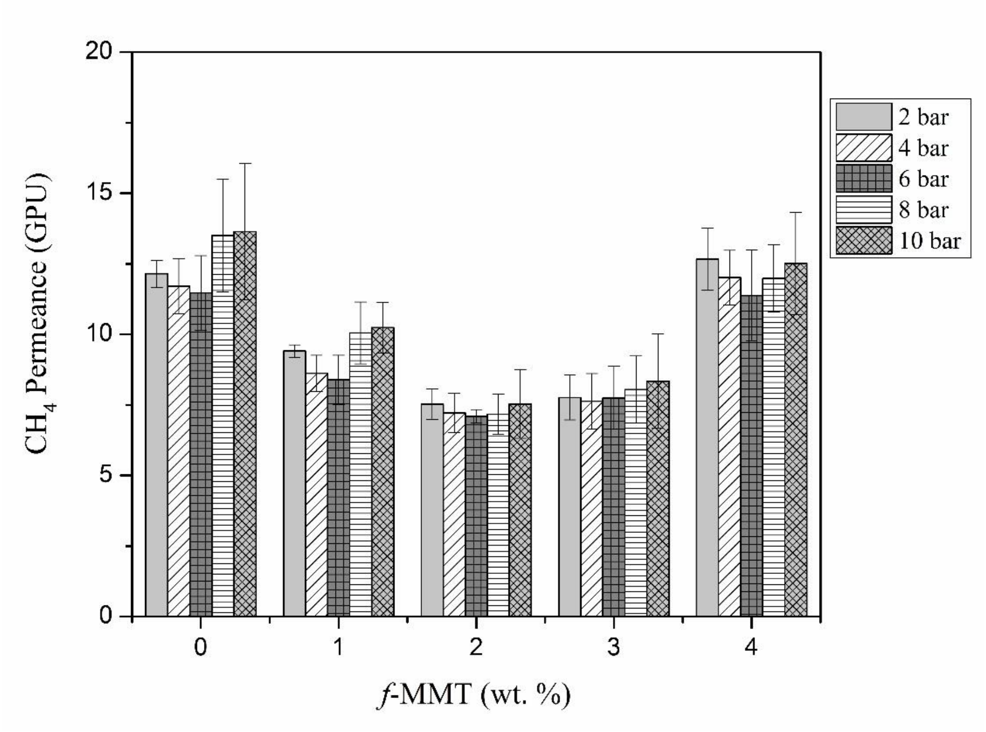

Figure 4-37: CH_4 permeance of coated PEI-*f*-MMT HFMM membranes at various *f*-MMT loadings.

76.1, 76.2, and 68.7% respectively. This is due to the suppression of voids at the membrane surface and CH_4 faced more obstruction compared to CO_2 gas molecule.

Figure 4-38 provides a similar trend as Figure 4-30 for uncoated membranes; however, the magnitude change is rather significant. Moreover, PEI-*f*-MMT (2) showed the highest ideal selectivity compared to neat and all other MMMs at all feed pressures. The maximum ideal selectivity achieved is 18.35 at 4 bar pressure which is 52.2 % higher than neat PEI HF membranes. Furthermore, in contrast to uncoated PEI-*f*-MMT (2) HFMM membrane, the CO_2/CH_4 ideal selectivity increment is 119.2 % higher at the same feed pressure.

The exfoliated morphology at 2 wt. % *f*-MMT loading shows the optimum gas separation performance. Beyond this loading, intercalated morphology of *f*-MMT exists which reduced the gas separation performance of PEI-*f*-MMT HFMM membrane. Although exfoliated geometry exists below 2 wt.% *f*-MMT loading, due to lower filler concentration, the diffusion pathways within the PEI matrix are not obstructed enough. Hashemifard et al. incorporated Cloisite 15, a type of clay, in PEI matrix to develop

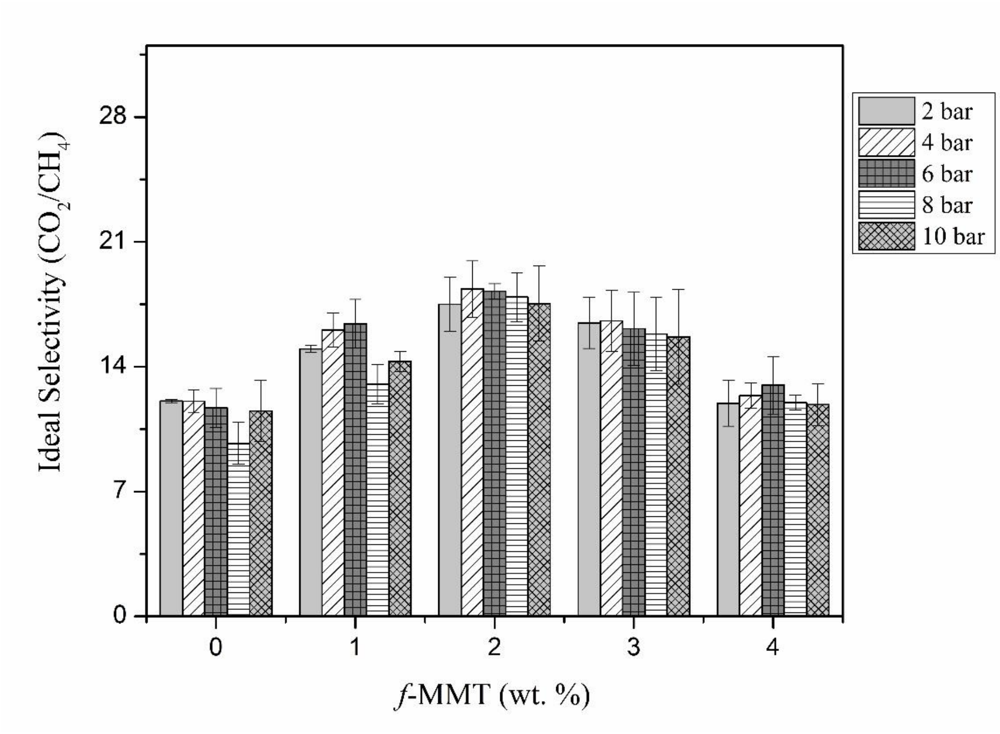

Figure 4-38: Ideal Selectivity of PEI-*f*-MMT HFMM membranes at various loadings.

asymmetric flat sheet MMM [100]. It was reported that below 2 wt. % loading, ideal morphology exists; beyond this loading, void morphology dominates the membrane surface which deteriorated the separation performance of membrane.

4.5 Polyetherimide-montmorillonite interfacial morphological analysis

Gas separation performance of MMMs are dependent on the polymer-filler interfacial interactions. Moore and Koros proposed the transport property morphological diagrams for small sized filler and polymer interactions [218]. Later, Hashimefard applied the same model for halloysite nano-filler (HNT) [219]. The non-ideal morphologies in MMMs governed the gas transportation and are classified in 5 different cases. Case **I** represents matrix rigidification, which shows good adhesion characteristics, nevertheless, polymer rigidifies around fillers and reduces the gas permeation whereas selectivity enhancement is observed. Case **II** represents the “sieve in a cage morphology” which shows higher permeability and constant or lower selectivity performance. Leaky interface represents Case **III** in the diagram, which shows

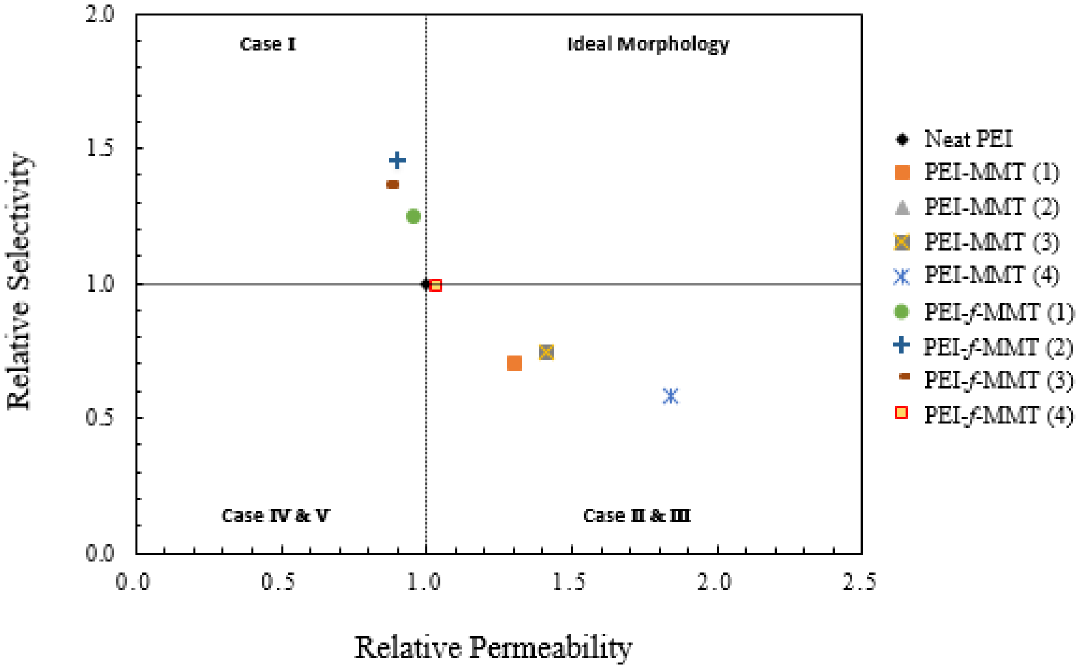

Figure 4-39: Incorporation of developed coated hollow fibre membranes data in morphological diagram.

significant increase in gas permeation with slight decrease in selectivity. Case **IV** and **V** present the filler pore blockage morphology in which permeation decreases at the expense of selectivity.

Figure 4-39 displays the experimental data of MMMs discussed in this study in a morphological diagram in order to determine the interfacial morphologies based on gas transport performance. PEI-MMT HFMM membranes are placed in the lower-right quadrant, showing leaky interface morphology due to significant permeation increase. Moreover, with increasing filler loading, the PEI-MMT interfacial interactions further decrease as 4 wt. % MMT loading showed the lowest selectivity and higher permeability values. This is due to filler agglomeration as depicted in FESEM images, wherein the voids present adjacent to MMT agglomerates deteriorate the separation performance. In addition, the hydrophilic MMT may adsorb water from the coagulant bath during asymmetric hollow fibre membrane fabrication, which affects the interfacial morphology [1].

Compared to MMT, *f*-MMT filler addition in PEI results in lower permeation and higher ideal selectivity performance, hence are placed at the left-top quadrant, which shows polymer chain rigidification near filler surface. MMMs for all *f*-MMT loadings are present in the same quadrant except at 4 wt. % loading. PEI chains rigidified around PEI-*f*-MMT interfacial morphology, which caused immobilization of PEI chains at interface which not only reduce gas sorption but permeation as well. Although PEI/*f*-MMT showed good interfacial interactions, nevertheless, due to rigidification, the selectivity enhancement is not significant. Moreover, with 4 wt. % *f*-MMT loading, the interfacial morphology shifted from matrix rigidification to "sieve in a cage" morphology as shown in Figure 4-40. The agglomeration formation at this wt. % leads to poor interactions with PEI chains. As a result, voids are created at the PEI/*f*-MMT interface, which affect the membrane performance adversely.

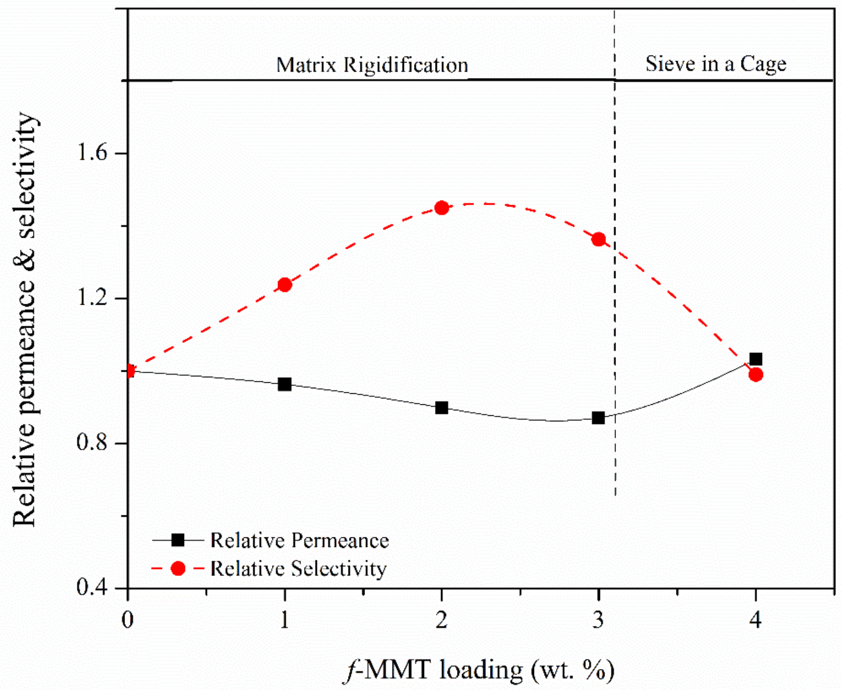

Figure 4-40: Effect of *f*-MMT loading on PEI-*f*-MMT HFMM membrane's CO_2 permeance and CO_2/CH_4 selectivity.

4.6 Performance study of developed PEI-*f*-MMT HFMM membranes in Robeson upper bound curve

Robeson developed upper performance curves for various gases that relate permeability and selectivity, also known as Robeson's upper bound curves [220]. Commercially attractive region is also shown in Figure 4-41. [221].

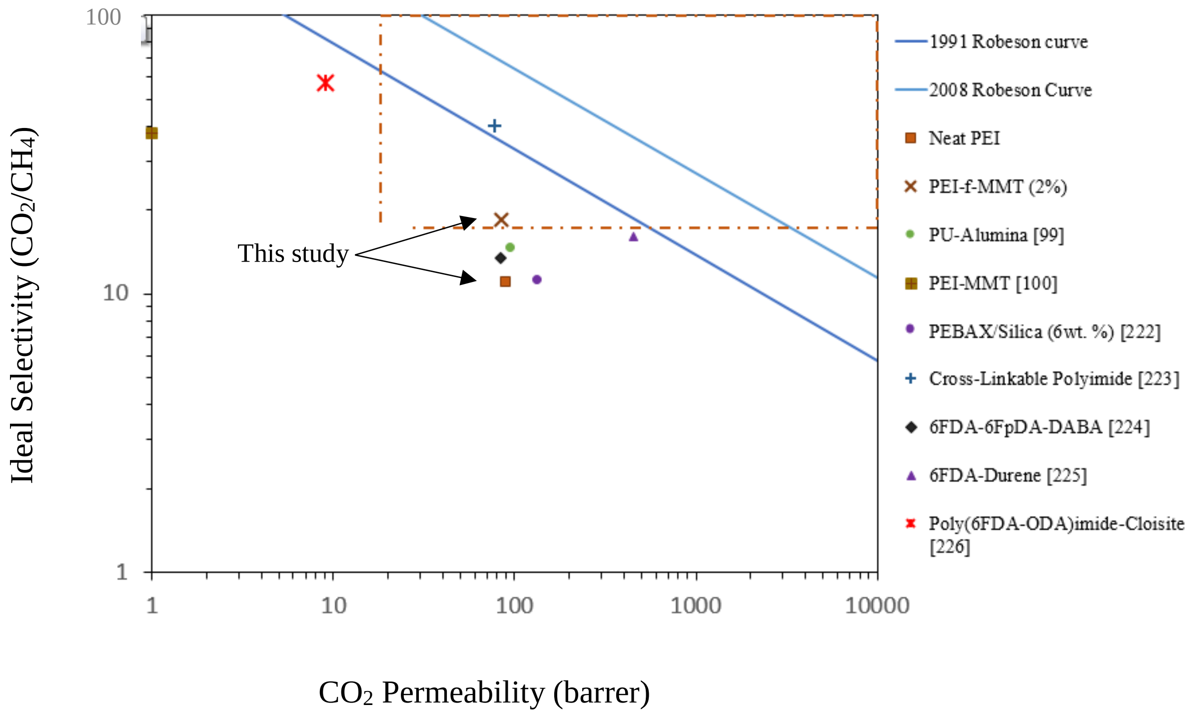

Figure 4-41: Incorporation of PEI-*f*-MMT HF membrane data in Robeson curve.

Figure 4-41 presents the current standing of developed PEI-*f*-MMT membranes compared to other reported membranes in Robeson upper bound curve [222-226]. It is noticed that the reported mixed matrix membranes containing non-porous fillers do not exist in the commercially attractive region. However, in this study, by applying the performance enhancement strategies, the developed PEI-*f*-MMT (2) hollow fibre membrane falls within the commercially attractive region. This is due to the fact that the developed membrane has very thin top layer. Furthermore, the optimization of spinning parameters has improved the permeability and selectivity of the aforementioned membrane. Moreover, it is noticed that CO_2/CH_4 ideal selectivity is increased by *f*-MMT loading at 2 wt. % compared to neat PEI membrane. This is due to the fact that good interfacial interactions exist until 2 wt. % loading. Beyond this point, fillers agglomerated and void morphology dominated.

4.7 Mixed gas performance of selected membranes

Table 4-7 presents the real gas selectivity data obtained via gas chromatography (GC). The real gas selectivity shows reduction in comparison to ideal selectivity for both neat and 2 wt. % *f*-MMT loaded PEI membranes. However, like ideal selectivity, the real selectivity also increased by the addition of *f*-MMT filler. The decrease in membrane performance is mainly due to the competitive environment from the coexistence of binary gas mixture in the feed stream [14]. In the presence of CH_4 gas, the sorption of CO_2 in glassy polymers faced decrement which affected the membrane performance. The large sized CH_4 molecules hindered the diffusion pathways for the small interactive CO_2 molecules.

Table 4-7: Pure and mixed (50%/50%) gas selectivity for neat and PEI-*f*-MMT (2) HF membranes.

Membrane	CO_2 Permeance (GPU)	CH_4 Permeance (GPU)	Ideal Selectivity	Real Selectivity
Neat PEI	83.54	10.23	12.07	8.17
PEI-*f*-MMT (2)	78.06	7.32	18.35	10.66

Similar observation was reported by Chen et al., when Matrimid membrane was tested under mixed gas conditions [227]. Jusoh et al. prepared dense flat sheet 6FDA-durene/silanated zeolite composite membranes and observed the decrease in real gas (CO_2/CH_4, 50/50 v/v %) selectivity to 7.30 compared to ideal selectivity of 19.10 [14]. The author speculated that along with the competitive effect due to binary gas mixture, gas polarization and non-ideal behavior of gas phase might deteriorate the mixed gas separation performance of the membrane.

4.8 Validation of developed PEI-*f*-MMT HFMM membranes' performance via existing permeation models

This section evaluates the performance of developed PEI-*f*-MMT HFMM membranes through existing gas permeance models followed by comparing theoretical values with experimental data.

- Nielsen Model: proposed a simple permeation model by considering regular and horizontal arrangement of platelets to the diffusion path.
- Cussler Model: improved the model by assuming layered arrangement of nanoparticles and each layer is separated by narrow slits.
- Yang-Cussler Model: further improved the model by considering mono dispersed nanoparticles with parallel alignment and varied aspect ratio.
- Lape-Cussler Model: considered rectangular platelets with similar aspect ratio are dispersed randomly in polymer matrix and aligned parallel to each other along the diffusion path.
- Bharadwaj model: developed model which takes into account the platelet orientation factor. This factor includes various dimensions whether horizontal, parallel or randomly distributed in the direction of the diffusion path.

4.8.1 Estimation of *f*-MMT aspect ratio

The permeation properties of polymer-layered silicates MMM are strongly dependent on organic-inorganic phase interaction, dispersion state, aspect ratio and the length of the inorganic flakes. In this study, different phenomenological models were used to study the permeation properties of PEI-*f*-MMT MMM, and to determine the dispersion state of the dispersed *f*-MMT in PEI matrix.

Theoretical permeation curves were generated from Nielsen, Cussler, Yang-Cussler, Lape-Cussler and Bharadwaj models as depicted in Figure 4-42. The relative permeation curves generated for all the models show a decreasing trend by increasing the flakes aspect ratio and volume fraction. In most studies, the average aspect ratio is determined using TEM analysis of the clay platelets, followed by permeation estimation through existing models [228-230]. However, it is also possible to estimate the aspect ratio by inserting the experimental permeation values in the theoretical models. The theoretical aspect ratio value, at which the experimental permeation values are in close agreement to the theoretical values is considered to be the filler's aspect ratio. For instance, Zulhairun and Ismail prepared PSf-cloisite flat sheet membranes and measured the gas permeance values experimentally [106]. These experimental relative permeability values were then used in phenomenological models to estimate the aspect ratio of the dispersed cloisite flakes in continuous phase. In this study, the permeance at 2 bar is considered for uncoated PEI-*f*-MMT HFMM membrane for the sake of simplicity. Low pressure was selected, as the effect of surface defects is minimum on membrane performance as depicted by experimental data. Furthermore, uncoated membrane depends on the effect of *f*-MMT only and is independent of PDMS coating characteristics. Figure 4-42 presents the experimental data points and theoretical curves generated at various aspect ratio of filler. Whereas, P_c, represents the permeance of MMM; P_o, is the permeance of neat membrane; and, a, is the aspect ratio of *f*-MMT within PEI matrix. Furthermore, it is observed that none of the data points fully fit the theoretical curves, nevertheless, they follow the same trend at volume fraction above 0.005 for CO_2 gas.

The relative permeance calculated using the aforementioned models show similar trend as experimentally determined relative permeation values. However, at volume fraction of 0.020, the relative permeability showed an abrupt increase, which might be due to agglomeration of clay at this loading as evident in EDX mapping (Figure 4-18). The relative permeance values of CO_2 gas measured through experiments and calculated by theoretical curves generated through Nielsen, Cussler, Yang-Cussler, Lape-Cussler and Bharadwaj models at aspect ratio of 40, 40, 60, 15 and 110, respectively are shown in Table 4-7. The average aspect ratio calculated by all these models is 53 for PEI-*f*-MMT. Equation 4-1 gives the average absolute relative error (%AARE), which is the tuning parameter that describes the close agreement between experimental and calculated values. For better fitting values, the % AARE value should be minimized.

$$\%AARE = \frac{100}{NDP}\sum_{J=1}^{NDP}\left|\frac{P^{cal}{}_i - P^{exp}{}_i}{P_i{}^{exp}}\right| \qquad (4\text{-}1)$$

Where $P^{cal}{}_i$ and $P^{exp}{}_i$ are the relative permeance for the *i*th experimental value and NDP represents the number of data points.

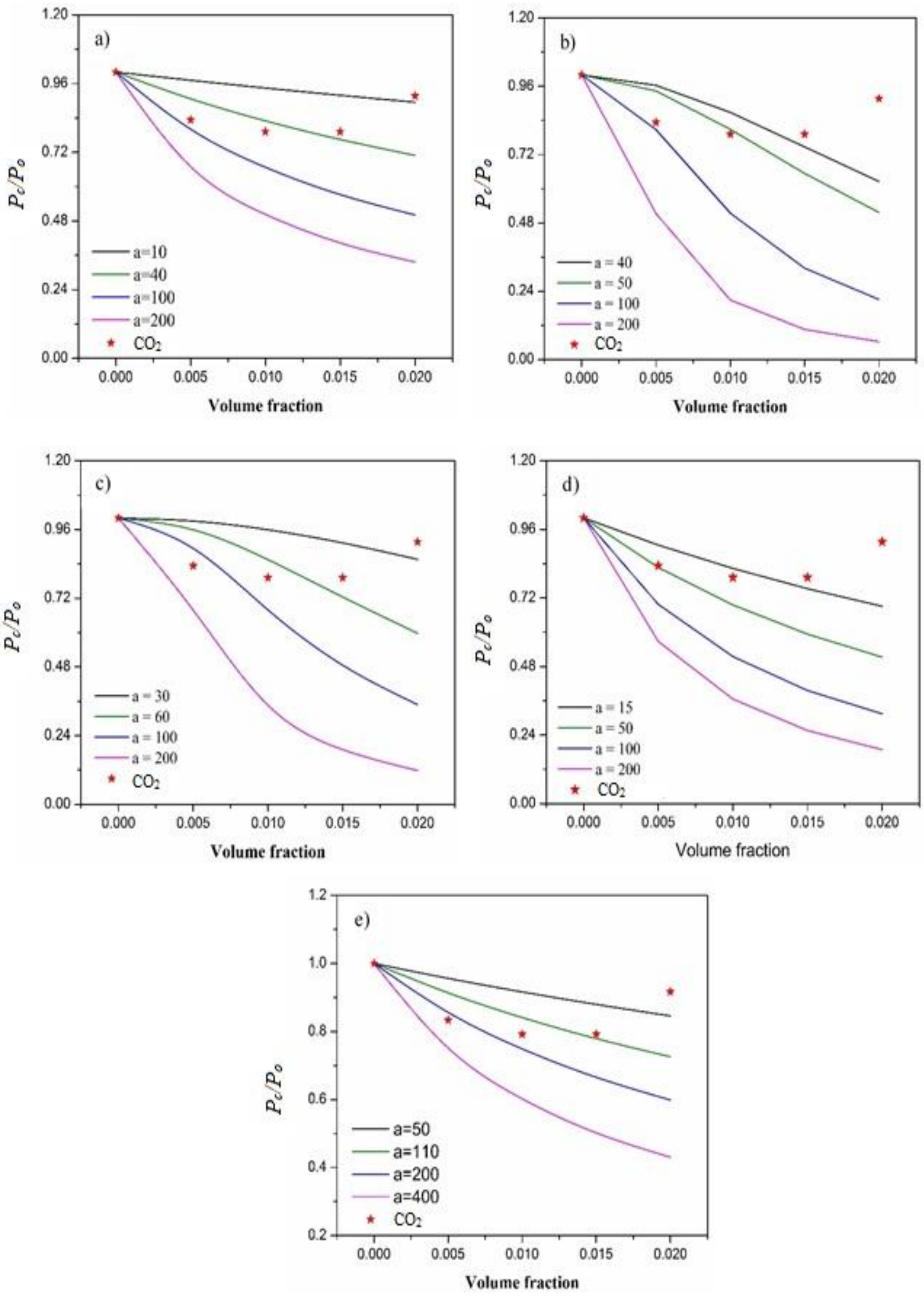

Figure 4-42 : Estimation of *f*-MMT aspect ratio by using a) Nielsen, b) Cussler, c) Yang-Cussler, d) Lape-Cussler and e) Bharadwaj permeation models.

Table 4-8 presents the calculated and experimental P_c/P_o values of all PEI-*f*-MMT HFMM membranes with %AARE at different aspect ratio of *f*-MMT. For volume fraction of 0.005 to 0.0015, %AARE values varied from +8.84 to –3.41 for Nielsen model, +8.61 to – 4.95 for Lape Cussler model, and +9.65 to -1.57 for Bharadwaj model. These %AARE values showed ±10 % deviation which showed the close agreement of experimental values to the theoretical curve. However, Cussler and Yang-Cussler models calculated approximately +15 %AARE for PEI-*f*-MMT (1). Moreover, for volume fraction of 0.002, agglomeration took place and abrupt permeation increase is observed. The aforementioned behavior is not considered in theoretical permeation models.

Bharadwaj proposed a method to approximate the number of stacks of flakes in a tactoid through aspect ratio of layered silicate [179]. Yano et al., studied the water permeability of polyimide-Na-MMT nano-composite and reported the average lateral dimension of Na-MMT as 218 nm. In this study, the number of stacks per unit tactoid is calculated by considering the lateral dimension of MMT as 218 nm with a width of 1 nm. Moreover, the polymer chains are expanded by MMT interlayer space to 1 nm as suggested by Bharadwaj [228]. The number of stacks per unit tactoid calculated using average aspect ratio is explained in Appendix C, which is approximately 4 for volume fraction of 0.005 to 0.020. This reflects excellent dispersion properties of *f*-MMT for 1 to 3 wt.% loading in PEI matrix. Although the dispersion state is not fully exfoliated, the layer delamination consists of only 3 stacks which is in agreement to reported literature. From Zulhairun and Ismail's study on Cloisite 15A mixed matrix membrane, the number of stacks per unit tactoid calculated by phenomenological models ranged from 2 to 4 [135]. On the other hand, Kim et al. prepared AMH-3 cellulose acetate membrane with high shear mixer to delaminate the AMH-3 layers and observed 2 to 3 stacks per unit tactoid for 2 to 6 wt.% AMH-3 loading [133]. In another study, Ismail et al., prepared PES/Cloisite 15A membrane for CO_2/CH_4 separation. 50% of the tactoids consist of 2-3 stacks per unit tactoid for 5 wt.% Cloisite 15A loading [200]. Picard et al. studied the water permeability of Nylon 6-Mt membranes prepared through melt blending process. The experimentally determined average aspect ratio was estimated at 20, whereas Lape-Cussler model provides a closer value of 17.2 [230].

Table 4-8: CO_2 permeance generated through models vs experimental values.

Model	Membrane	$P_c/P_{o(exp)}$	$P_c/P_{o(cal)}$	%AARE	Aspect Ratio
Nielsen	PEI-*f*-MMT (1)	0.8333	0.906966	8.840297	40
	PEI-*f*-MMT (2)	0.7917	0.82977	4.815206	
	PEI-*f*-MMT (3)	0.7917	0.764683	-3.40638	
	PEI-*f*-MMT (4)	0.9167	0.709065	-22.6469	
Cussler	PEI-*f*-MMT (1)	0.8333	0.9634	15.61272	40
	PEI-*f*-MMT (2)	0.7917	0.8686	9.725414	
	PEI-*f*-MMT (3)	0.7917	0.7470	-5.63492	
	PEI-*f*-MMT (4)	0.9167	0.6254	-31.7792	
Yang-Cussler	PEI-*f*-MMT (1)	0.8333	0.9590	15.08621	60
	PEI-*f*-MMT (2)	0.7917	0.8546	7.952845	
	PEI-*f*-MMT (3)	0.7917	0.7241	-8.52727	
	PEI-*f*-MMT (4)	0.9167	0.5974	-34.8311	
Lape - Cussler	PEI-*f*-MMT (1)	0.8333	0.9050	8.605915	15
	PEI-*f*-MMT (2)	0.7917	0.8233	3.998669	
	PEI-*f*-MMT (3)	0.7917	0.7525	-4.94589	
	PEI-*f*-MMT (4)	0.9167	0.6907	-24.6487	
Bharadwaj	PEI-*f*-MMT (1)	0.8333	0.913713	9.649894	110
	PEI-*f*-MMT (2)	0.7917	0.841133	6.250658	
	PEI-*f*-MMT (3)	0.7917	0.779236	-1.56811	
	PEI-*f*-MMT (4)	0.9167	0.725824	-20.8186	

At lower volume fraction, the degree of delamination or exfoliation is higher. This produced higher aspect ratio or lower number of stacks per unit tactoid. Also, the higher *f*-MMT loading hindered the polymer chains migration into interlayer space. As a result, lower degree of flake delamination took place. However, the relative permeance decrease of membrane is due to reduction in permeable phase. Therefore, it can be concluded that the modification of Na-MMT through aminolauric acid improved the flake dispersion and interaction with PEI matrix.

4.8.2 Modeling of spun PEI-*f*-MMT HFMMM

In order to validate the experimental CO_2 permeation values with existing theoretical models, Nielsen, Cussler, Yang-Cussler, Lape-Cussler and Bhardwaj models were considered at pressure range from 2 to 10 bar. The above stated models are available models that considered the layered form of dispersed filler. Since MMT is a type of clay and consists of alumino silicates in layered form, the aforementioned models were adopted for this study.

4.8.2.1 Nielsen model

Nielsen model considered the horizontal dispersion of *f*-MMT in the PEI matrix. Figure 4-43 presents the theoretical curves generated through Nielsen model for CO_2 permeance against feed. The theoretical curves generated at different wt. % of *f*-MMT present a downward trend with increasing pressure.

The experimentally determined value showed deviation from the theoretical values. However, it exhibits similar decreasing trend with pressure. MMM with 1 wt. % *f*-MMT

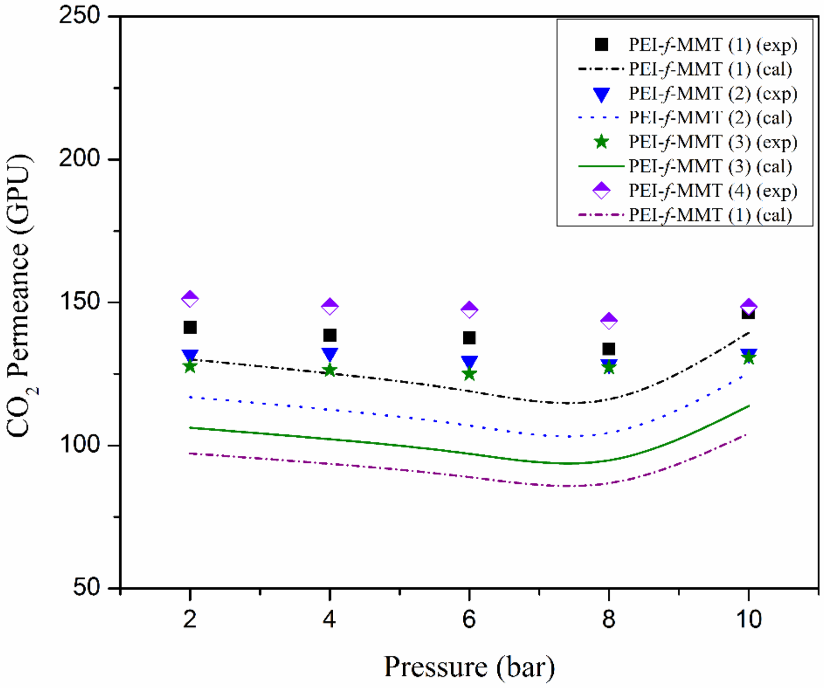

Figure 4-43: Nielsen model for PEI-*f*-MMT.

shows minimum deviation whereas highest deviation is observed for 4 wt. % *f*-MMT. The absolute average from the theoretically generated values are given as -8.46, 10.17, -14.08, -11.72 and -5.30 for 1 wt. % *f*-MMT loading at 2, 4, 6, 8 and 10 bar. For all other filler loadings, the %AARE value is in the range of ±10.

4.8.2.2 Cussler model

Cussler model showed a similar downward trend with increasing feed pressure until 8 bar for all developed PEI-*f*-MMT MMMs as depicted in Figure 4-44. Furthermore, the experimentally determined CO_2 permeance values for PEI-*f*-MMT (1) showed close agreement to the theoretically generated curves. In contrast, MMM containing 4 wt. % of *f*-MMT showed the maximum deviation from the theoretical curve. This is mainly due to agglomeration of *f*-MMT in PEI matrix, which was not considered in the models.

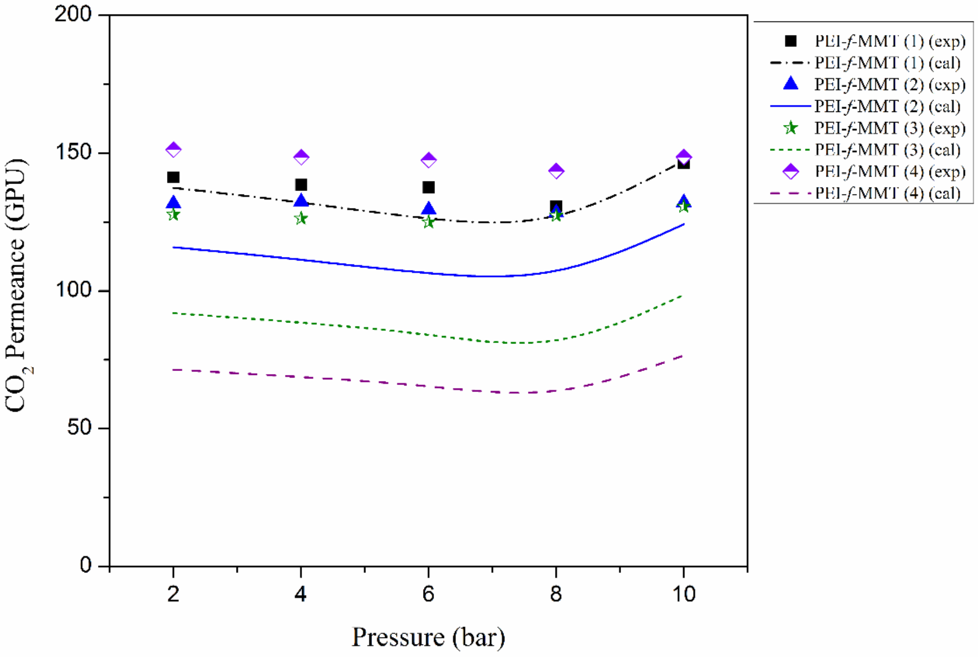

Figure 4-44: Cussler model for PEI-*f*-MMT HFMMM.

4.8.2.3 Yang-Cussler model

Figure 4-45 presents the theoretically generated curves by applying Yang-Cussler model at various feed pressure in comparison to experimentally determined values of HFMM membranes incorporated with *f*-MMT filler. Yang-Cussler model considered the mono dispersion of nano-filler containing variations in aspect ratio.

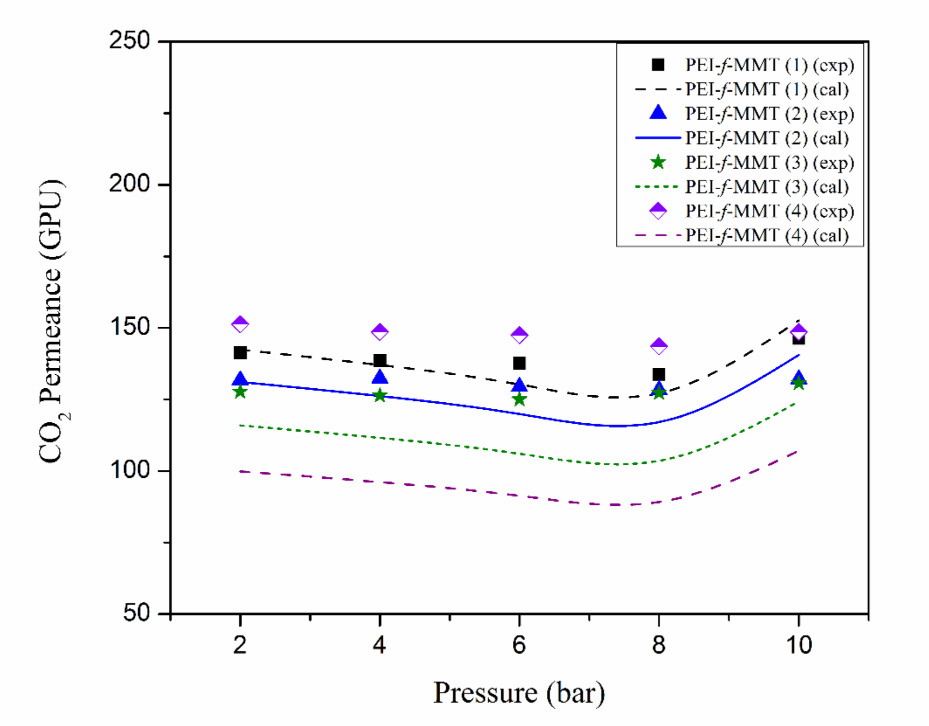

Figure 4-45: Yang-Cussler model for PEI-*f*-MMT HFMMM.

It can be seen that the CO_2 permeance values follow a similar trend with their respective theoretical curves. For 1 and 2 wt. % *f*-MMT addition in PEI polymer, the calculated %AARE values are less than ±10 as tabulated in Table 4-9. However, for PEI-*f*-MMT (3), the %AARE is ±20. This model is better suited to experimentally determined data compared to Nielsen and Cussler models. This is due to Yang-Cussler model incorporated the concept of flakes for filler, which is a relevant assumption for *f*-MMT structure. Thus, the theoretical and experimental values are in close agreement.

Table 4-9: %AARE of PEI-*f*-MMT membranes in comparison to Yang-Cussler model.

Pressure (Bar)	%AARE			
	PEI-*f*-MMT (1)	PEI-*f*-MMT(2)	PEI-*f*-MMT (3)	PEI-*f*-MMT (4)
2	0.49	-1.75	-11.49	-36.50
4	-1.39	-5.91	-13.90	-37.77
6	-5.69	-8.58	-17.30	-40.42
8	-3.09	-9.95	-20.72	-40.22
10	3.95	5.04	-7.29	-30.68

4.8.2.4 Lape-Cussler model

Figure 4-46 shows the theoretically generated curves via Lape-Cussler model and experimentally determined values for spun PEI-*f*-MMT MMMs. Lape-Cussler model considered the rectangular shape of incorporated fillers with random dispersibility in host polymer matrix. It is noted that the experimental points are poorly suited with theoretical curves. The minimum %AARE for any membrane at any pressure is between ±20 to ±60, which indicates the poor performance of developed membrane based on Lape-Cussler's assumptions. The assumption of parallel distribution of clay

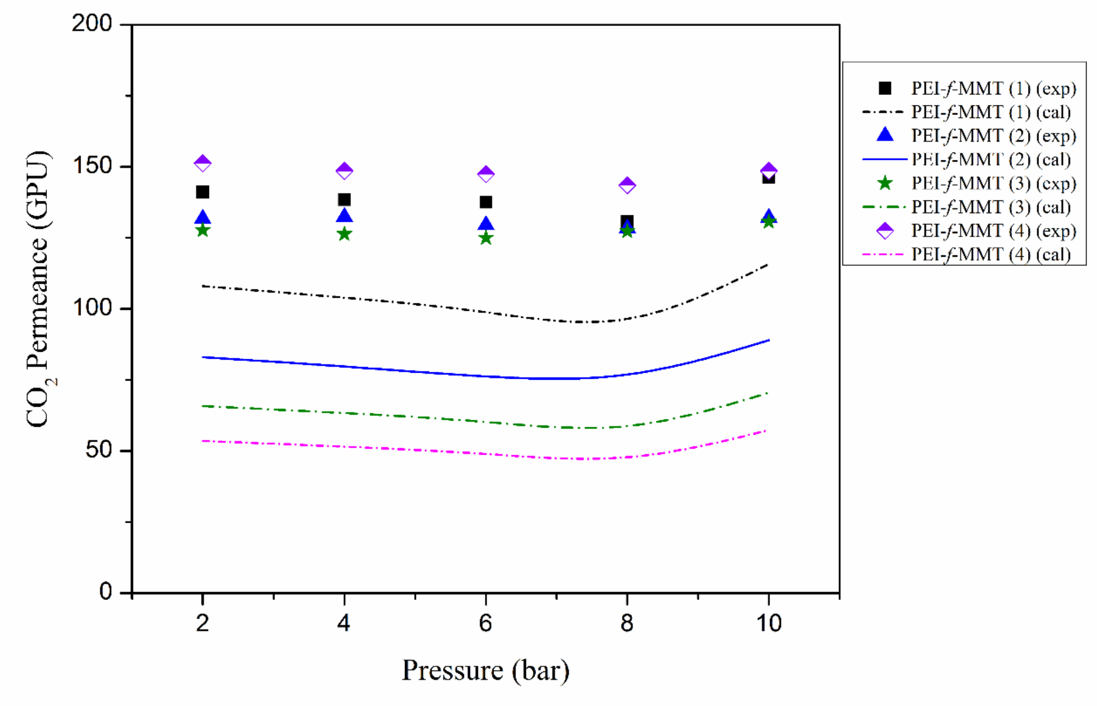

Figure 4-46: Lape-Cussler model for PEI-*f*-MMT MMMs.

platelets in the diffusion pathways was unable to relate to the actual distribution of clay platelets in PEI matrix.

4.8.2.5 Bharadwaj model

Figure 4-47 presents the experimental point for spun HFMM membrane in comparison to Bharadwaj model's generated curves. It is observed that CO_2 permeance trend against pressure by theoretical curve is the same as experimentally observed data points. Moreover, for 1 to 3 wt.% of *f*-MMT incorporation in PEI matrix, closer CO_2 permeance behavior is obtained compared to their respective theoretical curves. However, the model does not consider the agglomeration of filler. As a result, PEI-*f*-MMT (4) showed significant deviation compared to theoretically generated curve.

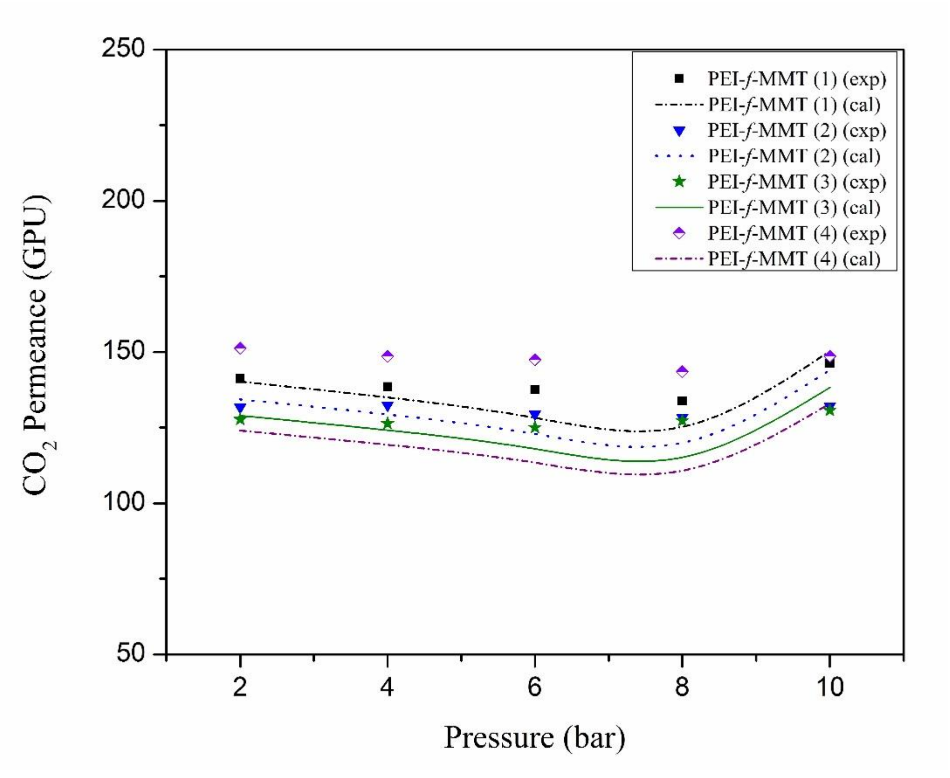

Figure 4-47: Bharadwaj model for PEI-*f*-MMT MMMs.

Table 4-10: %AARE of PEI-*f*-MMT membranes in comparison to Bharadwaj model.

Pressure (Bar)	%AARE			
	PEI-*f*-MMT (1)	PEI-*f*-MMT(2)	PEI-*f*-MMT (3)	PEI-*f*-MMT (4)
2	-0.92	1.53	0.36	-18.72
4	-2.77	-2.76	-2.37	-20.34
6	-7.01	-5.52	-6.23	-23.74
8	-4.45	-6.94	-10.11	-23.49
10	2.49	8.55	5.12	-11.27

Table 4-10 shows the %AARE calculated for each PEI-*f*-MMT HFMM membrane from theoretically generated curves. It is observed that for all feed pressure range, the PEI membranes incorporated with 1 to 3 wt. % of *f*-MMT has shown close agreement with %AARE less than ±10. This showed excellent performance of Bharadwaj model in order to fit the experimentally determined CO_2 permeance values at feed pressure of 2 to 10 bar for PEI-*f*-MMT HFMM membrane. However, PEI-*f*-MMT (4) showed higher deviation for all pressure ranges. This is because, the *f*-MMT agglomerated at 4 wt. % as observed in Figure 4-19, and Bharadwaj model does not consider the effect of filler agglomeration.

Bharadwaj model is the most advanced and versatile model which incorporates the orientation geometry of the dispersed filler. In this study, the random oriented geometry of *f*-MMT filler is taken into account to generate theoretical curves as it is the most practical approach. Due to this assumption, Bharadwaj model is best suited to PEI-*f*-MMT HFMM membrane at various feed pressure and *f*-MMT loadings, compared to Nielsen, Cussler, Yang- Cussler and Lape- Cussler models.

4.9 Summary of key experimental findings

This study involved the synthesis, characterization and gas separation performance of hollow fibre membranes, which included PEI, PEI-MMT and PEI-*f*-MMT before and after applying PDMS coating.

The Na-MMT was modified through covalent modification. FTIR confirmed the presence of relevant functional groups on MMT clay surface whereas XRD confirmed the presence of organic molecules in the interlayer surface of MMT. The basal spacing has increased from 12.38 to 17.22 Å. The *f*-MMT showed better dispersion compared to unmodified MMT as confirmed by EDX micrographs whereas MMT tend to form agglomeration even at lower loading due to incompatible properties from host polymer matrix. Improved filler dispersion resulted in improved gas separation performance of the MMM. PEI-*f*-MMT HFMM membranes have been tested for CO_2 and CH_4 gas permeance and it showed better gas separation performance compared to its counterpart PEI-MMT membranes. Furthermore, the developed PEI-*f*-MMT showed higher CO_2/CH_4 ideal selectivity at all pressure except plasticization pressure at which the membranes showed reverse selective behavior. The developed membranes contain surface defects as confirmed by FESEM micrographs that deteriorate the membrane performance. Thus, the developed membranes were coated with PDMS to overcome the surface defects and tested again for CO_2 and CH_4 gases to evaluate the performance. It is noticed that the coated membranes at all pressure and filler loadings showed better performance compared to uncoated membranes. This improvement in separation performance was the result of surface defects reduction that were generated during solvent exchange in phase inversion method. Furthermore, PEI-*f*-MMT (2) membrane showed better performance as depicted by Robeson upper bound curve compared to neat PEI and other developed MMMs.

Furthermore, the CO_2 permeance of PEI-*f*-MMT HFMM membranes were compared to the theoretical existing models and it is observed that the Bharadwaj model showed closer agreement to the developed membranes, as it considered random clay platelets orientation.

CHAPTER 5

CONCLUSIONS AND RECOMMENDATIONS

The negatively charged montmorillonite layers attract cations like Na^{+1} and Ca^{+2} which possess affinity for polar molecules such as water and other polar solvents. Due to these weakly bonded interlayer cations, MMT contains high cation exchange capacity, which makes it a promising inorganic filler in MMM development. Cation exchange method is easy and viable, besides that, the weak bonding between cations and MMT layers enhances the exfoliation in polymer matrix. The inorganic cations of MMT were replaced with organic cations of 12-aminolauric acid via cation exchange method. The attachment of organic cation to the MMT surface was confirmed by FTIR analysis. The presence of several new peaks for *f*-MMT at wave number 1713, 2850 and 3236 cm^{-1} are associated with the stretching vibration of carbonyl groups, C-H stretching and N-H stretching, respectively. These newly appeared peaks confirmed the attachment of 12-aminolauric acid to the MMT surface. TGA revealed that the mass loss in *f*-MMT occurred in two stages at 260 and 358˚C. The former confirmed the presence of organic cations at the interlayer space, whilst the latter is associated with the covalent bonding of Si-OH and Al-OH groups at the outer surface of *f*-MMT. Moreover, the extent of attached aminolauric acid was estimated by TGA and was approximately 21 wt. %. Furthermore, XRD analysis revealed that the basal spacing has increased from 12.38 to 17.22 Å for *f*-MMT. The enhanced interlayer distance weakens the van der Waals forces and promotes the exfoliated morphology in polymer matrix. Moreover, dispersibility analysis revealed that the *f*-MMT is more hydrophobic and organophilic in nature compared to MMT.

Polymer concentration and air gap distance were optimized to prepare macrovoids free morphology of the developed membranes. Hollow fibre membranes with PEI concentrations of 10 to 28 wt. % were developed and the morphology was analyzed via SEM. It was noticed that at 25 wt. % PEI, the macrovoids are eliminated and uniform thickness of top layer is observed. Furthermore, PEI membranes at various air gaps ranging from 0 to 35 cm were developed and the morphology was analyzed via SEM. The micrographs showed that the optimum air gap distance for PEI/NMP hollow fibre membrane was 15 cm. A very thin, defect-free outer skin was observed and contained uniform finger-like pores under the outer thin skin. This pore structure favors gas permeation through the membrane.

The FESEM analysis showed asymmetric and macrovoids free morphology with uniform skin layer of developed PEI-MMT HFMM membranes. Moreover, EDX micrographs showed the poor dispersion characteristics of MMT in PEI matrix after 2 wt. % loading due to filler agglomeration. Surface topology was studied via AFM, and it was observed that with increase in MMT, surface roughness also increased. The surface roughness factor of 41.79 nm is observed for 4 wt. % MMT loading. PEI-MMT MMMs are thermally stable until 500˚C with slight increase in T_g with MMT loading. In addition, PEI-MMT membranes showed hydrophilic characteristics and decrease in contact angle was observed with filler loading. The contact angle decreased from 60.85 to 55.95 with MMT loading of 1 to 4 wt. % in PEI matrix. In contrast, *f*-MMT addition showed improved membrane morphology and dispersion in PEI matrix. Uniform filler dispersion in PEI matrix was observed via EDX micrographs. Surface properties of PEI-*f*-MMT membranes have improved as depicted by AFM and hydrophobic behavior is observed via contact angle measurement. The developed membranes were stable up to 436.16˚C, in which decrease in T_g was noticed with increase in *f*-MMT loading. Furthermore, the *f*-MMT addition improved the hydrophobicity of developed MMM. PEI-MMT (2) showed the lowest surface roughness of 12.57 nm and higher hydrophobic characteristics.

Neat coated PEI membrane showed enhanced selectivity and decrease in permeance with increase in gas feed pressure up to plasticization pressure of 8 bar, which represented true glassy behavior. PEI-MMT MMMs showed upward trend for gas permeance and downward trend for ideal selectivity with MMT loading due to filler agglomeration and surface voids. The maximum ideal selectivity of 10.215 is obtained for coated PEI-MMT (1) at 6 bar pressure. The incorporation of *f*-MMT not only improved the morphological characteristics, enhancement in gas separation was observed as well. For both CO_2 and CH_4, decrement in permeance was observed with *f*-MMT addition up to 3 wt. %. The ideal selectivity increased until 2 wt. % beyond which a downward trend is observed. The maximum ideal selectivity of 18.35 is obtained at 2 wt. % *f*-MMT loading at 4 bar pressure. The morphological diagram revealed that good interfacial interactions exist for *f*-MMT loadings. Moreover, the *f*-MMT incorporation in PEI matrix improved the gas separation performance as depicted in Robeson curve. Due to good interfacial interactions with polymer, PEI-*f*-MMT (2) successfully crossed the commercially attractive region in Robeson curve.

Existing phenomenological models such as Nielsen, Cussler, Yang-Cussler, Lape-Cussler and Bhardwaj models were opted in order to validate the experimental data. Initially, the aspect ratio of the *f*-MMT filler was estimated by incorporating the experimentally determined permeation values in theoretical models. The average aspect ratio was found to be 53, with 3 number of stacks per tactoid, which showed that the intercalation morphology is the dominating dispersion state of *f*-MMT filler in PEI matrix. Subsequently, the experimental CO_2 permeation values were validated with existing theoretical models at pressure range from 2 to 10 bar. Bhardwaj model proved to be the most suitable model at all feed pressures. The Bhardwaj model is versatile in nature, which assumed both parallel and horizontal distribution of incorporated filler. For *f*-MMT loading of 1 to 3 wt. % regardless of pressure, the %AARE range from -10.11 to 8.55, which showed closer agreement to the experimentally determined permeation values. However, at further loading, *f*-MMT agglomeration started and deviation from the experimental data was observed.

5.1 Future recommendations

Based on the experimental analysis and modeling study as well as the discussion provided and conclusions drawn from the current studies on membranes, future work is suggested for providing more insight into membrane development.

The present study encompasses the fabrication of neat PEI and mixed matrix hollow fibre membranes using modified/unmodified MMT filler. Following the same formulation, dense membranes in both flat and hollow fibre geometries can be developed to provide further insight into membrane performance parameters. This will enhance further understanding about parameters that affect the gas separation performance of membranes. Moreover, during hollow fibre membrane spinning, the effect of humidity, coagulation bath temperature and coagulant composition could also be studied to determine the mechanism that define membrane morphology. These results may pave the way towards commercialization of PEI-MMT mixed matrix membrane.

The dispersion state of the clay platelets defines the morphology and gas separation performance of developed membranes. Techniques which are used to manufacture polymer composites can be applied to fabricate MMMs. For instance, melt compounding which may produce direct exfoliation without using organic solvents, is an environmentally friendly, practical, and stable process that could be applied to fabricate MMMs dispersed with layered silicate [231]. Typically, the phase boundary defects between layered silicate and polymer phase results in poor membrane performance, nevertheless, these can be solved via crosslinking, thermal treatment, and priming protocol. The orientation of layered silicates is also a critical factor in defining the gas separation performance of MMMs, thus it should be carefully controlled during membrane casting.

Furthermore, the CO_2 induced plasticization follows different mechanism in dense and asymmetric membranes. For asymmetric membranes, the plasticization behavior depends on the thickness of membrane skin layer and affect the performance range of membrane. The correlation between skin layer thickness and plasticization mechanism could be studied quantitatively in asymmetric membranes, to optimize the membrane performance which is important for scaling up of membrane separation process.

The reported work on modelling was carried out for dense flat sheet membranes. It can be extended to the development of new permeation models for asymmetric membranes This will further improve understanding about the deviation behavior of membranes from modeling parameters.

LIST OF PUBLICATIONS

1. Asif Jamil, Oh Pei Ching, Azmi M Shariff, “Current Status and Future Prospect of Polymer-Layered Silicate Mixed Matrix Membranes for CO_2/CH_4 Separations”, Chemical Engineering & Technology, 39 (8) 1393-1405, 2016. (Quartile: Q2, I.F = 1.588)

2. Asif Jamil, Oh Pei Ching, Azmi M Shariff, “Mixed matrix hollow fibre membrane comprising polyetherimide and modified montmorillonite with improved filler dispersion and CO_2/CH_4 Separation performance”, Applied Clay, 143 115-124, 2017. (Quartile: Q1, I.F = 3.641)

3. Asif Jamil, Pei Ching, Azmi M Shariff, “Polyetherimide-montmorillonite mixed matrix hollow fibre membranes: Effect of inorganic/organic montmorillonite on CO_2/CH_4 separation”, Separation and Purification Technology, 206, 256-267, 2018. (Quartile: Q1, I.F = 3.927)

4. Asif Jamil, Oh Pei Ching, Azmi M Shariff, “Macrovoids suppression in Polyetherimide (PEI) hollow fibre membranes by optimizing the air gap”, International Journal of Applied Engineering Research, 11 (19), 9684-9688, 2016. (Scopus)

5. Asif Jamil, Oh Pei Ching, Azmi M Shariff, “Minimizing morphological defects of Polyetherimide (PEI) hollow fibre membranes by optimizing the dope viscosity”, APRN Journal of Engineering and Applied Science, 11, 2016. (Scopus)

6. Asif Jamil, Oh Pei Ching, Azmi M Shariff, “Polymer-Nanoclay Mixed Matrix Membranes for CO_2/CH_4 Separation: A Review”, Applied Mechanics and Materials, 625, 690-695, 2014. (Scopus).

CONFERENCE PRESENTATIONS

1. 3rd International Conference on Process Engineering and Advance Material, ESTCON 2014, held in Kuala Lumpur Convention Centre, Malaysia. A presentation on “Polymer-Nanoclay Mixed Matrix Membranes for CO_2/CH_4 Separation: A Review”.

2. 28th Symposium of Malaysian Chemical Engineers (SOMChE 2015), held in Palm Garden Hotel, Putrajaya, Malaysia. A presentation on “Macrovoids suppression in Polyetherimide (PEI) hollow fibre membranes by optimizing the air gap”.

3. Malaysian Technical Universities Conference on Engineering and Technology (MUCET 2015) held in Johor Bahru, Malaysia. A presentation on “Minimizing morphological defects of Polyetherimide (PEI) hollow fibre membranes by optimizing the dope viscosity”.

REFERENCES

[1] S. Husain and W. J. Koros, "Mixed matrix hollow fiber membranes made with modified HSSZ-13 zeolite in polyetherimide polymer matrix for gas separation," *Journal of Membrane Science*, vol. 288, pp. 195-207, 2007.

[2] X. J. Zhong, "Polymeric gas separation membranes for carbon dioxide removal," PhD, National University of Singapore, 2012.

[3] R. S. Murali, T. Sankarshana, and S. Sridhar, "Air separation by polymer-based membrane technology," *Separation & Purification Reviews,* vol. 42, pp. 130-186, 2013.

[4] R. Rautenbach and A. Gröschl, "Separation potential of nanofiltration membranes," *Desalination,* vol. 77, pp. 73-84, 1990.

[5] W. Byrne, Reverse osmosis: a practical guide for industrial users: Tall Oaks Pub., 2002.

[6] M. Wesslein, A. Heintz, and R. Lichtenthaler, "Pervaporation of liquid mixtures through poly (vinyl alcohol)(PVA) membranes. I. Study of water containing binary systems with complete and partial miscibility," *Journal of Membrane Science,* vol. 51, pp. 169-179, 1990.

[7] V. Dindore, D. Brilman, F. Geuzebroek, and G. Versteeg, "Membrane–solvent selection for CO_2 removal using membrane gas–liquid contactors," *Separation and Purification Technology,* vol. 40, pp. 133-145, 2004.

[8] G. Maier, "Gas separation with polymer membranes," *Angewandte Chemie International Edition,* vol. 37, pp. 2960-2974, 1998.

[9] M. H. M. Ashnani, A. Johari, H. Hashim, and E. Hasani, "A source of renewable energy in Malaysia, why biodiesel?," *Renewable and Sustainable Energy Reviews,* vol. 35, pp. 244-257, 2014.

[10] Bakar, Wan Azelee Wan Abu, and Rusmidah Ali. "Natural gas." In natural gas. InTech, 2010.

[11] D. Q. Vu, "Formation and characterization of asymmetric carbon molecular sieve and mixed-matrix membranes for natural gas purification," PhD Thesis, The university of Texas, Austin, 2001.

[12] D. Aaron and C. Tsouris, "Separation of CO_2 from flue gas: a review," *Separation Science and Technology,* vol. 40, pp. 321-348, 2005.

[13] R. Ur Rehman, S. Rafiq, N. Muhammad, A. L. Khan, A. Ur Rehman, L. TingTing, *et al.*, "Development of ethanolamine-based ionic liquid membranes for efficient CO_2/CH_4 separation," *Journal of Applied Polymer Science,* vol. 134, p. 45395, 2017.

[14] N. Jusoh, Y. F. Yeong, K. K. Lau, and A. M. Shariff, "Fabrication of silanated zeolite T/6FDA-durene composite membranes for CO_2/CH_4 separation," *Journal of Cleaner Production,* vol. 166, pp. 1043-1058, 2017.

[15] R. W. Baker, "Future directions of membrane gas separation technology," *Industrial & Engineering Chemistry Research,* vol. 41, pp. 1393-1411, 2002.

[16] S. Hussain, "Mixed Matrix Dual Layer Hollow Fiber Membranes for Natural Gas Separation," Doctor of Philosophy, School of Chemical & Biomolecular Engineering, Georgia Institute of Technology, 2006.

[17] R. E. Kesting and A. Fritzsche, *Polymeric gas separation membranes*: Wiley-Interscience, 1993.

[18] S. Loeb and S. Sourirajan, "Saline Water Conversion-II," *Advances in chemistry series,* vol. 38, p. 117, 1963.

[19] S. B. Carruthers, "Integral-skin formation in hollow fiber membranes for gas separations, PhD Thesis, The university of Texas, Austin 2001.

[20] K. H. Oh, "Effect of shear, elongation and phase separation in hollow fiber membrane spinning, PhD diss., Georgia Institute of Technology, 2014.

[21] N. Peng, T-S. Chung, and K. Y. Wang, "Macrovoid evolution and critical factors to form macrovoid-free hollow fiber membranes," *Journal of Membrane Science,* vol. 318, pp. 363-372, 2008.

[22] S. Husain and W. J. Koros, "Macrovoids in hybrid organic/inorganic hollow fiber membranes," *Industrial & Engineering Chemistry Research,* vol. 48, pp. 2372-2379, 2009.

[23] J. Ren, Z. Li, and F.-S. Wong, "Membrane structure control of BTDA-TDI/MDI (P84) co-polyimide asymmetric membranes by wet-phase inversion process," *Journal of membrane science,* vol. 241, pp. 305-314, 2004.

[24] M. Khayet, "The effects of air gap length on the internal and external morphology of hollow fiber membranes," *Chemical engineering science,* vol. 58, pp. 3091-3104, 2003.

[25] N. Widjojo and T-S. Chung, "Thickness and air gap dependence of macrovoid evolution in phase-inversion asymmetric hollow fiber membranes," *Industrial & engineering chemistry research*, vol. 45, pp. 7618-7626, 2006.

[26] M. R. Kosuri and W. J. Koros, "Defect-free asymmetric hollow fiber membranes from Torlon, a polyamide–imide polymer, for high-pressure CO_2 separations," *Journal of Membrane Science*, vol. 320, pp. 65-72, 2008.

[27] H. Tsai, L. Li, K. Lee, Y. Wang, C. Li, J. Huang, *et al.*, "Effect of surfactant addition on the morphology and pervaporation performance of asymmetric polysulfone membranes," *Journal of Membrane Science*, vol. 176, pp. 97-103, 2000.

[28] A. F. Ismail, "Preparation of Carbon Membranes for Gas Separation," *Comprehensive Membrane Science and Engineering*, E. Drioli and L. Giorno, Eds., ed Oxford: Elsevier, 2010, pp. 275-290.

[29] B. Li, "Fabrication and characterization of multifunctional polyetherimide/carbon nanofiller composites," PhD Thesis, Washington State University, 2012.

[30] L-P. Cheng, D-J. Lin, and K-C. Yang, "Formation of mica-intercalated-Nylon 6 nanocomposite membranes by phase inversion method," *Journal of Membrane Science*, vol. 172, pp. 157-166, 2000.

[31] T-S. Chung, L. Y. Jiang, Y. Li, and S. Kulprathipanja, "Mixed matrix membranes (MMMs) comprising organic polymers with dispersed inorganic fillers for gas separation," *Progress in Polymer Science*, vol. 32, pp. 483-507, 2007.

[32] B. Chen, "Polymer–clay nanocomposites: an overview with emphasis on interaction mechanisms," *British Ceramic Transactions*, 2013.

[33] F. Uddin, "Clays, nanoclays, and montmorillonite minerals," *Metallurgical and Materials Transactions A*, vol. 39, pp. 2804-2814, 2008.

[34] V. Mittal, "Polymer layered silicate nanocomposites: a review," *Materials*, vol. 2, pp. 992-1057, 2009.

[35] N. R. Horn and D. R. Paul, "Carbon dioxide plasticization and conditioning effects in thick vs. thin glassy polymer films," *Polymer*, vol. 52, pp. 1619-1627, 2011.

[36] A. Zulhairun, Z. Fachrurrazi, M. N. Izwanne, and A. Ismail, "Asymmetric hollow fiber membrane coated with polydimethylsiloxane–metal organic framework hybrid layer for gas separation," *Separation and Purification Technology,* vol. 146, pp. 85-93, 2015.

[37] S. Madaeni, M. Badieh, and V. Vatanpour, "Effect of coating method on gas separation by PDMS/PES membrane," *Polymer Engineering & Science,* vol. 53, pp. 1878-1885, 2013.

[38] N. José, L. d. A. Prado, and I. Yoshida, "Synthesis, characterization, and permeability evaluation of hybrid organic–inorganic films," *Journal of Polymer Science Part B: Polymer Physics,* vol. 42, pp. 4281-4292, 2004.

[39] H. Siti Badriah, "Development of hybrid membrane (polysulfone and zeolites) for gas separation application," Universiti Malaysia Pahang, 2010.

[40] D. F. Mohshim, H. b. Mukhtar, Z. Man, and R. Nasir, "Latest development on membrane fabrication for natural gas purification: a review," *Journal of Engineering,* vol. 2013, 2012.

[41] A. S. H. Ghaanim, "Preparation and characterization of PLA polymeric membrane for pervaporation applications," Masters, Chemical Engineering Department, University of Technology, 2012.

[42] M. Knudsen, "The laws of molecular flow and of inner friction flow of gases through tubes," *Journal of Membrane Science,* vol. 100, pp. 23-25, 1995.

[43] R. W. Baker, *Membrane technology*: Wiley Online Library, 2000.

[44] D. Gottschlich, D. Roberts, and J. Way, "A theoretical comparison of facilitated transport and solution-diffusion membrane modules for gas separation," *Gas Separation & Purification,* vol. 2, pp. 65-71, 1988.

[45] M. Muhammad, Y. F. Yeong, K. K. Lau, and A. B. Mohd Shariff, "Issues and Challenges in the Development of Deca-Dodecasil 3 Rhombohedral Membrane in CO_2 Capture from Natural Gas," *Separation & Purification Reviews,* vol. 44, pp. 331-340, 2015.

[46] A. Mansourizadeh and A. F. Ismail, "Hollow fiber gas–liquid membrane contactors for acid gas capture: A review," *Journal of Hazardous Materials,* vol. 171, pp. 38-53, 2009/11/15/ 2009.

[47] M. Mulder, *Basic principles of membrane technology*, Second ed.: Kluwer Academic, 1996.

[48] E. Mason, "From pig bladders and cracked jars to polysulfones: an historical perspective on membrane transport," *Journal of membrane science,* vol. 60, pp. 125-145, 1991.

[49] D. R. Paul and Y. P. Yampol'skii, *Polymeric gas separation membranes*: CRC press, 1993.

[50] J. D. Figueroa, T. Fout, S. Plasynski, H. McIlvried, and R. D. Srivastava, "Advances in CO_2 capture technology", The U.S. Department of Energy's Carbon Sequestration Program," *International Journal of Greenhouse Gas Control,* vol. 2, pp. 9-20, 2008.

[51] Z. Y. Yeo, T. L. Chew, P. W. Zhu, A. R. Mohamed, and S.-P. Chai, "Conventional processes and membrane technology for carbon dioxide removal from natural gas: a review," *Journal of Natural Gas Chemistry,* vol. 21, pp. 282-298, 2012.

[52] A. F. Ismail, Matsuura, Takeshi, "Gas Separation Membranes Polymeric and Inorganic," ed, 2015, pp. 2, 2015.

[53] A. Basile, S. P Nunes. *Advanced membrane science and technology for sustainable energy and environmental applications* vol. 25: Woodhead Publishing, 2011.

[54] P. Bernardo, E. Drioli, and G. Golemme, "Membrane gas separation: a review/state of the art," *Industrial & Engineering Chemistry Research,* vol. 48, pp. 4638-4663, 2009.

[55] R. Nasir, H. Mukhtar, Z. Man, and D. F. Mohshim, "Material Advancements in Fabrication of Mixed Matrix Membranes," *Chemical Engineering & Technology,* vol. 36, pp. 717-727, 2013.

[56] Mubashir, M., Yeong, Y.F. and Lau, K.K.,. Ultrasonic-assisted secondary growth of deca-dodecasil 3 rhombohedral (DD3R) membrane and its process optimization studies in CO_2/CH_4 separation using response surface methodology. *Journal of Natural Gas Science and Engineering*, 30, pp.50-63, 2016.

[57] Y. Zhang, J. Sunarso, S. Liu, and R. Wang, "Current status and development of membranes for CO_2/CH_4 separation: A review," *International Journal of Greenhouse Gas Control,* vol. 12, pp. 84-107.

[58] S. Li, J. L. Falconer, and R. D. Noble, "Improved SAPO-34 Membranes for CO_2/CH_4 Separations," *Advanced Materials,* vol. 18, pp. 2601-2603, 2006.

[59] M. C. Lovallo, A. Gouzinis, and M. Tsapatsis, "Synthesis and characterization of oriented MFI membranes prepared by secondary growth," *AIChE journal,* vol. 44, pp. 1903-1913, 1998.

[60] T. Tomita, K. Nakayama, and H. Sakai, "Gas separation characteristics of DDR type zeolite membrane," *Microporous and Mesoporous Materials,* vol. 68, pp. 71-75, 2004.

[61] M. Ogawa and Y. Nakano, "Separation of CO_2/CH_4 mixture through carbonized membrane prepared by gel modification," *Journal of Membrane Science,* vol. 173, pp. 123-132, 2000.

[62] R. M. De Vos and H. Verweij, "Improved performance of silica membranes for gas separation," *Journal of Membrane Science,* vol. 143, pp. 37-51, 1998.

[63] J. Van Den Bergh, W. Zhu, F. Kapteijn, J. A. Moulijn, K. Yajima, K. Nakayama, *et al.*, "Separation of CO_2 and CH_4 by a DDR membrane," *Research on Chemical Intermediates,* vol. 34, pp. 467-474, 2008.

[64] L. Van den Broeke, W. Bakker, F. Kapteijn, and J. Moulijn, "Transport and separation properties of a silicalite-1 membrane. Operating conditions," *Chemical engineering science,* vol. 54, pp. 245-258, 1999.

[65] Y. Zhang, J. Sunarso, S. Liu, and R. Wang, "Current status and development of membranes for CO2/CH4 separation: A review," *International Journal of Greenhouse Gas Control,* vol. 12, pp. 84-107, 2013.

[66] T. H. Bae, J. S. Lee, W. Qiu, W. J. Koros, C. W. Jones, and S. Nair, "A High-Performance Gas-Separation Membrane Containing Submicrometer-Sized Metal–Organic Framework Crystals," *Angewandte Chemie International Edition,* vol. 49, pp. 9863-9866, 2010.

[67] K. J. Kim, S. H. Park, W. W. So, D. J. Ahn, and S.-J. Moon, "CO_2 separation performances of composite membranes of 6FDA-based polyimides with a polar group," *Journal of membrane science,* vol. 211, pp. 41-49, 2003.

[68] R. Wang, C. Cao, and T-S. Chung, "A critical review on diffusivity and the characterization of diffusivity of 6FDA–6FpDA polyimide membranes for gas separation," *Journal of membrane science,* vol. 198, pp. 259-271, 2002.

[69] Y. Liu, M. L. Chng, T-S. Chung, and R. Wang, "Effects of amidation on gas permeation properties of polyimide membranes," *Journal of membrane science,* vol. 214, pp. 83-92, 2003.

[70] D. Q. Vu, W. J. Koros, and S. J. Miller, "Effect of Condensable Impurities in CO_2/CH_4 Gas Feeds on Carbon Molecular Sieve Hollow-Fiber Membranes," *Industrial & Engineering Chemistry Research,* vol. 42, pp. 1064-1075, 2003.

[71] D. Syrtsova, A. Kharitonov, V. Teplyakov, and G.-H. Koops, "Improving gas separation properties of polymeric membranes based on glassy polymers by gas phase fluorination," *Desalination,* vol. 163, pp. 273-279, 2004.

[72] S. Sridhar, T. M. Aminabhavi, and M. Ramakrishna, "Separation of binary mixtures of carbon dioxide and methane through sulfonated polycarbonate membranes," *Journal of applied polymer science,* vol. 105, pp. 1749-1756, 2007.

[73] K. Ghosal, B. Freeman, R. Chern, J. Alvarez, J. De La Campa, A. Lozano, *et al.*, "Gas separation properties of aromatic polyamides with sulfone groups," *Polymer,* vol. 36, pp. 793-800, 1995.

[74] C. Cao, R. Wang, T. S. Chung, and Y. Liu, "Formation of high-performance 6FDA-2, 6-DAT asymmetric composite hollow fiber membranes for CO_2/CH_4 separation," *Journal of membrane science,* vol. 209, pp. 309-319, 2002.

[75] C. Cao, T.-S. Chung, Y. Liu, R. Wang, and K. Pramoda, "Chemical cross-linking modification of 6FDA-2, 6-DAT hollow fiber membranes for natural gas separation," *Journal of membrane science,* vol. 216, pp. 257-268, 2003.

[76] A. F. Ismail, S. J. Shilton, I. Dunkin, and S. L. Gallivan, "Direct measurement of rheologically induced molecular orientation in gas separation hollow fibre membranes and effects on selectivity," *Journal of Membrane Science,* vol. 126, pp. 133-137, 1997.

[77] G. Dong, H. Li, and V. Chen, "Factors affect defect-free Matrimid hollow fiber gas separation performance in natural gas purification," *Journal of Membrane Science,* vol. 353, pp. 17-27, 2010.

[78] T. Visser, N. Masetto, and M. Wessling, "Materials dependence of mixed gas plasticization behavior in asymmetric membranes," *Journal of Membrane Science,* vol. 306, pp. 16-28, 2007.

[79] L. Jiang, T. S. Chung, D. F. Li, C. Cao, and S. Kulprathipanja, "Fabrication of Matrimid/polyethersulfone dual-layer hollow fiber membranes for gas separation," *Journal of Membrane Science,* vol. 240, pp. 91-103, 2004.

[80] M. Rahmani, A. Kazemi, F. Talebnia, and P. Abbasszadeh Gamali, "Fabrication and characterization of brominated matrimid 5218 membranes for CO_2/CH_4 separation: application of response surface methodology (RSM)," *e-Polymers,* vol. 16, pp. 481-492, 2016.

[81] M. Suleman, K. Lau, and Y. Yeong, "Development and performance evaluation of Polydimethyl siloxane/Polysulfone (PDMS/PSF) composite membrane for CO_2/CH_4 separation," in *IOP Conference Series: Earth and Environmental Science*, pp. 012014, 2016.

[82] C. A. Scholes, G. W. Stevens, and S. E. Kentish, "Membrane gas separation applications in natural gas processing," *Fuel,* vol. 96, pp. 15-28, 2012.

[83] D. R. Paul and D. R. Kemp, "The diffusion time lag in polymer membranes containing adsorptive fillers," in *Journal of Polymer Science: Polymer Symposia*, pp. 79-93, 1973.

[84] C. M. Zimmerman, A. Singh, and W. J. Koros, "Tailoring mixed matrix composite membranes for gas separations," *Journal of Membrane Science,* vol. 137, pp. 145-154, 1997.

[85] H. Lin and B. D. Freeman, "Materials selection guidelines for membranes that remove CO2 from gas mixtures," *Journal of Molecular Structure,* vol. 739, pp. 57-74, 2005.

[86] D. Q. Vu, W. J. Koros, and S. J. Miller, "Mixed matrix membranes using carbon molecular sieves: Preparation and experimental results," *Journal of Membrane Science,* vol. 211, pp. 311-334, 2003.

[87] J. M. Duval, A. J. B. Kemperman, B. Folkers, M. H. V. Mulder, G. Desgrandchamps, and C. A. Smolders, "Preparation of zeolite filled glassy polymer membranes," *Journal of Applied Polymer Science,* vol. 54, pp. 409-418, 1994.

[88] R. Mahajan, R. Burns, M. Schaeffer, and W. J. Koros, "Challenges in forming successful mixed matrix membranes with rigid polymeric materials," *Journal of Applied Polymer Science,* vol. 86, pp. 881-890, 2002.

[89] R. Mahajan and W. J. Koros, "Factors Controlling Successful Formation of Mixed-Matrix Gas Separation Materials," *Industrial & Engineering Chemistry Research,* vol. 39, pp. 2692-2696, 2013.

[90] C. Rubio, B. Zornoza, P. Gorgojo, C. Tellez, and J. Coronas, "Separation of H_2 and CO_2 Containing Mixtures with Mixed Matrix Membranes Based on Layered Materials," *Current Organic Chemistry,* vol. 18, pp. 2351-2363.

[91] Y. K. Kim, H. B. Park, and Y. M. Lee, "Preparation and characterization of carbon molecular sieve membranes derived from BTDA-ODA polyimide and their gas separation properties," *Journal of Membrane Science,* vol. 255, pp. 265-273, 2005.

[92] M. Sadeghi, M. A. Semsarzadeh, M. Barikani, and M. Pourafshari Chenar, "Gas separation properties of polyether-based polyurethane-silica nanocomposite membranes," *Journal of Membrane Science,* vol. 376, pp. 188-195, 2011.

[93] M. Schwanninger, J. C. Rodrigues, H. Pereira, and B. Hinterstoisser, "Effects of short-time vibratory ball milling on the shape of FT-IR spectra of wood and cellulose," *Vibrational Spectroscopy,* vol. 36, pp. 23-40, 2004.

[94] P. S. Goh, A. F. Ismail, S. M. Sanip, B. C. Ng, and M. Aziz, "Recent advances of inorganic fillers in mixed matrix membrane for gas separation," *Separation and Purification Technology,* vol. 81, pp. 243-264.

[95] A. L. Khan, C. Klaysom, A. Gahlaut, A. U. Khan, and I. F. J. Vankelecom, "Mixed matrix membranes comprising of Matrimid and SO_3H functionalized mesoporous MCM-41 for gas separation," *Journal of Membrane Science,* vol. 447, pp. 73-79, 2013.

[96] D. Bera, P. Bandyopadhyay, S. Ghosh, and S. Banerjee, "Gas transport properties of aromatic polyamides containing adamantyl moiety," *Journal of Membrane Science,* vol. 453, pp. 175-191, 2014.

[97] S. Kim and E. Marand, "High permeability nano-composite membranes based on mesoporous MCM-41 nanoparticles in a polysulfone matrix," *Microporous and Mesoporous Materials,* vol. 114, pp. 129-136, 9/1/ 2008.

[98] S. Basu, A. Cano-Odena, and I. F. Vankelecom, "MOF-containing mixed-matrix membranes for CO_2/CH_4 and CO_2/N_2 binary gas mixture separations," *Separation and Purification Technology*, vol. 81, pp. 31-40, 2011.

[99] E. Ameri, M. Sadeghi, N. Zarei, and A. Pournaghshband, "Enhancement of the gas separation properties of polyurethane membranes by alumina nanoparticles," *Journal of Membrane Science*, vol. 479, pp. 11-19, 2015.

[100] S. A. Hashemifard, A. F. Ismail, and T. Matsuura, "Effects of montmorillonite nano-clay fillers on PEI mixed matrix membrane for CO_2 removal," *Chemical Engineering Journal*, vol. 170, pp. 316-325, 2011.

[101] D. Q. Vu, W. J. Koros, and S. J. Miller, "Effect of condensable impurity in CO_2/CH_4 gas feeds on performance of mixed matrix membranes using carbon molecular sieves," *Journal of Membrane Science*, vol. 221, pp. 233-239, 2003.

[102] S. B. Messaoud, A. Takagaki, T. Sugawara, R. Kikuchi, and S. T. Oyama, "Mixed matrix membranes using SAPO-34/polyetherimide for carbon dioxide/methane separation," *Separation and Purification Technology*, vol. 148, pp. 38-48, 2015.

[103] Q. Song, S. Nataraj, M. V. Roussenova, J. C. Tan, D. J. Hughes, W. Li, *et al.*, "Zeolitic imidazolate framework (ZIF-8) based polymer nanocomposite membranes for gas separation," *Energy & Environmental Science*, vol. 5, pp. 8359-8369, 2012.

[104] H-L. Tyan, Y-C. Liu, and K-H. Wei, "Thermally and mechanically enhanced clay/polyimide nanocomposite via reactive organoclay," *Chemistry of materials*, vol. 11, pp. 1942-1947, 1999.

[105] X. Fu and S. Qutubuddin, "Polymer–clay nanocomposites: exfoliation of organophilic montmorillonite nanolayers in polystyrene," *Polymer*, vol. 42, pp. 807-813, 2001.

[106] A. Zulhairun, A. Ismail, T. Matsuura, M. Abdullah, and A. Mustafa, "Asymmetric mixed matrix membrane incorporating organically modified clay particle for gas separation," *Chemical Engineering Journal*, vol. 241, pp. 495-503, 2014.

[107] P. Anado, L. F. Sato, R. R. Montes, and H. S. De Santis, "Polysulphone/montmorillonite nanocomposite membranes: Effect of clay

addition and polysulphone molecular weight on the membrane properties," *Journal of Membrane Science,* vol. 455, pp. 187-199, 2014.

[108] S. Choi, J. Coronas, Z. Lai, D. Yust, F. Onorato, and M. Tsapatsis, "Fabrication and gas separation properties of polybenzimidazole (PBI)/nanoporous silicates hybrid membranes," *Journal of Membrane Science,* vol. 316, pp. 145-152, 2008.

[109] A. Galve, D. Sieffert, E. Vispe, C. Tallez, J. n. Coronas, and C. Staudt, "Copolyimide mixed matrix membranes with oriented microporous titanosilicate JDF-L1 sheet particles," *Journal of Membrane Science,* vol. 370, pp. 131-140, 2011.

[110] P. Gorgojo, A. Galve, S. Uriel, C. Tallez, and J. n. Coronas, "Direct exfoliation of layered zeolite Nu-6 (1)," *Microporous and Mesoporous Materials,* vol. 142, pp. 122-129, 2011.

[111] H.-K. Jeong, S. Nair, T. Vogt, L. C. Dickinson, and M. Tsapatsis, "A highly crystalline layered silicate with three-dimensionally microporous layers," *Nature materials,* vol. 2, pp. 53-58, 2003.

[112] W-g. Kim, J. S. Lee, D. G. Bucknall, W. J. Koros, and S. Nair, "Nanoporous layered silicate AMH-3/cellulose acetate nanocomposite membranes for gas separations," *Journal of Membrane Science*, vol. 441, pp. 129-136.

[113] S. Choi, J. Coronas, J. A. Sheffel, E. Jordan, W. Oh, S. Nair*, et al.*, "Layered silicate by proton exchange and swelling of AMH-3," *Microporous and Mesoporous Materials,* vol. 115, pp. 75-84, 2008.

[114] M. Rezakazemi, A. E. Amooghin, M. M. Montazer-Rahmati, A. F. Ismail, and T. Matsuura, "State-of-the-art membrane based CO_2 separation using mixed matrix membranes: An overview on current status and future directions," *Progress in Polymer Science,* vol. 39(5), pp.817-861, 2014.

[115] M. E. Leonowicz, J. A. Lawton, S. L. Lawton, and M. K. Rubin, "MCM-22: A Molecular Sieve with Two Independent Multidimensional Channel Systems," *Science,* vol. 264, pp. 1910-1913, 1994.

[116] U. Daaz, "Layered Materials with Catalytic Applications: Pillared and Delaminated Zeolites from MWW Precursors," *ISRN Chemical Engineering,* vol. 2012.

[117] W-g. Kim, S. Choi, and S. Nair, "Swelling, functionalization, and structural changes of the nanoporous layered silicates AMH-3 and MCM-22," *Langmuir,* vol. 27, pp. 7892-7901, 2011.

[118] S.-T. Yang, J.-Y. Kim, J. Kim, and W.-S. Ahn, "CO_2 capture over amine-functionalized MCM-22, MCM-36 and ITQ-2," *Fuel,* vol. 97, pp. 435-442.

[119] J. Choi and M. Tsapatsis, "MCM-22/Silica Selective Flake Nanocomposite Membranes for Hydrogen Separations," *Journal of the American Chemical Society,* vol. 132, pp. 448-449, 2009.

[120] F. Z. Annabi-Bergaya, "Layered clay minerals. Basic research and innovative composite applications," *Microporous and Mesoporous Materials,* vol. 107, pp. 141-148, 2008.

[121] Q. T. Nguyen and D. G. Baird, "Preparation of polymer-clay nanocomposites and their properties," *Advances in Polymer Technology,* vol. 25, pp. 270-285, 2006.

[122] A. Okada and A. Usuki, "The chemistry of polymer-clay hybrids," *Materials Science and Engineering: C,* vol. 3, pp. 109-115, 1995.

[123] A. Usuki, A. Koiwai, Y. Kojima, M. Kawasumi, A. Okada, T. Kurauchi*, et al.*, "Interaction of nylon-6 clay surface and mechanical properties of nylon-6 clay hybrid," *Journal of Applied Polymer Science,* vol. 55, pp. 119-123, 1995.

[124] Y. Kojima, A. Usuki, M. Kawasumi, A. Okada, T. Kurauchi, O. Kamigaito*, et al.*, "Novel preferred orientation in injection molded nylon-6 clay hybrid," *Journal of Polymer Science Part B: Polymer Physics,* vol. 33, pp. 1039-1045, 1995.

[125] Y. W. Chen-Yang, Y. K. Lee, Y. T. Chen, and J. C. Wu, "High improvement in the properties of exfoliated PU/clay nanocomposites by the alternative swelling process," *Polymer,* vol. 48, pp. 2969-2979, 2007.

[126] A. K. Zulhairun, A. F. Ismail, T. Matsuura, M. S. Abdullah, and A. Mustafa, "Asymmetric mixed matrix membrane incorporating organically modified clay particle for gas separation," *Chemical Engineering Journal*, vol 241, pp.495-503, 2014.

[127] S. Pavlidou and C. D. Papaspyrides, "A review on polymer-layered silicate nanocomposites," *Progress in polymer science*, vol. 33, pp. 1119-1198, 2008.

[128] S. A. Hashemifard, A. F. Ismail, and T. Matsuura, "Effects of montmorillonite nano-clay fillers on PEI mixed matrix membrane for CO_2 removal," *Chemical Engineering Journal,* vol. 170, pp. 316-325.

[129] S. A. Hashemifard, A. F. Ismail, and T. Matsuura, "Mixed matrix membrane incorporated with large pore size halloysite nanotubes (HNT) as filler for gas separation: experimental," *Journal of colloid and interface science,* vol. 359, pp. 359-370, 2011.

[130] G. Defontaine, A. Barichard, S. Letaief, C. Feng, T. Matsuura, and C. Detellier, "Nanoporous polymer–clay hybrid membranes for gas separation," *Journal of colloid and interface science,* vol. 343, pp. 622-627, 2010.

[131] J. M. Herrera-Alonso, Z. Sedlakova, and E. Marand, "Gas barrier properties of nanocomposites based on in situ polymerized poly (n-butyl methacrylate) in the presence of surface modified montmorillonite," *Journal of Membrane Science,* vol. 349, pp. 251-257, 2010.

[132] C.-Y. Liang, P. Uchytil, R. Petrychkovych, Y.-C. Lai, K. Friess, M. Sipek, *et al.*, "A comparison on gas separation between PES (polyethersulfone)/MMT (Na-montmorillonite) and PES/TiO_2 mixed matrix membranes," *Separation and purification technology,* vol. 92, pp. 57-63, 2012.

[133] W-g. Kim, J. S. Lee, D. G. Bucknall, W. J. Koros, and S. Nair, "Nanoporous layered silicate AMH-3/cellulose acetate nanocomposite membranes for gas separations," *Journal of membrane science,* vol. 441, pp. 129-136, 2013.

[134] N. M. Ismail, A. F. Ismail, and A. Mustaffa, "Characterization of polyethersulfone/cloisite-15A mixed matrix membrane for CO_2/CH_4 separation," *Jurnal Teknologi,* vol. 69, 2014.

[135] A. Zulhairun and A. Ismail, "The role of layered silicate loadings and their dispersion states on the gas separation performance of mixed matrix membrane," *Journal of Membrane Science,* vol. 468, pp. 20-30, 2014.

[136] A. M. Herring, "Inorganic polymer composite membranes for proton exchange membrane fuel cells," *Journal of Macromolecular Science, Part C: Polymer Reviews,* vol. 46, pp. 245-296, 2006.

[137] S. J. Ahmadi, Y. D. Huang, and W. Li, "Synthetic routes, properties and future applications of polymer-layered silicate nanocomposites," *Journal of Materials Science,* vol. 39, pp. 1919-1925, 2004.

[138] N. Nassar, "Melt exfoliation in montmorillonite/polystyrene nanocomposites," in *Masters Abstracts International,* 2003.

[139] N. Takahashi and K. Kuroda, "Materials design of layered silicates through covalent modification of interlayer surfaces," *Journal of Materials Chemistry,* vol. 21, pp. 14336-14353, 2011.

[140] G. Defontaine, A. Barichard, S. Letaief, C. Feng, T. Matsuura, and C. Detellier, "Nanoporous polymer Clay hybrid membranes for gas separation," *Journal of Colloid and Interface Science,* vol. 343, pp. 622-627, 2010.

[141] J. M. Herrera-Alonso, Z. Sedlakova, and E. Marand, "Gas barrier properties of nanocomposites based on insitu polymerized poly (n-butyl methacrylate) in the presence of surface modified montmorillonite," *Journal of Membrane Science,* vol. 349, pp. 251-257, 2010.

[142] J. M. Herrera-Alonso, Z. Sedlakova, and E. Marand, "Gas transport properties of polyacrylate/clay nanocomposites prepared via emulsion polymerization," *Journal of Membrane Science,* vol. 363, pp. 48-56, 2010.

[143] E. Picard, H. Gauthier, J. F. Garard, and E. Espuche, "Influence of the intercalated cations on the surface energy of montmorillonites: consequences for the morphology and gas barrier properties of polyethylene/montmorillonites nanocomposites," *Journal of colloid and interface science,* vol. 307, pp. 364-376, 2007.

[144] C. Silvestre, D. Duraccio, and S. Cimmino, "Food packaging based on polymer nanomaterials," *Progress in Polymer Science,* vol. 36, pp. 1766-1782, 2011.

[145] J. P. G. Villaluenga, M. Khayet, M. A. Lapez-Manchado, J. L. Valentin, B. Seoane, and J. I. Mengual, "Gas transport properties of polypropylene/clay composite membranes," *European Polymer Journal,* vol. 43, pp. 1132-1143, 2007.

[146] H. M. C. d. Azeredo, "Nanocomposites for food packaging applications," *Food Research International,* vol. 42, pp. 1240-1253, 2009.

[147] P. C. Oh and N. A. Mansur, "Effects of Aluminosilicate Mineral Nano-Clay Fillers on Polysulfone Mixed Matrix Membrane for Carbon Dioxide Removal," *Jurnal Teknologi,* vol. 69, pp. 23-27, 2014.

[148] C-Y. Liang, P. Uchytil, R. Petrychkovych, Y.-C. Lai, K. Friess, M. Sipek, *et al.,* "A comparison on gas separation between PES (polyethersulfone)/MMT (Na-montmorillonite) and PES/TiO_2 mixed matrix membranes," *Separation and Purification Technology,* vol. 92, pp. 57-63.

[149] O. Gain, E. Espuche, E. Pollet, M. Alexandre, and P. Dubois, "Gas barrier properties of poly (e-caprolactone)/clay nanocomposites: Influence of the morphology and polymer/clay interactions," *Journal of Polymer Science Part B: Polymer Physics,* vol. 43, pp. 205-214, 2005.

[150] V. Goodarzi, S. H. Jafari, H. A. Khonakdar, S. A. Monemian, and M. Mortazavi, "An assessment of the role of morphology in thermal/thermo-oxidative degradation mechanism of PP/EVA/clay nanocomposites," *Polymer Degradation and Stability,* vol. 95, pp. 859-869, 2010.

[151] M. Frounchi, S. Dadbin, Z. Salehpour, and M. Noferesti, "Gas barrier properties of PP/EPDM blend nanocomposites," *Journal of membrane science,* vol. 282, pp. 142-148, 2006.

[152] S. S. Loeb S, "Sea water demineralization by means of anosmotic membrane.," *Saline water conversion—II.,* pp. 117–32, 1963.

[153] A. F. Ismail and P. Y. Lai, "Development of defect-free asymmetric polysulfone membranes for gas separation using response surface methodology," *Separation and purification technology,* vol. 40, pp. 191-207, 2004.

[154] D. Huang, B. Mu, and A. Wang, "Preparation and properties of chitosan/poly (vinyl alcohol) nanocomposite films reinforced with rod-like sepiolite," *Materials Letters,* vol. 86, pp. 69-72.

[155] M. Rezaei, A. F. Ismail, S. A. Hashemifard, and T. Matsuura, "Preparation and characterization of PVDF-montmorillonite mixed matrix hollow fiber membrane for gas-liquid contacting process," *Chemical Engineering Research and Design,* vol. 92(11), pp.2449-2460, 2014.

[156] A. K. Zulhairun and A. F. Ismail, "The role of layered silicate loadings and their dispersion states on the gas separation performance of mixed matrix membrane," *Journal of Membrane Science,* vol. 468, pp. 20-30, 2014.

[157] N. M. Ismail, A. F. Ismail, and A. Mustaffa, "Characterization of Polyethersulfone/Cloisite 15A Mixed Matrix Membrane for CO_2/CH_4 Separation," *Jurnal Teknologi,* vol. 69, 2014.

[158] N. Peng, N. Widjojo, P. Sukitpaneenit, M. M. Teoh, G. G. Lipscomb, T.-S. Chung, *et al.*, "Evolution of polymeric hollow fibers as sustainable technologies: past, present, and future," *Progress in Polymer Science,* vol. 37, pp. 1401-1424, 2012.

[159] M. A. Frommer and R. M. Messalem, "Mechanism of membrane formation. VI. Convective flows and large void formation during membrane precipitation," *Industrial & Engineering Chemistry Product Research and Development,* vol. 12, pp. 328-333, 1973.

[160] H. Strathmann, "Asymmetric polyimide membranes for filtration of non-aqueous solutions," *Desalination,* vol. 26, pp. 85-92, 1978.

[161] G. Bakeri, A. F. Ismail, M. Shariaty-Niassar, and T. Matsuura, "Effect of polymer concentration on the structure and performance of polyetherimide hollow fiber membranes," *Journal of Membrane Science,* vol. 363, pp. 103-111, 2010.

[162] R. E. Kesting, A. K. Fritzsche, M. K. Murphy, A. C. Handermann, C. A. Cruse, and R. F. Malon, "Process for forming asymmetric gas separation membranes having graded density skins," ed: Google Patents, 1989.

[163] D. Wang, K. Li, and W. Teo, "Preparation and characterization of polyetherimide asymmetric hollow fiber membranes for gas separation," *Journal of membrane science,* vol. 138, pp. 193-201, 1998.

[164] H. Tsai, C. Kuo, J. Lin, D. Wang, A. Deratani, C. Pochat-Bohatier, *et al.*, "Morphology control of polysulfone hollow fiber membranes via water vapor induced phase separation," *Journal of Membrane Science,* vol. 278, pp. 390-400, 2006.

[165] A. F. Ismail and W. Lorna, "Penetrant-induced plasticization phenomenon in glassy polymers for gas separation membrane," *Separation and purification technology,* vol. 27, pp. 173-194, 2002.

[166] S. Shahid and K. Nijmeijer, "Performance and plasticization behavior of polymer-MOF membranes for gas separation at elevated pressures," *Journal of Membrane Science,* vol. 470, pp. 166-177.

[167] A. F. Ismail and W. Lorna, "Suppression of plasticization in polysulfone membranes for gas separations by heat-treatment technique," *Separation and Purification Technology,* vol. 30, pp. 37-46, 2003.

[168] J. D. Wind, C. Staudt-Bickel, D. R. Paul, and W. J. Koros, "Solid-state covalent cross-linking of polyimide membranes for carbon dioxide plasticization reduction," *Macromolecules,* vol. 36, pp. 1882-1888, 2003.

[169] C. Cao, T-S. Chung, Y. Liu, R. Wang, and K. P. Pramoda, "Chemical cross-linking modification of 6FDA-2, 6-DAT hollow fiber membranes for natural gas separation," *Journal of membrane science,* vol. 216, pp. 257-268, 2003.

[170] D. Åzen, H. Kalaplar, and L. Yilmaz, "Development of polycarbonate based zeolite 4A filled mixed matrix gas separation membranes," *Journal of Membrane Science,* vol. 303, pp. 194-203, 2007.

[171] A. Bos, I. Pünt, H. Strathmann, and M. Wessling, "Suppression of gas separation membrane plasticization by homogeneous polymer blending," *AIChE Journal,* vol. 47, pp. 1088-1093, 2001.

[172] Y. Cui, S. Kumar, B. R. Kona, and D. van Houcke, "Gas barrier properties of polymer/clay nanocomposites," *RSC Advances,* vol. 5, pp. 63669-63690, 2015.

[173] Y. Yampolskii, "Polymeric gas separation membranes," *Macromolecules,* vol. 45, pp. 3298-3311, 2012.

[174] G. Choudalakis and A. Gotsis, "Permeability of polymer/clay nanocomposites: a review," *European Polymer Journal,* vol. 45, pp. 967-984, 2009.

[175] L. E. Nielsen, "Models for the permeability of filled polymer systems," *Journal of Macromolecular Science—Chemistry,* vol. 1, pp. 929-942, 1967.

[176] E. Cussler, S. E. Hughes, W. J. Ward, and R. Aris, "Barrier membranes," *Journal of Membrane Science,* vol. 38, pp. 161-174, 1988.

[177] C. Yang, W. Smyrl, and E. Cussler, "Flake alignment in composite coatings," *Journal of Membrane Science,* vol. 231, pp. 1-12, 2004.

[178] N. K. Lape, E. E. Nuxoll, and E. Cussler, "Polydisperse flakes in barrier films," *Journal of membrane science,* vol. 236, pp. 29-37, 2004.

[179] R. K. Bharadwaj, "Modeling the barrier properties of polymer-layered silicate nanocomposites," *Macromolecules,* vol. 34, pp. 9189-9192, 2001.

[180] Z. Navratilova, P. Wojtowicz, L. Vaculikova, and V. Sugarkova, "Sorption of alkylammonium cations on montmorillonite," *Acta Geodynamica et Geomaterialia,* vol. 4, p. 59, 2007.

[181] B. J. Saikia and G. Parthasarathy, "Fourier transform infrared spectroscopic characterization of kaolinite from Assam and Meghalaya, Northeastern India," *Journal of Modern Physics,* vol. 1, p. 206, 2010.

[182] M. Behroozi and M. Pakizeh, "Study the effects of Cloisite15A nanoclay incorporation on the morphology and gas permeation properties of Pebax2533 polymer," *Journal of Applied Polymer Science,* vol 134, pp.45302, 2017.

[183] A. Usuki, M. Kawasumi, Y. Kojima, A. Okada, T. Kurauchi, and O. Kamigaito, "Swelling behavior of montmorillonite cation exchanged for ω-amino acids by ∊-caprolactam," *Journal of Materials Research,* vol. 8, pp. 1174-1178, 1993.

[184] L. Zhou, H. Chen, X. Jiang, F. Lu, Y. Zhou, W. Yin*, et al.*, "Modification of montmorillonite surfaces using a novel class of cationic gemini surfactants," *Journal of colloid and interface science,* vol. 332, pp. 16-21, 2009.

[185] G. Bakeri, A. Ismail, M. Shariaty-Niassar, and T. Matsuura, "Effect of polymer concentration on the structure and performance of polyetherimide hollow fiber membranes," *Journal of membrane science,* vol. 363, pp. 103-111, 2010.

[186] A. Ismail and P. Lai, "Effects of phase inversion and rheological factors on formation of defect-free and ultrathin-skinned asymmetric polysulfone membranes for gas separation," *Separation and purification technology,* vol. 33, pp. 127-143, 2003.

[187] B. F. Kingsbury and K. Li, "A morphological study of ceramic hollow fibre membranes," *Journal of Membrane Science,* vol. 328, pp. 134-140, 2009.

[188] A. K. Itta, H.-H. Tseng, and M.-Y. Wey, "Effect of dry/wet-phase inversion method on fabricating polyetherimide-derived CMS membrane for H_2/N_2

separation," *international journal of hydrogen energy,* vol. 35, pp. 1650-1658, 2010.

[189] D. Wang, W. Teo, and K. Li, "Preparation and characterization of high-flux polysulfone hollow fibre gas separation membranes," *Journal of Membrane Science,* vol. 204, pp. 247-256, 2002.

[190] A. Salahi, T. Mohammadi, R. M. Behbahani, and M. Hemmati, "Asymmetric polyethersulfone ultrafiltration membranes for oily wastewater treatment: synthesis, characterization, ANFIS modeling, and performance," *Journal of Environmental Chemical Engineering,* vol. 3, pp. 170-178, 2015.

[191] Henis, J.M. and Tripodi, M.K.,. Composite hollow fiber membranes for gas separation: the resistance model approach. Journal of Membrane Science, vol 8, pp.233-246, 1981

[192] M. Rezaei, A. Ismail, S. Hashemifard, and T. Matsuura, "Preparation and characterization of PVDF-montmorillonite mixed matrix hollow fiber membrane for gas–liquid contacting process," *Chemical Engineering Research and Design,* vol. 92, pp. 2449-2460, 2014.

[193] J. M. Yeh, M. Y. Yu, and S. J. Liou, "Dehydration of water–alcohol mixtures by vapor permeation through PVA/clay nanocomposite membrane," *Journal of applied polymer science,* vol. 89, pp. 3632-3638, 2003.

[194] M. Rezaei, A. Ismail, S. Hashemifard, G. Bakeri, and T. Matsuura, "Experimental study on the performance and long-term stability of PVDF/montmorillonite hollow fiber mixed matrix membranes for CO_2 separation process," *International Journal of Greenhouse Gas Control,* vol. 26, pp. 147-157, 2014.

[195] H. Zhu, X. Jie, L. Wang, G. Kang, D. Liu, and Y. Cao, "Effect of MIL-53 on phase inversion and gas separation performance of mixed matrix hollow fiber membranes," *RSC Advances,* vol. 6, pp. 69124-69134, 2016.

[196] S. Bandyopadhyay, E. Giannelis, and A. Hsieh, "Thermal and thermo-mechanical properties of PMMA nanocomposites," *Polymeric Materials Science and Engineering(USA),* vol. 82, pp. 208-209, 2000.

[197] A. Usuki, Y. Kojima, M. Kawasumi, A. Okada, Y. Fukushima, T. Kurauchi, *et al.*, "Synthesis of nylon 6-clay hybrid," *Journal of Materials Research*, vol. 8, pp. 1179-1184, 1993.

[198] R. Nasir, "Synthesis, characterization and perfromance evaluation of amine mixed matrix membranes for CO_2/CH_4 separation," PhD, Universiti Teknologi Petronas, 2016.

[199] M. R. DashtArzhandi, A. Ismail, T. Matsuura, B. Ng, and M. Abdullah, "Fabrication and characterization of porous polyetherimide/montmorillonite hollow fiber mixed matrix membranes for CO_2 absorption via membrane contactor," *Chemical Engineering Journal*, vol. 269, pp. 51-59, 2015.

[200] N. M. Ismail, A. Ismail, A. Mustafa, T. Matsuura, T. Soga, K. Nagata, *et al.*, "Qualitative and quantitative analysis of intercalated and exfoliated silicate layers in asymmetric polyethersulfone/cloisite15A mixed matrix membrane for CO_2/CH_4 separation," *Chemical Engineering Journal*, vol. 268, pp. 371-383, 2015.

[201] M. R. DashtArzhandi, A. Ismail, and T. Matsuura, "Carbon dioxide stripping through water by porous PVDF/montmorillonite hollow fiber mixed matrix membranes in a membrane contactor," *RSC Advances*, vol. 5, pp. 21916-21924, 2015.

[202] McKelvey, S.A. and Koros, W.J., Phase separation, vitrification, and the manifestation of macrovoids in polymeric asymmetric membranes. *Journal of Membrane Science*, 112(1), pp.29-39, 1996.

[203] L. Y. Jiang, T. S. Chung, C. Cao, Z. Huang, and S. Kulprathipanja, "Fundamental understanding of nano-sized zeolite distribution in the formation of the mixed matrix single-and dual-layer asymmetric hollow fiber membranes," *Journal of membrane science*, vol. 252, pp. 89-100, 2005.

[204] N. Mansur, "Effects of Aluminosilicate Mineral Nano-Clay Fillers on Polysulfone Mixed Matrix Membrane for Carbon Dioxide Removal," 2014.

[205] P. Garg, R. Singh, and V. Choudhary, "Pervaporation separation of organic azeotrope using poly (dimethyl siloxane)/clay nanocomposite membranes," *Separation and purification technology*, vol. 80, pp. 435-444, 2011.

[206] R. Barrer, "Diffusivities in glassy polymers for the dual mode sorption model," *Journal of membrane science,* vol. 18, pp. 25-35, 1984.

[207] N. Muruganandam and D. Paul, "Gas sorption and transport in miscible blends of tetramethyl bisphenol-A polycarbonate and polystyrene," *Journal of Polymer Science Part B: Polymer Physics,* vol. 25, pp. 2315-2329, 1987.

[208] S. Shahid and K. Nijmeijer, "High pressure gas separation performance of mixed-matrix polymer membranes containing mesoporous Fe (BTC)," *Journal of membrane science,* vol. 459, pp. 33-44, 2014.

[209] S. Saedi, S. Madaeni, A. A. Shamsabadi, and F. Mottaghi, "The effect of surfactants on the structure and performance of PES membrane for separation of carbon dioxide from methane," *Separation and purification technology,* vol. 99, pp. 104-119, 2012.

[210] J. Xia, T.-S. Chung, P. Li, N. R. Horn, and D. Paul, "Aging and carbon dioxide plasticization of thin polyetherimide films," *Polymer,* vol. 53, pp. 2099-2108, 2012.

[211] G. Dong, H. Li, and V. Chen, "Plasticization mechanisms and effects of thermal annealing of Matrimid hollow fiber membranes for CO_2 removal," *Journal of membrane science,* vol. 369, pp. 206-220, 2011.

[212] W-H. Lin and T.-S. Chung, "Gas permeability, diffusivity, solubility, and aging characteristics of 6FDA-durene polyimide membranes," *Journal of Membrane Science,* vol. 186, pp. 183-193, 2001.

[213] S. Rafiq, Z. Man, A. Maulud, N. Muhammad, and S. Maitra, "Separation of CO_2 from CH_4 using polysulfone/polyimide silica nanocomposite membranes," *Separation and purification technology,* vol. 90, pp. 162-172, 2012.

[214] R. Nasir, H. Mukhtar, Z. Man, M. S. Shaharun, and M. Z. A. Bakar, "Effect of fixed carbon molecular sieve (CMS) loading and various di-ethanolamine (DEA) concentrations on the performance of a mixed matrix membrane for CO_2/CH_4 separation," *RSC Advances,* vol. 5, pp. 60814-60822, 2015.

[215] S. Rafiq, Z. Man, A. Maulud, N. Muhammad, and S. Maitra, "Effect of varying solvents compositions on morphology and gas permeation properties on membranes blends for CO_2 separation from natural gas," *Journal of membrane science,* vol. 378, pp. 444-452, 2011.

[216] J. M. Herrera-Alonso, E. Marand, J. C. Little, and S. S. Cox, "Transport properties in polyurethane/clay nanocomposites as barrier materials: effect of processing conditions," *Journal of Membrane Science,* vol. 337, pp. 208-214, 2009.

[217] A. F. Ismail, R. Norida, W. A. Rahman, T. Matsuura, and S. Hashemifard, "Preparation and characterization of hyperthin-skinned and high performances asymmetric polyethersulfone membrane for gas separation," *Desalination,* vol. 273, pp. 93-104, 2011.

[218] T. T. Moore and W. J. Koros, "Non-ideal effects in organic–inorganic materials for gas separation membranes," *Journal of Molecular Structure,* vol. 739, pp. 87-98, 2005.

[219] S. Hashemifard, A. Ismail, and T. Matsuura, "Mixed matrix membrane incorporated with large pore size halloysite nanotubes (HNTs) as filler for gas separation: morphological diagram," *Chemical engineering journal,* vol. 172, pp. 581-590, 2011.

[220] L. M. Robeson, "The upper bound revisited," *Journal of Membrane Science,* vol. 320, pp. 390-400, 2008.

[221] H. Sanaeepur, A. E. Amooghin, A. Moghadassi, and A. Kargari, "Preparation and characterization of acrylonitrile–butadiene–styrene/poly (vinyl acetate) membrane for CO_2 removal," *Separation and Purification Technology,* vol. 80, pp. 499-508, 2011.

[222] N. Azizi, T. Mohammadi, and R. M. Behbahani, "Comparison of permeability performance of PEBAX-1074/TiO_2, PEBAX-1074/SiO_2 and PEBAX-1074/Al_2O_3 nanocomposite membranes for CO2/CH4 separation," *Chemical Engineering Research and Design,* vol. 117, pp. 177-189, 2017.

[223] A. M. Hillock and W. J. Koros, "Cross-linkable polyimide membrane for natural gas purification and carbon dioxide plasticization reduction," *Macromolecules,* vol. 40, pp. 583-587, 2007.

[224] H.-K. Jeong, W. Krych, H. Ramanan, S. Nair, E. Marand, and M. Tsapatsis, "Fabrication of polymer/selective-flake nanocomposite membranes and their use in gas separation," *Chemistry of Materials,* vol. 16, pp. 3838-3845, 2004.

[225] S. Sridhar, B. Smitha, and T. Aminabhavi, "Separation of carbon dioxide from natural gas mixtures through polymeric membranes—a review," *Separation & Purification Reviews,* vol. 36, pp. 113-174, 2007.

[226] M. Rubal, C. W. Wilkins, P. E. Cassidy, C. Lansford, and Y. Yamada, "Fluorinated polyimide nanocomposites for CO_2/CH_4 separation," *Polymers for Advanced Technologies,* vol. 19, pp. 1033-1039, 2008.

[227] G. Q. Chen, C. A. Scholes, G. G. Qiao, and S. E. Kentish, "Water vapor permeation in polyimide membranes," *Journal of membrane science,* vol. 379, pp. 479-487, 2011.

[228] K. Yano, A. Usuki, and A. Okada, "Synthesis and properties of polyimide-clay hybrid films," *Journal of Polymer Science Part A: Polymer Chemistry,* vol. 35, pp. 2289-2294, 1997.

[229] Y. S. Bhole, S. D. Wanjale, U. K. Kharul, and J. P. Jog, "Assessing feasibility of polyarylate–clay nanocomposites towards improvement of gas selectivity," *Journal of membrane science,* vol. 306, pp. 277-286, 2007.

[230] E. Picard, A. Vermogen, J-F. Gérard, and E. Espuche, "Barrier properties of nylon 6-montmorillonite nanocomposite membranes prepared by melt blending: influence of the clay content and dispersion state: consequences on modelling," *Journal of Membrane Science,* vol. 292, pp. 133-144, 2007.

[231] C. Rubio, B. Zornoza, P. Gorgojo, C. Tellez, and J. Coronas, "Separation of H_2 and CO_2 containing mixtures with mixed matrix membranes based on layered materials," *Current Organic Chemistry,* vol. 18, pp. 2351-2363, 2014.

APPENDICES

APPENDIX A.1: GAS PERMEATION TEST RIG USED IN THIS RESEARCH

APPENDIX B: CALCULATIONS FOR HOLLOW FIBRE MEMBRANES

The gas permeance (CO_2, CH_4) was determined by passing the gas at certain volumetric flow rate. Digital flow meter installed at the permeation cell measured the gas flow rate across the membranes which was latter normalized to standard temperature and pressure. All the permeance tests were carried out at ambient temperature and varying feed pressure from 2 to 10 bars.

The calculation method is elaborated for PEI HF membrane. The effective surface area for hollow fibre membrane is 7.54 cm^2 with fibre length of 15 cm and 2 number of fibres in the module. The CO_2 flow rate recorded is 24 ml/min.

By conversion $Q = 0.4\ cm^3/s$

Normalization of 'Q' with STP, hence,

$$Q_{STP} = \frac{T_{STP}}{T_{25c}} \times Q$$

$$Q_{STP} = 0.367\ cm^3/s$$

CO_2 flux J, is calculated as:

$$J = \frac{Q_{STP}}{A}$$

$$J = 0.0486\ cm^3(STP)/cm^2.sec$$

The CO_2 permeance, P_{co_2}/l, is calculated by,

$$\frac{P_{CO2}}{l} = \frac{J}{\Delta P}$$

$$\frac{P_{CO2}}{l} = 323.98\ \text{GPU}$$

By following the same equations, the permeance of methane is calculated as;

$$\frac{P_{CH4}}{l} = 56.02 \text{ GPU}$$

The ideal selectivity is calculated by taking the ratio of permeance of CO_2 to CH_4;

$$\propto_{CO_2/CH_4} = \frac{P_{CO_2}/l}{P_{CH_4}/l}$$

$$\propto_{CO_2/CH_4} = 5.78$$

APPENDIX B.2: MIXED CO_2/CH_4 GAS PERMEANCE AND SELECTIVITY CALCULATIONS

For mixed (CO_2 & CH_4) gas analysis, the flow rate was noted from the permeation cell for any membrane at a certain pressure and calculated to gas permeance as described in Appendix B.1. For volumetric analysis of collected gases, GC analysis is required.

For instance, if the gas permeance is 125 GPU, and the composition of CO_2 and CH_4 is found to be 70 % and 30 %, respectively, the gas (CO_2 & CH_4) permeance is calculated as:

$$\frac{P_{CO2}}{l} = 70\ \% \times \frac{P_{mix}}{l}$$

$$\frac{P_{CO2}}{l} = 0.70 \times 125\ GPU$$

$$\frac{P_{CO2}}{l} = 0.70 \times 125\ GPU$$

$$\frac{P_{CO2}}{l} = 87.5\ GPU$$

Similarly,

$$\frac{P_{CH4}}{l} = 37.5\ GPU$$

The selectivity of the mixture is:

$$\propto_{CO_2/CH_4} = \frac{P_{CO_2}/l}{P_{CH_4}/l}$$

$$\propto_{CO_2/CH_4} = \frac{87.5}{37.5}$$

$$\propto_{CO_2/CH_4} = 2.33$$

Table A.1: Gas permeation performance of uncoated PEI-MMT hollow fibre membranes.

Sr. No	HFM	Pressure	Flow rate		Permeance		Selectivity
		bar	CO_2	CH_4	CO_2	CH_4	
1	PEI	2	24.0	4.2	324.0	56.0	5.78
2		4	51.0	8.6	344.2	57.9	5.94
3		6	72.0	12.0	324.0	54.0	6.00
4		8	95.0	16.1	320.6	54.4	5.89
5		10	121.0	24.3	343.9	68.9	4.99
1	PEI-MMT (1)	2	21.0	4.7	283.5	63.2	4.49
2		4	43.0	8.8	290.2	59.4	4.89
3		6	67.0	13.4	301.5	60.3	5.00
4		8	101.0	25.0	340.9	84.4	4.04
5		10	139.0	50.0	395.0	142.1	2.78
1	PEI-MMT (2)	2	22.0	5.0	297.0	67.5	4.40
2		4	42.0	9.5	293.5	64.1	4.58
3		6	66.0	14.0	297.0	63.0	4.71
4		8	96.0	24.0	324.0	81.0	4.00
5		10	137.0	51.0	389.3	144.9	2.69
1	PEI-MMT (3)	2	26.0	6.0	351.0	81.0	4.33
2		4	51.0	12.0	344.2	81.0	4.25
3		6	80.0	20.0	360.0	90.0	4.00
4		8	116.0	30.0	391.5	101.2	3.87
5		10	151.0	53.0	429.1	150.6	2.85
1	PEI-MMT (4)	2	29.0	8.0	391.5	108.0	3.63
2		4	59.0	17.0	398.2	114.7	3.47
3		6	89.0	26.0	405.0	117.0	3.46
4		8	119.0	39.0	401.6	131.6	3.05
5		10	152.0	57.0	432.0	162.0	2.67

Table A2: Gas permeance of Uncoated PEI-f-MMT hollow fibre mixed matrix membranes.

Sr. No	HFM	Pressure	Flow rate		Permeance		
		bar	CO_2	CH_4	CO_2	CH_4	Selectivity
1	PEI	2	24.0	4.2	324.0	56.0	5.78
2		4	51.0	8.6	344.2	57.9	5.94
3		6	72.0	12.0	324.0	54.0	6.00
4		8	95.0	16.1	320.6	54.4	5.89
5		10	121.0	24.3	343.9	68.9	4.99
1	PEI-*f*-MMT (1)	2	20.0	2.5	270.0	33.9	7.97
2		4	39.0	4.9	263.2	32.7	8.04
3		6	59.0	7.2	265.5	32.5	8.16
4		8	75.0	9.2	253.1	31.2	8.12
5		10	99.0	13.9	281.4	39.4	7.15
1	PEI-*f*-MMT (2)	2	19.0	2.3	256.5	31.5	8.16
2		4	37.0	4.4	249.7	29.8	8.37
3		6	55.0	6.7	247.5	33.1	7.48
4		8	72.0	8.8	243.0	29.6	8.20
5		10	102.0	14.8	289.9	42.1	6.88
1	PEI-*f*-MMT (3)	2	19.0	2.4	256.5	32.7	7.85
2		4	36.0	4.5	243.0	30.2	8.04
3		6	54.0	6.6	243.0	29.9	8.13
4		8	74.0	9.2	249.7	31.1	8.02
5		10	104.0	14.0	295.6	39.8	7.43
1	PEI-*f*-MMT (4)	2	22.0	3.0	297.0	40.5	7.33
2		4	45.0	6.0	303.7	40.5	7.50
3		6	69.0	8.7	310.5	39.2	7.93
4		8	92.0	12.0	310.5	40.5	7.67
5		10	114.0	17.0	324.0	48.3	6.71

Table A3: Gas permeance of PDMS coated PEI-MMT hollow fibre mixed matrix membranes.

Sr. No	HFM	Pressure	Flow rate		Permeance		Selectivity
		bar	CO_2	CH_4	CO_2	CH_4	
1	PEI	2	10.9	0.9	146.6	12.2	12.07
2		4	20.9	1.7	141.1	11.7	12.06
3		6	29.8	2.6	134.1	11.5	11.69
4		8	38.8	4.0	130.9	13.5	9.70
5		10	55.3	4.8	157.2	13.6	11.52
1	PEI-MMT (1)	2	14.2	1.7	192.2	22.8	8.43
2		4	27.9	3.1	188.3	20.9	9.00
3		6	42.0	4.1	189.0	18.5	10.22
4		8	60.0	6.9	202.5	23.3	8.69
5		10	77.0	8.9	218.8	25.2	8.69
1	PEI-MMT (2)	2	15.3	1.7	206.5	23.1	8.95
2		4	29.8	3.3	201.1	22.1	9.08
3		6	44.5	4.6	200.2	20.8	9.61
4		8	62.3	7.1	210.4	24.0	8.78
5		10	80.0	9.2	227.2	26.1	8.69
1	PEI-MMT (3)	2	17.0	2.1	229.5	28.4	8.09
2		4	33.4	4.0	225.2	27.0	8.34
3		6	50.0	6.1	225.0	27.5	8.20
4		8	70.0	9.2	236.2	31.1	7.61
5		10	87.5	11.6	248.7	33.0	7.54
1	PEI-MMT (4)	2	20.0	2.9	270.0	38.5	7.02
2		4	39.0	5.4	263.2	36.2	7.28
3		6	58.0	7.9	261.0	35.6	7.34
4		8	90.0	14.0	303.7	47.2	6.43
5		10	111.0	18.0	315.5	51.2	6.17

Table A4: Gas permeance of PDMS coated PEI-MMT hollow fibre mixed matrix membranes.

Sr. No	HFM	Pressure	Flow rate		Permeance		Selectivity
		bar	CO_2	CH_4	CO_2	CH_4	
1	PEI	2	10.9	0.9	146.6	12.2	12.07
2		4	20.9	1.7	141.1	11.7	12.06
3		6	29.8	2.6	134.1	11.5	11.69
4		8	38.8	4.0	130.9	13.5	9.70
5		10	55.3	4.8	157.2	13.6	11.52
1	PEI-*f*-MMT (1)	2	10.5	0.7	141.2	9.5	14.94
2		4	20.5	1.3	138.5	8.6	16.07
3		6	32.8	2.0	137.6	8.4	16.40
4		8	38.7	3.0	130.8	10.1	13.01
5		10	55.0	3.9	146.3	10.2	14.29
1	PEI-*f*-MMT (2)	2	10.5	0.6	131.7	7.5	17.50
2		4	21.1	1.2	132.4	7.2	18.35
3		6	30.0	1.8	129.5	7.1	18.23
4		8	41.0	2.3	128.4	7.2	17.90
5		10	50.0	2.8	132.1	7.5	17.54
1	PEI-*f*-MMT (3)	2	10.2	0.6	127.7	7.8	16.45
2		4	20.2	1.2	126.3	7.6	16.57
3		6	27.8	1.7	125.0	7.7	16.13
4		8	37.7	2.4	127.3	8.0	15.83
5		10	49.5	3.2	130.7	8.3	15.67
1	PEI-*f*-MMT (4)	2	12.0	1.0	151.3	12.7	11.95
2		4	22.0	1.8	148.6	12.0	12.37
3		6	35.0	2.7	147.5	11.4	12.96
4		8	45.5	3.8	143.6	12.0	11.98
5		10	55.8	4.7	148.6	12.5	11.87

APPENDIX C: STATE OF DELAMINATION

Bharadwaj proposed the method to calculate the delamination state of the dispersed layered filler in polymer matrix. The model is based on simple calculation steps and is explained in the following example.

The lateral dimension of MMT is given as 218 nm, and the aspect ratio value of 53 is estimated by permeation models. The width of the dispersed MMT tactoid can be calculated as;

$$aspect\ ratio = \frac{Length}{Width}$$

$$Width = \frac{218}{53}$$

$$Width = 4.11\ nm$$

According to Bharadwaj assumptions, each layer of MMT is 1 nm thick whereas polymer chain intercalation increased the interlayer distance to 1 nm as explained in the Figure.

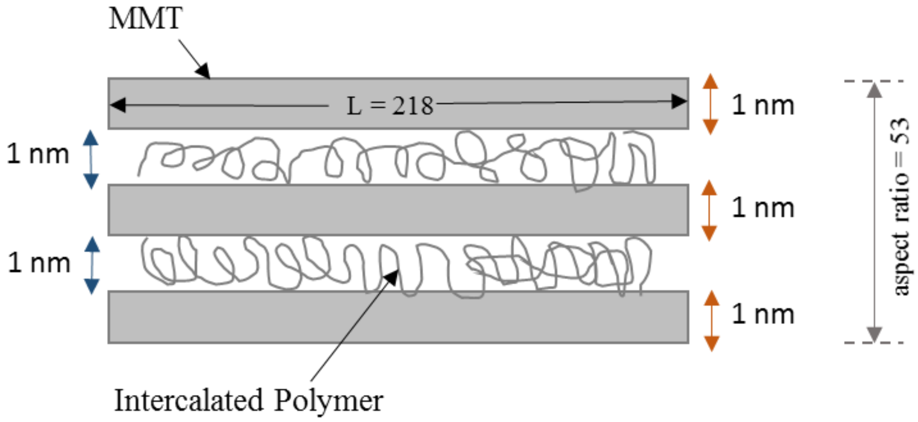

Since the width of the tactoid is more than 4, the tactoid consists of 3 layers of 1 nm each, and 2 interlayer galleries in which both are expanded to 1 nm. Hence, the tactoid consist of 3 stacks of MMT.